

#### **Copyright Undertaking**

This thesis is protected by copyright, with all rights reserved.

#### By reading and using the thesis, the reader understands and agrees to the following terms:

- 1. The reader will abide by the rules and legal ordinances governing copyright regarding the use of the thesis.
- 2. The reader will use the thesis for the purpose of research or private study only and not for distribution or further reproduction or any other purpose.
- 3. The reader agrees to indemnify and hold the University harmless from and against any loss, damage, cost, liability or expenses arising from copyright infringement or unauthorized usage.

#### **IMPORTANT**

If you have reasons to believe that any materials in this thesis are deemed not suitable to be distributed in this form, or a copyright owner having difficulty with the material being included in our database, please contact <a href="mailto:lbsys@polyu.edu.hk">lbsys@polyu.edu.hk</a> providing details. The Library will look into your claim and consider taking remedial action upon receipt of the written requests.

# PHYSICS INFORMED MACHINE LEARNING FOR STRUCTURAL RESPONSE PREDICTION AND HEALTH MONITORING

#### YUAN LEI

PhD

The Hong Kong Polytechnic University

2025

# The Hong Kong Polytechnic University Department of Civil and Environmental Engineering

# Physics Informed Machine Learning for Structural Response Prediction and Health Monitoring

#### YUAN Lei

A thesis submitted in partial fulfilment of the requirements for the degree of

Doctor of Philosophy

February 2025

# **Certificate of Originality**

I hereby declare that this thesis is my own work and that, to the best of my knowledge and
belief, it reproduces no material previously published or written, nor material that has been
accepted for the award of any other degree or diploma, except where due acknowledgement
has been made in the text

	(Signed)
YUAN Lei	_(Name of student)

#### **Abstract**

The rapid development of machine learning methods in recent years has provided researchers with alternative approaches to explain the physical world solely through data. These advanced data-driven methods offer great flexibility in handling various physical problems and have demonstrated superiority over traditional model-based methods in many fields. As a result, there is now a growing tendency to utilize these machine learning methods to tackle difficult problems in science and engineering, especially in physical problems involving uncertain systems. However, existing data-driven methods still face some limitations. Machine learning models trained from data are often hobbled by noise, imbalance, and sparsity in the training data, posing challenges to the generalization of the models. Additionally, since the intrinsic laws of physical systems are only represented at a shallow level from the training data, the trained machine learning models may produce physically implausible result predictions that violate the governing laws of physical systems.

Given the challenges existing in these data-driven methods, this study delves deeply into the application of physics-informed machine learning (PIML) in engineering physical systems. PIML is an emerging machine learning concept that aims to couple various prior physical constraints into the training of machine learning models, thereby enhancing the physical feasibility of the models and improving their generalization and robustness. The focus of this thesis is on the application of PIML in structural dynamic response and structural damage monitoring. Several PIML frameworks are proposed to integrate machine learning models and physical knowledge to address the difficulties encountered by current data-driven and

traditional physics-driven methods.

First, a framework named structural dynamics learner (SDL) is proposed to solve the forward problem of structural dynamics by integrating physical information with neural network models. In SDL, a novel recurrent convolutional neural network framework that integrates physical information described as the implicit Crank-Nicolson form of the system's motion equations is established to predict the dynamic response of linear/nonlinear structural systems. Afterward, the focus of this thesis shifted to the research of inverse problems in structural dynamics. The first inverse problem investigated is the reconstruction of external forces and dynamic responses of structures, where a physics-informed Markov parameters (PI-MP) framework is proposed to accurately reconstruct the external excitations and dynamic responses from partial vibration measurement data. Here, the neural network with strong characterization ability for reconstructing unknown external force input is coordinated with the Markov parameter for describing the motion equation of the structure in the state space to predict the acceleration response of the structure. By minimizing the deviation between the predicted structural acceleration response and the measured vibration response, PI-MP can locate and reconstruct the external excitation input of the structure and predict the vibration response of all nodes of the structure. Then, the application of PIML for structural damage identification with unknown external forces from vibration measurements is further investigated. A physics-informed Fourier feature neural networks (PI-FFNN) framework integrates Fourier neural networks with excellent multi-frequency characterization capabilities and the Newmark-beta scheme of the motion equation as physical information is presented to achieve this research goal. The integration of physical information makes this method unsupervised learning, which can be trained to accurately detect structural damage from vibration measurements without relying on any damage-related data labels. Finally, based on the physics-informed neural networks framework, we propose a PIML framework that can simultaneously identify the structural mechanical parameters, reconstruct the unknown external excitation on the structure, and establish a surrogate model for nonlinear systems. In this framework, two neural network models are employed to represent the structure's unknown external excitation and nonlinear internal restoring forces respectively, and the mechanical parameters of the structure are also updated together with the neural network model as trainable parameters. The physical information of the structural vibration equations is seamlessly integrated into the proposed machine learning framework through a set of mathematical equations that describe the Newmark-beta relations of the dynamic system. By minimizing the difference between the predicted structural response and the structural vibration observation, both the external excitation and the internal nonlinear restoring force of the structure can be reconstructed simultaneously and the exact values of the structural parameters can be discovered.

This thesis presents several innovative PIML frameworks for solving forward and inverse problems in structural dynamics. Under the constraints of physical information, these frameworks demonstrate the independence of complex and large training data and achieve efficient and accurate model training in a physically constrained search space. The embedding of physical information also gives the predictions of the proposed PIML frameworks with physical interpretation, outstanding noise robustness, and excellent generalization for physical systems in a variety of environments. The results of simulation analysis and real physical

experiments show that the proposed PIML frameworks have outstanding ability and performance to accurately model real physical systems. Looking ahead, more in-depth research is still needed to apply the promising PIML method to more complex physical systems, involving large structural degrees of freedom and complex nonlinearities.

#### **Publications**

#### **Journal Papers**

**Yuan, L.**, Ni, Y. Q., Deng, X. Y., & Hao, S. (2022). A-PINN: Auxiliary physics informed neural networks for forward and inverse problems of nonlinear integro-differential equations. Journal of Computational Physics, 462, 111260.

Sun, X., Guo, C., **Yuan, L.**, Kong, Q., & Ni, Y. (2022). Diffuse Ultrasonic Wave-Based Damage Detection of Railway Tracks Using PZT/FBG Hybrid Sensing System. Sensors, 22(7), 2504.

Rui, E. Z., Chen, Z. W., Ni, Y. Q., **Yuan, L.**, & Zeng, G. Z. (2023). Reconstruction of 3D flow field around a building model in wind tunnel: a novel physics-informed neural network framework adopting dynamic prioritization self-adaptive loss balance strategy. Engineering Applications of Computational Fluid Mechanics, 17(1), 2238849.

Ni, Y. Q., Liu, W. Q., Rui, E. Z., **Yuan, L.**, Chen, S. Y., & Zheng, Y. L. (2023). A novel computer vision-based vibration measurement and coarse-to-fine damage assessment method for truss bridges. Smart Structures and Systems, 31(4), 393-407.

Ye, X., Ni, Y. Q., Ao, W. K., & **Yuan, L.** (2024). Modeling of the hysteretic behavior of nonlinear particle damping by Fourier neural network with transfer learning. Mechanical Systems and Signal Processing, 208, 111006.

Zhang, W., Wang, S. M., Ni, Y. Q., Yuan, X., Feng, Y., Yuan, L., & Hao, S. (2024). Physics-enhanced multi-fidelity neural ordinary differential equation for forecasting long-term creep behavior of steel cables. Thin-Walled Structures, 112846.

**Yuan, L.**, Ni, Y. Q., Ye, X., Rui, E. Z. Structural dynamics learner: a physics-informed recurrent convolutional neural networks framework for dynamic response prediction of structural systems. Engineering Applications of Artificial Intelligence. (Under review)

Yuan, L., Ni, Y. Q., Hao, S., ZHANG, W. J. Physics-informed Markov parameters (PI-MP) framework for robust force localization and structural response reconstruction. Journal of Sound and Vibration. (Under review)

#### **Conference Papers**

Yuan, L., NI, Y. Q., Hao, S., & ZHANG, W. J. (2023). From Initial to Final State: Single Step Prediction of Structural Dynamic Response. STRUCTURAL HEALTH MONITORING 2023.

**Yuan, L.**, Ni, Y. Q., Rui, E. Z., & Zhang, W. (2024, June). Structural damage inverse detection from noisy vibration measurement with physics-informed neural networks. In Journal of Physics: Conference Series (Vol. 2647, No. 19, p. 192013). IOP Publishing.

Zhang, W., NI, Y. Q., **Yuan, L.**, Hao, S., & WANG, S. M. (2023). Structural Parameter Identification with a Physics-Informed Neural Networks-Based Framework. STRUCTURAL HEALTH MONITORING 2023.

Zhang, W., Yuan, X., Yuan, L., Ni, Y. Q., & Wang, S. M. (2023, October). Neural ODE-based data-driven approach for prediction of the creep behaviour of steel cables. In Proceedings of IASS Annual Symposia (Vol. 2023, No. 13, pp. 1-8). International Association for Shell and Spatial Structures (IASS).

#### Acknowledgements

Undertaking a Ph.D. has been an experience as enriching as it was challenging. It has been a great learning journey, one that involved honing many skills – from academic research to written and verbal communication. However, the path towards acquiring these skills is far from easy. It demands relentless learning, consistent practice, independent thinking, and most importantly, resilience in the face of failures. Now, as I stand at this penultimate milestone of my journey, the finish line within sight, I cannot help but feel a profound sense of pride and relief. With all its ups and downs, this journey has shaped me in ways I hadn't imagined, and I am profoundly grateful for that.

I am profoundly grateful to my supervisor, Prof. Yiqing Ni, whose guidance has been essential throughout my Ph.D. journey. Your exceptional blend of efficient leadership and passionate research has set a model for me to emulate. Your profound insight into the principles of quality research and the methodology to execute it has been truly invaluable. The knowledge and wisdom I have garnered under your tutelage, I firmly believe, will continue to illuminate my path in all future endeavors.

I would like to express my most sincere gratitude to my dearest and most precious life partner, my girlfriend Dr. Zhang Xiaozhe. During my doctoral studies, I suffered from complex diseases both physically and mentally, which made me sink into the quagmire without rescue. During this difficult time, Dr. Zhang gave me infinite patience, deep care and understanding, which became the driving force to support me to move forward. From the badminton court, the country park, the beautiful beach and the sea to the operating room, we have left many precious

memories together, which are moments worth remembering for my lifetime. In addition, I would also like to thank my friends on the badminton court and in my daily life. Thank you for bringing more colorful life during the boring doctoral studies.

My warmest appreciation extends to my family, notably my parents, who have been my pillars of support and strength during my Ph.D. journey. Your selfless love and unyielding support have profoundly touched my heart, and for this, I am forever grateful.

In addition, I must extend profound thanks to my friends and colleagues at the CNERC-Rail Research Center. The journey towards a Ph.D. can be daunting and taxing, but the constant presence of your unwavering support and companionship has lit the path in my darkest hours. You have imbued me with courage, faith, and happiness, bolstering my resilience during the most challenging moments. I cannot quantify the depth of my gratitude for the abundant laughter and joy we have shared. Your friendship is a gift for which I will remain forever thankful.

As I bid farewell to these transformative four years of my life, I will forever hold those memories we have created - moments of joy, moments of struggle, moments that have indelibly marked my journey. They all have shaped the person I am today.

### **Contents**

Certificate of Originalityi
Abstractii
Publications vi
Acknowledgements viii
Contentsx
List of Figuresxiv
List of Tablesxix
List of Abbreviationsxx
Chapter 1 Introduction
1.1 Background and Motivation1
1.2 Research Objectives
1.3 Thesis Outline
Chapter 2 Literature Review
2.1 Physics-informed machine learning
2.2 PIML for structural response prediction
2.3 PIML for structural health monitoring
2.4 Summary
Chapter 3 Structural dynamics learner framework for dynamic response prediction of
structural systems44
3.1 Introduction44

3.2 Problem statement	48
3.3 Methodology	49
3.3.1 Crank-Nicolson scheme of motion equation	50
3.3.2 Neural network architecture of SDL	52
3.3.3 Loss function and model training	55
3.3.4 Algorithm and computing platform	59
3.4 Numerical validation	60
3.4.1 2-DOF system	61
3.4.2 Five-story shear structure	65
3.4.3 3-DOF system with Bouc-Wen hysteresis	72
3.4.4 Plane truss structure	76
3.5 Summary	80
Chapter 4 PI-MP framework for force localization and structural response reconstruction	on
	82
4.1 Introduction	82
4.2 Background	87
4.2.1 Motion equations for structural system	87
4.2.2 Force and response reconstruction	88
4.2.3 Tikhonov regularization	89
4.2.4 Physics-informed neural networks	90
4.3 Methodology	92

4.4.1	4-degree-of-freedom system	98
4.4.2	Cantilever beam	103
4.4.3 I	Plane truss	106
4.5 Experir	mental validation	110
4.6 Summa	ary	115
Chapter 5 PI-FFN	NN for vibration based structural damage identifica	tion with unknown
external for	rces	117
5.1 Introdu	ction	117
5.2 Backgro	ound	124
5.2.1 1	Motion equation of structural system	124
5.2.2 I	Physics informed neural networks	126
5.3 Method	dology	128
5.4 Numeri	ical cases	134
5.4.1	Cantilever beam	134
5.4.2 I	Plane truss	153
5.5 Experir	mental verifications	157
5.5.1 I	Initial parameter identification	159
5.5.2 I	Damage detection of damaged beams	162
5.6 Summa	ary	164
Chapter 6 Structur	ral identification from unknown input excitations with	th physics-informed
neural netv	works	167
6.1 Introdu	action	167

6.2 Background	171
6.2.1 Motion equation of structural system	171
6.2.2 Physics informed neural networks	173
6.3 Methodology	175
6.4 Numerical cases	183
6.4.1 4-degree-of-freedom system	183
6.4.2 Bouc-Wen hysteresis system	194
6.5 Experimental case	202
6.6 Summary	208
Chapter 7 Conclusions and recommendations	210
7.1 Conclusions	210
7.2 Recommendations for Further Research	214
References	218

# **List of Figures**

Figure 2.1 Application areas of physics-driven and data-driven methods10
Figure 2.2 General PINNs framework for forward problems of nonlinear PDEs12
Figure 3.1 The comparison between the explicit scheme and implicit scheme51
Figure 3.2 Neural network architecture of the SDL framework
Figure 3.3 The CNN model in SDL framework
Figure 3.4 A linear two-degree-of-freedom system
Figure 3.5 The comparison of the predicted M1 displacement response of the 2-DOF
system with SDL model and numerical methods
Figure 3.6 The comparison of displacement response prediction of M1 with SDL model
and numerical methods64
Figure 3.7 A 5-story structure with nonlinear stiffness springs
Figure 3.8 The seismic acceleration excitation of EI Centro (N-S)
Figure 3.9 The benchmark solution of the seismic response of the 5-story structure67
Figure 3.10 The comparison of structural displacements and velocities of M1 and M5
predicted by the SDL model and PINNs method70
Figure 3.11 The comparison of frequency distribution of structural displacements and
velocities of M1 and M5 predicted by the SDL model and PINNs method71
Figure 3.12 A 3-DOF system with Bouc-Wen hysteresis
Figure 3.13 The comparison of the predicted displacement results of SDL model and
henchmark solutions 75

Figure 3.14 Restoring force loops for three Bouc-Wen hysteresis models. The three sub-
figures are results of model BW 1 (left), BW 2 (mid) and BW 3 (right)75
Figure 3.15 A plane truss structure
Figure 3.16 Comparison of the Y displacements of nodes 5, 6, and 7 predicted by the SDL
model and the PINNs model with the benchmark solution79
Figure 3.17 Convergence process of multiple loss functions in PINNs
Figure 4.1 The overall framework of the physics-informed Markov parameters93
Figure 4.2 4-degree-of-freedom system
Figure 4.3 Reconstructed external forces (Top: 0% noise input, bottom: 10% noise input)
100
Figure 4.4 Process of discovering the L matrix
Figure 4.5 Finite element model of the cantilever beam
Figure 4.6 Reconstructed external force with input data of different noise levels105
Figure 4.7 Reconstructed vertical displacement (top) of the cantilever beam and error in the
reconstructed vertical displacement (bottom)106
Figure 4.8 A plane truss system
Figure 4.9 The search process of the force position
Figure 4.10 Reconstructed external forces using the PI-MP method
Figure 4.11 Reconstructed vertical displacement (top) and velocity (bottom) of nodes 2 and
3109
Figure 4.12 Vibration test of a beam
Figure 4.13 Mechanical model of the test beam

Figure 4.14 Measured FRF and calculated FRF from FEM model
Figure 4.15 Measurement values from four accelerometers
Figure 4.16 Reconstructed external force and measured external force
Figure 4.17 Reconstructed acceleration response and measured values of accelerometer 114
Figure 5.1 The overall framework of PI-FFNN
Figure 5.2 The finite element model of the cantilever beam
Figure 5.3 The external force acting on the cantilever beam
Figure 5.4 Vibration data of the three accelerations (a) and the frequency spectrum (b) .137
Figure 5.5 lossz - lossa of 14 test schemes. (left) noise-free input data, (right) input data
with 1% noise. The values of $\alpha$ is given in brackets
Figure 5.6 Result of stiffness reduction identification
Figure 5.7 Results of external force reconstruction
Figure 5.8 Reconstructed external force prediction by Markov parameters method with
Tikhonov regularization
Figure 5.9 Convergence process of loss function of PINNs
Figure 5.10 Structural external forces predicted by the PINNs model
Figure 5.11 Structure of the plane truss
Figure 5.12 Acceleration observation data (a) and frequency spectrum (b)
Figure 5.13 Identified results of stiffness reduction
Figure 5.14 External forces of the plane truss reconstructed by PI-FFNN method157
Figure 5.15 The vibration test of an aluminum beam
Figure 5.16 The model of the aluminum beam and supports

Figure 5.17 Data acquisition and storage equipment
Figure 5.18 Measured acceleration response (top) and frequency spectrum (bottom)160
Figure 5.19 Location and depth of damage on the aluminum beam
Figure 5.20 Results of stiffness reduction identified by the PI-FFNN model
Figure 5.21 External force of the beam reconstructed by the PI-FFNN model164
Figure 6.1 The overall framework of the PINNs method for structural identification179
Figure 6.2 The architecture of the <i>FCNNin</i> model
Figure 6.3 4-DOF structural dynamic system
Figure 6.4 (a) Vibration response and (b) frequency spectrum of the structure calculated by
the numerical solver
Figure 6.5 Convergence process of loss function186
Figure 6.6 Structural displacement, velocity, and acceleration predicted by the model 187
Figure 6.7 Ground acceleration reconstructed by the model
Figure 6.8 The time series data of the internal restoring force
Figure 6.9 The acceleration responses predicted by PINNs model
Figure 6.10 Internal restoring force reconstructed from noisy training data
Figure 6.11 The calculated structural acceleration response of noisy cases
Figure 6.12 3-DOF system with Bouc-Wen hysteresis model
Figure 6.13 The amplified EI-Centro seismic acceleration
Figure 6.14 The time domain curves (a) and frequency distribution (b) of the acceleration
response of the 3DOF system
Figure 6.15 The convergence process of the loss function

Figure 6.16 The reconstructed displacement response of the 3-DOF system198
Figure 6.17 The reconstructed ground acceleration from <i>NNex</i> model198
Figure 6.18 The reconstructed internal restoring force generated by the Bouc-Wen model
Figure 6.19 The seismic acceleration of Chi-Chi earthquake
Figure 6.20 The structural vibration response predicted by the identified structural system
Figure 6.21 The hysteresis force calculated by the identified Bouc-Wen model202
Figure 6.22 Vibration test of aluminum beam
Figure 6.23 The collected vibration responses and frequency spectrum204
Figure 6.24 The comparison of the structural vibration response predicted by the model
(blue) and measured data (red)
Figure 6.25 Reconstructed moments from supports (top) and reconstructed external force
input (bottom)
Figure 6.26 The comparison of the structural vibration response predicted by PINNs (blue)
and the measured value (red)

## **List of Tables**

Table 3.1 The comparison of relative L2 error (a) and computation time (b) of different CNN
model schemes67
Table 4.1 Relative L2 errors in reconstructed external forces
Table 4.2 Relative L2 error of external force reconstruction for different measurement point
schemes
Table 4.3 Sensor positions and weights
Table 4.4 Parameter settings after model update
Table 5.1 The natural frequencies of the undamaged and damaged beams (Hz)135
Table 5.2 Test results of hyperparameters LNN and HNN
Table 5.3 Identified damage results of Markov parameters method with Tikhonov
regularization
Table 5.4 Damage results identified by PINNs model
Table 5.5 The results of the comparative experiment
Table 5.6 First ten natural frequencies of the plane truss (Hz)
Table 5.7 The installation positions and weights of accelerometers
Table 5.8 Results of mechanical parameter update
Table 6.1 Summary of the differences between proposed framework and PI-NODE 182
Table 6.2 Structural parameters identified from noisy training data
Table 6.3 Installation position and weight of accelerometers

#### List of Abbreviations

CFD Computational fluid dynamics
CNN Convolutional neural networks
DCAE Deep convolutional autoencoders

DCT Discrete cosine transforms

DPINN Direct physical information neural network
DR-RNN Deep residual recurrent neural network
ERA Eigensystem realization algorithm

ERK4 Fourth-order explicit Runge–Kutta method

ETD Explicit time-domain

ETDM Explicit time domain method FCNN Fully connected neural networks

FDAM Fault division autoencoder multiplexing

FDM Finite difference method FEA Finite element analysis FEM Finite element method

FFNN Fourier feature neural networks
FRF Frequency response functions
GPT Generative pretrained transformer

GRU Gated recurrent unit

KEMRO Kinetic energy matrix rank optimization

LSTM Long short-term memory MDOF Multi-degree-of-freedom

ML Machine learning

NODE Neural ordinary differential equation

OLS Ordinary least squares
OSP Optimal sensor placement
PCA Principal component analysis

PGNM Physical information gated recurrent unit network method

PIAE Physical information autoencoder
PIDL Physically-informed deep learning
PI-MP Physics-informed Markov parameters
PINNs Physics informed neural networks

PIPNN Physically informed parallel neural network
PI-VAE Physically-informed variational autoencoder
RCNN Recurrent convolutional neural networks

RNN Recurrent neural networks
SHM Structural health monitoring

TGSVD Truncated generalized singular value decomposition

TSVD Truncated singular value decomposition

UIR Unit impulse response

### UQ Uncertainty quantification

#### **Chapter 1 Introduction**

#### 1.1 Background and Motivation

In modern society, the safety and reliability of infrastructure are crucial to ensuring economic development and people's quality of life. In-service buildings, bridges, transportation systems, and other structures not only bear the load of daily operations but also face the impact of natural disasters, environmental changes, and human factors. Due to the ageing and fatigue of the structure and the wear and corrosion caused by the environment, potential damage and failure may lead to serious safety risks and economic losses. Therefore, regular monitoring and evaluation of structural health status is an important engineering task.

Structural health monitoring (SHM) is a comprehensive process that uses a series of technical tools and methods to evaluate and manage the safety and performance of structures. The main goal of SHM is to detect damage and deterioration in structures promptly to prevent potential safety risks and economic losses. The SHM process usually involves installing sensors on the structure to continuously collect data on its stress, strain, acceleration, and environmental conditions. These data can be analyzed and processed to identify the structural health status and evaluate the structural response under specific loading and environmental conditions.

In the SHM field, structural analysis is usually the basic process because it provides the necessary theoretical basis and data support for damage identification,

performance evaluation, and maintenance decisions by establishing structural models. Traditional structural analysis methods usually rely on physical models and empirical formulas. These methods perform well when dealing with simple linear systems but are often insufficient when faced with complex nonlinear behaviors, dynamic responses, and changing environmental conditions. For example, although the classic finite element analysis (FEA) can accurately describe the physical processes in the structural system, it is computationally expensive and requires detailed material and geometric data. In practical applications, obtaining accurate data is often difficult and time-consuming.

With the advancement of sensor technology and data collection methods, a large amount of structural monitoring data has been obtained. This data provides a rich foundation for data-driven methods such as machine learning. Machine learning enables models to adapt to complexity and uncertainty by learning patterns and relationships from data. However, pure data-driven methods have some drawbacks, such as a lack of physical interpretation, overfitting, and performance degradation in data-scarce conditions.

In this context, physics-informed machine learning (PIML) has been proposed and has received increasing attention. PIML provides a new solution by incorporating physical laws and constraints into machine learning models. This approach not only combines the flexibility of data-driven methods but also ensures that the model follows the basic laws of physics, thereby improving the accuracy and interpretability of the

model.

A major advantage of PIML is its ability to maintain good prediction performance even when data is limited or of low quality. By leveraging physical knowledge, PIML can more effectively capture the nonlinear characteristics of structural response and the changes in structural parameters while reducing the reliance on large amounts of training data. This feature is particularly important for SHM and response prediction, as obtaining high-quality, comprehensive, and balanced data is often a challenge in practical applications.

In real-world applications, PIML can provide structural engineers and designers with more advanced tools to help them make more scientific decisions during design and maintenance. With enhanced predictive capabilities, PIML can support timely maintenance measures, thereby extending the service life of structures, reducing maintenance costs, and improving the safety of public infrastructure. As the demand for structural health monitoring increases, the PIML method that combines physical knowledge with machine learning provides new perspectives and possibilities for addressing the limitations of traditional methods. This approach not only provides a stronger theoretical basis for structural response prediction but also provides data-driven support for strategies to maintain and manage infrastructure.

In light of these research motivations, this thesis delves into the development of PIML frameworks for structural response prediction and health monitoring. This work starts with the introduction of a novel machine learning framework that integrates PIML

and convolutional neural networks (CNN) to predict the response of linear or nonlinear structural systems under dynamic forces. Then, PIML is further investigated by integrating physics-informed neural networks (PINNs) with the Markov parameters method in structural dynamics. A physics-informed Markov parameters (PI-MP) method is proposed to reconstruct force and structural response from the measurement of structural vibrations. After that, the research of the PIML method is extended to structural damage identification from partial response observations of the structure. In this part, a novel vibration-based structural health monitoring method is proposed for vibration-based structural damage identification with unknown external forces. Finally, the focus of this work shifts to the structural identification of linear/nonlinear structural systems. A physics-informed neural networks framework based on the Newmark-beta numerical method is proposed to identify system parameters and unknown external forces from vibration measurements of nonlinear structural systems.

#### 1.2 Research Objectives

This study is intended to develop novel frameworks of PIML to accurately predict the dynamic response and detect the damage of linear and nonlinear structural systems.

The detailed research objectives are:

- To develop a novel PIML framework that successfully combines physical information and deep neural networks to accurately predict the dynamic response of linear and nonlinear structures under dynamic forces.
- 2) To develop a PIML framework for inverse problems of structural dynamics,

which can identify and reconstruct the external forces and responses of structures from partial structural vibration observations.

- 3) To expand the PIML framework for inverse problems of structural dynamics to detect damage based on vibration observations with unknown external forces.
- 4) To develop a novel PIML framework adapted to linear and nonlinear structural system identification.

#### 1.3 Thesis Outline

This thesis consists of the following seven chapters:

**Chapter 1** gives the research motivation, research objectives, and the outline of the thesis.

Chapter 2 presents a comprehensive review of research efforts on PIML, followed by the introduction of the latest applications of PIML in structural response prediction and PIML for structural health monitoring. The advantages and challenges of the existing PIML methods for structural dynamics are also discussed.

Chapter 3 develops a novel PIML framework called Structural Dynamics Learner (SDL) that integrates PIML and convolutional neural networks (CNN) to predict the response of linear or nonlinear structural systems under dynamic forces. After proper training, SDL can serve as a surrogate model of the structural system, capable of predicting the next dynamic response based on the current state. The governing equations of structural vibrations are incorporated into SDL to provide prior physical

knowledge for the training process.

Chapter 4 invests the physics-informed Markov parameters (PI-MP) method for force and structural response reconstruction. By integrating physics-informed neural networks and Markov parameters of structural dynamics, PI-MP can localize and reconstruct unknown external forces, as well as reconstruct unmeasured dynamic responses of the structure, from partial structural response observations.

Chapter 5 investigates the feasibility of a new framework named physics-informed Fourier feature neural networks (PI-FFNN) for structural damage detection from vibration observation with unknown external forces. Using a neural network model containing a Fourier feature layer to represent the unknown external forces and the Newmark-beta scheme of the motion equation as physical information, the PI-FFNN model is proven to accurately identify structural damage.

Chapter 6 investigates a promising approach for linear/nonlinear structure identification via physics-informed neural networks. The governing equations of structural motion are integrated as physical information with the neural network. A Fourier feature neural network model is utilized to represent the unknown external/internal forces of the structure. By minimizing the difference between the predicted structural vibration responses and the observed data, the structural mechanical parameters are updated to approach the exact values, and the external/internal forces of the structure are reconstructed. In addition, based on the reconstructed internal forces, a surrogate model can be trained to characterize the

nonlinear system in the structure.

**Chapter 7** provides a summary of the thesis, the major conclusions, and the potential future work.

#### **Chapter 2 Literature Review**

In this section, the current research state on PIML is introduced first, highlighting the distinctions between PIML and traditional machine learning methods. Subsequently, research efforts to apply PIML for structural response prediction are outlined and discussed. Following this, the applications of PIML in SHM are reviewed and summarized. Finally, the limitations and challenges of existing PIML methods in the realms of structural response prediction and health monitoring are analyzed and discussed.

#### 2.1 Physics-informed machine learning

In the past decades, great progress has been made in understanding physical processes in various fields by numerically solving the governing equations using computational methods such as finite difference methods and finite element methods. Although these methods can achieve satisfactory results in the analysis of fully informed physical systems, they still face severe difficulties for real physical problems with missing governing equations, gaps or noisy boundary conditions, and strong nonlinearities. In addition, for inverse problems of physical systems, i.e., inferring the parameters of the system or unknown physical principles from observed data, traditional numerical methods usually rely on expensive iterative procedures or the design of new algorithms.

To overcome these difficulties, people have turned their attention to observational

data obtained from actual physical systems. With the explosive growth of various sensors and data acquisition equipment installed, a large amount of multi-fidelity observational data has been collected, providing soil for the development of data-driven methods. Among data-driven methods, machine learning has played a revolutionary role in discovering real physical processes from multi-fidelity observational data because it can explore huge design spaces, identify multi-dimensional correlations, and manage ill-posed problems. In machine learning methods, deep learning methods are particularly outstanding as they can naturally extract deep features from observational data (Najafabadi et al., 2015).

Although machine learning methods have great promise and have achieved widespread success in various purely data-driven problems, most developed machine learning models are unable to obtain interpretable and robust physical information and knowledge from these data. In other words, these models usually act as a 'black box' to merely characterize the mapping relationships in the training data (Burkart & Huber, 2021). In addition, after well-training, these purely data-driven models may be highly consistent with the results of the observed data, but due to inference errors or observation biases, the model generalization performance may be poor, and its predictions may be physically inconsistent or unconvincing.

To overcome this shortcoming, a new machine learning concept called PIML was proposed in (Karniadakis et al., 2021). PIML is the process of improving the performance of machine learning algorithms by using prior knowledge derived from

our observations, experiences, physics, or mathematical understanding of the world. By providing machine learning models with 'informative priors,' i.e., strong theoretical constraints and inductive biases on top of observational constraints, PIML can 'teach' machine learning models about physical processes to integrate basic physical laws and domain knowledge. The comparison of the applicable areas of physics-driven methods, data-driven methods, and physical machine learning methods is shown in Fig. 2.1.

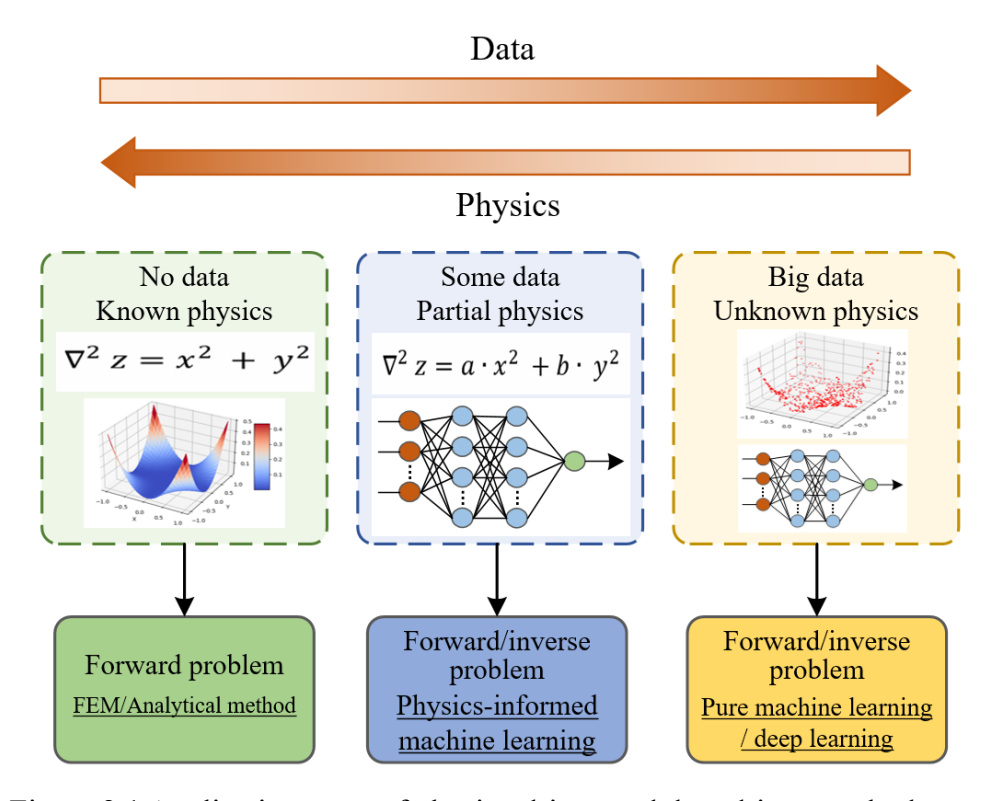


Figure 2.1 Application areas of physics-driven and data-driven methods

After PIML was proposed, it received widespread attention and experienced vigorous development. Researchers in various fields have designed a lot of different PIML frameworks to target specific physical problems according to a wide range of task requirements. Among these PIML frameworks, the most widely explored ones are

those frameworks that combine physical information with deep learning methods, especially PINNs proposed by (Raissi et al., 2019). PINNs use prior knowledge to construct the loss function of the deep neural network, thereby reducing the inference error of the model and 'teaching' the neural network model to learn prior physical information. After completing training, PINNs can seamlessly integrate physical information and deep neural network models so that the model's predictions are consistent with physical constraints. Using physical information, PINNs can solve the forward problem of nonlinear partial differential equations (PDEs) without any labeled data and can also accurately discover the accurate values of control parameters in the governing equations from noisy measurements. A general process of PINNs for solving the forward problem of nonlinear PDEs is shown in Fig. 2.2. In other extended studies, PINNs can not only solve the forward and inverse problems of PDEs, but their application scope has also been extended to fractional PDEs (Pang et al., 2019), integral-differential equations (Yuan et al., 2022) and stochastic differential equations (Yang et al., 2018, 2020).

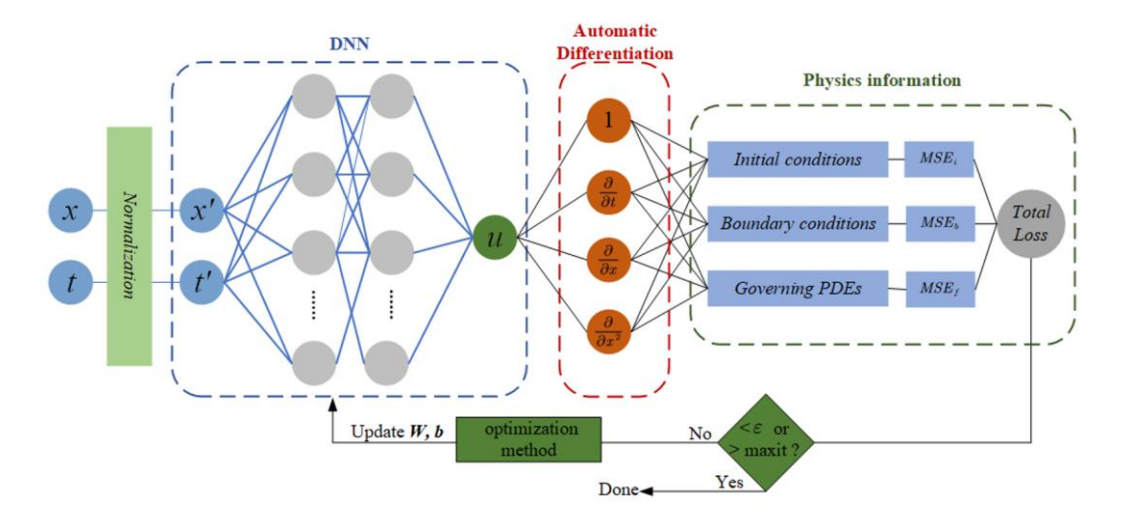


Figure 2.2 General PINNs framework for forward problems of nonlinear PDEs

Not only in the multi-layer perception (MLP) model, but physical information is also utilized in other deep learning methods to handle special tasks. For images or high-dimensional input data, the convolutional neural network (CNN) model is widely used in visual processing. It is also integrated with physical information into a series of novel PIML frameworks. Some typical PI-CNN frameworks have been developed in (Gao et al., 2021; Yuan et al., 2024; Zhang et al., 2023; Zhao et al., 2023). In these PI-CNN frameworks, the input of the neural network model is no longer (t, x) shown in Fig. 2.2 but is changed to multi-dimensional system states or coordinates after mapping the equation domain. Compared with the PINNs framework, PI-CNN can have better representation capabilities and improve the convergence speed for high-dimensional inputs (Fang, 2021; Lei et al., 2025).

For time series data, the Recurrent neural network (RNN), Gated recurrent unit (GRU), and Long Short-Term Memory (LSTM) model show excellent representation ability compared to the MLP model, because these models take into account the dependencies in the sequence data. When the output of the model is related to time series data, physical information can also be employed as prior information to train RNN, GRU, and LSTM models. For example, (Tang et al., 2022) proposed a PI-RNN model to characterize the time-domain response of optical resonances. (Zheng et al., 2023) used the PI-RNN model to predict and control the temporal state of nonlinear

systems. In (Chen, 2024), the MLP model in PINNs was replaced by a GRU network to improve the model's ability to characterize the time evolution of equation features. The proposed physical information gated recurrent unit network method (PGNM model) was shown to improve prediction accuracy and obtain better long-term prediction results. PI-LSTM models have also been developed for response prediction of engineering structures (Fangyu Liu et al., 2023; R. Zhang et al., 2020b) and prediction and health management of engineering systems (Ma et al., 2023). The results of the study show that embedding physics information into the LSTM model can not only alleviate the noise overfitting of the purely data-driven LSTM model and improve the robustness and generalization ability of the model but also obtain more accurate prediction results than the original PINNs model.

For dynamic processes described by differential equations, neural ordinary differential equation (NODE) is a special type of neural network model that treats the neural network as a continuous-time dynamic system rather than the traditional discrete-time model. NODE is shown to be able to process continuous time series data more naturally. In (Lai et al., 2021; O'Leary et al., 2022), physical information is also utilized as prior information for NODE training. The core idea of PI-NODEs is to use physical laws (usually in the form of differential equations) as part of the loss function to guide the learning process of the neural network.

Not only in deep learning methods, physics-informed concepts are also combined with classical kernel methods. The most famous of these is physics-informed Gaussian

process (PI-GP) proposed in (Nevin et al., 2021; Tartakovsky et al., 2023; Yang et al., 2019). Unlike PINNs, which integrates physics information through a specific loss function, the implementation of physics information in PI-GP is to design a specific kernel function to ensure that the model output conforms to the physics laws. This may involve adjusting the covariance matrix according to the physical equations to reflect the dynamic behavior of the system. However, compared to PINNs, due to the limitations of the kernel function in the Gaussian process, the PI-GP method has difficulties in dealing with nonlinear governing equations and high-dimensional spacetime differential operators. A detailed comparison between PI-GP and PINNs can be found in (Pang & Karniadakis, 2020).

Another major direction of PIML extension is to integrate physics information with numerical methods and machine learning to form hybrid models. Traditional numerical methods for solving partial differential equations, such as finite difference method (FDM) and finite element method (FEM), have been successfully developed with PIML. (Jiang et al., 2023) utilized finite differences to replace the automatic differentiation in the original PINNs to calculate the partial derivatives in the governing equations. The results show that finite difference-PINNs can improve the prediction accuracy of derivatives and have advantages in boundary condition integration and computational cost. (Würth et al., 2024) developed a neural finite element solver for non-stationary and nonlinear simulations on arbitrary meshes based on PINNs and mesh graph nets. This method has been shown to quickly and accurately solve non-

stationary and nonlinear PDEs on arbitrary meshes and can scale well to large and complex meshes. Some comparisons and discussions between PINNs and FEM methods can be found in (Grossmann et al., 2024; Rezaei et al., 2022). Runge-Kutta is also a popular numerical research method in PIML. One of the most classic methods is the discrete-time PINNs method (Raissi et al., 2019), which uses the output of the neural network to approximate the Runge-Kutta hidden step to accurately solve nonlinear partial differential equations with large time steps. Another study that combines Runge-Kutta with PIML is (Zhai et al., 2023), where PINNs are used to represent the force term in the equation, thereby using the Runge-Kutta method to solve the integral.

In order to implement PIML efficiently, some widely used general libraries for machine learning, such as TensorFlow and PyTorch, were used to build the PIML framework. In these libraries, neural network graphs and automatic differentiation can be easily implemented through built-in functions. On this basis, several specifically designed software libraries have also been designed to quickly implement PIML. The most famous software is DeepXDE (Lu, Meng, et al., 2021), which is designed based on the PINNs framework. DeepXDE can not only be used to solve the forward and inverse problems of ordinary differential equations and partial differential equations, but also fractional differential equations and integral-differential equations. DeepXDE is also adapted to complex nonlinear problems and irregular geometric domain problems and is developed to accelerate the operation using high-performance GPUs. Other PIML solvers include SimNet (Hennigh et al., 2021), PyDEns (Koryagin et al.,

2019), NeuroDiffEq (F. Chen et al., 2020), and NeuralPDE (Zubov et al., 2021).

In the comparative studies of (Grossmann et al., 2024; Karniadakis et al., 2021; Rezaei et al., 2022), it is discussed that PIML cannot surpass mature numerical methods such as FEM in solving well-posed forward problems of partial differential equations, but for ill-posed problems and inverse problems, PIML framework shows superior solving ability. Compared with pure data-driven methods and pure physics-driven methods, PIML also has obvious advantages in the following directions. The first is that in the learning of incomplete physical models or imperfect data, PIML shows stronger robustness. For example, PIML can effectively obtain accurate results for unbounded problems (Fang et al., 2024) or when boundary conditions are unknown (Mahmoudabadbozchelou et al., 2022). (S. Xu et al., 2023) also used PIML to reconstruct flow fields from sparse and missing imperfect data.

The second advantage of PIML is that it can learn generalizable models from a small amount of training data. For traditional machine learning models, a large amount of balanced training data is critical to improve model performance. However, in (Chen et al., 2021; Linka et al., 2022), PIML demonstrates its ability to train effective models using physical information from a small amount of sparse data.

The third strength of PIML is its uncertainty quantification (UQ) capability. In the PIML model, the uncertainty in the prediction results can come from three parts: the uncertainty of physical information, the uncertainty of training data, and the uncertainty of the machine learning model. The uncertainty of physical information usually refers

to the uncertainty of the stochastic partial differential equation or the control parameters of the equation. Regarding the solution of stochastic PDEs, several new PIML frameworks have been designed in (Yang et al., 2018; D. Zhang et al., 2020) using generative adversarial networks, the spectral dynamically orthogonal and borthogonal methods, respectively. Research on UQ in solving stochastic PDEs can be found in (Shin & Choi, 2023; D. Zhang et al., 2019). Some research on how to train PIML models under uncertain equation control parameters was conducted in (Zheng & Wu, 2023). Bayesian PINN (Yang et al., 2021) is a well-known framework based on Bayesian neural networks that can use physical laws and scattered noisy measurements to provide predictions and quantify the stochastic uncertainty caused by noisy data in a Bayesian framework. UQ tasks have also been addressed by developing new frameworks in (Yang & Foster, 2022; Yang & Perdikaris, 2019). Finally, due to the inference bias of the trained model, PIML's model will also bring uncertainty to the predicted results, which was studied in (Psaros et al., 2023; D. Zhang et al., 2019).

After the rapid development in recent years, researchers have explored the advantages of PIML in the above statement but also found that it has the following limitations. The first is the adaptability of PIML to multi-scale physical problems (Karniadakis et al., 2021). Since PIML relies on machine learning models to express the solutions of PDEs, for multi-scale physical processes, it may be difficult to represent the entire process using only one learning model. For example, there is a spectral bias (Wang et al., 2021) in the fully connected neural networks model, i.e., the model

preferentially learns the low-frequency components in the data represented, and may ignore the high-frequency components. To overcome this limitation, some improvements have been developed, such as the domain decomposition method (Jagtap & Karniadakis, 2020; Kharazmi et al., 2021; Shukla et al., 2021), which decomposes the equation domain into multiple subdomains, and Fourier neural networks that couple Fourier features into neural networks (Song & Wang, 2023; Wang et al., 2021), and multi-scale neural network models that can group multi-scales for training (Leung et al., 2022; Weng & Zhou, 2022).

PIML also faces the limitation of 'soft' constraints. This is because, in many PIML frameworks, the constraints are implemented by penalizing a loss function based on the constraints. It is difficult to ensure that this loss function converges to the global optimal solution so that the constraints are perfectly satisfied. In order to achieve 'hard' satisfaction of boundary conditions, some model techniques have been designed, such as the augmented Lagrangian method (Lu, Pestourie, et al., 2021b) and a smooth function that automatically satisfies boundary conditions (Xiao et al., 2024; Zhu et al., 2021). By combining the output of the neural network model with these techniques, the final prediction result can 'hard' satisfy all constraints.

Another limitation of PIML is the problem of balancing multiple damage functions.

The loss function of many PIML frameworks is a fixed weighted combination of observation data, boundary, and initial constraints, and PDE residuals. It has been observed that the training efficiency of the original PINN depends sensitively on the

weights associated with different loss terms. Many works focus on adjusting the relative importance of each loss term by changing the weights of different loss terms to meet the loss-balanced training of PINN. The first proposed improvement measure is the non-adaptive weight adjustment (Bai et al., 2023; Wight & Zhao, 2021), which determines the optimal weights through multiple tests. Later, the improvement measure that can adaptively adjust the weight coefficients was applied in (Hou et al., 2024; E.-Z. Rui et al., 2023; Xiang et al., 2022). Although adaptive loss function balancing techniques can improve the convergence of PIML, the balance between multiple loss functions remains an open problem.

As PIML is experiencing a booming development, hundreds of research papers on PIML applications are reported and published every year. Therefore, it is difficult to give a detailed and comprehensive review of PIML applications. Here, only some important application areas are listed as examples.

The first and most important applied research area for PIML is computational fluid dynamics (CFD), which often involves high-dimensional or strongly nonlinear governing equations and complex boundary conditions. The main advantage of PIML for CFD problems is that a unified framework can be used to solve both forward and inverse problems. Compared with traditional CFD solvers, PINNs are more flexible in integrating data and physics. A promising application is fluid visualization (Cai, Wang, Fuest, et al., 2021; Raissi et al., 2020) and reconstruction (Hosseini & Shiri, 2024; E.-Z. Rui et al., 2024; Shu et al., 2023), i.e., inferring the entire flow field from a few fluid

measurements. PIML has also been applied to solve various flow problems (Cheng & Zhang, 2021; Rao et al., 2020; Wessels et al., 2020), including compressible fluids (Mao et al., 2020), fluids in medicine (Arzani et al., 2021; Sen et al., 2024), turbulence (Hanrahan et al., 2023; Patel et al., 2024), free boundary (Y. H. Huang et al., 2023; Lu et al., 2024) and Stefan (Wang & Perdikaris, 2021) problems. Some detailed review reports on PIML for fluids can be found in (Cai, Mao, et al., 2021a; Sharma et al., 2023).

Another important application area of PIML is in heat conduction problems (Cai, Wang, Wang, et al., 2021a; J. Xu et al., 2023). Unknown thermal boundary conditions (Bowman et al., 2023; Cai et al., 2020) and multi-media heat conduction (Laubscher, 2021; B. Zhang et al., 2022), as well as the reconstruction of temperature fields (Zhao et al., 2023) are also popular research issues.

PIML has also been widely studied and applied in other engineering fields. In (Huang & Wang, 2022), the applications of PINNs in PIML in power systems are summarized, specifically including state/parameter estimation (Lakshminarayana, Sthapit, & Maple, 2022; Ngo et al., 2024; Zhao et al., 2022), dynamic analysis (Misyris et al., 2020; Stiasny et al., 2024), power flow calculation (Lei et al., 2020; Nellikkath & Chatzivasileiadis, 2022; H.-F. Zhang et al., 2024), optimal power flow (Nellikkath & Chatzivasileiadis, 2021), anomaly detection and location (Lakshminarayana, Sthapit, Jahangir, et al., 2022). Some examples of applications in weather and climate can also be found in (Brecht & Bihlo, 2024; Yao et al., 2023; Y. Zhang et al., 2024).

From the above review, it can be concluded that PIML makes up for the

shortcomings of traditional pure data-driven methods in terms of complexity, interpretability, and physical consistency by seamlessly combining prior physical laws and advanced machine learning models. PIML can make machine learning predictions more accurate in a physical perspective and generalization. In fuzzy boundaries, complex equation domains, ill-posed and sparse data problems, PIML shows strong learning and representation capabilities compared to pure data-driven methods through the enhancement of physical information. On the other hand, compared to pure physical solvers, PIML can flexibly use observational data to enhance the learning of uncertain factors in physical information (such as the control parameters of the equation), thereby avoiding the complex process of determining the exact value of the parameters. In addition, for the inverse problem of physical systems, pure physical methods are complicated to use iterations to continuously update unknown parameters or equation terms. In PIML, this is convenient and straightforward by using machine learning algorithms to reversely identify unknown parameters or represent unknown equation terms as a 'black box.' Moreover, for a fuzzy system, PIML can also combine search methods to directly discover unknown physical information from the data (Chen et al., 2021), which is impossible with traditional pure physical methods.

## 2.2 PIML for structural response prediction

In the previous section, the background knowledge and wide application fields of PIML are introduced. This section will shift our focus to the prediction of the dynamic response of structural systems.

Prediction of structural dynamic response is a key step in the design and research of infrastructure because infrastructure is inevitably affected by external dynamic forces such as wind, earthquake, and human-caused loads. In order to accurately analyze these structural dynamic responses, some traditional numerical methods such as FDM and FEM have undergone long-term development. For the forward problems of linear well-posed structural systems, these numerical methods can accurately solve them by directly solving the differential equations that govern the system vibration. However, for nonlinear or ill-posed systems, and inverse problems of the structural system, these traditional methods require some improvements or a lot of simulation analysis.

In recent years, the explosive development of machine learning technology has led to revolutionary changes in many industries. Researchers in the field of structural dynamics have also made a lot of attempts to utilize machine learning methods to solve such structural response prediction problems. Classic deep learning models, such as DNN models (Kim et al., 2019; Stoffel et al., 2018), CNN models (Oh et al., 2020; Wu & Jahanshahi, 2019), and LSTM models (Xue & Ou, 2021; R. Zhang et al., 2019) have become popular solutions for predicting responses of nonlinear structural systems. However, it should be noted that the essence of the above purely data-driven models is to represent the relationship in structural response through a 'black box' model. Because of this inherent foundation, these models always lack physical interpretability, and the model's predictions may be inconsistent with the well-known physics laws. In addition,

the performance of such models is highly dependent on the quantity and quality of training data. Machine learning models tend to have poor generalization in biased and noisy learning data. However, obtaining a large amount of high-quality labeled data from nonlinear systems is also a challenging task.

After the publication of the PINNs research results in (Karniadakis et al., 2021; Raissi et al., 2019), researchers found that the PIML method shows promising application capabilities for problems involving nonlinear systems. Therefore, in order to overcome the reliance of pure data-driven models on labeled data, some researchers tried to apply the PIML method to the modeling and analysis of nonlinear structural systems. The earliest successful application case is the Phy-LSTM model proposed in (R. Zhang et al., 2020b). In this study, a physics-informed multi-LSTM network was successfully designed for alternative modeling of nonlinear structural systems under data scarcity conditions. In this model, the physical laws of the equations of motion, state dependence, and hysteresis constitutive relations are used to construct the physical loss of the model. By embedding this physical constraint in the loss function to enhance model training, the model can accurately capture the potential nonlinear characteristics of the system even with limited available training datasets.

The main difference between the LSTM model and the ordinary RNN model is its special architecture that allows learning long-term temporal dependencies. However, in (Eshkevari et al., 2021), the Phy-LSTM model is stated to contain a large space of trainable variables, requiring a long training process. This problem is also solved in this

research by proposing an RNN architecture that uses neural connections inspired by exact numerical differential equation solvers to update the state from the current time step to the next step. The model is shown to be able to estimate the dynamics of linear and nonlinear multi-degree-of-freedom systems given a ground motion and estimate a complete set of responses including displacements, velocities, accelerations, and internal forces.

In (Fangyu Liu et al., 2023), a novel physics-based long short-term memory (PI-LSTM) network was proposed for structural response modeling by incorporating physical constraints into deep learning. The physical constraints were modified to accommodate the characteristics of linear and nonlinear structural systems. Two numerical experiments demonstrated that the improved PI-LSTM in this study has higher accuracy. Then, (Jiang et al., 2024) expanded the application of PI-LSTM to predict the nonlinear dynamic response of rotor systems by proposing a dynamic response prediction method based on a multi-LSTM network of physical information. Specifically, two multi-LSTM network architectures based on physical information were introduced here, and the physical laws of motion equations, state dependence, and hysteresis constitutive relations were considered to construct physical losses, thereby enhancing the physical interpretability of deep learning models. Another study on the prediction of the dynamic response of nonlinear systems can be found in (Su et al., 2024). Inspired by the explicit time domain method (ETDM), this study proposed a new PINNs framework based on ETDM, called E-PINN. This model can solve the limitation of the traditional PINN model due to the complexity of the global dynamic evolution mechanism of nonlinear systems.

How to effectively utilize the collected sensor data for modeling and predicting structural responses under future disasters remains a challenge. Most existing methods focus on extracting structural features (e.g., modal features) from the measured data and updating the model, such as model updating based on frequency response functions (FRF) (Esfandiari et al., 2009; Gang et al., 2014), Kalman filtering (Astroza et al., 2016; Song et al., 2020), and Bayesian inference (Rubio et al., 2018; Sun & Betti, 2015). However, these methods require excessive computational effort to update the simulation model when the model has high fidelity due to the large number of parameters that need to be updated and the limited available sensor data. Although lowfidelity models are more computationally cost-effective, it is difficult to maintain accuracy in the presence of uncertainty, especially for nonlinear response modeling. To address this shortcoming, some studies have attempted to couple physical information and the collected observational data to predict the response of the structure, especially under seismic excitation. The first attempt was the physics-guided convolutional neural network (PhyCNN) proposed in (R. Zhang et al., 2020a). PhyCNN is an alternative model for structural response prediction by training a deep convolutional neural network model based on a small amount of seismic input-output datasets and physical constraints. Known physical laws (e.g., governing equations of dynamics) can provide additional constraints on the output of the network model, alleviating the over-model

fitting problem and reducing the need for large training datasets, thereby improving the robustness of the trained model for more reliable predictions. The trained surrogate models can then be used to perform fragility analysis given certain limit state criteria. In recent years, transformers have become increasingly popular in natural language processing and time series data analysis due to their inherent self-attention mechanism, which can effectively capture the relationship between any position in the sequence. It is shown that transformer models can handle long-distance dependency problems without being limited by sequence length. A SeisGPT framework combining physics information and a transformer has also been developed in (Meng et al., 2024). This is a data-driven, large-scale physics information model that leverages deep neural networks based on the Generative Pretrained Transformer (GPT) architecture. The proposed SeisGPT is employed to predict the dynamic behavior of building structures under seismic forces in real-time.

In addition, due to the low frequency of extreme events such as earthquakes, it is difficult to collect enough training data with real labels. In order to reduce the dependence on labeled data and improve model accuracy, (Hu et al., 2023) introduced a new framework that combines the powerful learning ability of PINNs with the effectiveness of pseudo-labeling in data augmentation to improve the accuracy of structural seismic response prediction. (Ni et al., 2022) also used a convolutional NN to reconstruct the structural response of rare events under small data sets. This model takes acceleration at a limited number of locations as input. The output is the

displacement, velocity, and acceleration response at all locations. (Malik et al., 2023) proposed a new approach to evaluate the dynamic response of multi-degree-of-freedom (MDOF) systems using physics-informed recurrent neural networks. The focus of this research is on evaluating the seismic response of nonlinear structures under the limited availability of training data.

The above PIML methods for seismic response prediction all have a basic assumption that the equation of motion and mechanical parameters including mass matrices *M* and force distribution vector are available. In (Xiong et al., 2024), such a type of networks is considered difficult to apply in any real-world structures since the premise of availability of those dynamic parameters goes right against the nature of system complexity and ambiguity of real-world structures. To address this shortcoming, a novel physically informed deep 1D convolutional neural network compiled on top of extended state-space fusion (SSM-CNN) is proposed for seismic response modeling in this study. In SSM-CNN, an innovative parameter-free physical constraint mechanism is designed and embedded to improve performance by constructing differential connections of state variables derived from the state-space representation of the initial structural response.

The research scope of PIML has also been expanded in (Shen & Málaga-Chuquitaype, 2024) to simulate the rocking response of free-standing rigid blocks subjected to ground excitation. The proposed framework called PICNN is implemented by adding a physics-based component to a data-driven CNN to achieve a more accurate

estimation of the rocking response histories of ideally rigid blocks in a hybrid datadriven way.

In addition to discretized multi-DOF systems, the application of PIML in structural mechanics has also been extended to truss systems or continuum systems such as beams. An example of using PIML to study nonlinear trusses is shown in (Mai et al., 2023). For complex beam systems, (Kapoor et al., 2023) proposed a new framework using PINNs to simulate complex structural systems consisting of single and double Euler-Bernoulli or Timoshenko beams connected with Winkler foundations. The results showed that PINNs are a promising strategy for solving structural engineering and machine problems involving beam systems. The nonlinear bending of porous beams has also been studied in (Bazmara et al., 2023; Fallah & Aghdam, 2024). (Trinh et al., 2024) proposed a PINNs analysis model for functionally graded thin-walled beams with bi-symmetrical I-shaped and channel sections. To this end, an energy-based PINN method was used to determine the vertical displacement and torsion angle of the beam. Prediction of early time-dependent behavior of prestressed concrete beams has also been learned using PIML in (Park & Hwang, 2023). Specifically, this study proposed a PINN model to learn the time-dependent coupling between the effective prestress and several factors that affect the time-dependent behavior of beams, such as concrete creep and shrinkage, tendon relaxation, and changes in concrete elastic modulus.

In addition to seismic response prediction, wind-induced structural vibration is also an important research area in the forward problem of structural dynamics. (Li &

Zhang, 2022) implemented a hybrid approach to simulate the vibration of wind turbines. Specifically, the structural characteristics and linearized representation of the wind turbine system were used as physical constraints and applied to the recently proposed deep residual recurrent neural network (DR-RNN) to form a physics-informed deep learning model. (Tsai & Alipour, 2023) proposed a method to simulate wind-induced structural response with less training cost. In the proposed method, field monitoring data under conventional wind load conditions were used to train an LSTM network. However, by coupling physical information, the trained LSTM network can predict the wind-induced response under high and extreme wind conditions observed during structural monitoring.

For PIML to predict the dynamic response of structures, how to apply loads to the simulated structure is a complex issue, especially for non-uniformly distributed loads such as concentrated loads. This problem has been solved in recent studies. The first approach proposed in (Y. Li et al., 2024) was designed to use the partial response of the structure to estimate the arbitrarily distributed load as an equivalent load. Subsequently, the structural response was reconstructed using the finite element model. The modeling and analysis of moving loads was studied in (Liang et al., 2024). Here, the PINNs method is combined with the Fourier transform to solve partial differential equations in the frequency domain, thereby alleviating the spectral bias problem of neural networks when simulating multi-frequency functions.

From the above review, it is known that, for the prediction of structural dynamic

response, PIML focuses more on problems that are difficult to solve by numerical methods. The first is the modeling problem of nonlinear structural systems (Su et al., 2024; R. Zhang et al., 2020b). In the published studies, measured data is often employed to enhance the model representation of structural nonlinearity. The second study on PIML is the problem of inaccurate dynamic equations and mechanical parameters of the structure. In this problem, some nonparametric or weak physical information is integrated into the model training to enhance the model's learning even for sparse and noisy observation data. In both types of problems, the PIML methods demonstrate an outstanding ability to seamlessly couple physical information and training data to accurately predict the dynamic response of the structure.

However, some difficulties still exist in the current PIML method, especially PINNs, for predicting the dynamic response of structures, such as spectral bias in learning models, complex boundary condition representation, and hard boundary constraints. Some attempts have also been observed to address the spectral bias problem by applying frequency domain concepts (Liang et al., 2024) to PINNs. Another difficulty lies in the acquisition of training data. In the research results reported above, most PIML models are supervised machine learning models, which rely on high-quality training data to improve the results of their models. However, in structural systems, high-quality observational data may be difficult to obtain, especially in the design and analysis stage of the structure. Theoretically, the PINNs framework has been proven to accurately solve nonlinear governing equations without relying on any labeled data.

This property has not yet been well developed in structural response prediction.

Therefore, using the PIML method to forwardly establish a metamodel of linear/nonlinear structural systems to predict structural response without any observational data is still a promising research area.

### 2.3 PIML for structural health monitoring

With the popularity of various sensors applied to structures, data for structural health monitoring has become increasingly abundant, which provides a natural way for researchers to turn to the development of data-driven models. In fact, in the field of structural health monitoring, the use of data-driven methods such as machine learning models to explore the potential information in monitoring data has become very popular. Some early publications on the overview of machine learning models for structural health monitoring can be found in (Bao & Li, 2021; Worden & Manson, 2007; Yuan et al., 2020). Among these machine learning models, neural networks (Dadras Eslamlou & Huang, 2022), Gaussian processes (Teimouri et al., 2017), and support vector machines (Çevik et al., 2015; Zhou et al., 2021) have been widely used in solving classification and regression problems in structural diagnosis. These methods can directly learn the complex underlying relationships with structural damage from data, without the need for theoretical analysis of these structural systems. However, these methods are well-known 'black box' models, which reflect that their internal principles are unknowable, and their prediction results do not have clear physical meanings.

In addition, 'white' box models, which are completely built on known physical

laws, are also used to detect the damaged state of structures. In white-box modeling, the mechanical characteristics of a structure are simulated by building an abstract model of the structure (Gharehbaghi et al., 2022). Essentially, the actual structure is replaced by an idealized model that connects the input and output of the structure. Researchers have developed many methods for modeling, such as the finite element method (Haidarpour & Kong, 2020), the finite difference method (Lin & Yuan, 2005) and the spectral method (Kudela et al., 2020). The most typical application is to detect damage by updating the finite element model (Alkayem et al., 2018). During this process, the parameters and properties of the model are iteratively adjusted to simulate the damage on the structure. By using optimization methods to minimize the output of the model and the measured response of the structure, the model can be adjusted to be close to the actual state of the structure to detect the damage of the structure. Finite element model updating is a mature method that has been developed for many years. Some representative studies can be found in (Cheng et al., 2018; Giagopoulos et al., 2019; Schommer et al., 2017). However, there are some difficulties in deriving the damage of structures from the perspective of a 'white box,' i.e., from the perspective of motion equations and constitutive relations. The first is the input of the structure, i.e., the external force, which is difficult to measure accurately in actual engineering (Prawin & Rao, 2018). For example, for a high-rise building in operation, wind loads, machine operation, and human-caused loads affect its structural response all the time. Accurately measuring these extensive and chaotic loads is an impossible task. Another limitation

of physical models is the immeasurability of structural parameters and structural properties. Physical models are usually based on some assumptions, such as structural linearization and mass concentration, which are usually inconsistent with the nonlinearity and complexity of the actual structure. In addition, the parameters of the structure, which deeply affect the mechanical characteristics of the structure, may also change with time and external forces.

In recent years, some research on physics-based machine learning methods has been conducted to solve some problems in structural health monitoring. The goal of these studies is to combine the flexibility and power of state-of-the-art machine learning techniques with more structured and insightful physical models based on expertise in structural mechanics. These methods that share physics-based components and data-driven components are called gray-box models. Although the gray-box model is a long-standing method in the field of structural health monitoring, its early concept is called a hybrid model. After PIML was proposed, as a framework that seamlessly combines the prior physical laws described by the governing equations and various advanced machine learning algorithms, it immediately received widespread attention in the field of structural health monitoring.

Data acquisition of structural response observations is usually the first step in SHM. PIML has been applied in the acquisition and analysis of response data, especially for compressed sensing and data reconstruction. Compressed sensing and data reconstruction are advanced techniques that are usually used to reconstruct and

recover the original signal using a small amount of measured data. In (Russell & Wang, 2022), a novel compressed sensing scheme is proposed to integrate SHM domain knowledge such as frequency and mode by combining deep convolutional autoencoders (DCAE) with the physical information of local structure. In addition, fault division autoencoder multiplexing (FDAM) is proposed to mitigate the negative impact of multiple disjoint operating conditions on reconstruction fidelity. The results in two case studies show that physics-based DCAE compression shows superiority over popular data compression methods such as compressed sensing, principal component analysis (PCA), discrete cosine transform (DCT), and DCAE with standard loss functions. FDAM is shown to further improve the data reconstruction quality. Another technique to reconstruct the global responses of structures from local measurements is presented in (Lai et al., 2020). Here, a novel framework called physically informed sparse identification is proposed for full-field structural vibration tracking and analysis. The framework exploits sparse identification to assimilate the underlying structural dynamics in the assembly of a library matrix for characterizing the dynamics of the system. The global vibration of the structure can be approximated by a continuously expressed analytical function in a full-field manner, rather than being measured point by point as with conventional sensors.

In actual engineering, the external loads on a structural system are usually difficult to measure accurately. This is a more feasible path to inversely reconstruct the external loads on the structure by measuring the vibration response of the structure with some

reconstruction algorithms. The application of PIML in structural load reconstruction has also been studied. In (Liu et al., 2024), a PINNs framework was proposed to integrate the underlying modal transformation equations into the loss function of a fully connected neural network, which can effectively invert the uncertain modal responses. This method can use the predicted modal displacement/acceleration responses to identify modal loads, showing the advantages of low data requirements and high prediction performance. (M. Zhang et al., 2024) proposed a novel physically-informed deep learning (PIDL) framework, which consists of a data-driven convolutional neural network for structural excitation identification and a physically-informed variational autoencoder for explicit time-domain (ETD) vibration analysis, where the unit impulse response (UIR) signal of the measured structure is generated. This framework successfully combines a deep generative network with structural dynamics knowledge and is demonstrated in accurately identifying external excitation signals and underlying physical parameters under different damage modes. A case study of using the PIML method to identify external forces in actual engineering is presented in (Guo & Fang, 2024). In this study, the working mechanism of the autoencoder is first combined with the unique characteristics of the FRF to give a cross-signature assurance criterion. This criterion is then integrated into the loss function of PIML as a constraint to address the poor interpretability of pure data-driven methods in solving engineering problems. Following this paradigm, a physical information autoencoder (PIAE) network is used to reduce the dimensionality of FRF data when extracting key features. The reducedorder FRF data is paired with cable forces to form training samples, and the PIAE network is directly trained on these samples for cable force identification. Finally, the proposed method is verified on actual monitoring data of a cable-stayed bridge and a steel tube concrete arch bridge.

There are two main approaches to using PIML for structural damage identification. The first approach to structural damage identification is to directly solve the structural mechanics parameters using an approach similar to solving the inverse problem of partial differential equations. This approach is applied in (Haywood-Alexander & Chatzi, 2024) and (R. Zhang et al., 2024). The former used PINNs as constraint learners for system identification and response prediction. PINNs successfully discover the control parameters of the system by leveraging their applicability to complex boundary conditions, external forces, and governing equations and their ability to learn true data estimates from sparse data. The latter developed a physically informed parallel neural network (PIPNN) framework, which embeds the system's governing PDE and the associated continuity and equilibrium conditions as soft constraints into the neural network loss function. PIPNN learns to approximate the PDE and unknown structural parameters by minimizing the physically informed loss function. In the context of continuous systems, PIPNN successfully estimates the unknown structural parameters, which are then used to estimate the complete state of the system. Such system parameter identification methods can also be applied in complex structural systems with multiphysics damping models. In (Liu & Meidani, 2023), a novel physics-informed neural network method for nonlinear structural system identification, called PIDynNet, is proposed and is demonstrated in multi-physics situations where the damping term is controlled by separate dynamic equations. This method improves the estimation of nonlinear structural system parameters by integrating auxiliary physical loss terms.

The second PIML method for structural damage identification incorporates traditional finite element model updating techniques, which use physical information and observation data to guide the rapid update of the finite element model. A typical attempt is shown in (Zhang & Sun, 2021). Here, physics-guided machine learning is implemented through PINNs, and the original modal attribute-based features are extended with the damage identification results of the finite element model update. A physics-based loss function is designed to evaluate the difference between the output of the neural network model and the output of the finite element model update. The proposed PIML method successfully combines the advantages of physics-guided machine learning with data-driven and physics-based structural health monitoring methods, which can improve damage identification performance.

In terms of specific engineering application cases, PIML frameworks have been developed for damage detection of various structures, including MDOF systems, beams, plates, bearings, and complex nonlinear structures. The typical PIML framework for MDOF systems includes a fully nonlinear spring MDOF damage identification algorithm based on PINNs proposed by (Yamaguchi & Mizutani, 2024). This algorithm was also applied to an engineering case of a bridge pier to quantitatively evaluate

different types of local damage on the pier. Another example of an MDOF system is a direct physical information neural network (DPINN) proposed by (Mai et al., 2023) for analyzing the stability of truss structures.

For beam systems, (Yuan et al., 2020) present the results of dynamic modeling of beam structures using physics-based artificial neural networks. This study addresses the problem of damage identification of beams based on solving the forward and inverse problems of partial differential equations. By comparison, it is found that the proposed physics-informed approach significantly outperforms the purely data-driven approach and avoids overfitting. (Dat et al., 2023) applied PINNs to solve an inverse problem to identify the dynamic structural parameters of a prestressed concrete beam bridge built 40 years ago. The model input data are acceleration data measured by three sensors under vehicle loads in two states (i.e., before and after external prestressing cable reinforcement), combined with the PDE of beam bending and boundary conditions to minimize the loss function. The modal properties obtained from the PDE with the parameters identified by PINN were compared with the modal properties experimentally identified by the eigensystem realization algorithm (ERA) technique. In (Tondo et al., 2023), a physically informed GP model for the Timoshenko beam element is proposed. The model is constructed as a multi-output GP whose covariance and crosscovariance kernels are analytically derived based on differential equations for deflections, rotations, strains, bending moments, shear forces, and applied loads. Stiffness identification is performed in a Bayesian format by maximizing the posterior

model via a Markov chain Monte Carlo method, resulting in a stochastic model of the structural parameters.

For damage detection of plate structures, PIML methods are mainly studied from the perspective of wave propagation. The Kirchhoff–Love plate theory, which describes the physical laws of pressure and displacement in thin-walled plates, is usually integrated into PIML as physical information for damage detection of plate structures. A classic example is presented in (Zhou & Xu, 2024). This study proposes a baselinefree plate structure damage identification method using PINNs. By combining the Kirchhoff-Love plate theory with PINNs, the local anomalies caused by damage in the bending guided wave field of a damaged thin plate can be isolated and enhanced. The implementation of multiple boundary conditions of the Kirchhoff–Love plate is critical to correctly predict the structural response of the plate. How to improve the performance of PINNs in enforcing the boundary conditions of the plate and using sensor data at limited locations to capture the overall physical characteristics of the system is studied in (Al-Adly & Kripakaran, 2024). Another study using PIML to reconstruct the wave field in a plate-like structure is presented in (Zargar & Yuan, 2024). In this study, a physics-based deep learning framework is proposed to reconstruct the complete scattered spatiotemporal Lamb wave field in a plate-like structure from a set of sparse time-series sensor data. This reconstructed scattered wave field contains a wealth of information about the wave propagation phenomena, including any interactions between the propagating waves and structural damage. In addition to wave

fields for detecting structural damage, heat transfer is another research direction to detect damage in plates. This direction was studied in (Kulkarni & Sabato, 2024), by proposing a novel physically-informed variational autoencoder (PI-VAE) network for extending sparse temperature measurements to a full-field representation while detecting damage. The effectiveness of the proposed PI-VAE network was evaluated through analytical and experimental studies on metal plates under thermal excitation with various sizes and types of embedded defects. In an analytical study using finite element model data, PI-VAE accurately extended the full-field temperature distribution and identified the sizes of cracks, spalling, and hole-like defects.

PIML technology has also been used in damage detection of other engineering structures. Two application cases on bearing damage detection were reported in (Shen et al., 2021) and (Ni et al., 2023). In these two studies, physical information was fused with deep CNN and residual networks to automatically extract high-level features related to damage from the observed data of the bearing. These features were fully utilized to predict the health level of the bearing. Concrete structures are also a research object of interest in PIML. (Miele et al., 2023) and (Xu & Noh, 2021) studied damage monitoring of concrete structures from local and global perspectives, respectively. The former used the performance of several PIML models trained with different amounts of low-fidelity and high-fidelity data, which used nonlinear dynamics-based diagnostic techniques to locate hidden cracks in concrete structures. The latter introduced a new framework, namely, the physically informed multi-source domain adversarial network

(PhyMDAN), for transferring models learned from other buildings to diagnose structural damage states in target buildings without any labels. Damage detection of an offshore wind turbine structure was also reported in (Fushun Liu et al., 2023). Here, numerical simulations and field data were exploited to quickly and accurately solve the eigensystem governed by differential equations through recurrent neural networks. The results show that the proposed framework can adaptively identify modal parameters with higher computational efficiency than traditional methods, which can be used for intelligent monitoring and maintenance of engineering structures.

After several years of exploration, the PIML method for structural damage detection has been used in multiple engineering fields as shown above. Some phased summary and review studies have also been published. (Cross et al., 2022) provide an overview of various new approaches to PIML for grey-box modeling in a Bayesian context. The main machine learning tool discussed in this study is Gaussian process regression, and how to incorporate physical assumptions/models via constraints, mean functions, and kernel design, and finally in a state-space setting is stated here. A recent review report is (Wu et al., 2024). This study provides a comprehensive overview of PIML techniques in the context of condition monitoring, with a detailed examination of methods that integrate known physical principles into machine learning frameworks and their applicability to specific monitoring tasks. The unique advantages and limitations of each approach to incorporating physics into data-driven models are also detailed here, taking into account factors such as computational efficiency, model

interpretability, and generalizability to different systems in condition monitoring and fault detection.

In summary, PIML can couple data-driven techniques with a priori high-confidence physical information, which has obvious advantages in dealing with SHM tasks. In various mathematical and engineering problems, PIML methods have demonstrated powerful inverse problem-solving capabilities, which are very suitable for SHM problems such as the inverse discovery of system states from observations. For continuous structures such as beams and plates and nonlinear systems, PIML also shows a promising prospect.

## 2.4 Summary

Due to the limited scope of information search, it is difficult to review all the published research related to PIML. The author can only describe the research on structural response prediction and structural health monitoring of PIML as detailed as possible, from which we can get a glimpse of the current research status. As stated in many published research results, PIML has demonstrated desirable capabilities in various engineering and research problems, especially those involving differential equations. Many proposed PIML frameworks also demonstrate their flexibility to develop targeted PIML frameworks for certain specific tasks.

However, behind these successful cases, there are still some problems that have been found in PIML research that need further study. For structural response prediction, how to solve the spectral bias and hard implementation of boundary conditions in PIML

is still an open question, which will be solved in this study. In addition, how to fully expand the unsupervised learning capabilities of PIML that do not rely on any labeled data in structural response prediction will also be explored in subsequent studies. For the problem of structural health monitoring, the scarcity and imbalance of training data are also constraints on the further application of machine learning methods in this field. Although the damage of nonlinear structures has been explored in some studies, it is still a difficult problem due to its inherent complexity. These issues will be analyzed in the following sections as the focus of this study.

# Chapter 3 Structural dynamics learner framework for dynamic response prediction of structural systems

### 3.1 Introduction

Structural dynamics plays a vital role in modern engineering, especially in the design and maintenance of buildings, bridges, and other infrastructures. Accurately predicting the response of a structure under different dynamic loads not only helps to optimize the design but also effectively improves the safety and durability of the structure. Traditional structural dynamics analysis methods, such as the finite element method (Genikomsou & Polak, 2015) and modal analysis (Peeters & Ventura, 2003), are widely used to predict the dynamic response of structures in many applications, but they are computationally expensive and have limited adaptability to complex nonlinear behaviors. In addition, numerical methods based on numerical integration also face the problem of stiffness (Zhang, 2020) in structural dynamics equations, i.e., when solving the dynamic response of certain structures, the solver relies on very short time steps to maintain the stability of the solution. This not only increases the calculation time but also may lead to high demand for computing resources, limiting the scope of application of these methods in practical applications.

With the rapid development of machine learning, data-driven methods have gradually attracted attention in structural dynamic response prediction. For the task of structural response prediction, popular machine learning methods include Bayesian

models (Gardner et al., 2020), support vector machines (Dong et al., 2008), and deep neural networks (Stoffel et al., 2020). These methods can learn the dynamic behavior of structures from large amounts of data and offer greater flexibility as they do not rely on idealized model assumptions. However, a significant drawback of this type of approach is the reliance on large amounts of labeled data, especially when training deep learning models (Cunha et al., 2023). Obtaining sufficient high-quality labeled data is often time-consuming and costly, which limits the effectiveness and scalability of these methods in some practical applications.

Due to the difficulties faced by the above numerical methods and data-driven methods, an emerging machine learning framework called PINNs (Raissi et al., 2019) has been introduced into the prediction of structural dynamic response. By utilizing known physical information, such as partial differential equations, as prior information to train neural network models, PINNs thus significantly reduce the reliance on large amounts of labeled data in traditional machine learning methods, and the prediction of the model will inherently obey the constraints of the physical governing equations. This outstanding capability has enabled PINNs to find widespread applications across various research and engineering fields, such as in fluid mechanics (E. Z. Rui et al., 2023; E. Z. Rui et al., 2024; Sharma et al., 2023), heat transfer (Cai, Wang, Wang, et al., 2021b; He et al., 2021; Zobeiry & Humfeld, 2021), solid mechanics (Abueidda et al., 2021; Haghighat et al., 2021), structural dynamics (Jeong et al., 2023; Fangyu Liu et al., 2023; Liu & Meidani, 2023; Preetha Hareendran & Alipour, 2022; Tsai & Alipour,

2023) and medical diagnosis (Kissas et al., 2020; Sarabian et al., 2022).

Although PINNs have achieved positive results in many fields, there are still some defects in their practical application in structural dynamics. For example, the spectral bias problem (Farhani et al., 2022; Wang et al., 2021) leads to a decrease in the prediction accuracy of the model at different frequencies, affecting the overall response accuracy. In addition, the 'soft' embedding of constraints (Cao et al., 2023; Lu, Pestourie, et al., 2021a) limits the application of the model under complex boundary conditions and cannot effectively capture the real physical behavior. Finally, the multiloss function balance problem (Bai et al., 2023; E. Z. Rui et al., 2023; Xiang et al., 2022) makes it difficult to optimize multiple objectives simultaneously during training, resulting in the uneven performance of the model on different response characteristics.

To address these issues, this study proposes a novel framework called the structural dynamics learner (SDL) that combines recurrent convolutional neural networks (RCNN) and physical information to accurately predict the dynamic response of structural systems. This framework is not intended to surpass the well-established numerical analysis methods in structural dynamics but rather aims to overcome the limitations of existing PINNs by effectively integrating physical knowledge and advanced machine learning models. This method can also serve as an alternative to solving structural dynamics problems involving stiff equations. Specifically, a recurrent framework is established in SDL to predict the dynamic response sequence of the structural system at discrete time steps. In each recurrent block of the recurrent framework, a CNN model

is employed to predict the structural state at the next step from the current hidden state (displacement and velocity) of the structural system and the external force input. The implicit scheme of the governing equations of structural vibration is integrated as a priori physical information to train the CNN model in each recurrent block. Benefiting from physical information, SDL is an unsupervised learning model that does not rely on any labeled data for training. After 'hard'-embedded constraints, the prediction of the CNN model is output as the predicted dynamic response of the structure.

The main contributions of this study can be summarized as: (1) A novel physicsinformed recurrent convolutional neural network framework is proposed to predict linear/nonlinear structural dynamic responses based on the Crank-Nicolson scheme of motion equations. The key component of this framework is the CNN-based recurrent block, which is designed to capture the nonlinearities in the structural response. (2) The utilization of recurrent blocks gives the SDL framework a memory mechanism, where the CNN model parameters optimized in the previous time step can be used as the initial settings for the next time step. In this way, the convergence speed of the model is greatly improved, allowing the proposed model to fast and accurately infer structural response sequences. (3) The loss function is completely derived from the physical governing equations, thus avoiding the problem of balanced convergence of multiple loss functions. In addition, the model training can be performed without relying on any labeled training data, making the proposed model an unsupervised machine learning model and avoiding expensive data collection and data-induced errors. The loss

function is constructed based on the Crank-Nicolson scheme of the motion equation, which is an implicit numerical integration scheme, thus providing excellent solution stability from a mathematical principle. (4) The embedding of initial and boundary conditions is carefully designed into the framework to ensure that the prediction results of the SDL model rigidly meet the constraints, which also avoids the model prediction error on the constraints. Numerical outcomes demonstrate the superiority of the SDL framework in terms of mathematical rationality and solution stability and accuracy compared to vanilla PINNs solvers.

The rest of the study is organized as follows. Section 2 outlines the problem of structural dynamic response prediction. The details of the proposed SDL framework are demonstrated in Section 3. In Section 4, the effectiveness and advantages of the proposed SDL framework are verified through several numerical cases. Section 5 summarizes the research results and conclusions.

#### 3.2 Problem statement

Consider a d-degree-of-freedom structural system subjected to an external dynamic force F(t). The vibration of the structural system follows the governing equation.

$$M\ddot{u}(t) + C\dot{u}(t) + Ku(t) + f(u, \dot{u}) = F(t)$$
 (3.1)

Here, M is the d-dimensional system mass matrix. C is the system damping matrix and K is the stiffness matrix.  $u, \dot{u}, \ddot{u}$  are the system displacement, velocity, and acceleration vectors, respectively.  $f(u, \dot{u})$  is a nonlinear term, usually representing a nonlinear

restoring force or nonlinear damping, which depends on system displacement u and velocity  $\dot{u}$ . F(t) is the external force acting on the system.

The general task of dynamic response prediction of structural systems is to calculate the structural response  $[u(t), \dot{u}(t), \ddot{u}(t)]$  under various dynamic loads F(t). The structural system can be linear or nonlinear, depending on the existence of the nonlinear term  $f(u, \dot{u})$  in Eq. (3.1). This study is limited to the forward problem of the structural system, i.e., to solve the governing equation in the space-time domain mainly by analyzing the physical dynamics forward under the condition that the system parameters M, C, and K are determined. In this study, the entire domain is discretized while considering mainly the regular physical domains, where the time domain is discretized into uniform time steps and the space domain is discretized into multiple degrees of freedom.

## 3.3 Methodology

In this section, a physics-informed machine learning framework based on RCNN is proposed for learning the governing equations of structural systems in the spatiotemporal domain. Previous studies have shown that CNN models are more convenient and efficient than fully connected neural networks (FCNN) in solving time-dependent differential problems (Qu et al., 2022). The primary goal of this study is not to prove that the proposed model outperforms traditional numerical methods, but rather to offer new perspectives and alternatives for simulating structural systems that balance time efficiency with desirable accuracy. The mathematical concepts, network

architecture, and implementation details of the proposed model are discussed in this section.

## 3.3.1 Crank-Nicolson scheme of motion equation

The Crank-Nicolson method is a finite difference method based on the trapezoidal rule, commonly used to numerically solve the heat equation and partial differential equations (Frei & Singh, 2024; Liu & Hao, 2022). It is a second-order implicit method in time and has proven to be A-stable, which can overcome the effects of equation stiffness and adapt to large time step sizes (Qu & Liang, 2017). For an ordinary differential equation

$$\frac{dy}{dt} = f(t, y) \tag{3.2}$$

The Crank-Nicolson method can discretize this equation in the time domain and recursively solve the equation from the initial value as

$$y_{n+1} = y_n + \frac{\Delta t}{2} \cdot (f(t_n, y_n) + f(t_{n+1}, y_{n+1}))$$
(3.3)

Here, the right side of Eq. (3.3) is also dependent on  $y_{n+1}$ , which shows that the Crank-Nicolson method is implicit where a system of algebraic equations must be solved to obtain the next value  $y_{n+1}$  at each time step. If the ordinary differential equation is nonlinear, the discretized algebraic equation is also nonlinear.

To apply the Crank-Nicolson scheme to the motion equation of Eq. (3.1), a system state z is first defined as  $z = [u, \dot{u}]^T$  in the state space. Then, the motion equation can be written in the form of a first-order differential equation as

$$\dot{z} = K^* \cdot z + B^* \cdot (F(t) - f(z)) = g(t, z, F(t), f(z))$$
(3.4)

where,  $K^* = \begin{bmatrix} 0 & I \\ -M^{-1}K & -M^{-1}C \end{bmatrix}$  and  $B^* = [0, M^{-1}]^T$ . g is a function referring to the entire right terms, which depends on t, z, F(t) and f(z). Using the Crank-Nicolson method in Eq. (3.3), Eq. (3.4) can be discretized as

$$z_{n+1} = z_n + \frac{\Delta t}{2} \cdot \left[ g(t_n, z_n, F(t_n), f(z_n)) + g(t_{n+1}, z_{n+1}, F(t_{n+1}), f(z_{n+1})) \right]$$
(3.5)

Here, the prediction of the system state  $z_{n+1}$  is implicit, which depends not only on the current structural state  $z_n$  and  $F(t_n)$ , but also on the next system state  $z_{n+1}$  and external force  $F(t_{n+1})$  at time step n+1. The comparison between the implicit numerical scheme and the explicit scheme is shown in Fig. 3.1. In explicit scheme methods, such as the Euler forward method and the explicit Runge-Kutta method, the system state  $z_{n+1}$  is predicted using  $z_n$  and  $F(t_n)$  at the current time step with simple forward calculation. In the implicit scheme, the information of  $F(t_{n+1})$  and  $z_{n+1}$  is also required to predict the structural response. In traditional implicit numerical methods, iterative calculations are relied upon to make the value of  $z_{n+1}$  converge to the exact value. In this study, machine learning architecture is employed to predict  $z_{n+1}$ . The details of the architecture will be described in the next section.

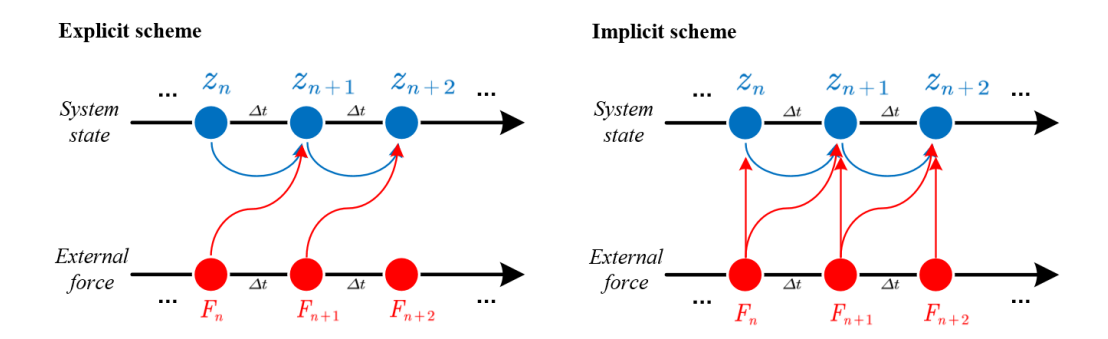


Figure 3.1 The comparison between the explicit scheme and implicit scheme

## 3.3.2 Neural network architecture of SDL

In this section, the architecture of the proposed SDL framework is outlined. From the perspective of architectural form, SDL is a type of recurrent neural network, which is composed of a series of CNNs based on a recurrent architecture. The architecture diagram is shown in Fig. 3.2, which demonstrates that the SDL framework is composed of a series of recurrent blocks. The overall input of the SDL framework is the initial system state  $z_0$  and the external force series F(t), and outputs the system state series Z(t) of time steps.

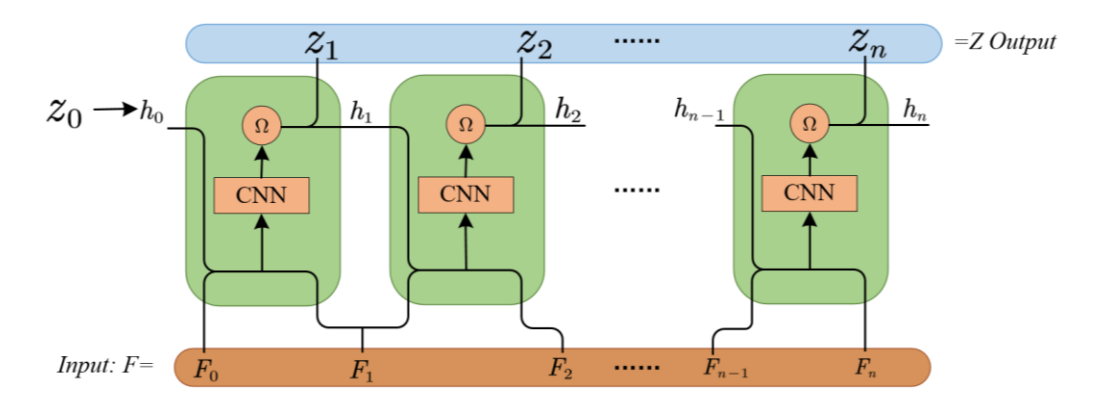


Figure 3.2 Neural network architecture of the SDL framework.

As shown in Fig. 3.2, at each time step, a recurrent block is built to update the hidden state h and predict the structural response z. The hidden state h is defined as  $h = [u, \dot{u}]^T$ , which is employed to pass the system state information to the next recurrent block. The first recurrent block takes hidden state  $h_0$  set to the initial system state  $h_0$  and the external force  $h_0$ ,  $h_0$  as input to infer new hidden states  $h_0$  and output the predicted system state  $h_0$  as input to infer new hidden states  $h_0$  and output the predicted system state  $h_0$  as input to infer new hidden states  $h_0$  and output the predicted system state  $h_0$  as input to infer new hidden states  $h_0$  and output the predicted system state  $h_0$  as input to infer new hidden states  $h_0$  and output the predicted system state  $h_0$  as input to infer new hidden states  $h_0$  and output the predicted system state  $h_0$  as input to infer new hidden states  $h_0$  and output the predicted system state  $h_0$  as input to infer new hidden states  $h_0$  and output the predicted system state  $h_0$  as input to infer new hidden states  $h_0$  and output the predicted system state  $h_0$  as input to infer new hidden states  $h_0$  and output the predicted system state  $h_0$  as input to infer new hidden states  $h_0$  and  $h_0$  are  $h_0$  are  $h_0$  are  $h_0$  and  $h_0$  are  $h_0$  are  $h_0$  and  $h_0$  are  $h_0$  are  $h_0$  are  $h_0$  and  $h_0$  are  $h_0$  are  $h_0$  are  $h_0$  and  $h_0$  are  $h_0$  are  $h_0$  are  $h_0$  are  $h_0$  are  $h_0$  and  $h_0$  are  $h_0$  are  $h_0$  are  $h_0$  are  $h_0$  and  $h_0$  are  $h_0$ 

external force  $(F_{n-1}, F_n)$  as the recurrent block input. The outputs of all N recurrent blocks are combined into the system state time series  $Z = [z_0, z_1, z_2, \cdots, z_N]$  as the output of the entire SDL model.

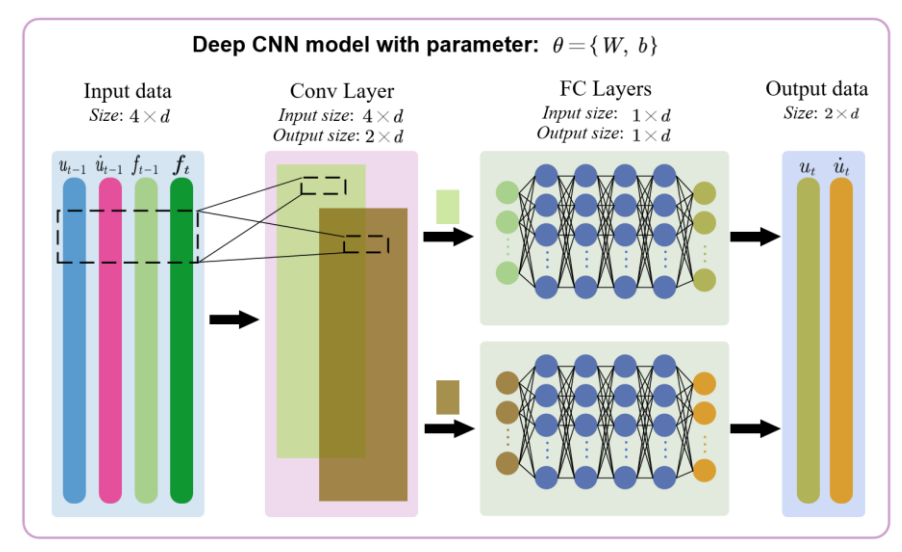


Figure 3.3 The CNN model in SDL framework

In each recurrent block, a CNN model as shown in Fig. 3.3 is utilized to update the hidden state. The input of the model is  $[u_{n-1}, \dot{u}_{n-1}, F_{n-1}, F_n]^T$  with a size of (4, d). After normalization by the hyperbolic tangent function, a convolution layer is utilized to perform convolution calculations on the input data. There are two convolution kernels in the convolution layer to reduce the input 4-dimensional data to two dimensions. The size of the convolution kernels is  $3 \times 3$ , the stride and padding are one. These two convolution kernels are used to extract the feature information related to the structural response u and  $\dot{u}$  respectively. Then, the extracted features of the two convolution kernels are passed into an FCNN model separately. FCNN models have L hidden layers, each containing H neurons. The hyperbolic tangent function

serves as the activation function to provide a nonlinear representation ability. The input and output sizes of the FCNN models are both (1,d). Then, the outputs from FCNN models are merged into an output  $O_{CNN}$  of size (2,d), which is also the output of the whole CNN model. The trainable parameters of the CNN model include the weights and biases of the convolutional layer and the fully connected layers. The model hyperparameters include the number of fully connected hidden layers L and the number of neurons H. Here, the pooling layer in the traditional CNN model is not used as the pooling operation can filter out the feature information of some degrees of freedom in the input data.

In order to make the output of the CNN model rigidly meet the boundary condition constraints, a 'hard' embedding operation  $\Omega$  of the boundary conditions is performed on the CNN model output  $O_{CNN}$ . For multi-DOF systems, boundary conditions are usually imposed by setting u or  $\dot{u}$  to specific values, for example, u and  $\dot{u}$  of nodes on the fixed boundary are constrained to zero. To achieve such a 'hard' embedding of boundary conditions, the output  $O_{CNN}$  of the CNN model is processed as

$$h^{pred} = M_k \circ O_{CNN} + V \tag{3.6}$$

Here,  $h^{pred}$  is the predicted hidden state of the recurrent block, and  $M_k$  is a Boolean mask matrix of size (2,d). The  $M_k$  matrix controls where the  $O_{CNN}$  matrix is constrained by setting the values of the constrained positions are zero and unconstrained positions are one. Operator  $\circ$  is the Hadamard product which returns a matrix of the

multiplied corresponding elements. V is a value matrix of size (2,d), where the values of the unconstrained positions are zero, and the values of the constrained positions are set according to the boundary conditions. In this way, the predicted hidden state  $h^{pred}$  is forced to rigidly couple the boundary conditions.

## 3.3.3 Loss function and model training

To train the SDL model, a loss function needs to be constructed to update the weights and biases in the CNN model. Different from traditional supervised learning, which relies on labeled data of input-output pairs to train the model, inspired by PINNs, an unsupervised model training that integrates physical information as prior information is utilized in this study. According to the Crank-Nicolson scheme of motion equation in Eq. (3.5), a loss function of the *n*-th recurrent block is constructed as

$$loss_n = ||res_n||_2^2 \tag{3.7}$$

$$res_{n} = h_{n}^{pred} - h_{n-1} - \frac{\Delta t}{2} \cdot \left[ g(t_{n-1}, h_{n-1}, F_{n-1}, f(h_{n-1})) + g(t_{n}, h_{n}^{pred}, F_{n}, f(h_{n}^{pred})) \right]$$
(3.8)

Here, the output  $h_n^{pred}$  of the n-th recurrent block is combined with the input of the recurrent block to construct the loss function  $loss_n$ . By minimizing  $loss_n$ , the residual of Eq. (3.5) can be gradually reduced, so that the hidden state  $h_n^{pred}$  can approximate the true structural response. Although in the SDL framework, all recurrent blocks can be trained together like traditional RNN models, it will make model training prone to gradient explosion and gradient vanishing (Ribeiro et al., 2020). In addition, as the number of time steps increases, the complexity and time consumption of model training will also significantly increase, thereby increasing the difficulty of model convergence.

Actually, the loss function  $loss_n$  described in Eq. (3.7) has the advantage in that the loss function of the previous recurrent block is independent of subsequent output. To take advantage of this, the SDL framework adopts a sequential training technique, i.e., training recurrent blocks in sequence according to the time steps. Specifically, starting from the first recurrent block, a gradient descent-based optimizer, such as Adam (Kingma, 2014), is employed to minimize  $loss_1$  until the relative error  $\epsilon$  converges to the defined error tolerance  $\epsilon_{tol}$ . The relative error  $\epsilon$  is defined as

$$\epsilon = \frac{\sqrt{\|res_n\|_2^2}}{\sqrt{\|h_n^{pred}\|_2^2}} \tag{3.9}$$

The error tolerance  $\epsilon_{tol}$  is a commonly used convergence criterion in implicit methods, and the value set is studied in (González--Pinto et al., 2004). In the n-th time step, the optimized CNN model parameters in the previous time step are inherited to initialize the CNN model, and the optimizer is employed again to minimize  $loss_n$ . This inheritance and training process is repeated until all N-time steps are completed. At each time step, the converged  $h^{pred}$  will be output as the predicted structural dynamic response  $z^{pred}$ .

The sequential training technique has another advantage in that it retains the characteristic of the recurrent architecture in capturing short-term dependencies of sequence data. This advantage can be fully utilized in structural response prediction because the structural responses at adjacent time steps are always evolutionarily similar. In the SDL framework, the CNN network of the next recurrent block is initialized with

the optimized CNN model parameters in the previous recurrent block, namely the memory mechanism. In this way, the CNN model is initialized on the memory of the previous recurrent block instead of random initialization, which can greatly accelerate the convergence process of the CNN model.

The SDL framework relies on iterative training to converge the loss function to the error tolerance, which means that it is impossible to have an efficiency advantage over explicit numerical methods such as the Euler forward method and explicit Runge-Kutta method. However, the integration of implicit physical information can bring excellent stability, as the Crank-Nicolson scheme has been proven to be unconditionally stable (Qu & Liang, 2017). This feature is very powerful in structural dynamics problems, which always involve stiff equations. In contrast, traditional explicit numerical methods rely on extremely short step sizes to keep the solution stable and convergent in stiff equations.

Due to the adaptability of the Crank-Nicolson scheme to nonlinear equations, it is convenient to implement the SDL model to solve nonlinear dynamic systems involving nonlinear stiffness and damping. Adaptability to nonlinear partial differential equations is also an inherent advantage of the PINNs methods. However, the SDL framework also breaks through several obstacles that hinder the implementation of PINNs in structural response prediction. The first is the spectral bias in the neural network, which is manifested by the phenomenon that the neural network model tends to prioritize the low-frequency components in the data and ignore the high-frequency components. This

shortcoming becomes more serious in the structural response prediction because structural responses often consist of multiple components with frequencies spanning a wide range. However, this obstacle is overcome in the SDL framework by predicting the structural response in the time domain step by step to avoid using a single model to represent the information of the entire time domain. The 'soft' embedding of constraints is also a well-known defect of the PINNs framework. In the prediction of structural response, constraints including initial conditions and boundary conditions are vital prior information to ensure the uniqueness of the structural response. The residual on the constraints also brings additional errors to the prediction results of the structural response. In the SDL framework, by directly inputting the initial state to the first recurrent block and 'hard' embedding of the boundary conditions through Eq. (3.6), the constraints are hard embedded without residual, thereby eliminating this constraint error. Another benefit of the 'hard' embedding of constraints is to avoid the problem of balancing multiple loss functions in PINNs. In PINNs, initial conditions, boundary conditions, and governing equations are 'soft' embedded through defined loss functions, and these loss functions are summed as the total loss function. However, research results show that in PINNs, it is difficult to maintain balanced convergence of multiple loss functions, which is still an unresolved issue in the field of PINNs (Wang et al., 2022; Xiang et al., 2022). In the SDL framework, since the constraints are 'hard'embedded, there is only a governing equation residual in the loss function, which fundamentally avoids the instability caused by the competition of multiple loss

functions.

It is also noted that combining CNN, RNN, or numerical methods such as the Runge-Kutta method with PINNs is not innovative. The most well-known include PhyCNN (R. Zhang et al., 2020a) and PI-LSTM (Fangyu Liu et al., 2023) for predicting the seismic response of structures. However, these models are supervised learning that relies on structural response observation for training, and physical information only plays an auxiliary role in improving the robustness and generalization ability of the model. This study does not intend to show the advantages of the SDL framework over these methods but provides an unsupervised learning method that does not require any training data to accurately predict the structural response.

## 3.3.4 Algorithm and computing platform

The overall implementation process of SDL framework is shown in Algorithm 3.1.

**Algorithm 3.1.** The implementation of SDL framework

**Input:** Mass matrix M, stiffness matrix K, damping matrix C, nonlinear function  $f(u, \dot{u})$ , mask matrix  $M_k$ , value matrix V, initial state  $z_0$ , force series F(t), number of time steps N, time step size dt

**Parameter:** Learning rate  $l_r$ , error tolerance  $\epsilon_{tol}$ , CNN model hyperparameters L and H

Output: Structural system state series Z

- 1: Initialize hidden state  $h_0 = z_0$ , system state list  $Z[0] = z_0$ , relative error  $\epsilon = 1.0$ , randomly initialize CNN model
- 2: **for** i = 1 to N **do**
- 3: Calculate  $t_{i-1} = (i-1) * dt$ ,  $t_i = i * dt$
- 4: Get external force  $F_{i-1} = F(t_{i-1})$ ,  $F_i = F(t_i)$
- 5: Concatenate CNN model input  $x_i = [h_{i-1}, F_{i-1}, F_i]$
- 6: **while**  $\epsilon > \epsilon_{tol}$  **do**
- 7: Forward propagation  $O_{CNN} = CNN(x_i)$

- 8: Predict hidden state  $h_i^{pred} = M_k \circ O_{CNN} + V$  with boundary conditions
- 9: Update the CNN model by the optimizer with learning rate =  $l_r$
- 10: Update the relative error  $\epsilon$
- 11: end while
- 12: Predict the structural response  $z_i^{pred} = h_i^{pred}$ , set  $Z[i] = z_i^{pred}$
- 13: Update  $h_{i-1} = h_i^{pred}$ , reset relative error  $\epsilon = 1.0$
- 14: **end for**

All codes in this study are compiled in Python 3.8. The neural network framework is based on PyTorch (Paszke et al., 2019), a mature deep learning library. All codes are run on the Windows platform with an Intel Core i7-10700 CPU and an NVIDIA GeForce RTX 3080 Ti GPU.

#### 3.4 Numerical validation

In this section, several numerical examples are carried out to demonstrate the effectiveness and accuracy of the SDL method. First, a two-degree-of-freedom system example involving a stiff equation is calculated to demonstrate the stability of the SDL method. Then, the SDL method is employed to predict the seismic response of a 4-story frame structure involving nonlinear stiffness. The hyperparameter settings of the SDL method are discussed in this example. The improvement of the efficiency of the recurrent architecture is also demonstrated here. The third example involving nonlinear Bouc-Wen hysteretic models is conducted to demonstrate the applicability of SDL to nonlinear hysteretic systems. How to integrate the unobservable variables of the nonlinear hysteretic model into the hidden states of the SDL method is also explained in this example. Finally, a plane truss example is utilized to demonstrate the 'hard'

embedding of boundary conditions in the SDL framework.

## **3.4.1 2-DOF system**

A linear two-degree-of-freedom system (2-DOF) as shown in Fig. 3.4 is first studied. The masses of the two degrees of freedom are set to  $M_1 = 3.0 \, kg$ ,  $M_2 = 2.0 \, kg$ . The spring stiffness is  $k_1 = 10 N/m$ ,  $k_2 = 10 N/m$ ,  $k_3 = 3000 N/m$ . The damping coefficients are  $c_1 = 0.1 N/(m/s)$ ,  $c_2 = 0 N/(m/s)$ ,  $c_3 = 3.0 N/(m/s)$ . The exact response of this system under harmonic force can be obtained by the modal decomposition method (Paz & Kim, 2018).

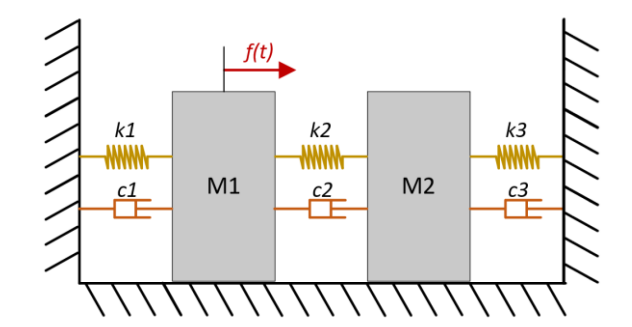


Figure 3.4 A linear two-degree-of-freedom system

According to Eq. (3.4), a first-order differential equation describing the motion of this 2-DOF system is built as

$$\dot{z} = K^* \cdot z + B^* \cdot F(t) \tag{3.10}$$

The four eigenvalues  $\lambda$  of  $K^*$  are calculated as [-0.0167 + 2.58j, -0.0167 - 2.58j, -0.750 + 38.8j, -0.750 - 38.8j]. According to the stiff equation criterion in (Spijker, 1996), the  $K^*$  matrix's  $\frac{\max|Real(\lambda)|}{\min|Real(\lambda)|} = 44.9 \gg 1$ , the differential equation for this 2-DOF system is stiff.

To demonstrate the stability of our proposed method for stiff systems, an SDL model is built to first analyze the free vibration of this system with large time steps. The external force of this system is first set to 0 and the initial displacement is [0.1, 0]. The exact structural dynamic response obtained by the modal decomposition method can serve as the benchmark solution, with a time step of  $0.01 \, s$  and a calculation duration of 1s. The Euler forward method and the fourth-order explicit Runge–Kutta (ERK4) method (Iserles, 2008) are also employed to calculate the numerical solution for comparison. The time step size of these numerical methods is  $0.1 \, s$ . The SDL models with a time step size of  $0.1 \, s$  and  $0.5 \, s$  are tested separately. The hyperparameters of the CNN model are set as L=1 and H=100. The optimizer Adam is employed to train the SDL model with a learning rate  $l_r=0.001$ . The error tolerance  $\epsilon_{tol}$  of the convergence criterion is set as 1e-4. The calculated results of the displacement response of  $M_1$  are compared in Fig. 3.5.

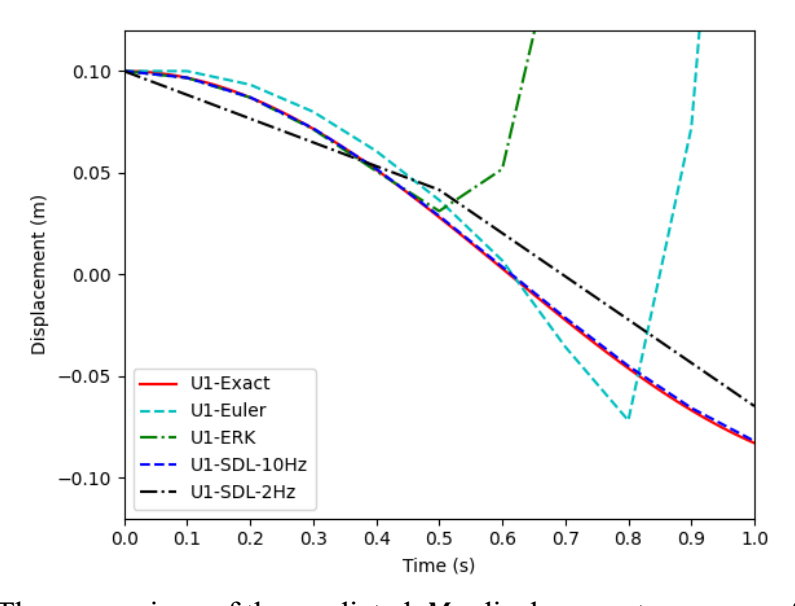


Figure 3.5 The comparison of the predicted  $M_1$  displacement response of the 2-DOF

Fig. 3.5 shows that the SDL model can obtain stable converged solutions at both  $0.1 \, s$  and  $0.5 \, s$  time step sizes. Affected by the error caused by the large step size, the error of the result predicted by the SDL model with a  $0.5 \, s$  time step is larger than the SDL model with a  $0.1 \, s$  time step. The result predicted from the SDL model with a  $0.1 \, s$  time step is highly consistent with the exact solution. The explicit numerical methods including Euler forward and ERK4 methods cannot maintain solution stability at a time step  $dt = 0.1 \, s$ . This case demonstrates that based on the Crank-Nicolson scheme, the SDL method shows outstanding stability for stiff systems.

A forced vibration case of this 2-DOF system is analyzed in order to verify the accuracy of the SDL model in predicting the structural response under external force. An external force  $F(t) = 500 \cdot sin(\pi/2 \cdot t)$  is applied to  $M_1$  to make the system vibrate from rest. The benchmark solution is the exact system response obtained by the modal decomposition method, with a time step of 0.01 s and a duration of 1 s. The time step of the Euler forward method and ERK4 method is reduced to 0.01 s to improve the solution stability. The time step of the SDL model is also set as 0.01 s, and the other parameters of the SDL model are set as the same as the free vibration case. The comparison of predicted displacement responses of  $M_1$  with the SDL model and numerical methods is shown in Fig. 3.6.

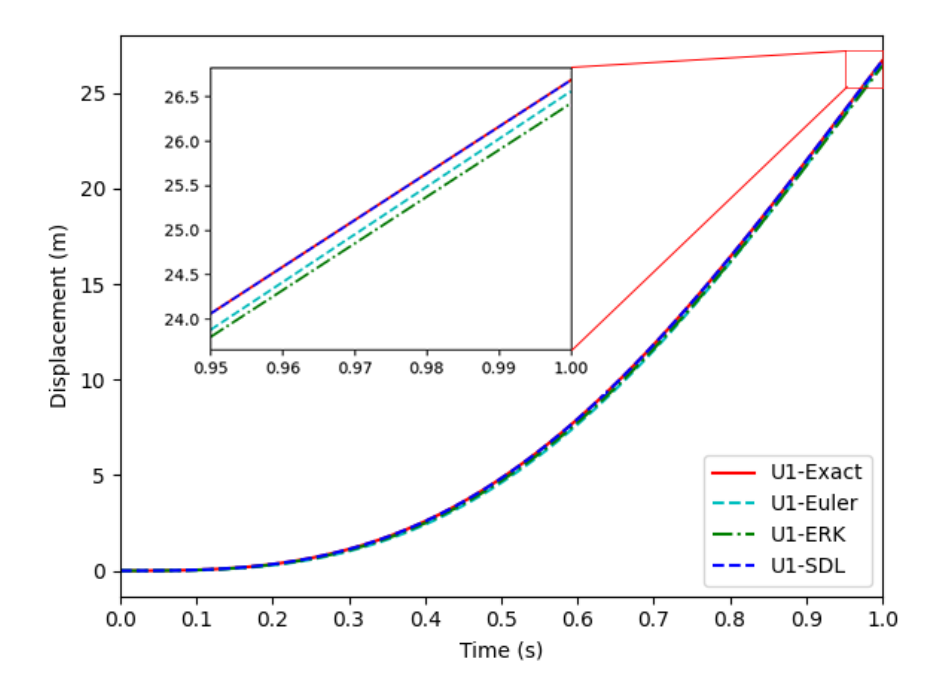


Figure 3.6 The comparison of displacement response prediction of  $M_1$  with SDL model and numerical methods

The results of Fig. 3.6 show that the SDL model successfully predicts the displacement response of  $M_1$ , which shows high consistency with the exact solution. To quantify the error with the benchmark solution, the relative L2 error is calculated as

$$Relative L2 = \frac{\sqrt{\|u^{pred} - u^{exact}\|_{2}^{2}}}{\sqrt{\|u^{exact}\|_{2}^{2}}}$$
(3.11)

According to the calculation results, the relative L2 error in the predicted displacement response  $u_1^{pred}$  of the SDL model is 0.00506%, while the relative L2 errors of the Euler forward method and ERK4 method are 1.74% and 1.42%, respectively. In this case, the SDL method shows significantly higher accuracy than these two explicit numerical methods.

## 3.4.2 Five-story shear structure

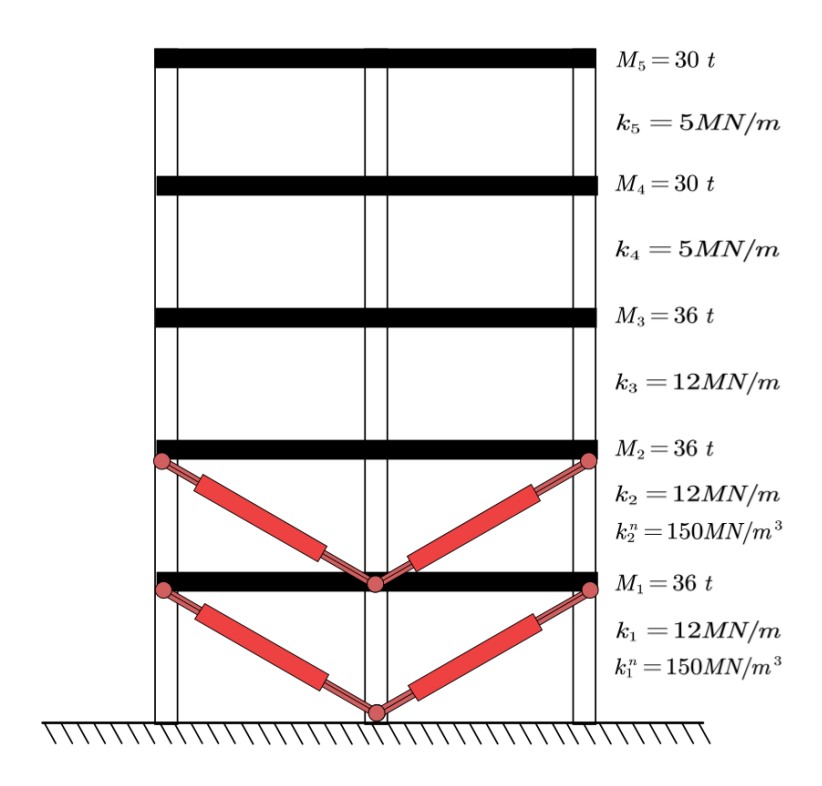


Figure 3.7 A 5-story structure with nonlinear stiffness springs

The seismic response of a 5-story structure with nonlinear stiffness springs as shown in Fig. 3.7 is analyzed with the SDL method. The inter-story stiffnesses and masses are also given in Fig. 3.7. The damping of the structure is set to give a damping ratio of 1% for the first and second natural frequencies. Cubic stiffness springs  $k_1^n$  and  $k_2^n$  act on the first and second layers. Then the governing equation of the structure vibration can be written as

$$M\ddot{u}(t) + C\dot{u}(t) + Ku(t) + K^n \cdot u(t)^3 = M\ddot{u}_g(t)$$
 (3.12)

Here,  $K^n$  is the cubic stiffness matrix and  $\ddot{u}_g(t)$  is the ground seismic acceleration. This 5-story structure vibrates under the seismic acceleration excitation of EI Centro (N-S) shown in Fig. 3.8. The sampling frequency of seismic acceleration is 50 Hz.

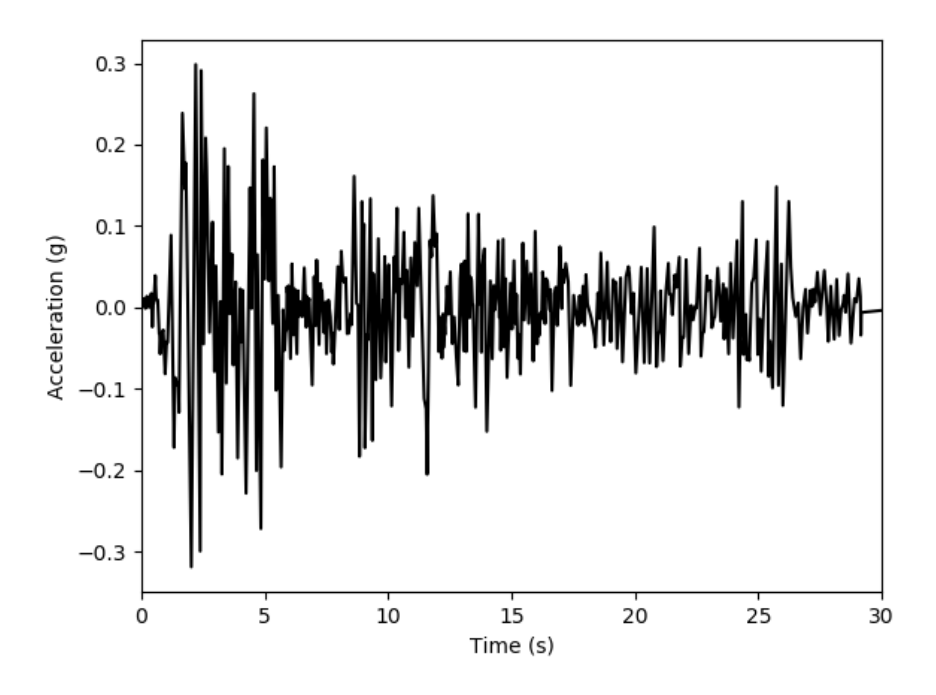


Figure 3.8 The seismic acceleration excitation of EI Centro (N-S)

The ERK4 method with a time step of 0.001 s is employed to solve the vibration response  $z = [u, \dot{u}]$  of the structure as the benchmark solution, which is shown in Fig. 3.9. The total computation duration is 5 s. Since the explicit method does not require iterative convergence, a small time step is adopted to ensure the accuracy of the solution. In this case, the hyperparameters of the SDL model including the number of hidden layers L and the number of neurons H in the CNN model are first tested. Specifically, 20 CNN model schemes as shown in Table 3.1 are tested to calculate the seismic response of the structure respectively. The time step of the SDL model is set to 0.01 s. An Adam optimizer with a learning rate of 0.001 is employed to train the SDL model until the relative error  $\epsilon$  converges to the error tolerance  $\epsilon_{tol}$  of 1e-4. The relative L2

error of the structural responses predicted by all CNN model schemes to the benchmark solution is calculated as the criterion of model accuracy and the model training time is also recorded to evaluate the training efficiency. The results of model accuracy and training time are shown in Table 3.1.

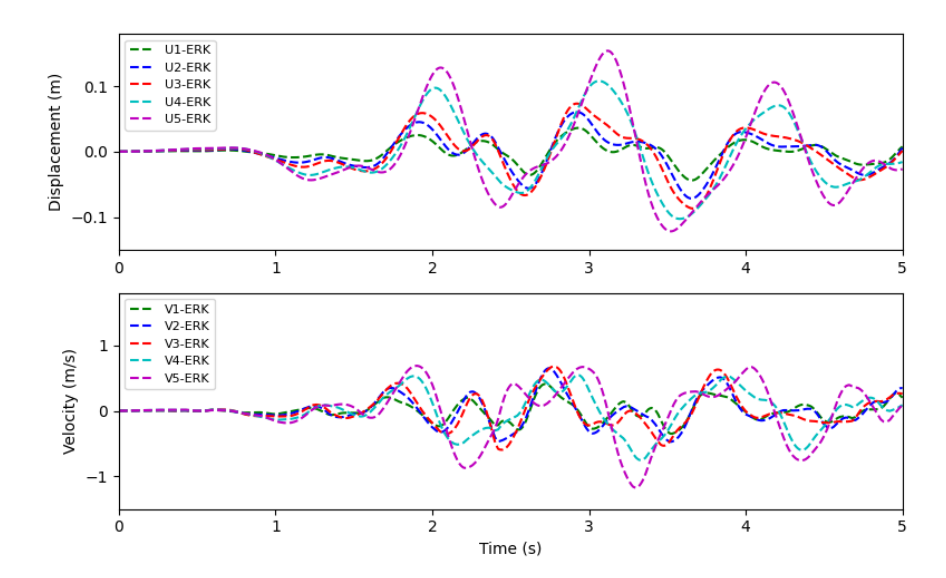


Figure 3.9 The benchmark solution of the seismic response of the 5-story structure

Table 3.1 The comparison of relative L2 error (a) and computation time (b) of different CNN model schemes

(a)						
	H\L	1	2	4	8	Avg
	10	4.36%	4.41%	4.24%	4.37%	4.35%
	20	4.29%	4.24%	4.10%	4.49%	4.28%
	40	4.19%	4.24%	4.23%	4.33%	4.25%
	80	4.27%	4.48%	4.10%	4.11%	4.24%
	100	4.34%	4.35%	4.22%	4.16%	4.27%
	Avg	4.29%	4.34%	4.18%	4.29%	

(b) 2 4 8 H\L 1 Avg 299.91 389.22 633.46 **10** 338.51 415.27 20 270.30 283.81 411.03 682.79 411.98 40 279.84 345.71 397.29 648.81 417.91 80 247.14 300.23 383.58 387.44 618.81 **100** 268.27 312.13 374.83 389.78 603.89 308.36 391.19 Avg 280.81 637.55

Unit: second

The results in Table 3.1(a) show that the SDL model of all CNN schemes accurately predicts the seismic response of the structure, with the largest relative L2 error of 4.49% and the smallest of 4.10%. It is also observed that the accuracy of the prediction results with different CNN hyperparameters has no significant difference. This means that the accuracy of the prediction results of the proposed SDL model with error tolerance  $\epsilon_{tol}$  as the convergence criterion is not sensitive to the hyperparameters L and H settings. The results of calculating time in Table 3.1(b) indicate that as the number of fully connected layers L increases, the training time of the SDL model also increases significantly. But increasing the width of the hidden layer H has no significant impact on the model efficiency and can slightly improve the accuracy of the solution. Therefore a 'shallow' but the 'wide' FCNN model is a better setting for the SDL method.

Here, the PINNs method proposed in (Raissi et al., 2019) is also employed to predict the structural response for comparison. Specifically, in PINNs, an FCNN with two inputs (t, x) is employed to predict the displacement response u(t, x) of the structure. Here t is the time domain of the equation, ranging from 0 - 5 s. x is the number of the system's degrees of freedom, ranging from 1 - 5. The number of hidden layers L of the neural network model is set to 4, and the number of neurons H is 100. The hyperbolic tangent function is utilized as the activation function of the neural network. Using the governing equation of Eq. (3.12), the loss function of PINNs is

constructed as

$$Loss_{pinn} = Loss_i + Loss_f (3.13)$$

where

$$Loss_{i} = \frac{1}{N_{i}} \sum_{i=1}^{N_{i}} \left| u_{i}^{pred}(0, x_{i}) - u_{i}'(0, x_{i}) \right|^{2} + \frac{1}{N_{i}} \sum_{i=1}^{N_{i}} \left| \dot{u}_{i}^{pred}(0, x_{i}) - \dot{u}_{i}'(0, x_{i}) \right|^{2}$$
(3.14)

and

$$Loss_f = \frac{1}{N_f} \sum_{i=1}^{N_f} \left| M \ddot{u}_i^{pred} + C \dot{u}_i^{pred} + K u_i^{pred} + K^n \cdot u_i^{pred^3} - M \ddot{u}_g \right|^2$$
(3.15)

Here,  $Loss_i$  is the loss function of the initial constraint condition.  $N_i = 5$  is the number of sampling points  $(0, x_i)$  sampled on the initial condition of the structural system, where  $x_i$  is 1-5. u' and  $\dot{u}'$  are the initial displacement and initial velocity of the structure, respectively. Loss function  $Loss_f$  is defined to constrain the satisfaction of the structural governing equation. Here the  $N_f$  collocation points are fully sampled on all 5 degrees of freedom with a time step of  $0.01 \, s$ , totaling 2505 points. The Adam optimizer with  $l_r = 0.001$  is employed to minimize the total loss  $Loss_{pinn}$ . The loss function  $Loss_{pinn}$  converges after 100,000 training iterations. The structural displacements and velocities of  $M_1$  and  $M_5$  predicted by the SDL model and PINNs method are shown in Fig. 3.10 as examples and compared with benchmark solutions.

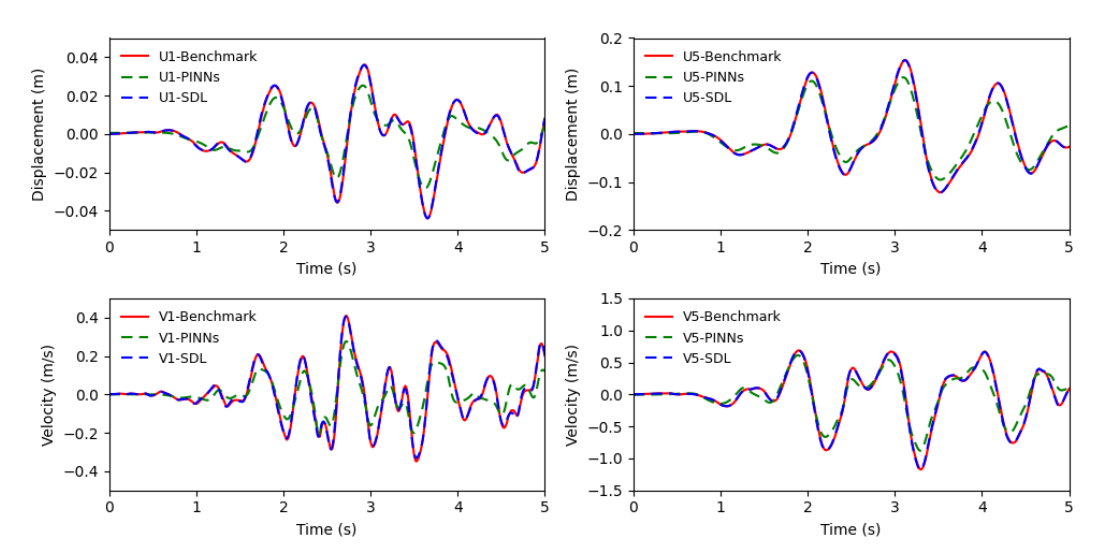


Figure 3.10 The comparison of structural displacements and velocities of  $M_1$  and  $M_5$  predicted by the SDL model and PINNs method.

Fig. 3.10 shows that the results of the SDL model are consistent with the benchmark solution, while the results of PINNs have obvious errors. The relative L2 error of the predicted displacement and velocity responses for all degrees of freedom is calculated to quantify the accuracy of the SDL and PINNs results. The calculated relative L2 error of the SDL is 4.34%, while that of the PINNs is 36.08%. This indicates that SDL can achieve more accurate structural response predictions than the PINNs method in this case. To compare the frequency distributions, the Fourier transform is performed on the structural displacements and velocities of  $M_1$  and  $M_5$  shown in Fig. 3.10, and the frequency distribution results are shown in Fig. 3.11.

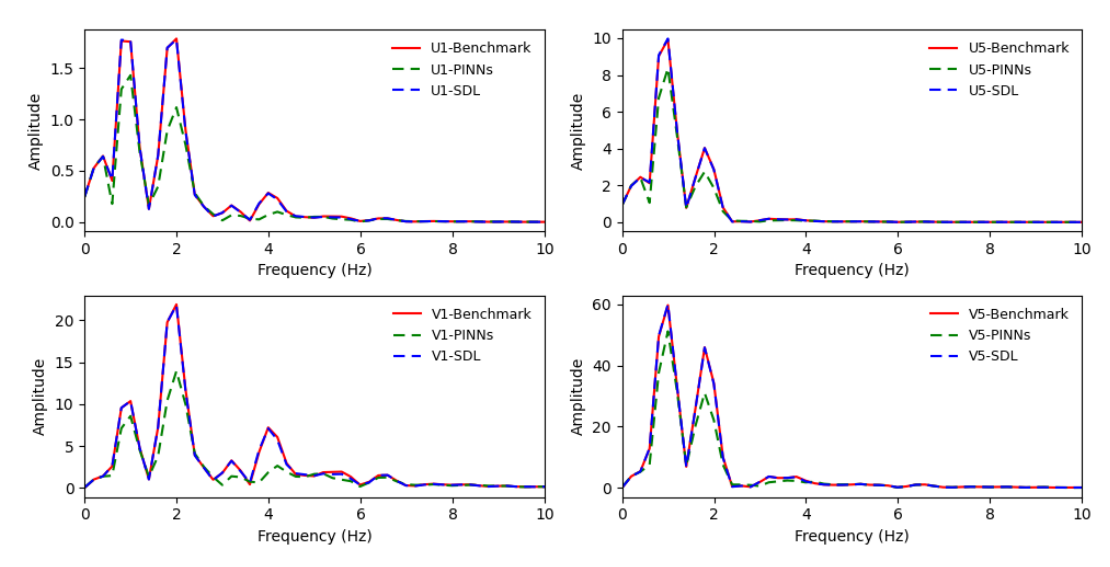


Figure 3.11 The comparison of frequency distribution of structural displacements and velocities of  $M_1$  and  $M_5$  predicted by the SDL model and PINNs method.

Fig. 3.11 shows that even when the dynamic response in this case only involves frequency components  $f < 10 \, Hz$ , the PINNs method still loses some frequency components of  $f > 2 \, Hz$ , and preferentially learns frequency components of  $f \le 2 \, Hz$ , especially in the predicted  $u_1$  and  $\dot{u}_1$ . The SDL method successfully solves the defect of the spectral bias in PINNs, which is reflected in the frequency distribution consistent with the benchmark solution.

In this case, we also compared the running efficiency of several algorithms listed above by recording their running time. In addition, in order to analyze the improvement of the memory mechanism of the recurrent architecture on the efficiency of the SDL model, an ablation test without the memory mechanism is conducted. For comparison, the most efficient CNN model scheme in Table 3.1 (L=1, H=80) is used, but it is randomly initialized in each time step instead of being initialized from the memory of

the previous time step. The rest settings are the same as the above SDL model. After testing, the training time of the model without the memory mechanism is 3051.69 s, while the training time with the memory mechanism is 247.14 s. In this case, the memory mechanism in the SDL framework can improve the model training efficiency by 12.34 times. In comparison, the running time of PINNs is 2318.3 s, while the explicit 4th-order Runge-Kutta method of the benchmark method only takes 1.5 s. From this, we can see that the explicit algorithm that does not require iterative calculations or training has an incomparable efficiency advantage. The SDL framework based on the memory mechanism also has a significant efficiency advantage over PINNs.

## 3.4.3 3-DOF system with Bouc-Wen hysteresis

The Bouc-Wen model is one of the widely used hysteretic models employed to describe the nonlinear hysteretic system. The latent hysteretic displacement has dynamics which is governed by a nonlinear differential equation that depends on the system's velocity. The hysteretic dynamics equation of the Bouc-Wen model for an *N*-DOF system can be expressed as:

$$M\ddot{u} + Ku + C\dot{u} + K_{hw} \cdot z_{hw} = F(t) \tag{3.16}$$

Here,  $K_{bw}$  is the stiffness between the restoring force of the Bouc-Wen model and the latent hysteretic displacement  $z_{bw}$ .  $z_{bw}$  is the non-observable hysteretic displacement that obeys the following nonlinear differential equation with zero initial condition  $(z_{bw}=0)$ , which is calculated as:

$$\dot{z}_{bw} = A\dot{u} - \beta |\dot{u}(t)| |z_{bw}(t)|^{n-1} \cdot z_{bw}(t) - \gamma \dot{u}(t) |z_{bw}(t)|^n$$
(3.17)

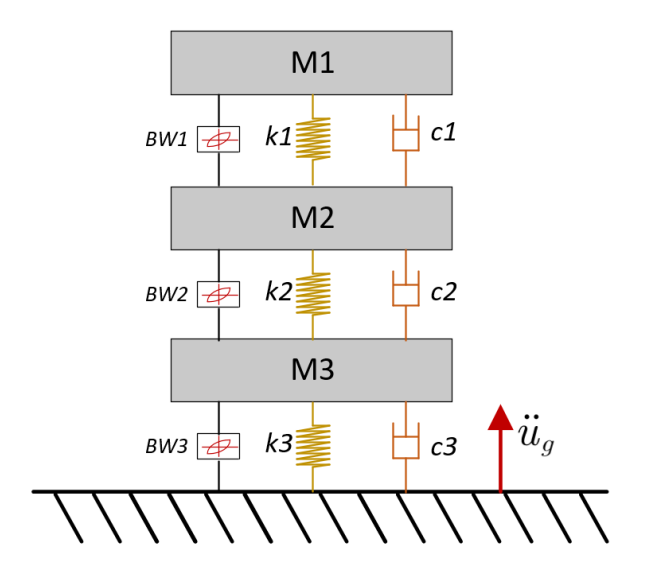


Figure 3.12 A 3-DOF system with Bouc-Wen hysteresis

In this case, a 3-DOF system with Bouc-Wen hysteresis as shown in Fig. 3.12 is analyzed. The mass of the system is set as  $m_1 = 1.0 \ kg$ ,  $m_2 = 2.0 \ kg$ ,  $m_3 = 3.0 \ kg$ . Linear stiffness is set as  $k_1 = 20N/m$ ,  $k_2 = 25N/m$ ,  $k_3 = 30N/m$ . The damping matrix is set as the damping ratio of 1% for the first and second-order natural frequencies. Three Bouc-Wen hysteresis models are installed with parameters  $k^{bw} = 25N/m$ , A = 0.5,  $\beta = 0.5$ ,  $\gamma = 0.5$ , n = 1. In this case, the system state is described as  $z = [u, \dot{u}, z_{bw}]^T$  in state space. According to Eq. (3.16) and (3.17), the system state equation can be expressed as

$$\dot{z} = \begin{bmatrix} \dot{u} \\ \ddot{u} \\ \dot{z}_{bw} \end{bmatrix} = \begin{bmatrix} \dot{u} \\ M^{-1}[F(t) - (Ku + C\dot{u} + K_{bw} \cdot z_{bw})] \\ A\dot{u}_{bw} - \beta |\dot{u}_{bw}||z_{bw}|^{n-1} \cdot z_{bw} - \gamma \dot{u}_{bw}|z_{bw}|^{n} \end{bmatrix} = g(t, z, F(t)) \quad (3.18)$$

Here  $\dot{u}_{bw}$  is different from  $\dot{u}$  in the system state, which is the relative velocity of the Bouc-Wen model.  $\dot{u}_{bw}$  can be calculated as

$$\dot{u}_{bw} = \begin{bmatrix} 1 & -1 & 0 \\ 0 & 1 & -1 \\ 0 & 0 & 1 \end{bmatrix} \cdot \dot{u} \tag{3.19}$$

 $K_{bw}$  is the hysteretic stiffness matrix, set as

$$K_{bw} = \begin{bmatrix} 25 & 0 & 0 \\ -25 & 25 & 0 \\ 0 & -25 & 25 \end{bmatrix}$$
 (3.20)

This 3-DOF system vibrates from rest under the action of seismic acceleration  $\ddot{u}_g = 10 sin(2\pi \cdot t) + 5 sin(6\pi \cdot t)$ . The ERK4 method with a time step of 0.001s is employed to solve Eq. (3. 18) as the benchmark solution. The total calculation duration is 5 s.

In this case, the SDL model is employed to predict the dynamic response with additional hidden states including hysteretic displacements. In the SDL model for this 3-DOF system, the hidden state h of the system is defined as  $h = [u, \dot{u}, z_{bw}]^T$ . The CNN in the SDL model includes a convolutional layer and three FCNN models. The input of the convolutional layer is a 5-dimensional matrix as  $x_n = [u_{n-1}, \dot{u}_{n-1}, z_{bw_{n-1}}, f_{n-1}, f_n]^T$ , and the output is 3-dimensional. These three dimensions in the output are respectively input into an FCNN model with one hidden layer of 100 neurons. The outputs of the three FCNNs are combined as the output of the CNN model  $O_{CNN}$  to approximate the hidden state  $[u, \dot{u}, z_{bw}]$ . Since no boundary conditions are embedded, the output  $O_{CNN}$  is directly used as the predicted system hidden state  $h_n^{pred}$ . The loss function of the SDL model is also constructed according to Eq. (3.7) and Eq. (3.8). The Adam optimizer with a learning rate of 0.001 is employed to minimize the loss function until the relative error  $\epsilon$  converges to the error tolerance

 $\epsilon_{tol} = 1e - 4$ . The predicted displacement results of the SDL model and benchmark solutions are shown in Fig. 3.13.

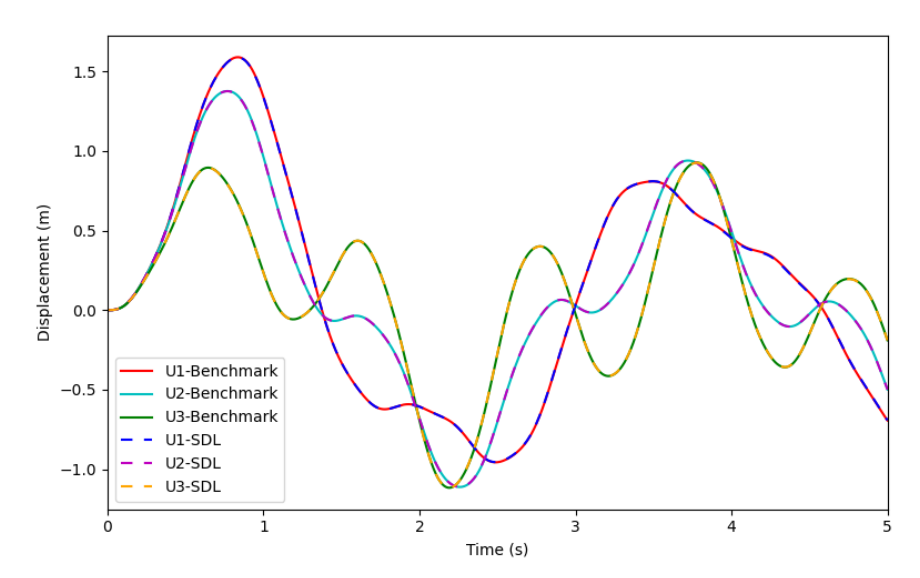


Figure 3.13 The comparison of the predicted displacement results of SDL model and benchmark solutions

Fig. 3.13 shows that the displacement responses predicted by the SDL model are highly consistent with the benchmark solution. The calculated relative *L*2 error between the predicted displacement responses and the benchmark solution is 0.271%. The restoring forces loops of the three Bouc-Wen hysteresis models are also shown in Fig. 3.14. As can be seen from Fig. 3.14, the SDL model also accurately predicts the hysteresis force of these three Bouc-Wen models.

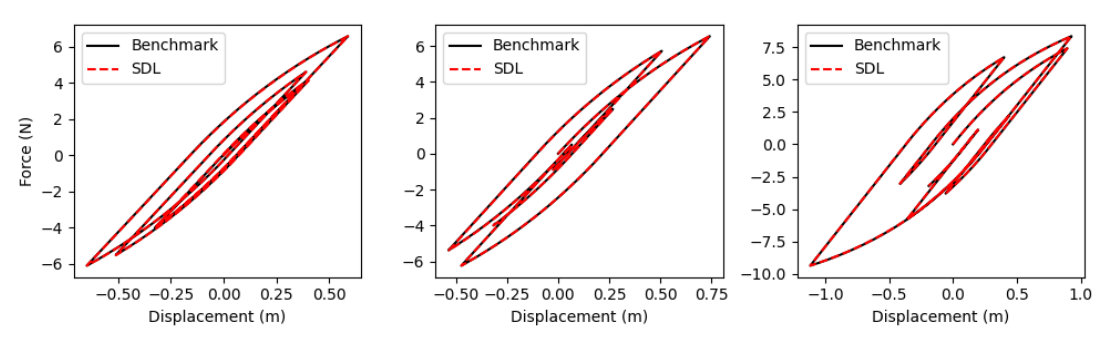


Figure 3.14 Restoring force loops for three Bouc-Wen hysteresis models. The three

sub-figures are results of model BW 1 (left), BW 2 (mid) and BW 3 (right).

#### 3.4.4 Plane truss structure

In order to verify the effectiveness of the SDL framework for 'hard' embedding of constraint conditions, the dynamic response of a plane truss structure as shown in Fig. 3.15 is analyzed. This truss consists of 19 rods with a total of 11 nodes. Truss members are considered as 2-node linear elements in the X-Y plane with consistent mass matrices. The length of the rods is 10 m and the cross-sectional area is  $0.01 m^2$ . The material density of the rods is  $2000 kg/m^3$  and the elastic model is 80 MPa. This truss is constrained at the left side (node 1 in the X and Y directions) and at the right side (node 11 in the Y direction). Two Y-direction forced displacements are applied as external excitations at nodes 5 and 7 to make the truss vibrate from the static state. The forced displacements are  $u_5^Y(t) = 0.1 * \sin(2\pi * t) + 0.3 * \sin(\pi * t)$ ,  $u_7^Y(t) = 0.25 * \sin(2\pi * t) + 0.1 * \sin(\pi * t)$ . The external forces on the unconstrained nodes are 0. The ERK4 method with dt = 0.001 is utilized to calculate the dynamic response of the truss structure as the benchmark solution. The calculation duration is 1 s.

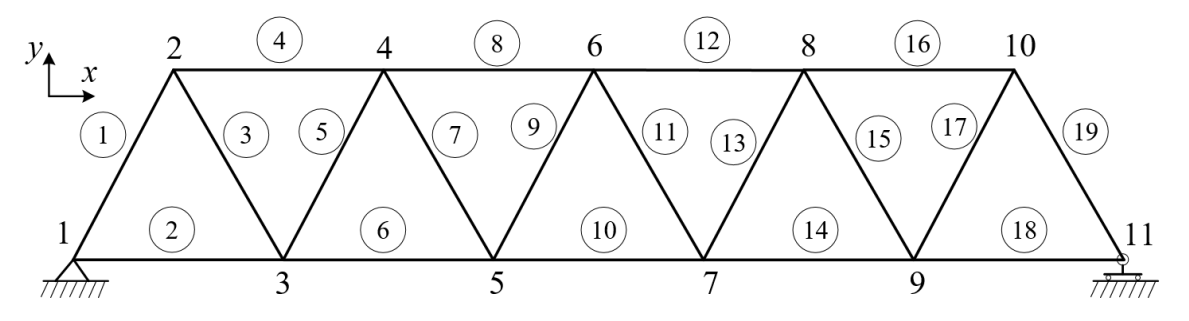


Figure 3.15 A plane truss structure

An SDL model is constructed to calculate the vibration response of the truss. The input of the SDL recurrent block is the hidden state  $h_{n-1} = [u_{n-1}, \dot{u}_{n-1}]^T$ , and the output is  $z_n = [u_n, \dot{u}_n]^T$  . In each recurrent block, a CNN model with input  $[h_{n-1}, f_{n-1}, f_n]$  (size  $4 \times 22$ ) is employed to predict the output  $O_{CNN}$  (size  $2 \times 22$ ). Then, the output  $O_{CNN}$  is processed to integrate the boundary conditions by Eq. (3.6). In this case, there are 5 constraint conditions, three of which are boundary conditions on nodes 1 and 11, and two are displacement constraints on nodes 5 and 7. Therefore, the mapping matrix  $M_k$  has 0 elements in positions of node 1 (X and Y directions), and of nodes 5, 7, and 11 (Y direction). The rest elements of matrix  $M_k$  are ones. The elements of the value matrix V in positions of nodes 5 and 7 (Y direction) are set according to the forced displacement, and the other values are 0. In the CNN model, there is one hidden layer with 100 neurons. An Adam optimizer with a learning rate of 0.001 is employed to train the CNN model until the relative error converges to the error tolerance  $\epsilon_{tol} = 1e - 4$ . The time step size of the SDL model is 0.01 s, and the number of time steps is 100.

For comparison, a PINNs model with 'soft' constraint embedding is also built to predict the vibration response of the truss. The input of the FCNN model in PINNs is t and x, and the output is the predicted node displacement  $u^{pred}(t,x)$ . t ranges from 0-1s, and x is the degree of freedom of the structure numbered from 1 to 22. The degrees of freedom of the n-th node in the X direction are numbered 2n-1, and the degrees of freedom in the Y direction are numbered 2n. The FCNN model has 4 hidden

layers with 200 neurons. The activation function between layers is the hyperbolic tangent function. In this case, the loss function  $Loss_{pinn}$  of PINNs consists of 4 parts as

$$Loss_{pinn} = Loss_i + Loss_b + Loss_u + Loss_f$$
 (3.21)

Here,  $Loss_i$ ,  $Loss_b$ ,  $Loss_u$ , and  $Loss_f$  are loss functions of the initial conditions, boundary conditions, displacement constraints and governing equations, respectively, which are calculated as

$$Loss_{i} = \frac{1}{N_{i}} \sum_{i=1}^{N_{i}} (\left| u^{pred}(0, x_{i}) \right|^{2} + \left| \dot{u}^{pred}(0, x_{i}) \right|^{2})$$
 (3.22)

$$Loss_{b} = \frac{1}{N_{b}} \sum_{i=1}^{N_{b}} (\left| u^{pred}(t_{i}, 1) \right|^{2} + \left| u^{pred}(t_{i}, 2) \right|^{2} + \left| u^{pred}(t_{i}, 22) \right|^{2})$$
(3.23)

$$Loss_{u} = \frac{1}{N_{u}} \sum_{i=1}^{N_{u}} (\left| u^{pred}(t_{i}, 10) - u^{exact}(t_{i}, 10) \right|^{2} + \left| u^{pred}(t_{i}, 14) - u^{exact}(t_{i}, 14) \right|^{2})$$
(3.24)

and

$$Loss_{f} = \frac{1}{N_{f}} \sum_{i=1}^{N_{f}} \left| M \ddot{u}^{pred}(t_{i}, x_{i}) + C \dot{u}_{i}^{pred}(t_{i}, x_{i}) + K u_{i}^{pred}(t_{i}, x_{i}) \right|^{2}$$
(3.25)

Here,  $N_i$  sampling points of initial conditions are sampled on 22 degrees of freedom at t=0.  $N_b$  sampling points of the boundary condition are sampled at node 1 (X, Y direction) and node 11 (Y direction).  $N_u$  sampling points of displacement constraint are sampled at node 5 (Y direction) and node 7 (Y direction).  $u^{exact}(t_i, 10)$  and  $u^{exact}(t_i, 14)$  are the exact displacements from the constraint conditions.  $N_f$  collocation points are sampled on all unconstrained degrees of freedom. The partial derivatives of u are calculated using the automatic differentiation technique in the PINNs framework. In the time domain, the sampling is uniform with dt=0.01s. The Adam optimizer with  $l_r=0.001$  is employed to train the PINNs model for 100,000

iterations. The displacement responses of nodes 5, 6, and 7 in the Y direction predicted by the trained SDL model, PINNs model, and benchmark solution are shown in Fig. 3.16.

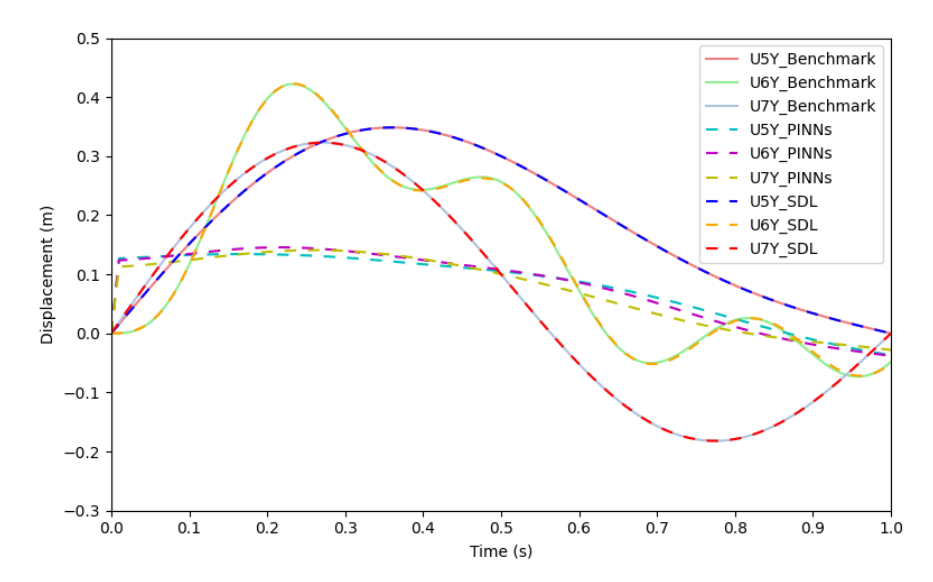


Figure 3.16 Comparison of the Y displacements of nodes 5, 6, and 7 predicted by the SDL model and the PINNs model with the benchmark solution

Fig. 3.16 shows that benefiting from 'hard' constraint embedding, the SDL model accurately expresses the displacement constraints at nodes 5 and 7, while PINNs failed to successfully satisfy these two constraints. The SDL model also successfully predicts the displacement response of node 6 with a relative L2 error of 0.898%. The reason for the failure of PINNs is the imbalance of multiple loss functions as shown in Fig. 3.17. Fig. 3.17 shows that in PINNs, the optimizer prioritizes minimizing  $Loss_i$ ,  $Loss_b$ , and  $Loss_f$ , while  $Loss_u$  is not significantly reduced.

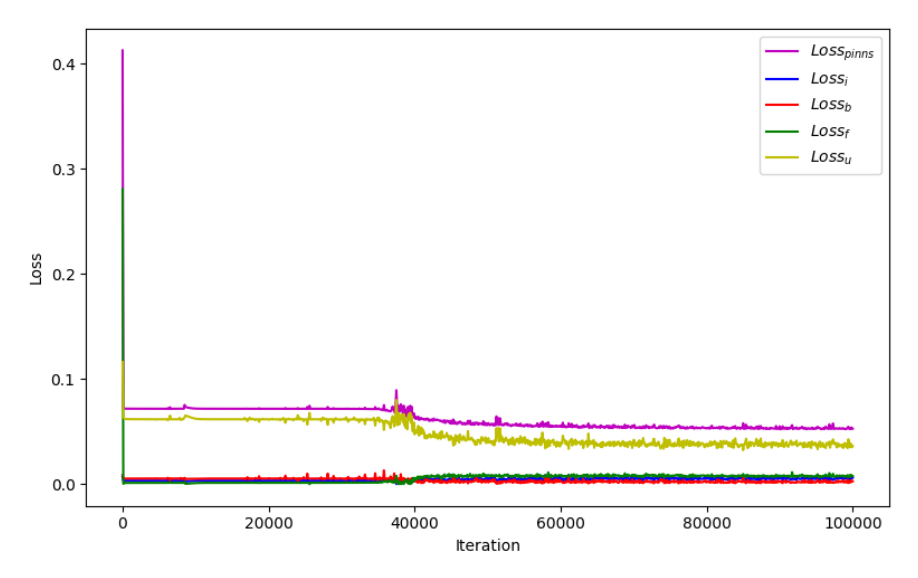


Figure 3.17 Convergence process of multiple loss functions in PINNs

## 3.5 Summary

In this study, a novel recurrent convolutional neural network framework named the structural dynamics learner (SDL) is proposed to predict the dynamic response of linear/nonlinear structural systems. A recurrent architecture consisting of a series of recurrent blocks containing convolutional neural network models is built to accurately predict the unknown structural response at discrete time steps with the system state and external force inputs. The implicit Crank-Nicolson form of the system's motion equations is incorporated into the SDL framework as physical information, which also provides excellent stiff equation stability for the framework. A 'hard' embedding of boundary conditions is adopted to ensure the rigid satisfaction of constraints and eliminate the residual errors of constraints. Several numerical examples are carried out to demonstrate the accuracy and stability of the proposed framework. In the vibration analysis of a 2-DOF system, the SDL framework shows better stability for the structural

system involving stiff equations, compared with explicit numerical algorithms such as the Euler forward method and the explicit Runge-Kutta method. The accuracy comparison between the PINNs method and the SDL framework is carried out on a 5-DOF system involving nonlinear stiffness. The results show the improved accuracy of SDL over the PINNs method and address the spectral bias drawback of PINNs. How to integrate other hidden states of the structural system such as hysteretic displacements into the SDL framework is also demonstrated in an example of a 3-DOF system with Bouc-Wen hysteresis. Finally, the benefits of 'hard' embedding of boundary conditions are also verified in an example of a plane truss. The results of the numerical examples demonstrate the excellent ability of the SDL framework as a reliable alternative to simulate vibration responses of the structural systems.

# Chapter 4 PI-MP framework for force localization and structural response reconstruction

#### 4.1 Introduction

Accurate knowledge of the dynamic forces acting on a structure is the foundation for structural vibration prediction, structural design, and structural health monitoring. Generally, for a structural system, predicting the structural response using known structural system parameters and external forces is referred to as a forward problem. Many mature methods have been established to solve these forward problems, which can accurately calculate the structural response. Unfortunately, in actual engineering projects, it is often difficult to directly measure the external forces acting on the vibrating structure. Although advanced force sensors have been developed, directly installing them on the structure or in the force transmission path can inevitably affect the properties of the system and the acting forces. In this case, an alternative approach to estimating these forces is to measure the structural response and then reconstruct the forces using computational methods, which points to an important inverse problem known as force reconstruction.

In recent years, various methods for force reconstruction have been proposed, which can be broadly divided into three groups: direct calculation, regularization method, and probabilistic method (Sanchez & Benaroya, 2014). The direct calculation method establishes a mathematical or physical relationship between the structural

response and the external forces, then directly computes the external forces using this mapping and the measured structural response. For example, Jacquelin and Hamelin (Jacquelin & Hamelin, 2003) successfully calculated the external forces on a bar by establishing a relationship between the force and the strain of the Hopkinson bar and measuring the three-dimensional strain of the bar. Other direct calculation methods have also been developed for Bernoulli-Euler beams (Law et al., 1997). While direct calculation methods are computationally efficient, they are highly sensitive to the measuring noise, which is unavoidable in real-world vibration data due to sensor errors or environmental influences.

To address the sensitivity to noise inherent in direct calculation methods, regularization approaches have been developed. These methods incorporate additional mathematical or physical constraints to suppress the influence of noise (Qiao et al., 2020; Wang et al., 2019). The most widely used regularization methods in recent years are the truncated singular value decomposition (TSVD) (Shi et al., 2024; Yang, 2024) and the Tikhonov regularization (Li Wang et al., 2020) method based on L2-norm penalty. For instance, (Ren et al., 2019) employed an improved Tikhonov regularization method to identify dynamic forces between a conical pick and a coal seam. (H. P. Zhu et al., 2014) combined the transmissibility concept in the state-space domain with Tikhonov regularization to find the unknown input excitation of a structure. (Chen & Chan, 2017) proposed a truncated generalized singular value decomposition (TGSVD) method to obtain a more stable solution to the ill-posed problem in load identification,

making the results less sensitive to noise disturbances.

Among the probabilistic methods, the most commonly used is the Bayesian method, which assumes that the external force obeys a prior distribution, such as Gaussian distribution, and uses Bayesian reasoning to obtain the posterior probability distribution of the external force using the response observation according to the relationship between the structural response and the external force. Some studies based on Bayesian methods to reconstruct forces can be found in (Li & Lu, 2019), (Feng et al., 2020), and (Chen et al., 2023). Another classic probabilistic method is the Kalman filter, which uses the current structural response measurement and the previous structural state estimate to calculate the optimal current system state estimate through the Kalman gain. Then, based on the current state estimate and state equation, the unknown input force at the current moment can be inferred. The application and improvements of Kalman filter methods are discussed in (Niu et al., 2015), (Lourens et al., 2012), (Wei et al., 2022), and (Petersen et al., 2022). For a more comprehensive review of force reconstruction methods, the work of (Sanchez & Benaroya, 2014) and (Beltran Carbajal, 2012) provides further discussions.

With the rapid advancements in machine learning, various deep learning techniques have been explored for reconstructing forces acting on structures. Recent studies have demonstrated the potential of deep neural networks (Liu et al., 2022; Lei Wang et al., 2020), graph neural networks (C. Huang et al., 2023), and long short-term memory (Denkena et al., 2020) networks in tackling the inverse problem of force

reconstruction. These data-driven machine learning approaches have shown promising results, highlighting the broad applicability of deep learning methods in this domain. Recently, a class of novel machine learning frameworks known as physics-informed machine learning (Karniadakis et al., 2021) has gained significant attention across diverse scientific and engineering disciplines. By seamlessly integrating physical information, often described by partial differential equations or integro-differential equations, with powerful deep learning architectures, PIML has highlighted remarkable application prospects. Prominent examples include successful deployments in fluid mechanics (Sharma et al., 2023), heat conduction (Cai, Wang, Wang, et al., 2021a), and material design (Zheng et al., 2022). The key advantage of PIML lies in its ability to effectively combine data and physical models, even when the models are nonlinear, partially informed, or high-dimensional. Moreover, PIML has also demonstrated strong adaptability in solving ill-posed problems and inverse problems in the presence of noisy data (Gao et al., 2022; Raissi et al., 2019).

In this study, we propose a physics-informed Markov parameters (PI-MP) framework to reconstruct the structural external force by integrating the Markov parameters of the structural vibration governing equations with the physics-informed neural networks (PINNs) in the state space. Specifically, in the PI-MP framework, a deep neural network is built to predict the unknown external forces of the structure. Then, the governing equations of structural vibration are employed to derive the relationship between the structural vibration responses and the external forces,

represented by Markov parameters. The calculated Markov parameters are integrated into the neural network model as prior physical information to guide the model training. With the external forces predicted by the neural network model and Markov parameters, the predicted structural responses can be calculated and then used to construct a loss function by calculating the residuals from the measured structural responses. A regularization term based on the derivatives of the predicted forces is also added to the loss function to improve solution smoothness and avoid noise overfitting. By minimizing the loss function, the predicted structural responses of PI-MP tend to be consistent with the measured responses, and the reconstructed external forces can approach the true values. With the reconstructed external forces, the responses of the entire structure can also be reconstructed. In addition, for the case where the force location is also unknown, by considering an L1 norm of the force mapping matrix in the loss function and designing a special optimization algorithm to minimize the loss function, the force location on the structure can also be discovered.

The rest of this study is organized as follows: In Section 2, the background knowledge of the proposed method is introduced briefly. In Section 3, our proposed PI-MP framework is described in detail. In Sections 4 and 5, we validate the proposed PI-MP framework in three numerical cases and an experimental case, respectively. Lastly, some conclusions are summarized in Section 6.

# 4.2 Background

# 4.2.1 Motion equations for structural system

For a linear, time-invariant structural system subjected to dynamic forces, the equation of motion can be written as

$$[M]{\ddot{x}} + [C]{\dot{x}} + [K]{x} = [L]{F}$$
(4.1)

where M, C, and K are the mass, damping, and stiffness matrices, respectively. The matrix L is the mapping matrix for the external forces, which is a diagonal Boolean matrix with diagonal elements of 0 (without external forces) or 1 (with external forces).  $\ddot{x}$ ,  $\dot{x}$ , and x represent the system's acceleration, velocity, and displacement responses, respectively. The vector F represents the external forces acting on the structural system. By defining the state vector of the structural system as  $X = [x, \dot{x}]$  in the state space, Eq. (4.1) can be rewritten as

$$\dot{X} = K^*X + B^*LF \tag{4.2}$$

where,  $K^* = \begin{bmatrix} 0 & I \\ -M^{-1}K & -M^{-1}C \end{bmatrix}$ ,  $B^* = \begin{bmatrix} 0 \\ M^{-1} \end{bmatrix}$ . The response observation y is set as  $y = R_a * \ddot{x} + R_v * \dot{x} + R_x * x \tag{4.3}$ 

where,  $R_a$ ,  $R_v$ ,  $R_x$  are diagonal Boolean mapping matrices of acceleration, velocity, and displacement observations, respectively. Each of these matrices has diagonal elements of 1 (observed) or 0 (not observed). Using Eq. (4.1), Eq. (4.3) can be expressed as

$$y = RX + DLF (4.4)$$

where  $R=[R_x-R_aM^{-1}K,R_v-R_aM^{-1}C]$  and  $D=R_aM^{-1}$ . According to the

exponential matrix algorithm, Eq. (4.2) and (4.4) can be expressed as

$$X_{i+1} = AX_i + BLF_i \tag{4.5}$$

$$y_j = RX_j + DLF_j$$
,  $j = 1, 2, \dots, N$  (4.6)

where,  $A = \exp(K^*h)$  and  $B = K^{*-1}(A - I)B^*$ . Here, h is the time step length and N is the number of time steps. Following Eq. (4.5) and Eq. (4.6), the state  $X_j$  at time step j can be calculated as

$$X_j = \sum_{k=0}^{j-1} A^k B L F_{j-k-1} + A^j X_0, j = 1, 2, \dots, N$$
(4.7)

Then the observation  $y_i$  at time step j is

$$y_i = \sum_{k=0}^{j} H_k L F_{i-k} + R A^j X_0, j = 1, 2, \dots, N$$
 (4.8)

where,  $H_0 = D$  and  $H_k = RA^{k-1}B$ . Here  $H_k$  are called Markov parameters, which represent the structural response of the external force at the previous time steps. For a linear system, Markov parameters are unique and represent the inherent characteristics of the system in response to external forces. Eq. (4.8) can be expressed in Toeplitz matrix form as

$$\begin{pmatrix} y(0) \\ y(1) \\ \vdots \\ y(N) \end{pmatrix} = \begin{bmatrix} H_0 & 0 & \cdots & 0 \\ H_1 & H_0 & \cdots & 0 \\ \vdots & \vdots & \ddots & \vdots \\ H_N & H_{N-1} & \cdots & H_0 \end{bmatrix} \begin{bmatrix} L \\ L \\ \vdots \\ L \end{bmatrix} \begin{Bmatrix} F(0) \\ F(1) \\ \vdots \\ F(N) \end{Bmatrix} + \begin{bmatrix} RA^0 \\ RA^1 \\ \vdots \\ RA^N \end{bmatrix} X_0$$
 (4.9)

Eq. (4.9) can also be simplified as

$$Y = H_L F + A_R X_0 \tag{4.10}$$

where  $H_L$  and  $A_R$  are the corresponding Toeplitz and state transition matrices.

# 4.2.2 Force and response reconstruction

When the external forces on the system are unobservable, an alternative approach

is to reconstruct the external forces by measuring the vibration response of the structure. If we know the initial state  $X_0$  of the system and obtain some observation data Y, according to Eq. (4.10), theoretically, the external force can be inversely reconstructed by

$$F_{rec} = H_L^+(Y - A_R X_0) (4.11)$$

Here,  $H_L^+$  is the pseudo-inverse of  $H_L$ . This approach, however, is a well-known ill-posed problem due to limitations in the number of measurement points, as well as the presence of noise and measurement errors (Mao et al., 2010; H. P. Zhu et al., 2014). Another way to reconstruct the unknown external force is to minimize the error by the ordinary least squares (OLS) method as

$$min \|H_L F_{rec} + A_R X_0 - Y\|_2^2 \tag{4.12}$$

After obtaining the predicted external force, Eq. (10) can also be employed to reconstruct the unobserved structural response. Through defining the observed structural response as  $Y_1$  and the unobserved structural response as  $Y_2$ , according to Eq. (4.10), the derivation relationships between  $Y_1$ ,  $Y_2$  and F are listed as

$$\begin{cases} Y_1 = H_{L1}F + A_RX_0 \\ Y_2 = H_{L2}F + A_RX_0 \end{cases}$$
 (4.13)

With the external force  $F_{rec}$  reconstructed from Eq. (4.12), the unknown structural response  $Y_2$  can be reconstructed as

$$Y_{2r} = H_{L2}F_{rec} + A_RX_0 (4.14)$$

# 4.2.3 Tikhonov regularization

Regularization is a commonly used technique in optimization problems to ensure

smoothness and convergence of solutions by adding additional constraints. In the study of force reconstruction, noise in the measured data may significantly degrade the accuracy of the external force reconstructed from Eq. (4.12). A technique called Tikhonov regularization (Gockenbach, 2016) is often applied to keep the solution stable and reduce the influence of noise. The force reconstruction with Tikhonov regularization (Mao et al., 2010) is calculated as

$$min\|H_L F_{rec} + A_R X_0 - Y\|_2^2 + \alpha \|L F_{rec}\|_2^2$$
 (4.15)

Here,  $\alpha$  is the regularization parameter which controls the balance between the goodness of fitness and the regularization term. The classic method to determine the optimal value of parameter  $\alpha$  is the L-curve method (Johnston & Gulrajani, 2000). By setting various  $\alpha$  values and employing an optimizer to solve Eq. (4.15), a series of value pairs  $(log(\|H_LF_{rec} + A_RX_0 - Y\|_2^2), log(\|LF_{rec}\|_2^2))$  for different  $\alpha$  values is obtained. These value pairs can be plotted and fit into an L-shaped curve. On one side of this curve, the method can fit the observed data well, but the solution may be less smooth, potentially indicating overfitting to noise. On the other hand, the solution is smoother, but the fit to the observed data is reduced. The optimal value of  $\alpha$  is typically chosen as the value corresponding to the "corner" of the L-curve, where the trade-off between data fit and solution smoothness is balanced.

# 4.2.4 Physics-informed neural networks

Physics-informed neural networks are a popular class of physics-informed machine learning methods that aim to incorporate physical information into deep neural

network models (Raissi et al., 2019). The key idea behind PINNs is to define a neural network NN(x,t) that can approximate the solution u(x,t) of a mathematical governing equation.

$$D(u(x,t),\theta) = f(x,t) \tag{4.16}$$

where D is a mathematical operator controlled by parameter  $\theta$ , which can be a linear or nonlinear partial differential operator, integral differential operator, etc. To train the PINNs model for the forward problem, i.e., predicting the exact value of u(x,t) given some constraints, a total loss function that consists of two parts is defined as

$$Loss_{total} = Loss_f + Loss_u (4.17)$$

where,  $Loss_f$  is the loss function that penalizes the deviation of the neural network output from satisfying the governing equation as

$$Loss_{f} = \frac{1}{N_{f}} \sum_{i=1}^{N_{f}} \|D(u(x_{f}, t_{f}), \theta) - f(x_{f}, t_{f})\|^{2}$$
 (4.18)

Here,  $N_f$  is the number of collocation points randomly sampled in the domain of the governing equation. The second term  $Loss_u$  of Eq. (4.17) enforces the neural network output to satisfy the defined constraints by

$$Loss_{u} = \frac{1}{N_{u}} \sum_{i=1}^{N_{u}} ||u(x_{u}, t_{u}) - u^{*}(x_{u}, t_{u})||^{2}$$
(4.19)

where,  $N_u$  is the number of randomly sampled points on the constraints.  $u^*(x_u, t_u)$  is the exact value given by the defined constraints. By minimizing the total loss  $Loss_{total}$  using an optimizer, the PINNs model can learn to approximate the exact solution of the governing equation while satisfying the given constraints.

For the inverse problem, where the goal is to discover the unknown parameter  $\theta$ 

in the governing equation through some observations  $u^*(x_m, t_m)$ , the PINNs model can treat the unknown parameters  $\theta$  as trainable variables that are initialized and learned alongside the neural network weights and biases. The total loss function for the inverse problem is defined as

$$Loss_{total} = Loss_f + Loss_m (4.20)$$

Here,  $Loss_f$  is calculated by following Eq. (4.18) to enforce the neural network output to satisfy the governing equation (4.16). The additional term  $Loss_m$  penalizes the deviation between the neural network predictions  $u(x_m, t_m)$  and the observed values  $u^*(x_m, t_m)$  by

$$Loss_{m} = \frac{1}{N_{m}} \sum_{i=1}^{N_{m}} ||u(x_{m}, t_{m}) - u^{*}(x_{m}, t_{m})||^{2}$$
(4.21)

where,  $N_m$  is the number of observation points. By minimizing the total loss  $Loss_{total}$  using an optimizer, the PINNs model can learn to approximate both the solution u(x,t) and the unknown parameters  $\theta$  in the governing equation of Eq. (4.16). The implanted mathematical constraints will guide the parameter  $\theta$  to approach its exact value that best fits the observations  $u^*(x_m, t_m)$ .

## 4.3 Methodology

Consider a linear time-invariant structural system with d degrees of freedom. The relationship between the system's dynamic response and the external force can be expressed using the Markov parameters described in Eq. (4.10). We propose a novel neural network framework called physics-informed Markov parameters (PI-MP) that combines the strengths of PINNs and the Markov parameters to reconstruct the external

force and the system response. The overall framework of PI-MP is shown in Fig. 4.1.

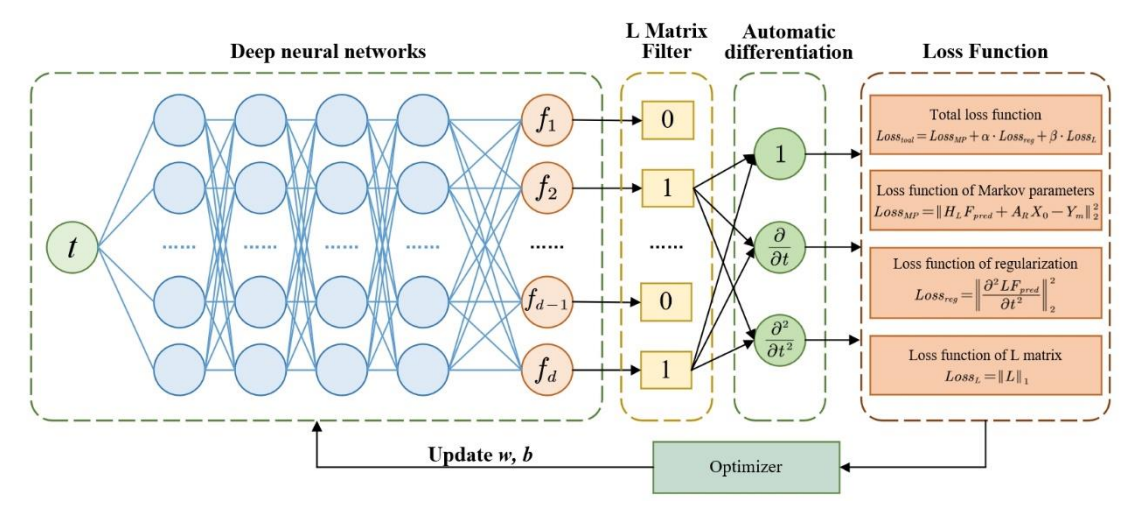


Figure 4.1 The overall framework of the physics-informed Markov parameters

As shown on the left side of Fig. 4.1, a deep neural network model is utilized to predict the external force f acting on all degrees of freedom with the input of time t. In the filtering step, the predicted external force f is transformed using the mapping matrix L defined in Eq. (4.1) to obtain the filtered external force  $F_L$  acting on the system. The matrix L can be either determined (if the force location is known) or undetermined, in which case it can be discovered using the method described below. Next, the PI-MP framework employs automatic differentiation of the neural network model to calculate the derivative of  $F_L$  with respect to the input t. This derivative information will be used to construct the loss function in the next optimization step.

The total loss function of the PI-MP framework consists of three parts. The first part is the loss function of the Markov parameters, calculated as the mean square error of the residual of Eq. (4.10) by

$$Loss_{mp} = \|H_L F_{pred} + A_R X_0 - Y_m\|_2^2$$
 (4.22)

where  $F_{pred}$  is the external force predicted by the neural network model, and  $Y_m$  is the measured structural response. By changing the settings of the  $R_a$ ,  $R_v$  and  $R_x$  in Eq. (4.3), we can adapt Eq. (4.22) to different structural response (displacement, velocity, and acceleration) measurements. To prevent the neural network model from overfitting the noise in the measured data, a regularization term which penalizes the second-order derivative of  $F_L$  with respect to time t is introduced as

$$Loss_{reg} = \left\| \frac{\partial^2 (LF_{pred})}{\partial t^2} \right\|_2^2 \tag{4.23}$$

When the L matrix is not determined, i.e., the force application points are unknown, following the assumption that only a few degrees of freedom are subject to external forces, an additional term is added to the loss function to promote sparsity in the L matrix, as defined in

$$Loss_L = ||L||_1$$
 (4.24)

Finally, the total loss function of the PI-MP framework is the weighted sum of these three terms as

Loss<sub>total</sub> = 
$$\|H_L F_{pred} + A_R X_0 - Y_m\|_2^2 + \alpha \cdot \|\frac{\partial^2 (L F_{pred})}{\partial t^2}\|_2^2 + \beta \cdot \|L\|_1$$
 (4.25) where,  $\alpha$  and  $\beta$  are the weights of the regularization term and the  $L$  matrix norm, respectively.  $\alpha$  controls the balance between the goodness of fit and smoothness of the predicted forces, which can be determined by the L-curve method described in Section 4.2.3.  $\beta$  controls the sparsity of the  $L$  matrix, which is set to 0.01 according to our tests.

When the L matrix is determined, the  $Loss_L$  also becomes a fixed value. To omit

this fixed value term in the loss function, the corresponding weight  $\beta$  is set as 0. Then, a gradient descent-based optimizer such as Adam (Kingma & Ba, 2014) is employed to minimize the total loss function  $Loss_{total}$ , so that the outputs of the neural network model can approximate the exact external force. However, when the L matrix is not determined, the optimal problem of  $Loss_{total}$  becomes more challenging. Due to the sparsity and the discontinuity of the diagonal values in the L matrix, it is difficult to directly use a gradient descent-based optimizer to minimize  $Loss_{total}$ . To address this problem, in the PI-MP framework, we use a greedy algorithm combined with the Adam optimizer, as outlined in Algorithm 4.1, to minimize the total loss function  $Loss_{total}$ . After training the model using this optimization strategy, the PI-MP framework can accurately locate the position of the external force and predict the external force  $F_{pred}$  from the neural network model. These predicted forces can then be used to reconstruct all unknown structural responses by following Eq. (4.10).

## **Algorithm 4.1** Greedy algorithm with Adam optimizer for minimizing Loss<sub>total</sub>

```
1. Initialize L as a zero matrix
```

2. Repeat

Use Adam to minimize  $Loss_{total}$ , record the minimum loss as  $Loss_{min}$ 

Set updated = False

For each inactivated diagonal element  $L_{ii}$  in L matrix (i.e.,  $L_{ii} = 0$ ):

Activate  $L_{ii}$  by setting  $L_{ii} = 1$ , resulting in matrix  $L_i$ 

Use Adam to minimize  $Loss_{total}$ , record the matrix  $L_i$  and minimum loss

 $Loss_i$ 

If  $min(Loss_i) < Loss_{min}$ :

Update L matrix by setting matrix  $L = L_i$ ,  $i = argmin(Loss_i)$ 

Set updated = True

- 3. Until updated = False
- 4. Return final *L* matrix

In the above PI-MP framework, we have described the processes to locate the

positions of external forces, reconstruct the time series of external forces, and reconstruct the unobserved structural responses using partial system response observations. However, there is still a challenge that needs further analysis. As the size of the Toeplitz matrix defined in Eq. (4. 9) increases linearly with the number of time steps and the degree of freedom of the structure, for long-term response observation of structures with large degrees of freedom, the entire Toeplitz matrix will consume a significant amount of computer memory resources, which will reduce the computation efficiency. To address this issue, in the PI-MP framework, we employ a moving window technique to decompose the entire long time series data into short fragments. Specifically, the long-term structural response data is divided into windows of hundreds or thousands of time steps (depending on the size of available computer memory), with a certain overlap between adjacent windows. Within each window, the PI-MP framework is employed to reconstruct the corresponding external forces and structural responses. Finally, the external forces and responses from all the windows are spliced together to obtain the results for the entire time series. This moving window technique avoids the need to compute the entire Toeplitz matrix at once, which helps to conserve computer memory resources and maintain the efficiency of the PI-MP framework.

#### 4.4 Numerical cases

To assess the accuracy and capabilities of the proposed PI-MP framework, three numerical examples are presented in this section. We first consider a 4-degree-of-freedom system and compare the performance of the PI-MP framework against the

ordinary least squares method (described in Section 4.2.2) and the Tikhonov regularization method (described in Section 4.2.3). The impact of factors such as the number and positions of structural response measurement points, as well as the noise level in the response data, on the reconstruction accuracy are also investigated. Additionally, this case also illustrates how to accurately identify the force location when it is unknown. The second case involves reconstructing the external forces and dynamic responses of a cantilever beam from noisy measurements. In the third case of a truss system, the PI-MP framework is used to discover the external force location and reconstruct the external forces and structural responses from noisy measurements. For all three numerical experiments, a neural network model with two hidden layers of 100 neurons and a sine activation function is built to approximate the unknown external forces, respectively. The Adam optimizer with a learning rate of 0.001 is employed to minimize the total loss function.

# 4.4.1 4-degree-of-freedom system

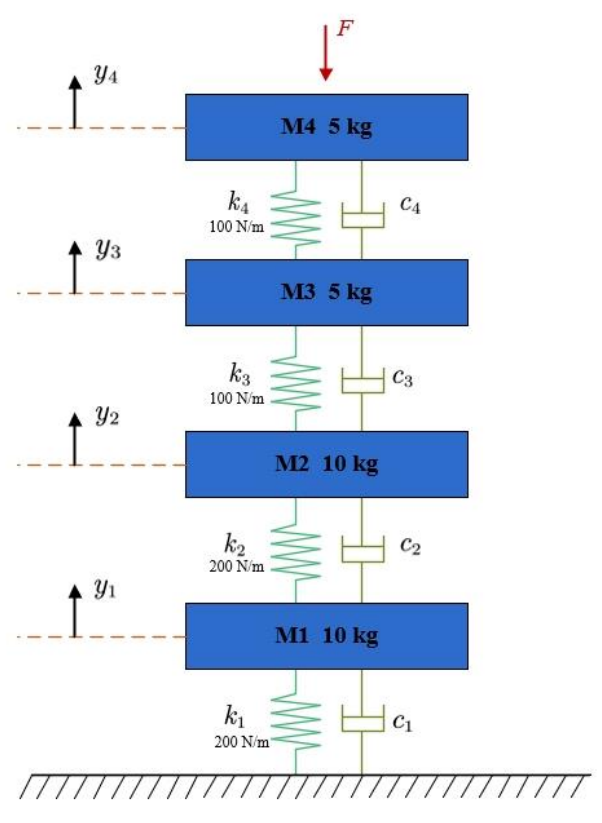


Figure 4.2 4-degree-of-freedom system

Consider a 4-degree-of-freedom system as shown in Fig. 4.2. The mass of each degree of freedom and the stiffness of the connections are presented in the figure. The damping of the structure is set as C = 0.005 \* K + 0.001 \* M. The system vibrates under the external force action on M4 as shown in Fig. 4.3. Using the Newmark method with a time step of 0.001 s, the structural response is calculated for a duration of 1 s, which serves as the observation data. To simulate observation data with different noise levels, Gaussian noise is added to the calculated response data as

$$y_{noise} = y_{cal} * (1 + \eta * N(n, m))$$
 (4.26)

where,  $y_{noise}$  is the noisy observed data,  $y_{cal}$  is the calculated data from the Newmark

method, and  $\eta$  is the noise level ranging from 0 to 1. N(n, m) is a random number matrix of shape (n, m) generated using a standard Gaussian distribution. Here, n is the length of the input data, and m is the system degree of freedom as m = 4.

Let us first consider the case where the point of force application is known, i.e., L=diag (0, 0, 0, 1). The calculated acceleration data of M1 and M3 are used as the observation data, with noise levels of 0%, 1%, 5%, and 10%, respectively. Using the L-curve test, the weight of the regularization term  $\alpha$  is set to  $10^{-8}$ , and the weight of the L matrix norm  $\beta$  is set to 0.01. The Adam optimizer is employed for 20,000 iterations to minimize the total loss function. Since the input data has only 1,000 time steps and 4 degrees of freedom, the entire input data can be used as a single window for the calculations. For comparison, the ordinary least squares method described in Eq. (4.12) and the Tikhonov regularization method described in Eq. (4.15) are also applied to predict the unknown force. The weight of the regularization term in the Tikhonov regularization method is set to  $10^{-7}$ . The reconstructed external forces using the three methods are plotted in Fig. 4. 3, with 0% and 10% noisy input data, respectively.

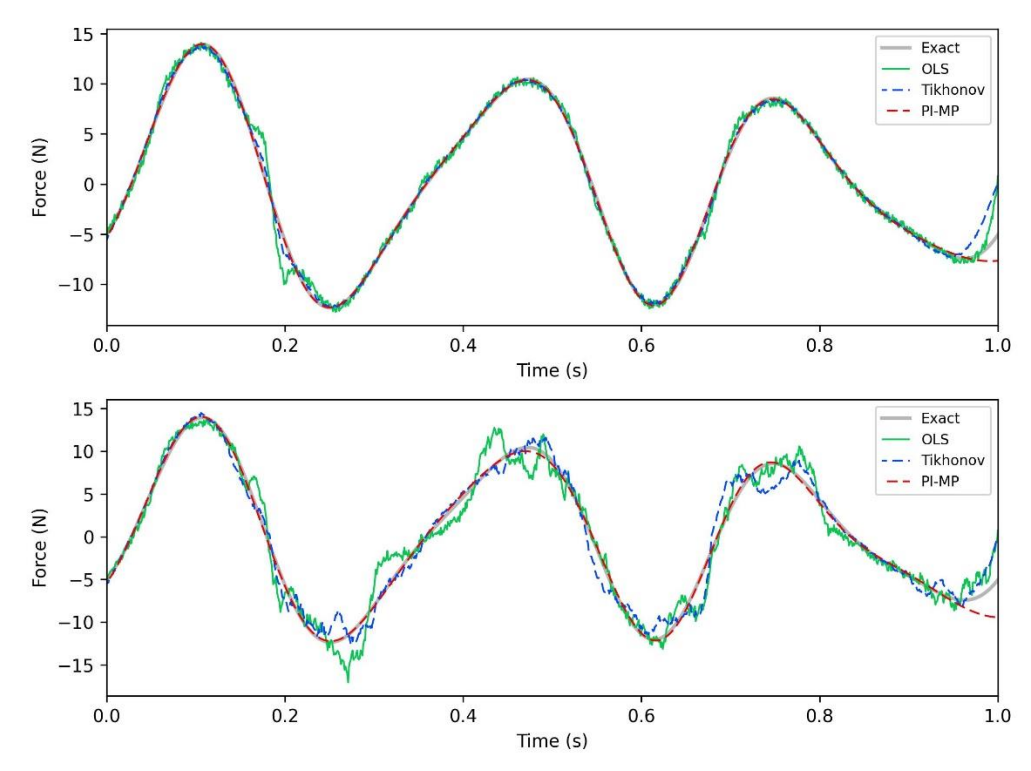


Figure 4.3 Reconstructed external forces (Top: 0% noise input, bottom: 10% noise input)

Fig. 4.3 shows that when the input data is noise-free, all three methods are able to accurately reconstruct the unknown external force. However, when there is 10% noise in the input data, the OLS method and Tikhonov regularization method tend to overfit the noise, while the PI-MP method can effectively suppress the noise overfitting. To quantify the accuracy of the results, the relative L2 error of the solutions is calculated by following Eq. (4.27). The relative L2 errors of the three methods with input data of different noise levels are shown in Table 4.1.

Relative L2 = 
$$\frac{\sqrt{\sum (f^{pred} - f^{exact})^2}}{\sqrt{\sum f^{exact^2}}}$$
 (4.27)

Table 4.1 Relative L2 errors in reconstructed external forces

Method	Noise level			
	0%	1%	5%	10%
OLS	11.147%	11.126%	21.785%	51.774%
Tikhonov regularization	9.088%	9.355%	17.936%	31.246%
PI-MP	3.502%	4.394%	7.410%	9.104%

The results in Table 4.1 show that as the noise level increases, the errors in the external forces reconstructed by the three methods also increase. However, the PI-MP method consistently achieves more accurate results than the other two methods. In order to compare the computational efficiency of the above methods, the computation time of the proposed PI-MP method and benchmark methods including the OLS method and Tikhonov regularization method was recorded. The results show that the PI-MP method took 83.69 seconds to complete 20,000 iterations, while the OLS method and Tikhonov regularization method took 104.64 seconds and 105.80 seconds to complete 20,000 iterations respectively. In terms of computational efficiency, PI-MP has a slight advantage over the OLS method and Tikhonov regularization.

To further analyze the impact of the number and positions of measurement points on the accuracy of the PI-MP method, 15 different measurement point schemes are set up, as listed in Table 4.2. The input data for these schemes is the noise-free measurement of the acceleration at the positions indicated in the table.

Table 4.2 Relative L2 error of external force reconstruction for different measurement point schemes

Measurement	Relative L2	Measurement	Relative L2
location	error	location	error
1	79.573%	2,4	0.266%

2	33.770%	3,4	0.236%
3	3.085%	1,2,3	3.619%
4	0.250%	1,2,4	0.239%
1,2	37.809%	1,3,4	0.279%
1,3	3.257%	2,3,4	0.226%
1,4	0.276%	1,2,3,4	0.245%
2,3	3.502%		

From Table 4.2, it is observed that increasing the number of measurement points can significantly improve the accuracy of force reconstruction of the PI-MP method. When the number of measurement points is limited, the accuracy of force reconstruction can also be improved by bringing the measurement points closer to the point of force application.

When the L matrix is unknown, i.e., the force application points are undetermined, PI-MP can be employed to identify the exact force location. In this test case, external forces are applied to M2 and M4, and the Newmark method is used to calculate the vibration responses of the structure under these external forces. The total calculation duration is 1s, with a time step of 0.001 s. The calculated acceleration data at M1 and M3 are used as the noise-free measurement data, and 1% noise is added to make the noisy input data for the PI-MP method. Using the greedy algorithm and Adam optimizer described in Algorithm 1, the PI-MP method successfully identified the exact value of the *L* matrix to discover the exact force location. The detailed discovery process is shown in Fig. 4.4.

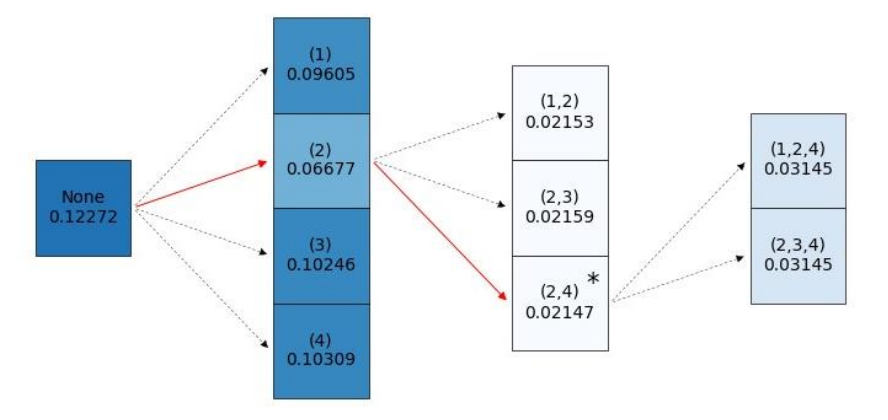


Figure 4.4 Process of discovering the L matrix

(The settings of force positions are shown in brackets, and the numbers below represent the corresponding loss values)

## 4.4.2 Cantilever beam

In this case, a cantilever beam structure shown in Fig. 4.5 is considered. The length, width, and thickness of the beam are 1 m, 50 mm, and 5 mm, respectively. The material of the beam is steel, with a density of  $7850 kg/m^3$  and an elastic modulus of 206 GPa. Using the finite element model, this cantilever beam is discretized into 10 elements. The beam elements are considered as two-node Euler-Bernoulli beams with a consistent mass matrix. This beam model has 11 nodes and 22 degrees of freedom (vertical displacement and rotation). The damping ratio of the first two modes is set to 0.5%. The displacement and rotation of the cantilever beam are constrained at the left end (node 0), and a vertical dynamic force is applied on the right end (node 10) to induce vibration. Using the Newmark method, the vibration response of the beam under the external force shown in Fig. 4.6 is calculated. The total calculation duration is 2s, and the time step is 0.0001 s. To simulate observation data with noise, different levels

of Gaussian noise are added to the calculation results according to Eq. (4.26).

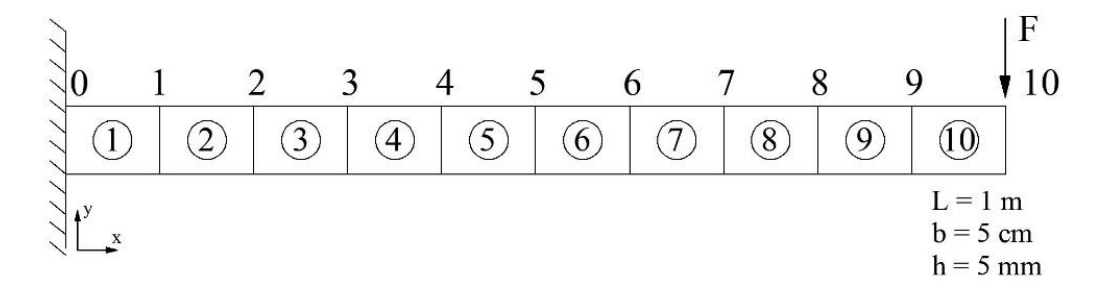


Figure 4.5 Finite element model of the cantilever beam

Let us first consider the case where the point of force application is known, i.e., the L matrix is determined. The calculated vertical acceleration data of nodes 5 and 9 are used as the observation data, with noise levels of 0%, 1%, 5%, and 10%, respectively. According to the L-curve test, the weight  $\alpha$  of the regularization term is set as  $10^{-6}$ , and the weight  $\beta$  of the L matrix norm is set to 0. The Adam optimizer with a learning rate of 0.001 is used to minimize the total loss function, and the number of iterations is 10,000.

Since the input data has 20,000 time steps and 22 degrees of freedom, it cannot be directly calculated as a single window due to our computer memory limitations. Therefore, the calculation is performed in windows of 1,000 time steps with a 50% overlap rate, resulting in a total of 40 windows covering the 2-second duration. Using the input data with different noise levels, the external force is successfully reconstructed as shown in Fig. 4.6. The relative L2 errors of the reconstructed external force compared to the exact data with 0%, 1%, 5%, and 10% noise input are 2.240%, 4.090%, 12.594%, and 23.990%, respectively. It is found that as the noise level in the data increases, the

error in the reconstructed force also increases. At low noise levels ( $\leq 1\%$ ), the PI-MP method can accurately reconstruct the external force time series.

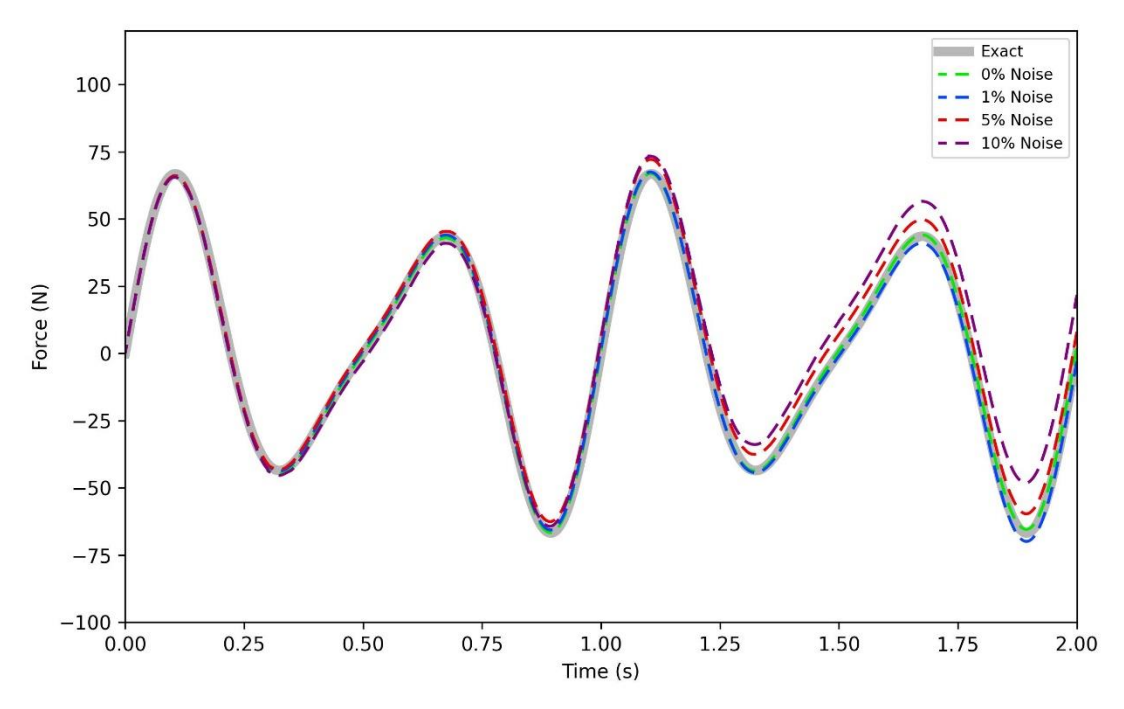


Figure 4.6 Reconstructed external force with input data of different noise levels

With the reconstructed external forces shown in Fig. 4.6, the unmeasured node responses of the cantilever beam can be reconstructed by following Eq. (4.14). For example, Fig. 4.7 shows the predicted vertical displacements of all nodes and the errors in the predicted values when using 1% noise input data. Fig. 4.7 shows that the reconstructed displacements from the PI-MP method are highly consistent with the exact values.

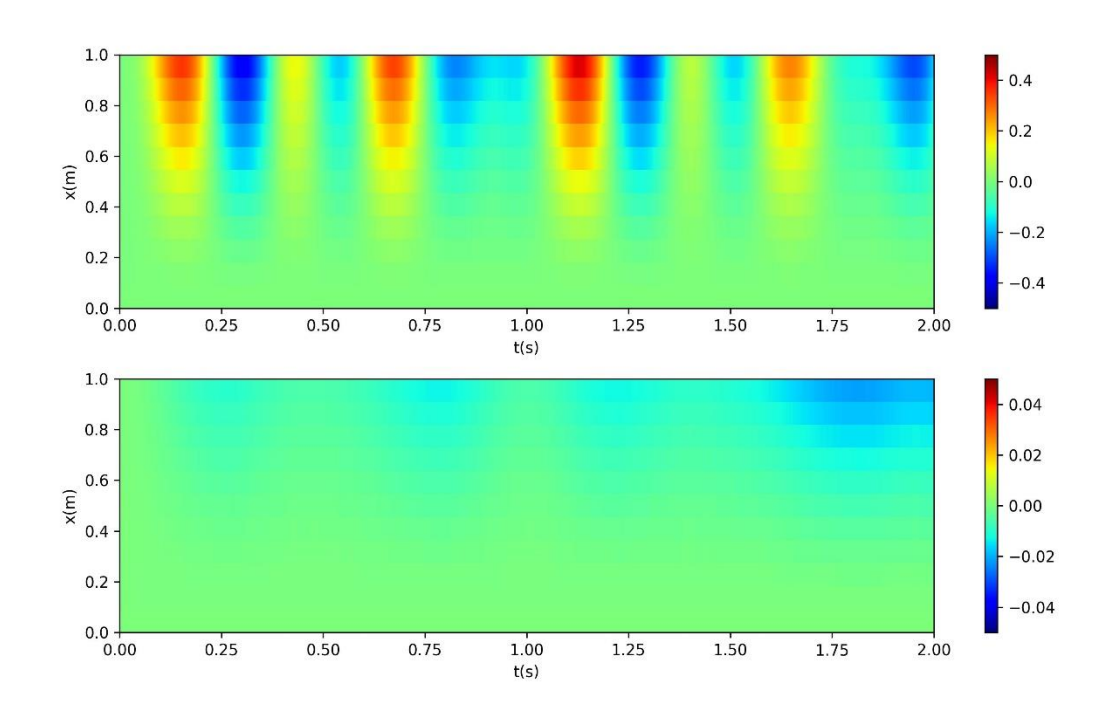


Figure 4.7 Reconstructed vertical displacement (top) of the cantilever beam and error in the reconstructed vertical displacement (bottom)

## 4.4.3 Plane truss

Consider a two-dimensional plane truss system composed of 15 rods as shown in Fig. 4.8. Each rod is 10 m long and made of steel with a density of  $7850 kg/m^3$  and an elastic modulus of 210 GPa. The cross-section of the rods is 5 cm\*5 cm. The truss is supported at the left and right corners as the lateral and vertical displacements of nodes 0 and 4 are fixed. A finite element model of this truss is established with 9 nodes and 18 degrees of freedom. Truss members are considered as 2-node linear elements in the X-Y plane with consistent mass matrices. The damping ratio of the first two modes of the truss is set to 0.5%. The truss vibrates under the action of a force at a random location. The Newmark method is used to calculate the vibration response of the truss

as the observation data, with a duration of 1 s and a time step of 0.0001 s. The vertical acceleration data of nodes 5 and 6 with 1% noise is used as observations. Since the position of the force is unknown, the PI-MP method is used to first discover the exact *L* matrix to determine the force position and then reconstruct the time series of the external force.

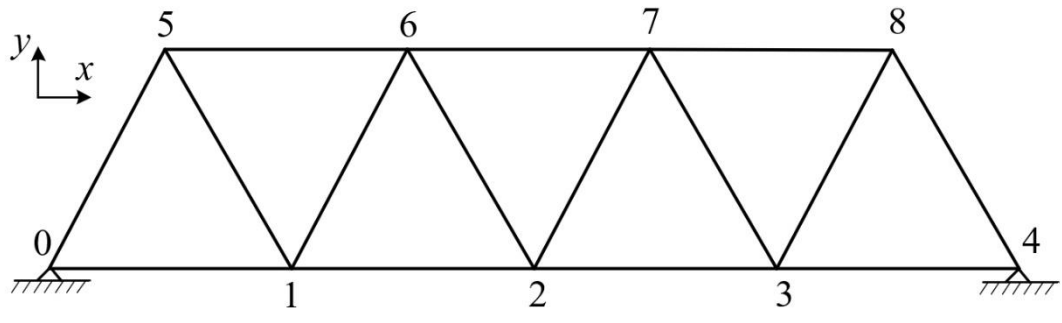


Figure 4.8 A plane truss system

Due to computer memory limitations, the calculation is performed in windows of 1,000 time steps with a 50% overlap, resulting in a total of 20 windows. The first window is used to discover the L matrix, and then the entire external force is reconstructed by sequentially calculating 20 windows. According to the L-curve test, the weight of the regularization term  $\alpha$  in the loss function is set to  $10^{-8}$ , and the weight of the L matrix norm  $\beta$  is set to 0.01. The iteration number in each window is 10,000. The process of discovering the force position is shown in Fig. 4.9.

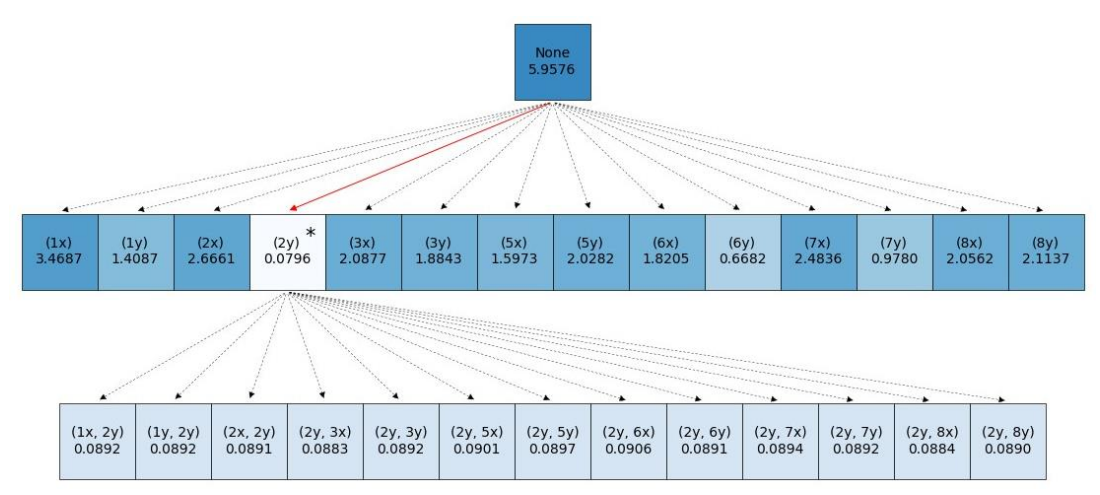


Figure 4.9 The search process of the force position

(The nodes and directions of the force settings are in brackets, and the numbers below are the corresponding loss values)

Through the search process shown in Fig. 4.9, it is successfully discovered that the force is acting on node 2 in the y direction. Using the discovered L matrix, the entire time series of the external force is reconstructed through 20 windows and plotted in Fig. 4.10.

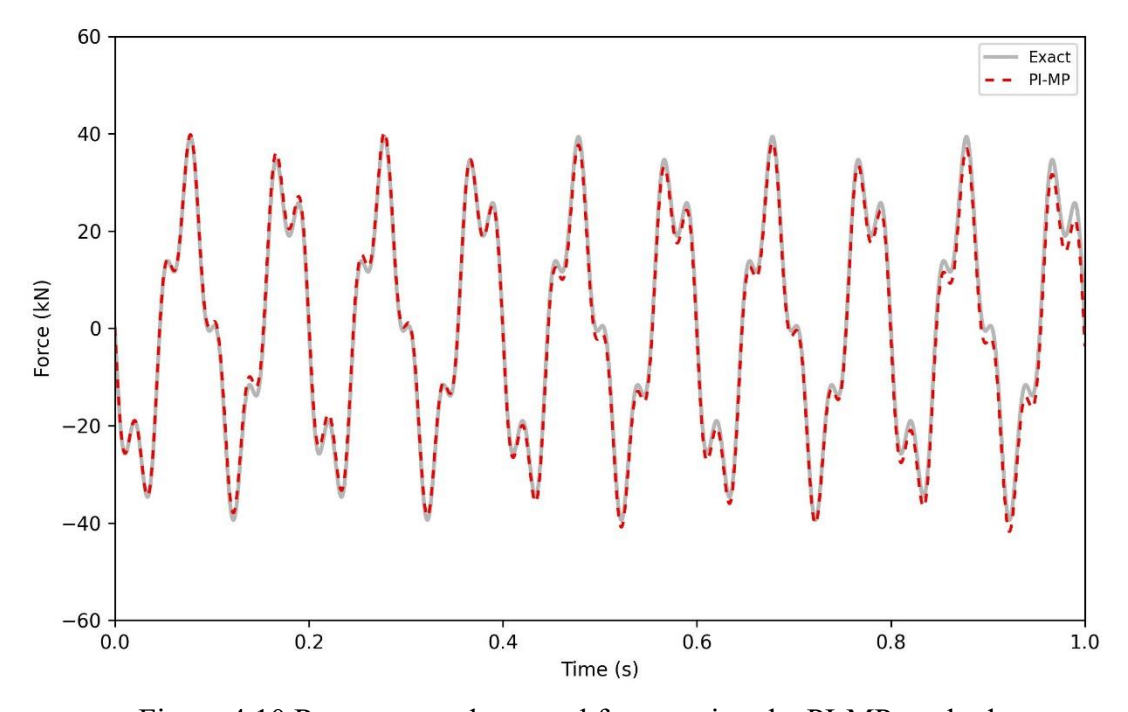


Figure 4.10 Reconstructed external forces using the PI-MP method

From Fig. 4.10, it is shown that the PI-MP method accurately reconstructs the entire time series of the external forces. Using the reconstructed external force, other unmeasured responses of the truss are also accurately reconstructed, such as the vertical displacement and velocity of nodes 2 and 3, as shown in Fig. 4.11.

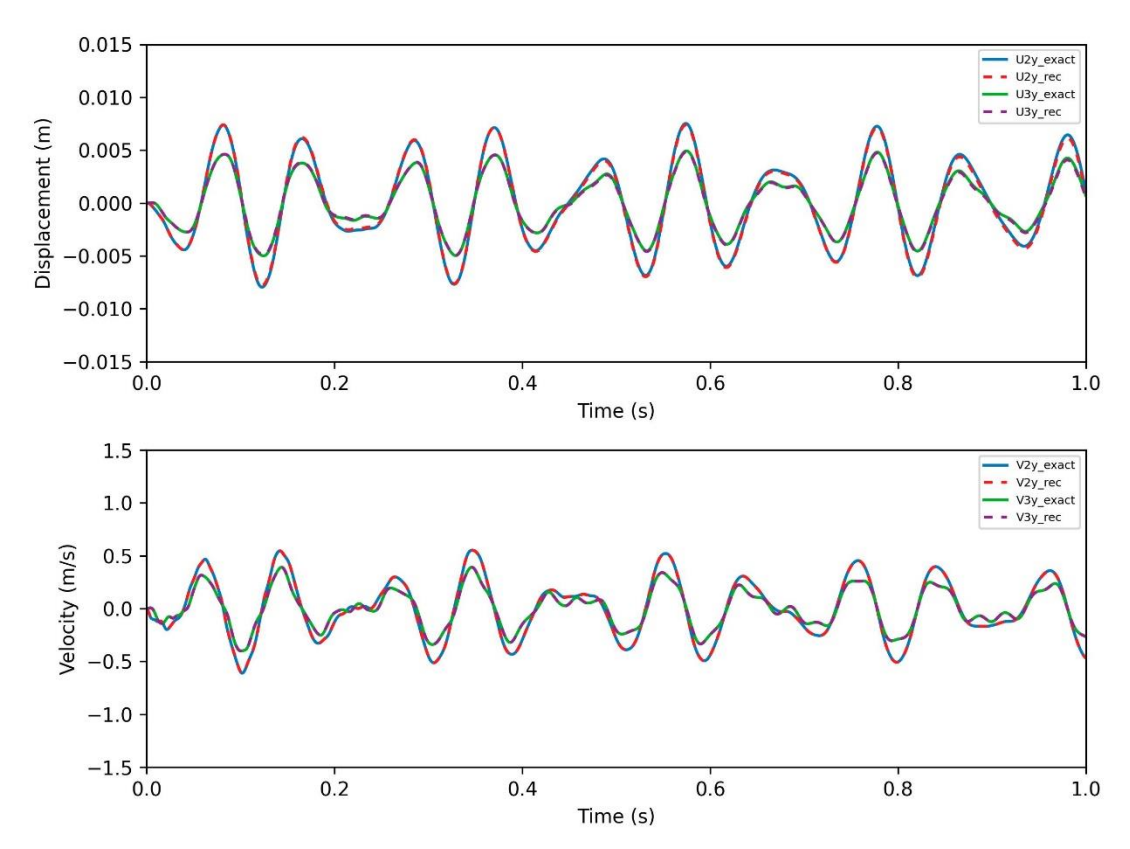


Figure 4.11 Reconstructed vertical displacement (top) and velocity (bottom) of nodes 2 and 3

# 4.5 Experimental validation

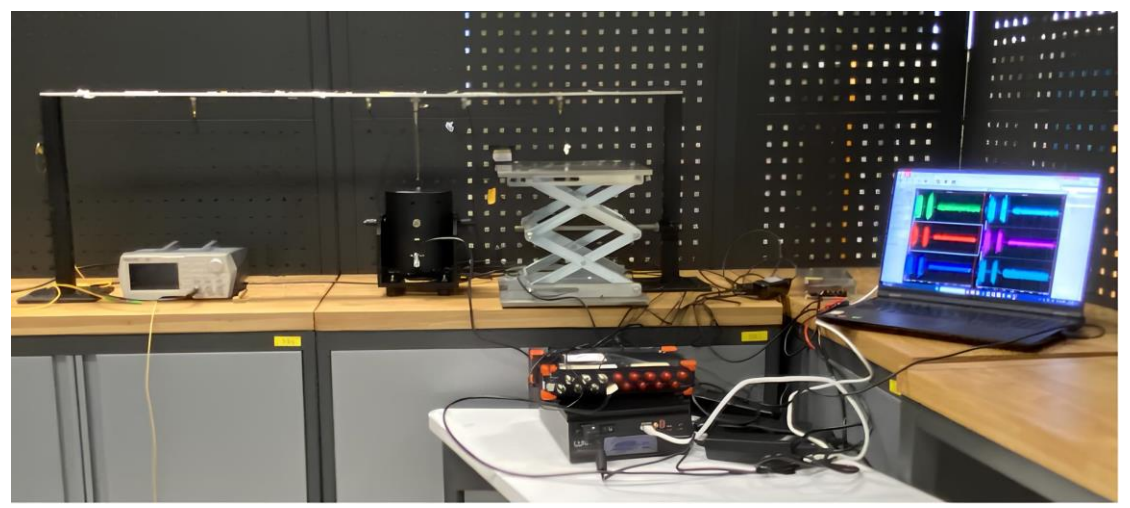


Figure 4.12 Vibration test of a beam

A vibration test of a beam is carried out in the laboratory as shown in Fig. 4.12. The mechanical model of the beam is also shown in Fig. 4.13. The total length of the beam is 130 cm, and the free section length is 126 cm. The beam width is 31 mm, and the thickness is 5 mm. The material of the beam is aluminum alloy with a density measured as  $2774 \, kg/m^3$  and an initial elastic modulus set to  $68.5 \, GPa$ . The damping of the structure is set as C = a \* M + b \* K, where a and b are the damping parameters to be determined. The beam is fixed to the supports with bolts at the left and right ends. Four accelerometers are installed on the beam to measure the vertical vibration, and a shaker equipped with a force sensor is installed to generate dynamic force to make the beam vibrate. The specific location and mass of the sensors are shown in Table 4.3. All acceleration and force data are collected by a Dewesoft data logger with a sampling frequency of 5,000 Hz.

A finite element model of the beam is built by discretizing the free section of the

beam into 2 cm beam elements. The beam element is a 2-node Euler-Bernoulli beam element with a consistent mass matrix. The model has a total of 63 elements, 64 nodes, and 128 degrees of freedom. The vertical displacement of the leftmost node 0 and the rightmost node 63 is constrained to 0. Semi-rigidity at the two supports is considered as rotational springs. The weights of the four accelerometers and the force sensor are also considered as additional masses at the nodes in the finite element model.

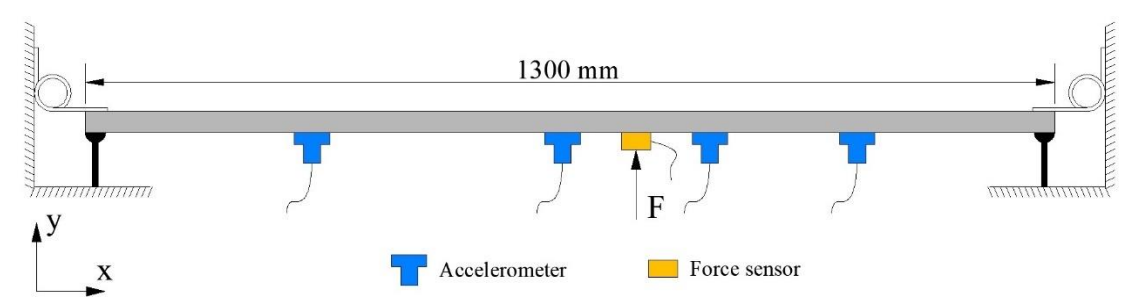


Figure 4.13 Mechanical model of the test beam

Table 4.3 Sensor positions and weights

Sensor	x	Weight		
		(Including mounting base)		
Accelerometer 1	30 cm	24.3 g		
Accelerometer 2	64 cm	24.3 g		
Accelerometer 3	84 cm	24.4 g		
Accelerometer 4	104 cm	24.6 g		
Force sensor	74 cm	24.4 g		

We first input a white noise excitation to the beam and record the structural response measured by four accelerometers for finite element model update. The frequency response function curve of the measured acceleration data is calculated, and the 10-100 Hz interval is set as the benchmark to update the parameters of the finite element model. Fig. 4.14 shows the FRF curve calculated by the finite element model after the model update and the measured benchmark. Table 4.4 shows the parameter

settings after the model update.

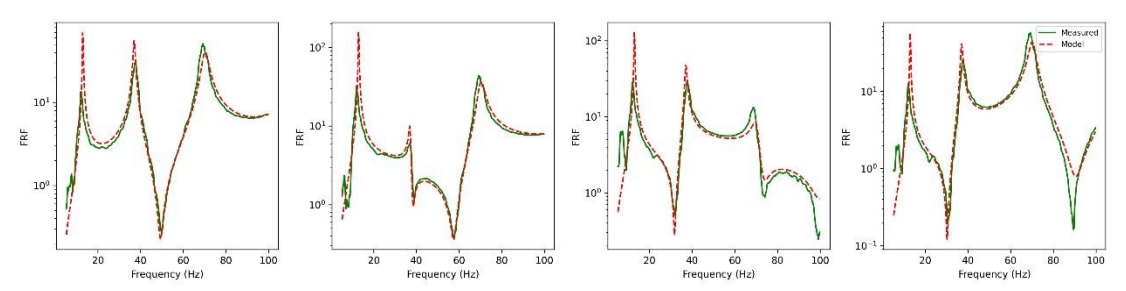


Figure 4.14 Measured FRF and calculated FRF from FEM model

(from left to right: accelerometers 1, 2, 3, 4)

Table 4.4 Parameter settings after model update

Parameter	Initial value	Scaling factor	Updated value
Elastic modulus	68.500 <i>GPa</i>	0.8764	60.03 <i>GPa</i>
Damping coefficient a	0.005	1.6189	0.00809
Damping coefficient b	0.005	0.0184	0.0000919
Rotational stiffness of left support	100 kN/m	0.0650	$6.50 \ kN/m$
Rotational stiffness of right support	100 kN/m	0.0946	9.46 <i>kN/m</i>

After the model is updated, we input another white noise excitation to the structure again and measure the acceleration responses with the four accelerometers as shown in Fig. 4.15. The data duration is 0.1 s, the sampling frequency is 5,000 Hz, and the data length is 500 time steps. The structural vibration collected by accelerometers 1, 2, and 3 as the input of the PI-MP method is used to reconstruct the dynamic force applied by the shaker to the structure. The force data collected by the force sensor is used as the benchmark for the force reconstruction result.

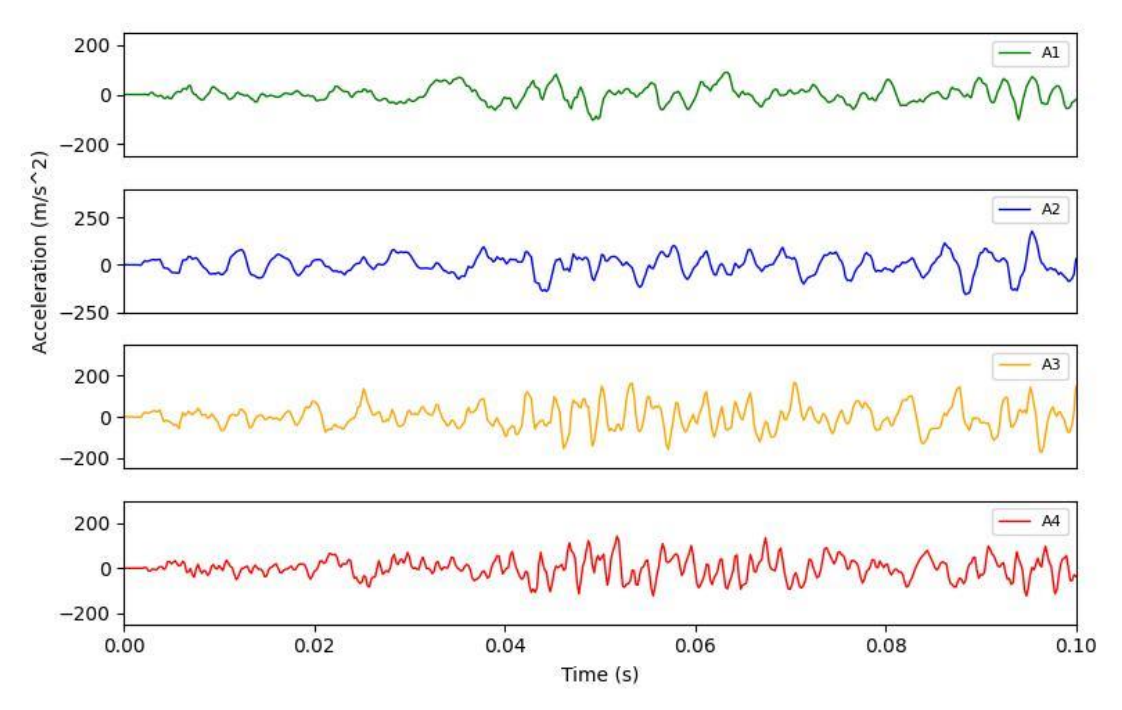


Figure 4.15 Measurement values from four accelerometers

We divide the above 500 time steps into 10 windows of length 100 time steps and an overlap of 50%. In each window, a neural network model with 2 hidden layers of 100 neurons is employed to predict the unknown external force, and the activation function of the neural network model is the sine function. The optimizer Adam with a learning rate of 0.001 is employed to minimize the loss function. In the loss function, according to the L curve test, the weight  $\alpha$  of the regularization term is set to  $10^{-8}$ . Since the L matrix has been determined, the weight  $\beta$  of the L matrix norm is set to 0. In each window, the neural network model is trained for 20,000 iterations.

The reconstructed external force and measured values are shown in Fig. 4.16. It is shown that the reconstructed external force is highly consistent with the measured value, but there are still some numerical errors, which may come from the finite element model

and measurement noise. Using the reconstructed external force, the acceleration response at accelerometer 4 is also successfully reconstructed, which is shown in Fig. 4.17.

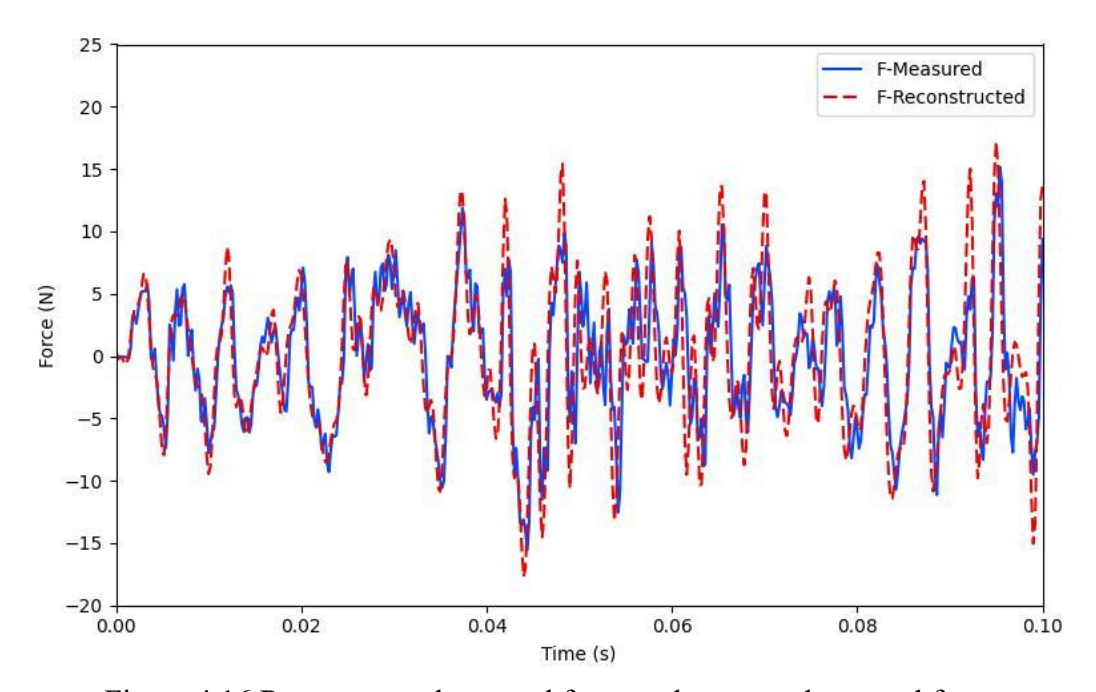


Figure 4.16 Reconstructed external force and measured external force

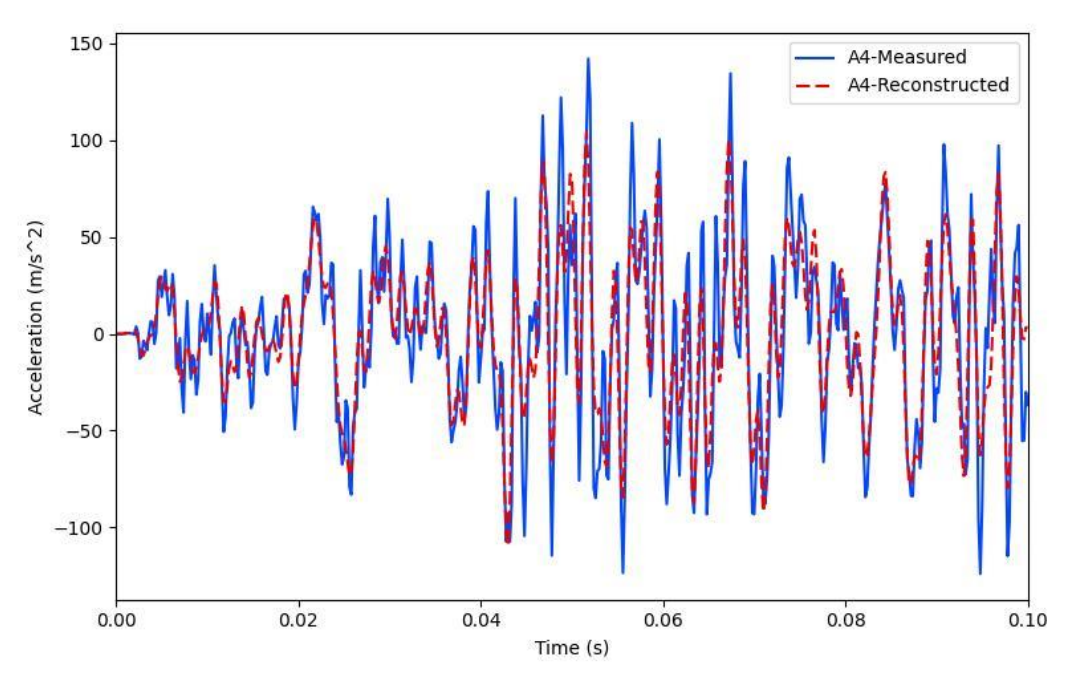


Figure 4.17 Reconstructed acceleration response and measured values of

accelerometer

## 4.6 Summary

This study presents a novel method called physics-informed Markov parameters (PI-MP) for reconstructing structural dynamic forces and responses by integrating physics-informed neural networks (PINNs) and Markov parameters in the state space. In the PI-MP framework, the strong representational capability of deep neural networks is leveraged to predict unknown external forces. By simultaneously minimizing a loss function based on Markov parameters and a regularization term of the second-order derivative of predicted forces, PI-MP successfully couples the measured structural responses to reconstruct the unknown forces while maintaining smoothness and avoiding noise over-fitting. Using the reconstructed forces and the Markov parameters, all the dynamic responses of the structure can also be reconstructed. Furthermore, by adding an L1 norm term of the force mapping matrix to the total loss function and designing an optimization strategy coupling a greedy algorithm and the Adam optimizer, PI-MP can successfully locate the force positions when they are unknown.

Through a four-degree-of-freedom case, PI-MP is demonstrated to achieve more accurate force reconstruction results even in noisy inputs than traditional methods such as ordinary least squares and Tikhonov regularization. Increasing the number of response measurement points and moving the measurement points closer to the force application point can increase the accuracy of PI-MP reconstruction. Additional numerical cases of a cantilever beam and a planar truss, as well as an experimental case on a beam, have also been conducted to demonstrate the effectiveness and accuracy of

the proposed method.

# Chapter 5 PI-FFNN for vibration based structural damage identification with unknown external forces

## 5.1 Introduction

In-service infrastructure inevitably suffers from damage caused by environmental factors and inherent material degradation. These external or internal damages lead to a decline in the mechanical performance of the structure and pose a threat to its normal functionality. Structural health monitoring technologies, which can timely detect and assess the severity of damage at an early stage, have been widely applied in various infrastructures. By utilizing SHM technologies, damaged engineering structures can be repaired in a timely manner, which can reduce maintenance costs and prevent structural failures, thereby improving the safety and reliability of structural systems. Over the past decade, vibration-based damage detection (Avci et al., 2021; Das et al., 2016; Sun et al., 2023) has been extensively researched due to its ease of implementation and capability for global damage detection. These vibration-based damage detection methods are based on the fact that structural damage will lead to changes in the vibration characteristics of the structure, which is reflected in the natural frequency (Yang & Wang, 2010), mode shape (Yazdanpanahla & Seyedpoor, 2015) and vibration data (Shang et al., 2021). Based on this, researchers have conducted studies to try to explore the vibration features that represent the occurrence of structural damage. The majority of existing methods can be broadly divided into two categories: physics-driven

methods and data-driven methods.

Physics-driven methods primarily exploit the physical laws of the structural system, such as motion equations and constitutive models, to extract information about the structural damage evolution from measured data. The most common practice of physics-driven structural damage identification method is finite element model (FEM) updating (Arora, 2011). In the model updating approach, a FEM that describes the physical laws of the structural system is first constructed to predict the dynamic response of the structure with measured external forces input. In the FEM, the structural mechanical parameters are updated by minimizing the difference between the predicted vibration response and the measured data. By comparing the updated model parameters with the parameters of the structural health state, whether the structure is damaged can be identified. This process was carried out by (Hua et al., 2009) to detect structural damage in cable-stayed bridges and achieved satisfactory results. Additionally, Jafarkhani and Masri (Jafarkhani & Masri, 2011) developed a stochastic optimization algorithm to improve the global optimization process of model updating, which enhances the accuracy of damage identification. Model updating has also been utilized in (Mousavi et al., 2021), with the detection results validated through numerical and laboratory tests.

Although the physics-driven approach has been extensively studied and has formed a mature implementation process, as mentioned in (Ereiz et al., 2022), the foundation of the physics-driven approach relies on an accurate FEM model that can

correctly reflect the structural vibration characteristics. However, this is difficult to achieve due to the uncertainties and complex interactions in real structural systems. Another limitation of the physics-driven approach is that it is an input-output damage detection method (Wang et al., 2018), which means that not only the vibration response of the structure but also the external force input of the structure needs to be accurately measured. However, in-service engineering structures are often affected by complex external forces, and it is impossible to obtain precise information on all the external forces applied. In addition, due to the limitations of the observation equipment, the noise and uncertainty in the measurement data will also seriously affect the performance of physics-driven damage identification (Hua et al., 2012).

On the other hand, data-driven methods represented by machine learning (ML) have developed rapidly in recent years. ML models such as support vector machines (Gui et al., 2017) and neural network models (Pan & Yang, 2020), rely on measurement data for training, studying, and solving structural damage identification by considering it as a pattern recognition problem. Unlike physics-driven models, ML methods no longer rely on precise physical models but directly discover the potential relationship between the vibration characteristics of observed data and structural damage. This feature enables ML models to identify structural damage more accurately than physics-driven methods under the influence of fuzzy physical models and noisy measurement data. For example, Ghiasi et al. (Ghiasi et al., 2016) took advantage of this feature of ML methods and built a least square support vector machine to detect damage in a four-

story steel structure and a 120-bar dome truss. Delgadillo and Casas (Delgadillo & Casas, 2022) also successfully discovered the degradation of the mechanical properties of the bridge structure from noise measurements based on the ML method of the improved completed ensemble empirical mode decomposition.

Although data-driven methods have made some promising progress, the drawbacks from data scarcity, low fidelity, and tedious feature engineering still pose challenges to their reliability. Generally, training a stable and reliable ML model requires a large amount of training data, which is often difficult to obtain in practical engineering. Even if researchers collect enough training data, the generalization ability of machine learning models is easily affected by the imbalance of damage severity. For example, for engineering structures that are frequently maintained such as rails and bridge cables, vibration measurement data of the healthy state of the structure is easy to obtain, while training data of multiple damage states is very scarce. In addition, noise from sensors, acquisition equipment, and the environment can also have a negative impact on the accuracy of model predictions (Ding et al., 2019). The uncertainty in model predictions comes not only from noisy training data, but also from the inherent 'black' box mechanism of machine learning models, where the physical laws of the model are unknown and the predicted output depends on data fitting (Rudin, 2019). Lastly, how to select appropriate damage-related features and machine learning models is also an open question worth studying for data-driven methods (Peng et al., 2022). Currently, this problem usually relies on researchers' prior knowledge and experience to determine, which also poses challenges to the application of ML models.

In order to address the above challenges in existing ML methods, a promising solution is to incorporate physical knowledge into the deep learning process, which is also called physics-informed machine learning (PIML). By seamlessly integrating the ML framework with physical information described as prior information of various equations, PIML has demonstrated strong applicability in many fields of physics and engineering. Recently, the application of PIML in dynamic response prediction and structural damage identification in structural engineering has also received increasing attention. (Lai et al., 2021) exploits a new physics-informed neural ordinary differential equations (NODE) to perform linear/nonlinear structure identification. The research results show that the NODE model integrating physical information can successfully learn the highly nonlinear behaviors of complex systems. (Jeong et al., 2023) proposes a novel physics-informed neural network-based topology optimization framework that can obtain optimized topology without labeled data or FEA, even in various types of complex domains. (R. Zhang et al., 2020b) introduces an innovative physics-informed multi-LSTM network model for metamodeling of nonlinear structural systems with scarce data. Experimental results show that embedded physics can alleviate the overfitting problem in regular LSTM models, reduce the need for large training datasets, and improve the robustness of trained models, leading to more reliable predictions with extrapolation capabilities. (Fangyu Liu et al., 2023) applied a physics-informed long short-term memory (PI-LSTM) network to structural response modeling by

incorporating physics constraints into regular LSTM. Through an SDOF system and a six-story building case, the proposed PI-LSTM network exhibited a more concentrated and higher accuracy performance.

Although these developed PIML methods for structural dynamics successfully integrate physical information and machine learning frameworks to enable models to be trained from small amounts of observed data. However, these methods still cannot get rid of their dependence on data and are still semi-supervised or supervised learning methods. In these existing PIML methods for damage identification, training data with structural damage labels still need to be obtained from simulations or laboratory tests, which significantly limits the applicability of such algorithms to actual engineering. To address these limitations, this study proposes a physics-informed Fourier feature neural network (PI-FFNN) framework to reversely identify the structural damages from vibration response observations without any damage labels and force measurement. In this framework, a Fourier-featured neural network is employed to represent the unknown external force input. The structural damage index is embedded in the neural network model as a trainable parameter and trained together with the model parameters. The physical information described as the governing equations of structural vibration is integrated into the framework as prior information by building a mapping relationship between external forces, structural parameters, and calculated vibration responses. The neural network model and damage index are trained by minimizing the difference between the calculated structural response and the vibration observation. The PI-FFNN framework is an output-only detection method that does not require measurements of external forces as input. By integrating the governing equation into the neural network model, the PI-FFNN framework can complete stable training without relying on any labeled data. The basic mechanism of PINNs in the framework also enhances the robustness of the PI-FFNN framework to noisy measurement data.

The main contributions of this study are: (1) A new neural network framework that incorporates physics knowledge into deep learning to identify structural damage without damage label data. This physics and data-coupled architecture can explore and retain damage-sensitive characteristics while complying with the physical laws of the structural system. (2) The proposed method does not require external force measurement. In contrast, the force can be reconstructed from the output of the FFNN model. (3) The embedding of the Fourier feature layer in the neural network enhances the multi-frequency feature capability of the PINNs model, which can improve the model's representation of the complex external force. (4) Numerical studies on beam and plane truss structures and experimental tests have demonstrated the accuracy and stability of the proposed PI-FFNN framework. Test results prove that the PI-FFNN can accurately detect structural damage from only a small amount of vibration measurement even noise.

The rest of this study is organized as follows: In Section 2, the basics of structural motion equations and PINNs are briefly introduced. Section 3 detailly introduces our proposed PI-FFNN framework for damage detection. Two numerical experiments are

carried out in Section 4 and a laboratory test is presented in Section 5. Lastly, the whole study is concluded in section 6.

# 5.2 Background

# 5.2.1 Motion equation of structural system

The motion equation of a linear structure system with n degrees of freedom can be expressed as

$$M\ddot{x}(t) + C\dot{x}(t) + Kx(t) = L \cdot F(t)$$
 (5.1)

where M, K, and C are the mass matrix, stiffness matrix, and damping matrix of the structure, F(t) is the external forces vector applied to the structure, and L is the mapping matrix for the forces, which is a diagonal Boolean matrix to determine where the force acts.  $\ddot{x}$ ,  $\dot{x}$ , and x represent the acceleration, velocity, and displacement responses of the structure, respectively. Traditionally, numerical integration methods are utilized to obtain the vibration response of the structure by solving Eq. (5.1). Among these numerical methods, the Newmark-beta method is widely applied due to its good numerical stability and ease of use. In this study, the Newmark-beta method is also adopted to calculate the vibration response of the structure. At each time step in the Newmark-beta method, the following four equations are established as

$$M\ddot{x}_n + C\dot{x}_n + Kx_n = f_n \tag{5.2}$$

$$\dot{x}_{n+1} = \dot{x}_n + (1 - \gamma) \, \Delta t \, \ddot{x}_n + \gamma \, \Delta t \, \ddot{x}_{n+1} \tag{5.3}$$

$$x_{n+1} = x_n + \Delta t \, \dot{x}_n + \frac{\Delta t^2}{2} ((1 - 2\beta) \, \ddot{x}_n + 2\beta \, \ddot{x}_{n+1})$$
 (5.4)

and

$$M\ddot{x}_{n+1} + C\dot{x}_{n+1} + Kx_{n+1} = f_{n+1} \tag{5.5}$$

Here,  $0 \le \gamma \le 1$  and  $0 \le 2\beta \le 1$  are the control parameters of the Newmark-beta method. By solving the above four equations, the structural response  $(x_{n+1}, \dot{x}_{n+1}, \ddot{x}_{n+1})$  can be recursively calculated using the current structural state  $(x_n, \dot{x}_n)$  and external force input  $(f_n, f_{n+1})$ . By setting different value combinations of  $\gamma$  and  $\beta$ , the Newmark-beta can become an explicit or implicit method, such as the explicit central difference scheme  $(\gamma = 0.5, \beta = 0.25)$ .

Vibration-based structural damage identification usually assumes that structural damage will cause changes in structural parameters (such as stiffness, mass, and damping), which in turn will change the vibration characteristics of the structure. In this study, the stiffness reduction is considered as damage to the structure. A set of scalar variables is utilized to represent the stiffness reduction rate of the given structure. The damaged stiffness is updated as

$$k_i^d = (1 - z_i) * k_i^0 (5.6)$$

Here,  $k_i^d$  is the damaged stiffness value of the *i*th element and  $k_i^0$  is the initial stiffness value. The  $z_i$  represents the stiffness reduction index, ranging from 0 (no damage) to 1 (complete damage). In general, the vibration-based structural damage detection method is designed to iteratively update the physical parameters by minimizing the differences between the calculated vibration characteristics (frequency and mode shape) or time series with the measured response. However, in the physics-

data coupling method, the calculated structural response will not only be consistent with the measured data, but also inherently satisfy the governing equation, thereby improving the accuracy and reliability of damage identification.

### 5.2.2 Physics informed neural networks

PINNs (Raissi et al., 2019) is a deep learning framework designed to solve forward and inverse problems of linear and nonlinear partial differential equations as

$$D(u(x,t),x,t;\theta) = f(u(x,t),x,t)$$
(5.7)

Here, D is a differential operator controlled by the parameter  $\theta$ . u(x,t) is the solution of the equation dependent on variables x and t, and f is the source term. In the forward problem of partial differential equations, where boundary and initial conditions are imposed to calculate the solution of u, the PINNs framework utilizes a neural network to approximate u(x,t) with inputs x and t. A loss function is formulated based on the residual of the governing equation, defined as

$$\mathcal{L}_{f} = \sum_{i=1}^{N_{f}} \left[ D\left(u_{pred}(x_{i}^{f}, t_{i}^{f}), x_{i}^{f}, t_{i}^{f}; \theta\right) - f\left(u_{pred}(x_{i}^{f}, t_{i}^{f}), x_{i}^{f}, t_{i}^{f}\right) \right]^{2}$$
 (5.8)

Here,  $(x_i^f, t_i^f)$  are collocation points sampled from the equation's definition domain to measure the residual error of the model predictions  $u_{pred}$  on the governing equations. Additionally, a constraint-based loss function is defined to measure the residual error of the model prediction on the constraints as

$$\mathcal{L}_{c} = \sum_{i=1}^{N_{c}} \left[ u_{pred}(x_{i}^{c}, t_{i}^{c}) - u_{exact}(x_{i}^{c}, t_{i}^{c}) \right]^{2}$$
 (5.9)

Here,  $(x_i^c, t_i^c)$  are points sampled on the constraints, and  $u_{exact}$   $(x_i^c, t_i^c)$  represents the exact solution obtained from these constraints. The total loss function of the PINNs

model combines both losses as

$$\mathcal{L}_{pinns} = \mathcal{L}_f + \mathcal{L}_c \tag{5.10}$$

By employing a gradient descent-based optimizer to minimize  $\mathcal{L}_{pinns}$ , the neural network model can be trained so that the model output can gradually satisfy both the governing equation and the defined constraints, thereby approaching the exact solution of the equation.

In the PINNs framework for inverse problems, the objective is to identify unknown parameters  $\theta$  from measurement data while ensuring that the underlying physical laws are satisfied. The inverse problem can be formalized as modifying the loss function to incorporate both the data-driven approach and the physics-informed constraints. To achieve this, a data loss function  $\mathcal{L}_d$  that quantifies the difference between the predicted solution from the neural network  $u_{pred}(x_i^d, t_i^d)$  and the observed data  $u_{obs}(x_i^d, t_i^d)$  is defined as

$$\mathcal{L}_{d} = \sum_{i=1}^{N_{d}} \left[ u_{pred}(x_{i}^{d}, t_{i}^{d}) - u_{obs}(x_{i}^{d}, t_{i}^{d}) \right]^{2}$$
 (5.11)

In addition to the data loss, the governing equation loss  $\mathcal{L}_f$  defined in Eq. (5.11) is also included to ensure that the predicted solution adheres to the physical laws. The total loss function of the PINNs model for inverse problems is constructed as

$$\mathcal{L}_{pinns} = \mathcal{L}_f + \mathcal{L}_d \tag{5.12}$$

The unknown parameter  $\theta$  in Eq. (5.10) is initialized and trained together with the neural network model as a trainable variable. By minimizing  $\mathcal{L}_{pinns}$  using a gradient descent-based optimizer, the PINNs can not only learn to approximate the

observed data but also adjust the parameters  $\theta$  to fit the governing equation, which means that parameters  $\theta$  will approach the exact value.

Based on the principles introduced above, the integration of data-driven insights with physical principles makes PINNs a powerful tool for solving forward and inverse problems across various applications, including fluid dynamics (Cai, Mao, et al., 2021b), material analysis (E. Zhang et al., 2022), and other fields where data and physical laws intersect.

# 5.3 Methodology

Consider a multi-degree-of-freedom (MDOF) structural system with stiffness reduction damage. The goal of vibration-based structural damage identification is to inversely discover the location and severity of stiffness reduction using the measured vibration response. In this study, a PI-FFNN framework is proposed to achieve this goal by using physical information described by structural motion equations and vibration response measurements as input. The overall framework of PI-FFNN is shown in Fig. 5.1.

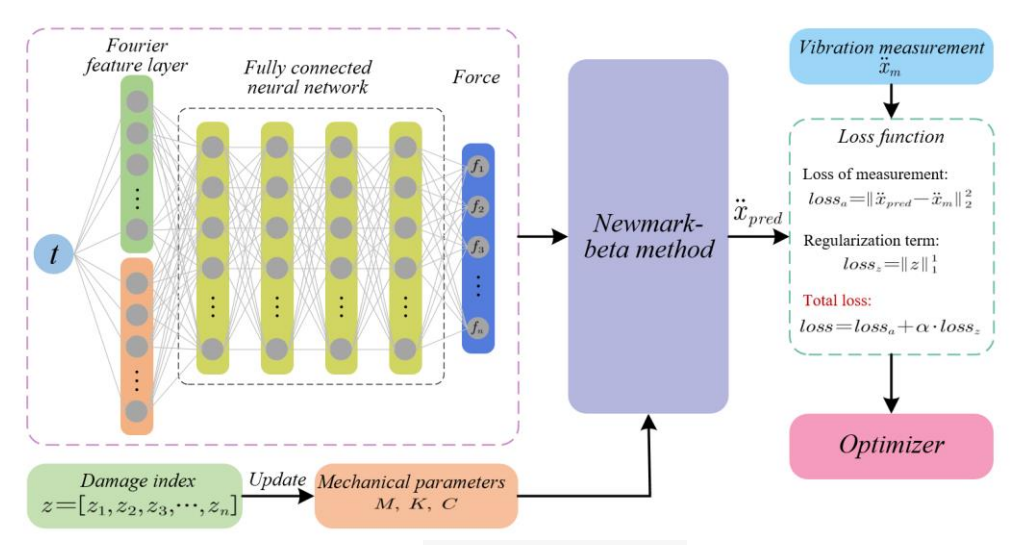


Figure 5.1 The overall framework of PI-FFNN

In Fig. 5.1, it is shown that the PI-FFNN framework takes vibration response measurements  $\ddot{x}_m$  as inputs, and outputs the identified damaged structural stiffness  $K^d$  and the reconstructed external force  $F^{rec}$ . The core component of the PI-FFNN framework is a Fourier feature neural network (FFNN) model, which aims to inversely reconstruct the external force with physical information of the motion equation parameterized by mechanical parameters  $\theta = [M, K, C]$ . The physical relationship of the FFNN model can be expressed as  $FFNN(\ddot{x}_m, \theta) \rightarrow F^{rec}$ . Spectral bias (Chai et al., 2024; Xu et al., 2024) is a well-known defect of neural networks, which is manifested in that neural networks preferentially learn the low-frequency components in the data and ignore the high-frequency components. Because the external force of the structure is usually a mixture of multiple frequency components, using a traditional PINNs model to represent the external force is prone to the difficulty of spectral bias. The FFNN proposed in (Jin et al., 2024; Sallam & Fürth, 2023; Song & Wang, 2023; Wang et al.,

2021) has been proven to effectively eliminate the spectral bias of the neural network by using a Fourier feature layer to extract the broad frequency characteristics of the input data. Inspired by this, a Fourier feature layer is embedded in the PINNs model in the proposed method to balance the convergence speed of various frequencies, thereby reducing the spectral bias and improving the overall model's representing performance. Specifically, the Fourier feature layer is implemented by

$$L_{FF}(t,W) = \begin{bmatrix} \cos(2\pi W^T t) \\ \sin(2\pi W^T t) \end{bmatrix}$$
 (5.13)

Here, the input of the Fourier feature layer is t, and the output is multiple frequency features of t. The trainable parameter of the Fourier feature layer is weight W, which is initialized as a Gaussian distribution  $N(0, \sigma^2)$ , where  $\sigma$  is the hyperparameter controlling the value distribution of W. In the proposed PI-FFNN framework,  $\sigma$  is determined according to the frequency range of the structural vibration measurements.

Through Eq. (5.13), multiple frequency features of input t are established. Then, these features are input to a fully connected neural network (FCNN) model, which outputs the reconstructed structural external force  $F^{rec}$ . The FCNN model has  $L_{NN}$  hidden layers, each with  $H_{NN}$  neurons. The width of the Fourier layer, i.e., the size of W, is also set to the width H. In addition, a damage index vector z is defined to update the damaged mechanical parameters according to Eq. (5.6). The values of z are limited to [0, 1]. Using these reconstructed external forces and updated structural mechanical parameters, the Newmark-beta method is employed to calculate the structural response  $\ddot{x}_{pred}$  and maintain the differentiability of the structural response output to the neural

network parameters, which will be utilized for the backpropagation of the loss function. The physical relationship of the Newmark-beta method can be expressed as  $Newmark(F^{rec},\theta) \to \ddot{x}_{pred}$ . By calculating the residual between the structural response obtained from the Newmark-beta method and the vibration measurement, a loss function  $loss_a$  is defined as

$$loss_a = \frac{1}{N} \sum (\ddot{x}_{pred} - \ddot{x}_m)^2$$
 (5.14)

In addition, to improve the sparsity of the identification result of z and improve the robustness of PI-FFNN to noise, a regularization term of z is defined as

$$loss_{z} = \sum |z| \tag{5.15}$$

The loss function of PI-FFNN is set as the weighted sum of these two losses

$$loss = loss_a + \alpha * loss_z$$
 (5.16)

where  $\alpha$  controls the weight of the regularization term, which can be determined by analyzing the L-curve of  $loss_z / loss_a$  (Hansen & O'Leary, 1993). Using a gradient descent-based optimizer to update the parameters of the neural network and the damage index z by minimizing the loss, the structural response calculated by Newmark-beta will be close to the vibration response measurements  $\ddot{x}_m$ . In this way, the output of the neural network will reconstruct the external force of the structure, and the damage index can characterize the location and severity of damage in the structure. The specific implementation process of the PI-FFNN framework is illustrated in Algorithm 5.1.

**Algorithm 5.1:** The implementation process of PI-FFNN framework

**Input:** Initial parameters  $M^0$ ,  $K^0$ ,  $C^0$ , initial state  $u_0$ ,  $v_0$ , vibration measurement  $\ddot{x}_m$ , force mapping matrix L, vibration mapping matrix R, time step dt

**Parameter:** Neural network hyperparameters  $L_{NN}$ ,  $H_{NN}$  and  $\sigma$ , Newmark-beta parameters  $\beta$ ,  $\gamma$ , regularization weight  $\alpha$ , number of iterations  $N_{it}$  and learning rate  $l_r$ 

**Output:** Identified damage index  $z^{idf}$  and reconstructed external force  $F^{rec}$ 

- 1: Initialize z to an all zero vector. Set i = 1. Randomly initialize the FFNN model
- 2: while  $i \leq N_{it}$  do:
- 3: Forward propagation FFNN model to obtain the reconstructed force  $F^{rec}$ , and filter into  $F_L^{rec}$  with the mapping matrix L
- 4: Update the mechanical parameters as  $K^d = (1 z) \cdot K^0$
- 5: Calculate  $\ddot{x}_{pred}$  with Newmark-beta method and filter with mapping matrix R
- 6: Calculate the  $loss_a$ ,  $loss_z$  and sum as  $loss = loss_a + \alpha * loss_z$
- 7: Back propagate loss to calculate gradients of FFNN parameters and z
- 8: Employ the optimizer to update the FFNN model and z
- 9: Limit the value of z in the range [0, 1], update i = i + 1

#### 10: end while

11: Output the identified damage index  $z^{idf} = z$  and reconstructed force  $F_L^{rec}$ 

According to the above introduction, the PI-FFNN framework is established for identifying structural damage from vibration measurements without knowledge of the external force on the structure. The hyperparameters of the framework include parameter  $\sigma$  of the Fourier layer, the depth  $L_{NN}$  and width  $H_{NN}$  of the FCNN model, and the weight  $\alpha$  of the regularization term. This should also be noted that to ensure the solvability and uniqueness of this inverse problem, the number of structural vibration measurements must exceed the number of unknown forces acting on the structure.

In traditional numerical methods such as finite element analysis, both model parameters and external force input are required to calculate the response of the structure. Therefore, the damage identification method based on these numerical methods must input the measurement of the external force, which may not be feasible

in some practical projects. Other damage detection methods based on no external forces, such as the sensitivity method (H.-P. Zhu et al., 2014), usually use the physics model of the initial structural parameters to reconstruct the external force from part of the response and then use the reconstructed external force to update the damage index based on another part of the response. However, accurate structural parameters and accurate external force reconstruction are interdependent. Errors in structural parameters will lead to incorrect estimation of external forces, which may in turn increase the errors in structural parameter identification. This interdependent mechanism will reduce the convergence and stability of these traditional damage detection methods. In addition, the noise in vibration measurement will introduce errors to the reconstructed external forces, which will also affect the accuracy of damage identification. In the PI-FFNN framework, the reconstructed external forces and damage index are trained simultaneously. By using an optimizer to minimize these two errors simultaneously, the PI-FFNN framework can ensure the synchronous convergence of the interdependent force reconstruction and parameter identification processes. Compared with common supervised machine learning models for structural damage detection, by directly inputting the time domain signal of vibration responses, PI-FFNN can avoid the reliance on a large amount of measurement data, which can be costly in structural health monitoring. By using physical information to train the neural network model instead of relying on damage-labeled data, as an unsupervised model, PI-FFNN can also be better implemented on actual engineering structures whose damage labels are difficult to

obtain. In addition, feature engineering (Chegeni et al., 2022; Guo et al., 2020; Pan et al., 2019), which plays a key role in the performance of traditional machine learning models, is completely eliminated here to improve the ease of use of PI-FFNN.

### 5.4 Numerical cases

In this section, two numerical examples are carried out to verify the effectiveness and accuracy of the proposed PI-FFNN framework. The first is a cantilever beam structure case, where the hyperparameter settings of the PI-FFNN framework are explained and analyzed. In this case, the results of the PI-FFNN framework are also compared with the classical numerical algorithm without force measurement and the original PINNs model for damage identification and force reconstruction in noise-free and noisy data. In the second case, the stiffness reduction of a planar truss is identified, where the robustness of PI-FFNN to noise in the measured data is demonstrated.

### **5.4.1 Cantilever beam**

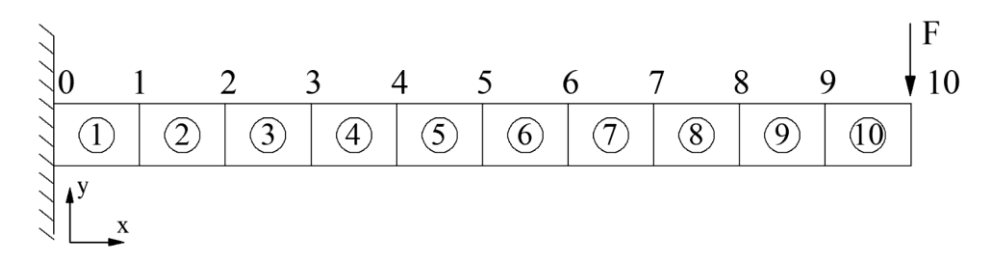


Figure 5.2 The finite element model of the cantilever beam

To demonstrate the performance of the proposed PI-FFNN framework, a cantilever beam is analyzed as a numerical example in this section. The length, width, and thickness of the cantilever beam are 1 m, 50 mm, and 5 mm respectively. The

material of the beam is steel with a density of 7850  $kg/m^3$  and an elastic modulus of 206 GPa. The finite element model of the beam is presented in Fig. 5.2, where the cantilever beam is numerically modeled as 10 elements, each of which is 0.1 m long. Using the finite element model, this cantilever beam is discretized into 10 elements. The beam elements are considered as two-node Euler-Bernoulli beams with a consistent mass matrix. This beam model has 11 nodes and 22 degrees of freedom (vertical displacement and rotation). The vertical displacement and rotation of the beam are constrained to 0 at the left end of the beam (node 0). A vertical dynamic force is applied to the right end of the beam (node 10) to make the beam vibrate. The damping of the beam is set to a damping ratio of 0.5% for the first two order natural frequencies. Elements 4 and 8 are assumed to be damaged with stiffness reduction of 15% and 20%, respectively. The first five-order natural frequencies of the intact and damaged beams are listed in Table 5.1. To obtain vibration response for model training, the explicit fourth-order Runge-Kutta method (ERK4) (Iserles, 2008) is utilized to calculate the vibration response of the damaged beam under the external force shown in Fig. 5.3. The time step of the calculation is 0.00001 s and the duration is 1s.

Table 5.1 The natural frequencies of the undamaged and damaged beams (Hz)

	$f_1$	$f_2$	$f_3$	$f_4$	$f_5$
Undamaged Beam	4.14	25.93	72.62	142.41	235.79
Damaged Beam	4.10	25.51	69.99	139.35	231.67

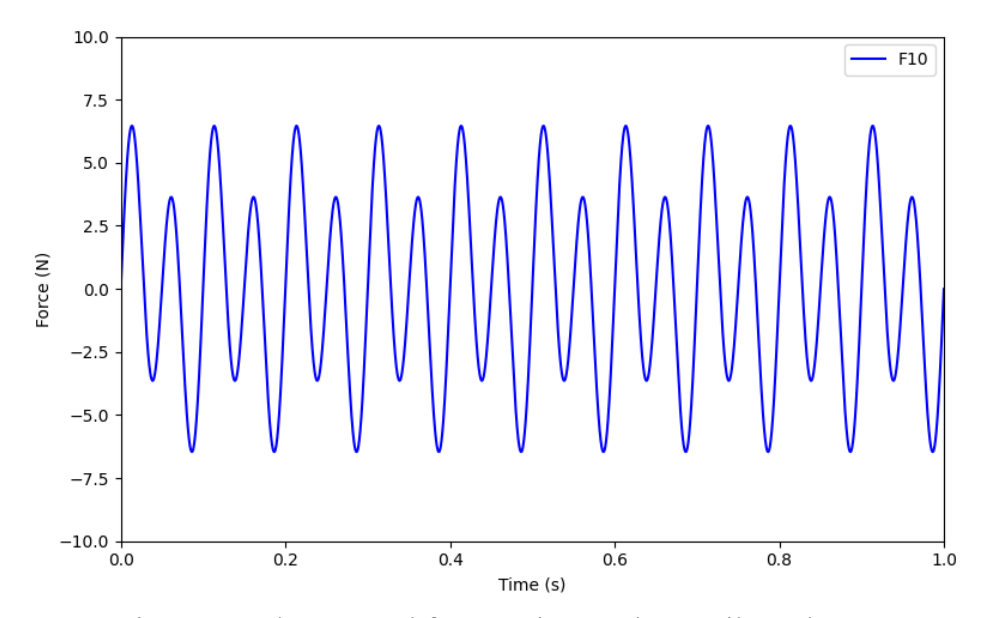


Figure 5.3 The external force acting on the cantilever beam

In actual engineering, it is difficult to accurately measure the rotation of the beam compared to the vertical vibration. So, the rotation is set as the unobservable structural response in this test. The vibration accelerations of three nodes are recorded to simulate the accelerometer measurement. In order to obtain the optimal sensor placement, kinetic energy matrix rank optimization (KEMRO) (Castro-Triguero et al., 2013; Heo & Jeon, 2016) for optimal sensor placement (OSP) is carried out. According to the analysis results of KEMRO, the optimal sensor locations of the three vertical acceleration sensors are nodes 4, 7, and 10.

#### 5.4.1.1 Hyperparameter testing

The PI-FFNN model involves several hyperparameters including the weight  $\alpha$  of the regularization term, the hyperparameter  $\sigma$  of the Fourier feature layer, the width  $H_{NN}$ , and the depth  $L_{NN}$  of the FCNN model. Before evaluating the performance of the PI-FFNN model, how to set these hyperparameters is studied first. In addition, other

parameters in the PI-FFNN model are also determined here. The parameters of the Newmark-beta method are set to  $\beta = 1/4$ ,  $\gamma = 1/2$  (average acceleration method). A gradient descent optimizer Adam (Kingma, 2014) is chosen to train the FFNN model with a learning rate of 0.001. The FFNN model is trained for 10,000 iterations, where the loss function is observed to have converged.

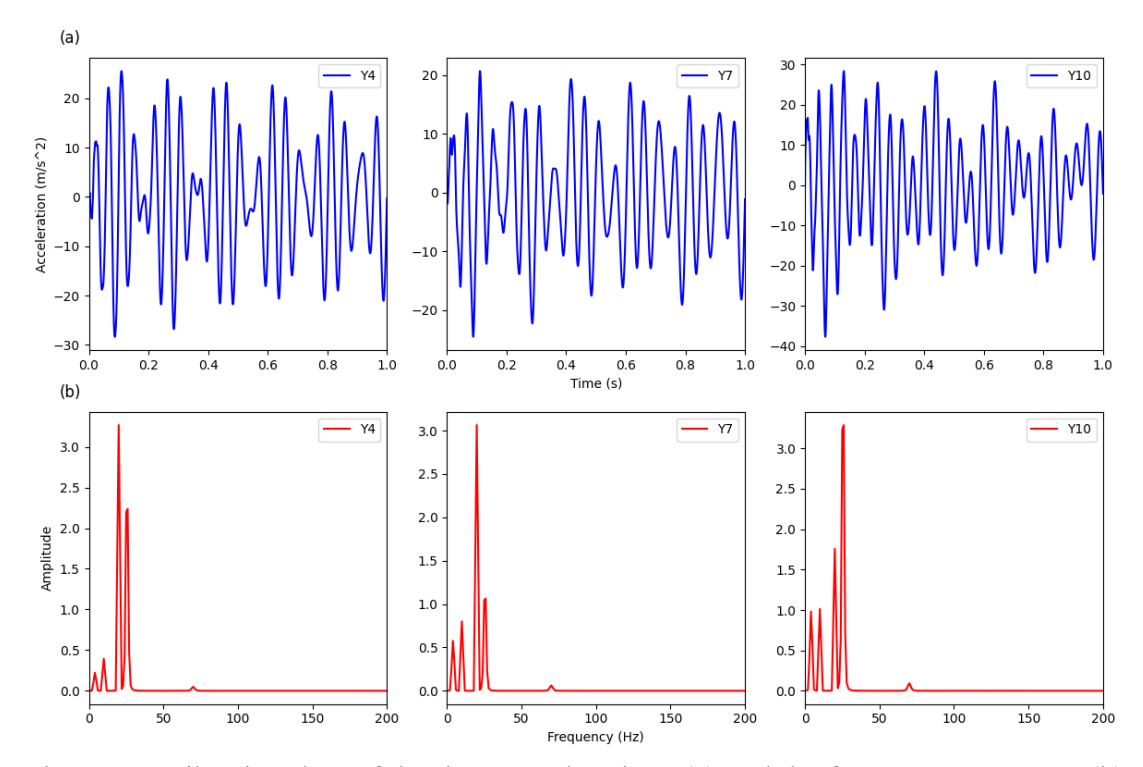


Figure 5.4 Vibration data of the three accelerations (a) and the frequency spectrum (b)

Consider the acceleration data of the three nodes (Y4, Y7, Y10) shown in Fig. 5.4(a) as the input data of the PI-FFNN model. The frequency spectrum analysis of the acceleration data is also demonstrated in Fig. 5.4(b). It is observed that the main frequency range of the three accelerations is 0-100 Hz. Accordingly, the hyperparameter  $\sigma$  of the FFNN model is set to 100 to establish the frequency characteristics of the input. In order to improve computational efficiency, the vibration data recorded from the

ERK4 method is resampled to 10000 Hz. The first 500 time steps are utilized as training data. Both noise-free and noisy training data are considered. The data calculated by the ERK4 method is considered noise-free. The noisy data are generated by adding Gaussian noise to the noise-free data by

$$\ddot{x}_{noise} = \ddot{x}_{exact} + \eta \cdot \mathcal{N}(0, \sigma_{exact}^2)$$
 (5.17)

Here,  $\ddot{x}_{exact}$  is the calculated noise-free data,  $\eta$  is the noise level, and  $\mathcal{N}(0, \sigma_{exact}^2)$  represents Gaussian noise with a mean of 0 and a variance of  $\sigma_{exact}^2$ .  $\mathcal{N}(0, \sigma_{exact}^2)$  has the same shape as  $\ddot{x}_{exact}$ .  $\sigma_{exact}$  is the standard deviation of  $\ddot{x}_{exact}$ . In this case, the noise of  $\eta = 1\%$  is added to the noise-free data to generate noisy data. The hyperparameter  $\alpha$  is investigated in both noise-free and noisy vibration data. A simple FFNN model with  $L_{NN} = 2$ ,  $H_{NN} = 40$  is utilized first to test the setting of  $\alpha$  values. A total of 14 schemes are tested, with  $\alpha$  values of [1.0, 1e-1, 1e-2, 1e-3, 1e-4, 1e-5, 0.0] in both noise-free and noisy data. All 14 schemes are trained with 10,000 iterations, and the converged  $loss_{\alpha}$  and  $loss_{z}$  are recorded and plotted as curves in Fig. 5.5.

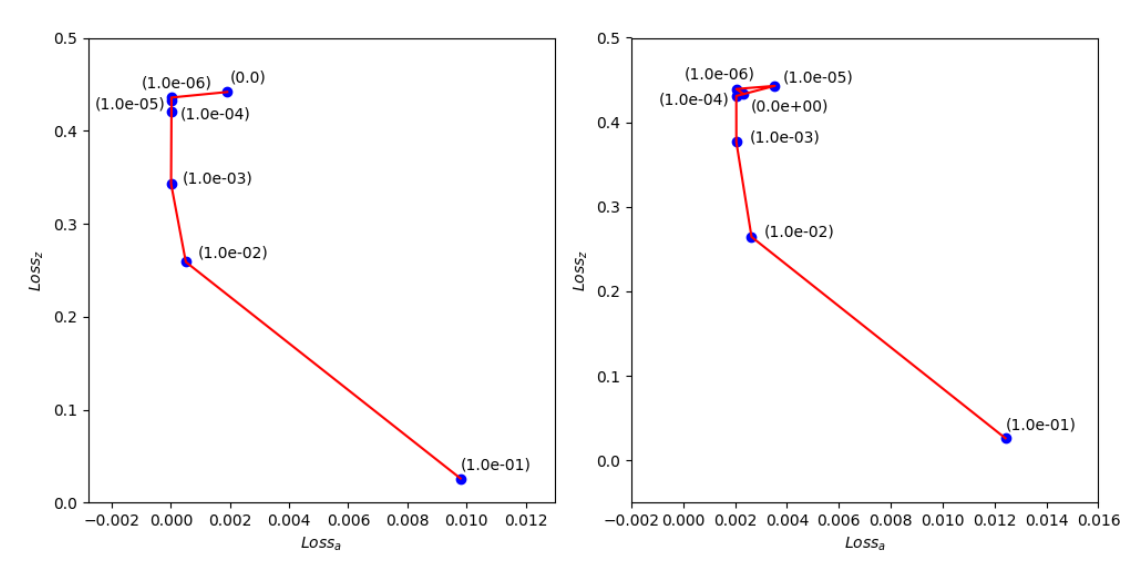


Figure 5.5  $loss_z$  -  $loss_a$  of 14 test schemes. (left) noise-free input data, (right) input data with 1% noise. The values of  $\alpha$  is given in brackets.

Fig. 5.5(a) shows that in the case of noise-free input data, as the  $\alpha$  value gradually decreases from 0.1 to 0, the value of  $loss_z$  shows a gradually increasing trend. While  $loss_a$  decreases first as the  $\alpha$  value gradually decreases and then increases when  $\alpha$  is less than 1e-3. Fig. 5.5(b) shows the changes of  $loss_z$  and  $loss_a$  with  $\alpha$  value in input data with 1% noise, which also shows similar trends as in Fig. 5.5(a). According to Fig. 5.5, it can be inferred that in this case when  $\alpha$  is set to 0.1 and 0.01, the PI-FFNN model is underfitting where damage is underestimated, and when  $\alpha$  is less than 1e-3, the model is overfitting where PI-FFNN overestimates the structural damage. The result of the identification  $z^{idf}$  also supports this inference. When  $\alpha$  is 0.1 or 0.01, the value of  $z^{idf}$  is smaller than the exact value and when  $\alpha$  is less than 1e-3, the sparsity of  $z^{idf}$  decreases significantly. Therefore, in this case,  $\alpha$ =1e-3 is considered the optimal hyperparameter setting.

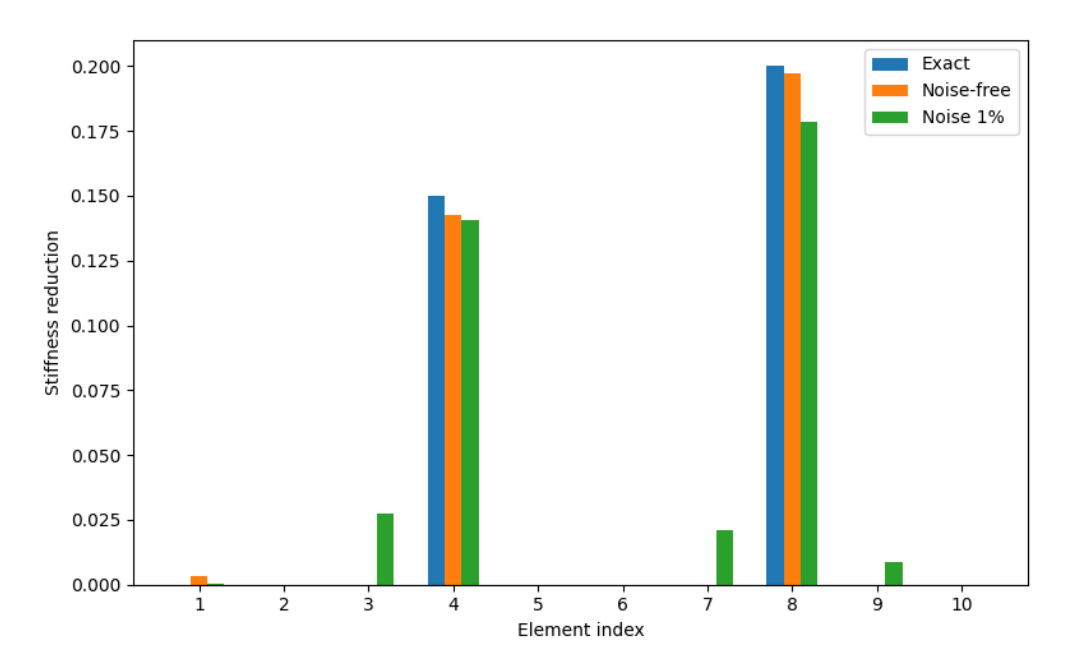


Figure 5.6 Result of stiffness reduction identification

In the scheme of  $\alpha$ =1e-3, the result of the identified  $z^{idf}$  is shown in Fig. 5.6. The result shows that in the vibration observation data with no noise and 1% noise, the PI-FFNN model successfully identified the decrease in structural stiffness. To quantify the overall accuracy of the identified stiffness reduction index  $z^{idf}$ , the average error is calculated as

$$\varepsilon_z = \frac{1}{N} \sum_{i=1}^{N} \left| z_i^{idf} - z_i^{exact} \right| \tag{5.18}$$

The average error of the stiffness reduction identification result of the noise-free input data is calculated to be 0.133%, while the error of the input data with 1% noise is 0.886%. The external force acting on node 10 is also reconstructed by the PI-FFNN model as plotted in Fig. 5.7.

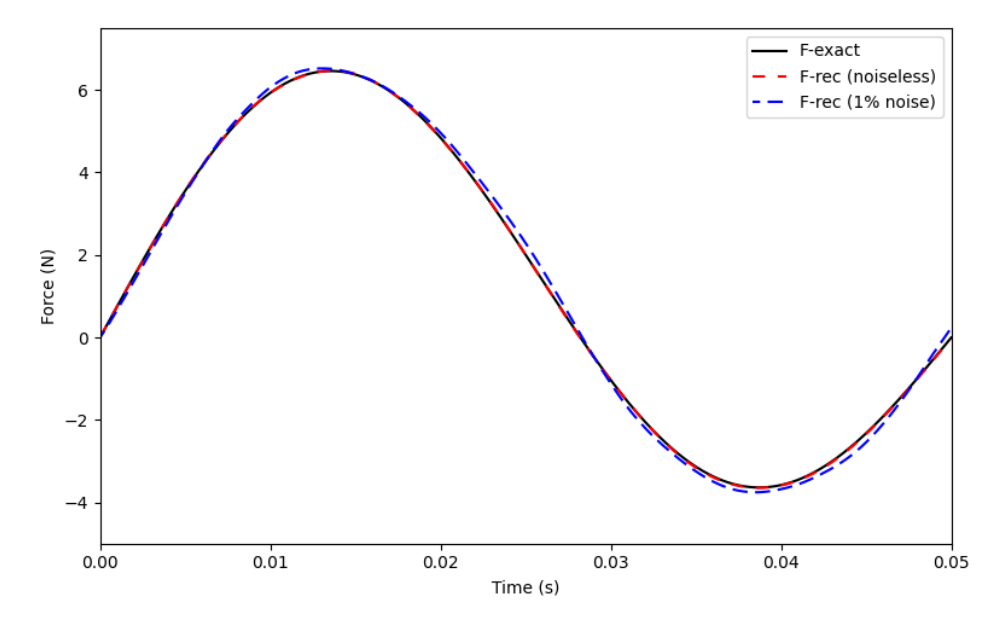


Figure 5.7 Results of external force reconstruction

Fig. 5.7 demonstrates that with both noise-free and noisy input data the PI-FFNN model accurately reconstructs the external forces of the structure. In order to quantify the accuracy of the external force reconstruction, the relative L2 error is calculated according to

$$\varepsilon_f = \frac{\sqrt{\sum (F^{rec} - F^{true})^2}}{\sqrt{\sum F^{true^2}}}$$
 (5.19)

According to the calculation, the relative L2 error of the reconstructed external force from the noise-free vibration data is only 0.323%, while that from the 1% noisy data is 3.536%. The hyperparameters  $L_{NN}$  and  $H_{NN}$  of the FCNN model are also investigated in this case. With the noise-free vibration measurement as input, the 16 neural network model schemes listed in Table 5.2 are tested respectively and the average error of damage identification results and the relative L2 error of force reconstruction are calculated. The running time is also recorded to evaluate the

efficiency of the models. The results are shown in Table 5.2.

Table 5.2 Test results of hyperparameters  $L_{NN}$  and  $H_{NN}$ .

(a) average error of damage identification results (%), (b) relative L2 error of force reconstruction (%), (c) running time (unit: s)

(a)

$H_{NN}/L_{NN}$	1	2	4	8	Avg
20	0.294	0.139	1.040	3.030	1.126
40	0.355	0.276	1.191	0.953	0.694
80	0.932	0.148	1.451	2.186	1.179
160	1.210	1.818	0.972	3.388	1.847
Avg	0.698	0.595	1.163	2.389	

(b)

$H_{NN}/L_{NN}$	1	2	4	8	Avg
20	0.084	0.114	0.185	0.551	0.233
40	0.180	0.155	0.196	0.131	0.166
80	0.418	0.195	0.170	0.322	0.276
160	0.359	0.371	0.150	1.093	0.493
Avg	0.260	0.209	0.175	0.525	

(c)

$H_{NN}/L_{NN}$	1	2	4	8	Avg
20	1406.03	1381.22	1385.22	1470.39	1410.72
40	1386.29	1374.57	1391.04	1457.25	1402.29
80	1373.56	1373.60	1414.82	1526.02	1422.00
160	1408.60	1401.25	1482.35	1737.13	1507.33
Avg	1393.62	1382.66	1418.36	1547.70	

From Table 5.2, it is observed that as  $H_{NN}$  and  $L_{NN}$  increase, the errors in both

the identified damage and the reconstructed force increase. This shows that increasing the width and depth of the FCNN model has a negative effect on improving the accuracy of PI-FFNN. In addition, as the number of hidden layers  $L_{NN}$  increases, the model training time will become significantly longer, so the efficiency will decrease. Therefore, based on the test results, a small FCNN model, such as  $L_{NN}=2$  and  $H_{NN}=40$ , is a better parameter setting for building the PI-FCNN model.

#### **5.4.1.2** Comparative experiments

Since the external force input of the beam model is unknown, traditional finite element model updating and frequency response function-based methods are not applicable in this case. In addition, since no labels related to damage severity are collected, all supervised machine learning frameworks are also not feasible due to the lack of training datasets. For comparison, classic Markov parameters with Tikhonov regularization utilized in (H.-P. Zhu et al., 2014) and the original PINN for the inverse problem proposed in (Raissi et al., 2019) are also employed to detect damage on the beam structure with noise-free and 1% noise input data.

Markov parameters with Tikhonov regularization (Mao et al., 2010; H.-P. Zhu et al., 2014) are a classic method to detect structural damage without the need for external force measurements. In the state space, by defining the state vector as  $X(t) = [x(t), \dot{x}(t)]^T$ , Eq. (5.1) can be transformed into a standard state equation as

$$\dot{X}(t) = K^*X(t) + B^*LF(t)$$
 (5.20)

where, system matrix  $K^* = \begin{bmatrix} 0 & I \\ -M^{-1}K & -M^{-1}C \end{bmatrix}$ , control matrix  $B^* = \begin{bmatrix} 0 \\ M^{-1} \end{bmatrix}$ .

According to the system state and input, the output variable y(t) is defined as

$$y(t) = RX(t) + DLF(t)$$
(5.21)

where output matrix  $R = [R_d - R_a M^{-1}K, R_v - R_a M^{-1}C]$  and feed-forward matrix  $D = R_a M^{-1}$ .  $R_a$ ,  $R_v$ , and  $R_d$  correspond to the mapping matrices of acceleration, velocity, and displacement, respectively. These mapping matrices are all diagonal matrices whose diagonal elements are 0 (not output) or 1 (output). According to the exponential matrix algorithm, adjacent system states can be transitioned by following

$$X_{t+1} = AX_t + BLF_t (5.22)$$

where, state transition matrix  $A = \exp(K^* \cdot h)$  and  $B = K^{*-1}(A - I)B^*$ . Here, h is the time step length. With Eq. (5.22), the system state at time step j can be calculated from the initial state  $X_0$  as

$$X_j = \sum_{k=0}^{j-1} A^k B L F_{j-k-1} + A^j X_0, j = 1, 2, \dots, N$$
 (5.23)

Here, N is the number of time steps. Then the observation  $y_j$  at time step j can be calculated according to

$$y_j = \sum_{k=0}^{j-1} RA^k BLF_{j-k-1} + RA^j X_0 + DLF_j, j = 1, 2, \dots, N$$
 (5.24)

Let  $H_0 = D$  and  $H_k = RA^{k-1}B$  (k > 0), then Eq. (5.24) can be expressed as

$$y_j = \sum_{k=0}^{j} H_k L F_{j-k} + R A^j X_0, j = 1, 2, \dots, N$$
 (5.25)

Here  $H_k$  is called the Markov parameters of the state-space model, which is a structural intrinsic property that represents the response relationship of the structural system to external forces. Eq. (5.25) can be expressed in Toeplitz matrix form as

$$\begin{cases}
y(0) \\
y(1) \\
\vdots \\
y(N)
\end{cases} = \begin{bmatrix}
H_0 & 0 & \cdots & 0 \\
H_1 & H_0 & \cdots & 0 \\
\vdots & \vdots & \ddots & \vdots \\
H_N & H_{N-1} & \cdots & H_0
\end{bmatrix} \begin{bmatrix} L \\ L \\ \vdots \\ L \end{bmatrix} \begin{Bmatrix} F(0) \\ F(1) \\ \vdots \\ F(N) \end{Bmatrix} + \begin{bmatrix} RA^0 \\ RA^1 \\ \vdots \\ RA^N \end{bmatrix} X_0$$
(5.26)

Eq. (5.26) can be rewritten simply as

$$Y = H_L F + A_R X_0 \tag{5.27}$$

where  $H_L$  and  $A_R$  are the corresponding Toeplitz matrix and transition matrices of the initial state. Assume that the measured structural response is divided into two data sets, namely  $Y_1$  and  $Y_2$ . Then the following mapping relationship can be established between them and the external force:

$$\begin{cases} Y_1 = H_{L1}F + A_RX_0 \\ Y_2 = H_{L1}F + A_RX_0 \end{cases}$$
 (5.28)

The first equation in Eq. (5.28) gives the reconstructed external force  $F^{rec}$  as:

$$F^{rec} = H_{L1}^+(Y_1 - A_R X_0) (5.29)$$

Here,  $H_{L1}^+$  is the pseudo-inverse matrix of  $H_{L1}$ . Then  $Y_2$  can be reconstructed according to:

$$Y_2^{rec} = H_{L2}F^{rec} + A_RX_0 = H_{L2} \cdot H_{L1}^+ (Y_1 - A_RX_0) + A_RX_0$$
 (5.30)

But Eq. (5.29) and Eq. (5.30) are well-known ill-posed problems. Therefore, regularization techniques are used to add additional constraints to obtain stable solutions. Tikhonov regularization is the most commonly used regularization technique, which solves  $F^{rec}$  by adding an L2 norm to F as:

$$F^{rec} = min\{\|H_{L1}F + A_RX_0 - Y_1\|_2^2 + \alpha^2 \cdot \|LF\|_2^2\}$$
 (5.31)

The reconstruction force  $F^{rec}$  is obtained by minimizing the above residual and regularization term by employing an optimizer. Using this reconstruction force,

 $Y_2$  can be reconstructed according to:

$$Y_2^{rec} = H_{L2}F^{rec} + A_RX_0 (5.32)$$

Now assume that the structure is damaged and its damage is quantified by a damage index vector  $\lambda$ , so that the Markov Parameter and transition matrices of the initial state of the structure are controlled by  $\lambda$  as  $H_k(\lambda)$  and  $A_R(\lambda)$ . By minimizing the deviation between the reconstructed  $Y_2$  and the observed value as Eq. (5.33), the damage index vector  $\lambda$  of the structural system can approximate the true structural damage and thus detect the damage of the structure.

$$\lambda = \min(\|Y_2^{rec}(\lambda) - Y_2^{obs}\|_2^2)$$
 (5.33)

Markov parameters with Tikhonov regularization have one hyperparameter  $\alpha$ , which controls the weight of the regularization term and can be determined by the L-curve method.

In the cantilever beam case of this study, the vertical accelerations of node 4 and node 10 of the cantilever beam are used as data set 1  $Y_1$  to reconstruct the unknown force, and the vertical acceleration the node 5 is used as data set 2  $Y_2$  to detect the damage of the structure. According to the L-curve method test, the value of  $\alpha$  is determined to be 0.001. The observation data without noise and with a noise level of 1% are used as input data to detect the damage of the structure. The damage results detected by the Markov parameters method with Tikhonov regularization are listed in Table 5.3.

Table 5.3 Identified damage results of Markov parameters method with Tikhonov regularization

Noise level		Element									
	1	2	3	4	5	6	7	8	9	10	
0%	0.000	0.000	0.000	0.000	0.000	0.000	0.000	0.000	0.000	0.454	
1%	0.000	0.000	0.000	0.000	0.000	0.000	0.000	0.000	0.000	0.462	

Table 5.3 shows that the Markov parameters method with the Tikhonov regularization method failed to detect the damage of elements 4 and 8, and incorrectly located the damage location as element 10. The error  $\varepsilon_{\lambda}$  of damage detection is calculated to be 8.035% (noiseless data) and 8.124% (1% noise data). The reconstructed external forces are also shown in Fig. 5.8.

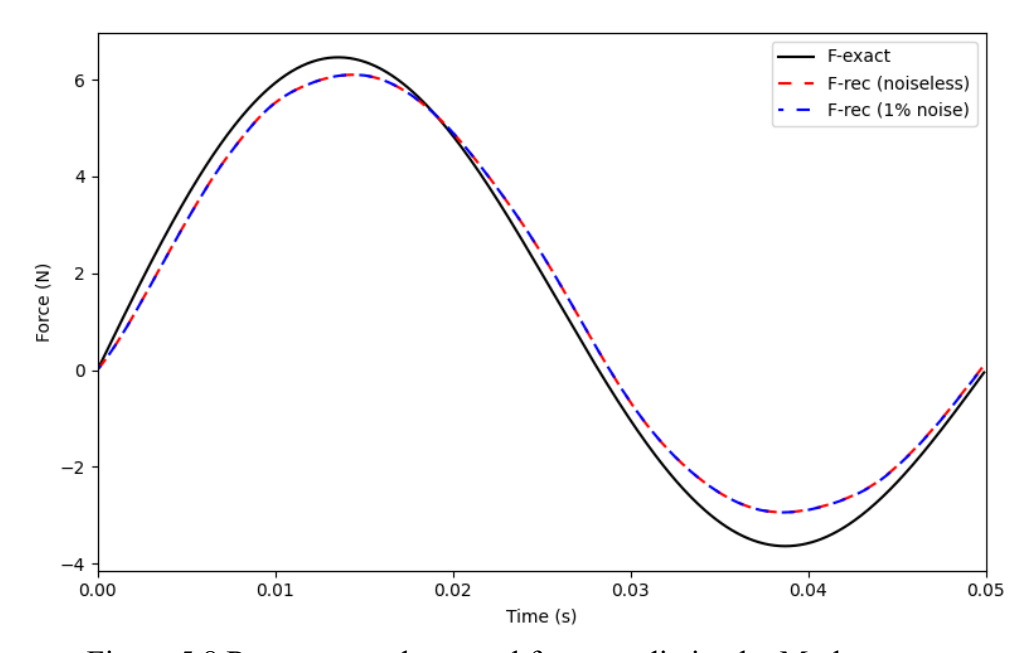


Figure 5.8 Reconstructed external force prediction by Markov parameters method with Tikhonov regularization

As shown in Fig. 5.8, the external force predicted by the Markov parameters method with Tikhonov regularization deviates from the exact value of the external force, and the relative L2 error is calculated to be 11.136% (0% noise) and 11.096% (1%

noise).

Physics-informed neural networks (PINNs) are a framework proposed by (Raissi et al., 2019) for solving direct and inverse problems of partial differential equations. PINNs show a remarkable ability to discover unknown parameters in differential equations. For a differential equation, its governing equation is described as:

$$N(u(t,x),t,x;\lambda) = f(t,x)$$
(5.34)

Where N is a differential operator parameterized by  $\lambda$ . u(t,x) is the solution to the equation. f(t,x) is the force term of the equation. The inverse problem of Eq. (5.34) is to discover the unknown parameter  $\lambda$  in the governing equation inversely given some measured values of  $u^{obs}(t,x)$ . In the PINNs framework, a neural network model is employed to predict  $u^{obs}(t,x)$  with inputs t and x. The unknown parameter  $\lambda$  is also initialized and updated together with the neural network model. The derivatives of the differential operator can be calculated by a technique called automatic differentiation (Baydin et al., 2018) of the neural network. A loss function based on the observed data is defined as Eq. (5.35) to quantify the residual between the neural network output and the observed data. A loss function based on the governing equation is also defined as Eq. (5.36) to quantify the residual of the governing equation.

$$L_{obs} = \frac{1}{N_m} \sum_{i=1}^{N_m} ||u^{pred}(t^m, x^m) - u^{obs}(t^m, x^m)||_2^2$$
 (5.35)

$$L_f = \frac{1}{N_f} \sum_{i=1}^{N_f} ||N(u^{pred}(t^f, x^f), t^f, x^f; \lambda) - f(t^f, x^f)||_2^2$$
 (5.36)

Here  $N_m$  is the number of observation points  $(t^m, x^m)$ .  $u^{pred}(t^m, x^m)$  and  $u^{obs}(t^m, x^m)$  are the predicted value and observed value of the neural network at the

observation point  $(t^m, x^m)$ .  $N_f$  is the number of collocation points  $(t^f, x^f)$ , which are randomly sampled in the domain of the equation. These two loss functions will be summed as  $L_{pinn} = L_{obs} + L_f$  as the loss function of the PINNs model. The output of the neural network model can gradually approach the exact solution of the equation and the unknown parameter  $\lambda$  will gradually approach its accurate value by utilizing an optimizer to minimize the loss function.

In this case, the PINNs method is also utilized to detect the structural damage of the cantilever beam. Since the external force is also unknown, two neural network models are built to predict the external force f(t, x) and the displacement response u(t, x) of the structure, respectively. The neural network models have 2 inputs (t, x) and 20 outputs. Here x is the node number from 0 to 10. The neural network models have 2 hidden layers of 100 neurons. Through the automatic differentiation of the neural network, the displacement response  $u^{pred}(t,x)$  predicted by the neural network can inversely calculate the velocity response  $v^{pred}(t,x)$  and the acceleration response prediction  $a^{pred}(t,x)$ . The acceleration response prediction can be combined with the observed data  $a^{obs}(t^m,x^m)$  to construct the loss function as

$$L_{obs} = \frac{1}{N_m} \sum_{i=1}^{N_m} ||a^{pred}(t^m, x^m) - a^{obs}(t^m, x^m)||_2^2$$
 (5.37)

Here  $N_m$  is the number of observed data  $(t^m, x^m)$  of the acceleration response. In addition, according to the initial conditions  $(u_0, v_0)$ , the loss function of the initial conditions is constructed as

$$L_{ini} = \|u^{pred}(0, x^0) - u_0\|_2^2 + \|v^{pred}(0, x^0) - v_0\|_2^2$$
 (5.38)

The governing equations of the structural system are also used as physical information to train the neural network model using a loss function as

$$L_{f} = \frac{1}{N_{f}} \sum_{i=1}^{N_{f}} \left\| M \cdot a^{pred}(t^{f}, x^{f}) + C \cdot v^{pred}(t^{f}, x^{f}) + K(\lambda) \cdot u^{pred}(t^{f}, x^{f}) - f(t^{f}, x^{f}) \right\|_{2}^{2} (5.39)$$

Here,  $N_f$  is the number of collocation points  $(t^f, x^f)$  of the acceleration response. The collocation points are generated according to the predetermined time step and full sampling of degrees of freedom. Finally, the loss function of PINNs is the sum of the above three loss functions as

$$L_{pinn} = L_{obs} + L_{ini} + L_f (5.40)$$

By using a gradient descent-based Adam optimizer to minimize  $L_{pinn}$  to reduce the residual of the neural network output to the observation data and the governing equation, the output of the neural network model will theoretically gradually approach the unknown external force and the true response of the structural system. The noise-free observation data and the observation data of 1% noise are used as the observation data of PINNs, respectively. After training 1e5 times, the loss function of PINNs has converged. Fig. 5.9 shows the convergence process of the PINNs loss function when the noise-free observation data is used as the input data.

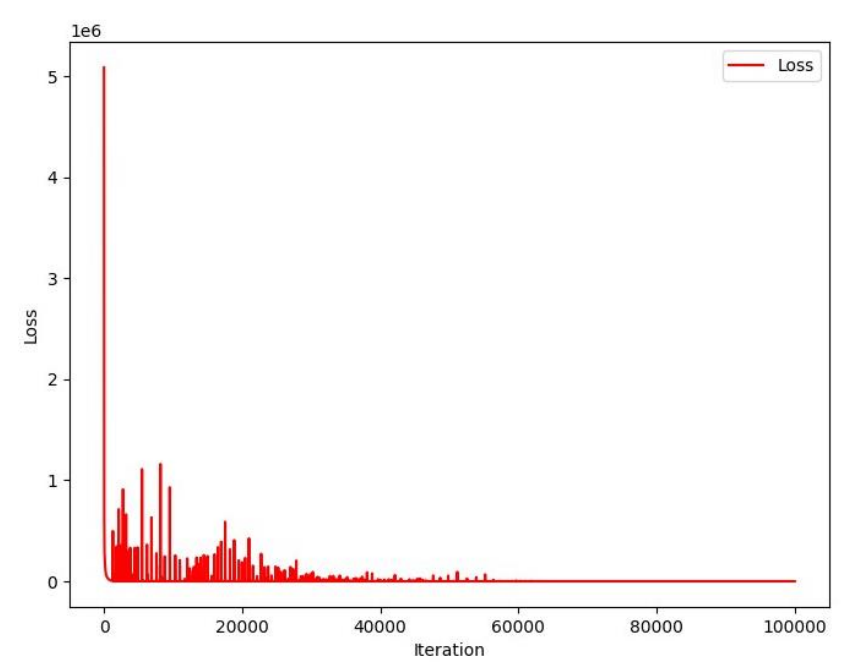


Figure 5.9 Convergence process of loss function of PINNs

After the loss function converges, the damage of the structure predicted by PINNs is extracted as shown in Table 5.4.

Table 5.4 Damage results identified by PINNs model

Noise level					Eler	nent				
Noise level	1	2	3	4	5	6	7	8	9	10
0%	0.010	0.010	0.011	0.013	0.014	0.016	0.015	0.014	0.012	0.012
1%	0.010	0.017	0.016	0.016	0.018	0.018	0.017	0.015	0.013	0.012
Exact	0	0	0	0.15	0	0	0	0.2	0	0

As shown in Table 5.4, PINN fails to detect the damage of the structure. The error between its detection results and the true result is 4.241% (0% noise) and 4.388 % (1% noise). Fig. 5.10 shows the structural external forces predicted by the PINNs model.

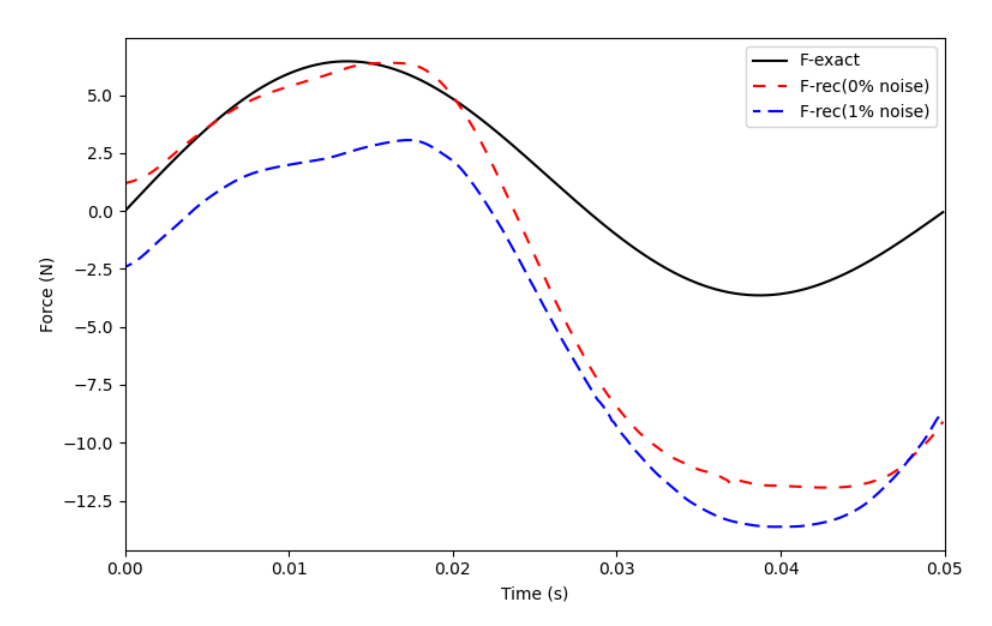


Figure 5.10 Structural external forces predicted by the PINNs model

As shown in Fig. 5.10, the PINNs model also fails to reconstruct the unknown structural external forces on the cantilever beam. The relative L2 errors between the reconstructed external forces and the true values are 152.618% (0% noise) and 183.350% (1% noise). Overall, the comparison results of average error  $\varepsilon_z$  of identified damage index and relative L2 error  $\varepsilon_f$  of reconstructed external force are listed in Table 5.5.

Table 5.5 The results of the comparative experiment

Method	Noise level	${m \mathcal E}_Z$	$oldsymbol{arepsilon}_f$
PI-FFNN	0%	0.133%	0.323%
I 1-1/1/1N1N	1%	0.886%	3.536%.
Tikhonov	0%	8.035%	11.136%
TIKHOHOV	1%	8.124%	11.096%
PINNs	0%	4.241%	152.618%
PININS	1%	4.388%	183.350%

Table 5.5 shows that the proposed PI-FFNN method can achieve more accurate results than Markov parameters with Tikhonov regularization and the original PINN in

both noisy and noiseless observation data in this case. In addition, the Tikhonov method took 9340 seconds to calculate 1000 iterations, while the PINNs took 3340 seconds to train 100,000 iterations. The PI-FFNN method successfully identified the damage of the structure in only 1375 seconds, showing higher efficiency.

# 5.4.2 Plane truss

A plane truss structure as shown in Fig. 5.11 is considered as the second numerical example. The truss consists of 19 bars and 11 nodes. The bars are all 10 m long and have a rectangular cross-section of  $5 cm \times 5 cm$ . The bar material is steel with a density of  $7850 kg/m^3$  and an elastic modulus of 210 MPa. The 12 truss elements are considered as 2-node linear truss elements with consistent mass matrices. The truss is set to vibrate in the X-Y plane and is constrained in the X and Y directions at node 0 and in the Y direction at node 10. Under the constraints, the truss has a total of 19 degrees of freedom. Considering that the truss is damaged in bars 5, 9, and 12, with the stiffness reduction of 15%, 20%, and 25% respectively. The damping ratio of the truss is considered to be 0.5% of the first two-order natural modes. The first ten natural frequencies of the healthy truss and damaged truss are shown in Table 5.6.

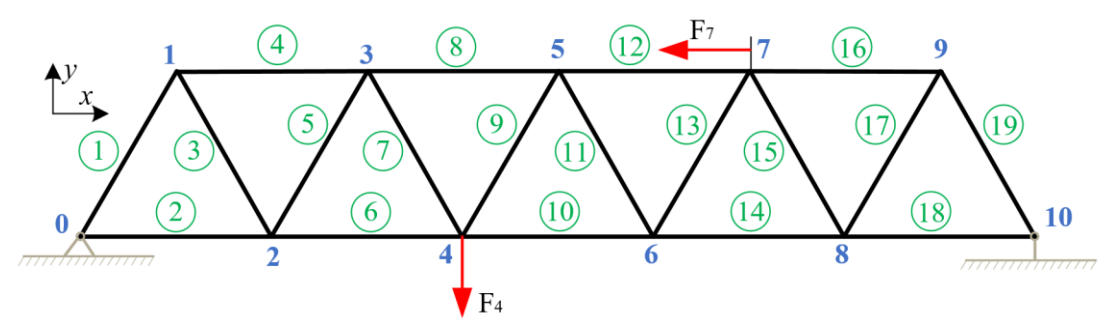


Figure 5.11 Structure of the plane truss

Table 5.6 First ten natural frequencies of the plane truss (Hz)

	$f_1$	$f_2$	$f_3$	$f_4$	$f_5$	$f_6$	$f_7$	$f_8$	$f_9$	$f_{10}$
Intact	8.05	16.06	26.54	46.57	50.07	71.79	76.91	81.98	95.13	101.45
Damaged	7.90	15.76	26.22	45.82	48.54	69.45	75.34	81.88	93.16	99.25

The truss vibrates under the action of the  $F_4^Y$  (Y-direction force on node 4) and the  $F_7^X$  (X-direction force on node 7).  $F_4^Y = 30 \sin(20\pi \cdot t) + 10 \sin(70\pi \cdot t) kN$ ,  $F_7^X = 25 \sin(30\pi \cdot t) + 7.5 \sin(80\pi \cdot t) kN$ . According to the calculation results of KEMRO for the optimal sensor position, the optimal positions of the four sensors are node 4 in the Y direction (4Y), node 5 in the X direction (5X), node 9 in the Y direction (9Y) and node 10 in the X direction (10X). The vibration response is calculated as the observation using the ERK4 method with a time step of 0.0001 s. The observation data of the four accelerations and the frequency spectrum are shown in Fig. 5.12.

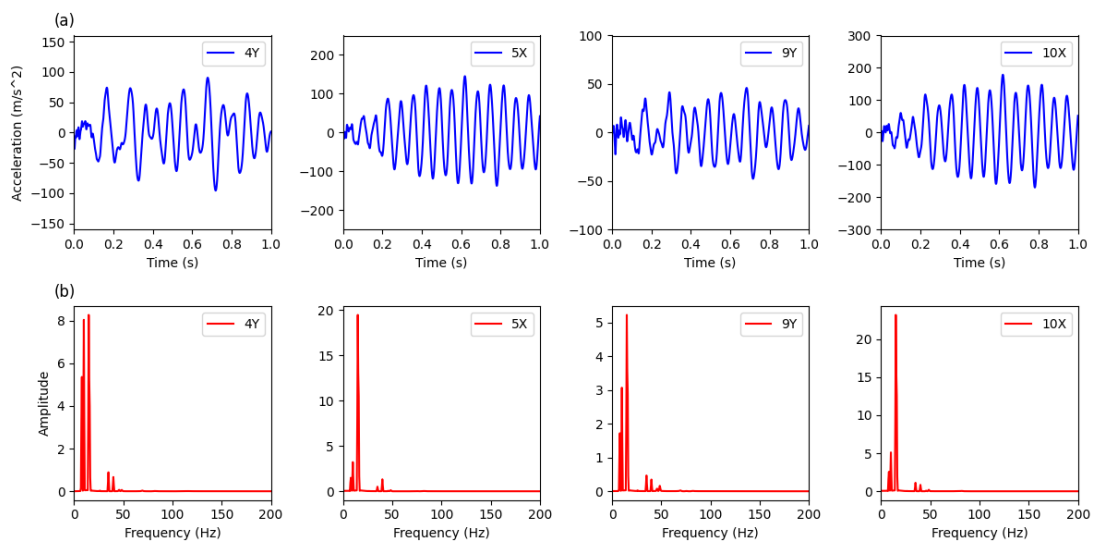


Figure 5.12 Acceleration observation data (a) and frequency spectrum (b)

A PI-FFNN model is built to reversely detect the damage of the plane truss, where

an FFNN model with  $L_{NN}=2$ ,  $H_{NN}=40$  is employed to approximate the unknown nodal forces. According to the frequency spectrum shown in Fig. 5.12, the frequency of the vibration response is mainly distributed in 0-100 Hz. So, the hyperparameter  $\sigma$  of the Fourier feature layer is set to 100 to establish the frequency characteristics of the external force.  $\alpha$  is set to 1e-3 to maintain the balanced convergence of  $loss_a$  and the regularization term  $loss_z$ . The parameters of the Newmark-beta method are set to  $\beta=1/4$ ,  $\gamma=1/2$ . A gradient descent optimizer Adam is chosen to train the FFNN model with a learning rate of 0.001. The FFNN model is trained for 5000 iterations, where the loss function is observed to have converged. In this case, vibration observation data without noise and with 1% and 5% noise are studied, respectively. The time step length is 0.0001 s, and the input data length is 500 time steps. After training, three calculation schemes with observation data of different noise levels identify the structural damage.

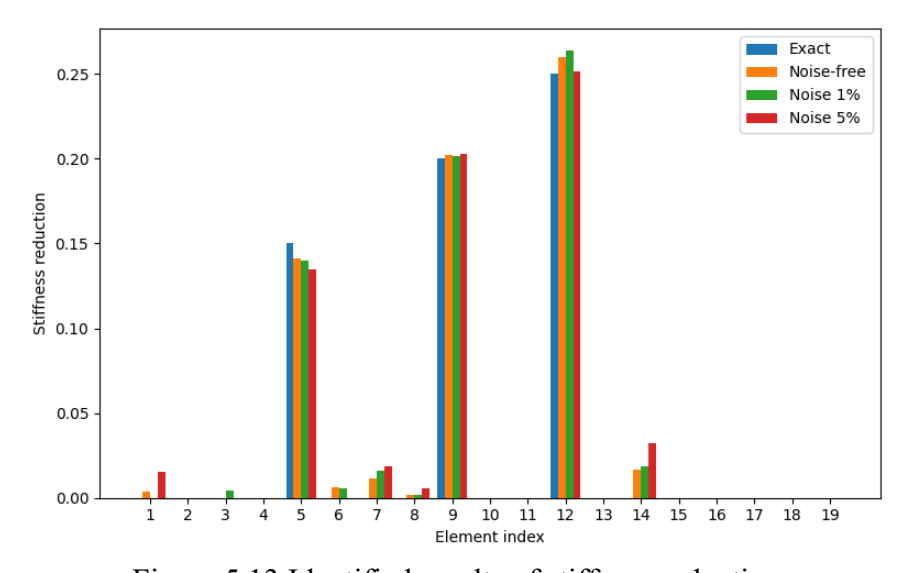
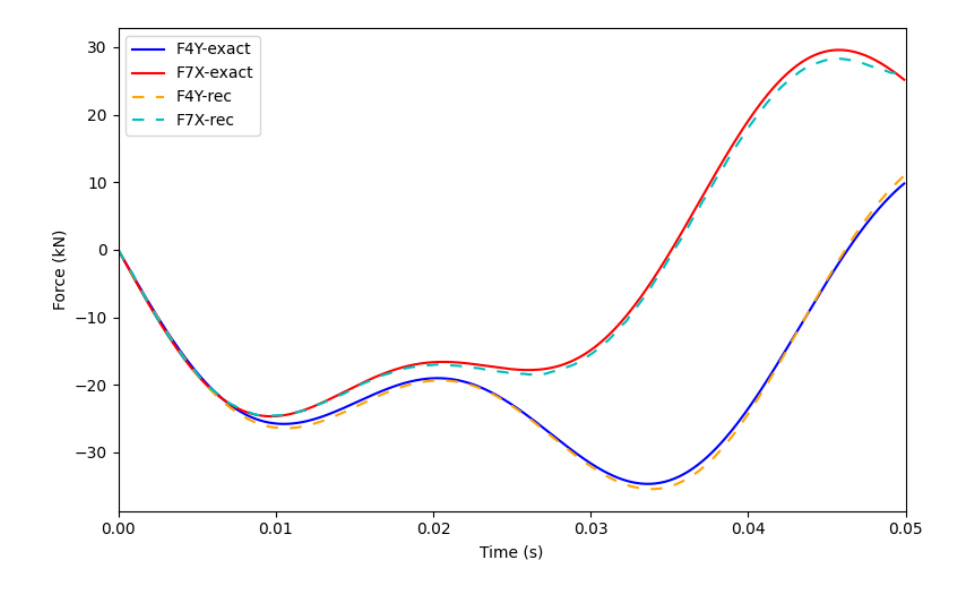


Figure 5.13 Identified results of stiffness reduction

From Fig. 5.13, it is shown that PI-FFNN can accurately identify the stiffness reduction of the plane truss from vibration observations with no noise, 1% noise, and 5% noise. The errors of the damage identification results are calculated to be 0.321% (noiseless), 0.375% (1% noise), and 0.483% (5% noise) respectively. In this case, the robustness of the PI-FFNN method to the noise in the measurement data is demonstrated. The outputs of the Fourier feature neural network model also successfully reconstruct the unknown external forces on the truss. As an example, Fig. 5.14 shows the reconstructed external forces from noise-free input data. To quantify the accuracy of the force reconstruction, the relative L2 error  $\varepsilon_f$  of the reconstructed external forces is calculated. The errors of the external force reconstruction are calculated to be 3.00% (noise-free), 3.03% (1% noise), and 4.07% (5% noise) respectively. This case shows that the PI-FFNN method can accurately detect the damage of this plane truss and reconstruct the external forces even in noisy measurements.



### 5.5 Experimental verifications

A vibration test of aluminum beams shown in Fig. 5.15 was carried out in the laboratory to verify the proposed PI-FFNN method. An intact and a damaged aluminum beam were respectively installed and vibration tested. The testing of the intact aluminum beam was designed to determine the initial stiffness of the beam, while the damaged aluminum beam was utilized to identify the stiffness reduction based on the initial stiffness. The model of the aluminum beams and supports is shown in Fig. 5.16. The total length of the aluminum beams is 126 cm, and the free section length is 120 cm. The thickness of the intact beam is 5 mm, and the width is 30 mm. The measured mass of the intact beam is 506.7 g, while the mass of the damaged beam is 497.1 g. The calculated densities are  $2683.08 \, kg/m^3$  and  $2644.43 \, kg/m^3$ respectively. The initial elastic modulus is considered to be 65.0 GPa. The left and right ends of the installed beam were bolted to the supports. The vertical displacement at both ends of the beam is considered to be constrained to 0, and the angular semirigidity of the supports is considered with an initial stiffness of  $1000N \cdot m/rad$ . The damping of the aluminum beam is considered to be Rayleigh damping, set as C = a.  $M + b \cdot K$ , where a and b are also parameters to be identified. In the finite element model of the aluminum beam, the beam is divided into 12 2-node Euler-Bernoulli beam elements with consistent mass matrices. Each element is 10 cm long. So, the finite element model of the aluminum beam has a total of 12 elements, 13 nodes, and 26 degrees of freedom.

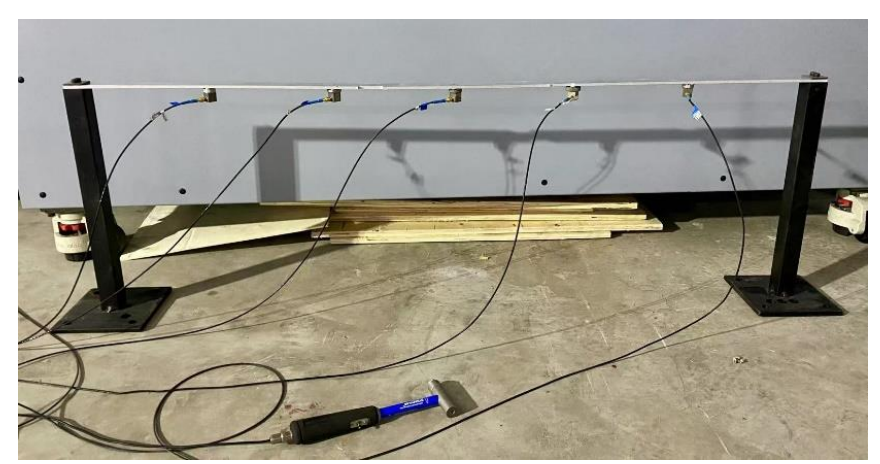


Figure 5.15 The vibration test of an aluminum beam

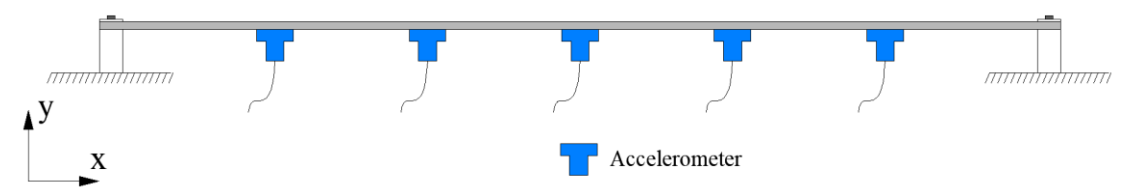


Figure 5.16 The model of the aluminum beam and supports

Five accelerometers were used to record the acceleration response of the structure, and a hammer with a force sensor was utilized to apply force at the mid-span to generate vibration. The installation positions and weights of all accelerometers are listed in Table 5.7. A Dewesoft data logger and laptop displayed in Fig. 5.17 were used to record the data of all sensors, with a sampling frequency of 10000 Hz.

Table 5.7 The installation positions and weights of accelerometers

Sensor ID	Installation position	Weight (including magnet mount)
A1	x = 20 cm	29.3 g

A2	$x = 40 \ cm$	31.8 g
A3	x = 60 cm	29.6 g
A4	x = 80 cm	35.8 g
A5	x = 100 cm	29.5 g



Figure 5.17 Data acquisition and storage equipment

# 5.5.1 Initial parameter identification

In the first step, the intact beam was installed and tested to determine the initial mechanical parameters of the beam model. The vibration test of the beam was repeated three times to enhance the reliability of the data. As an example, the vibration signals collected by the five accelerometers in the first test are shown in Fig. 5.18.

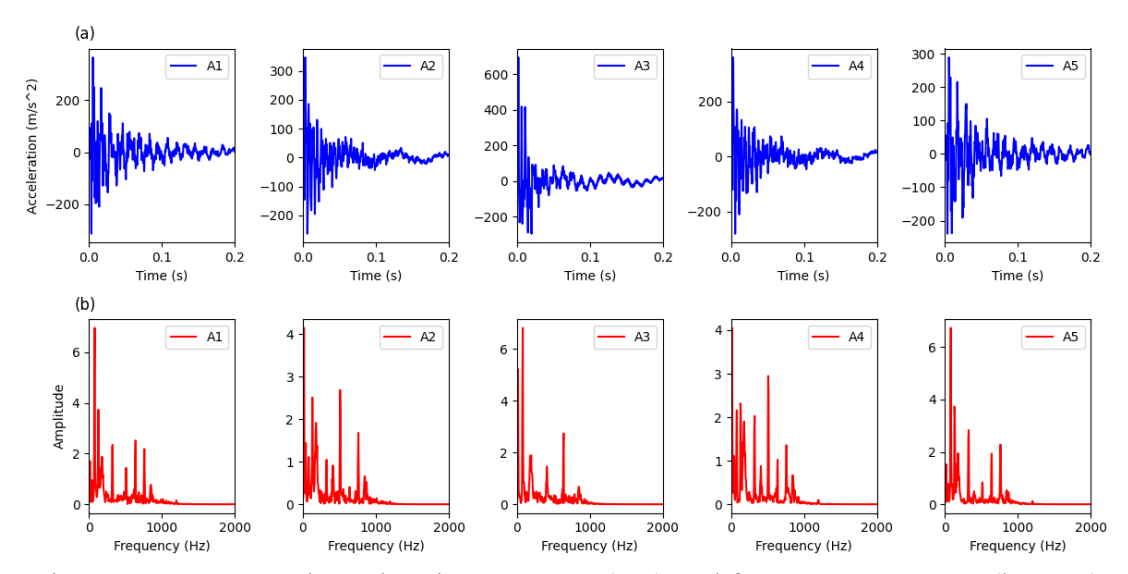


Figure 5.18 Measured acceleration response (top) and frequency spectrum (bottom)

At this stage, the beam is assumed to be homogeneous and each element has the same mass and stiffness. The elastic modulus E, the damping coefficients a and b of the beam and the rotational stiffnesses  $k_1$  and  $k_2$  of the two supports are considered as updateable parameters. The initial values and updated coefficient ranges of these parameters are listed in Table 5.8.

A PI-FFNN model is built to update these parameters with structural vibration measurements. According to the frequency spectrum shown in Fig. 5.18, the main distribution of the vibration response is 0-1000 Hz. Therefore, the hyperparameter  $\sigma$  of the FFNN is set to 1000. The depth  $L_{NN}$  of the FFNN model is set to 2, and the width  $H_{NN}$  is set to 40. Since all beam elements are intact, there is no need to increase the sparsity of the results, so  $\alpha$  is set to 0. The input data of the model are the first 200 time steps of the vibration measurements of the five accelerometers with  $dt = 0.0001 \, s$ . The vibration measurements collected from three tests are respectively input

into the model for parameter update. The force mapping matrix is set to have external forces only on the mid-span nodes. The Newmark-beta method with  $\beta = 1/4$ ,  $\gamma = 1/2$  is set to calculate the vibration response of the beam. The FFNN model is trained for 5,000 iterations with an Adam optimizer of 0.001 learning rate. The parameter update results of the three tests are listed in Table 5.8.

Table 5.8 Results of mechanical parameter update

Parameter	Initial value	Coefficient range	Test ID	Identified coefficient	Updated value	Average value
			1	1.0771	7.001E+10	
E	6.50E+10	[0.5, 1.5]	2	1.0747	6.986E+10	6.988E+10
			3	1.0736	6.978E+10	
			1	40.176	4.018E+00	
a	1.00E-01	[1E-2, 1E2]	2	39.574	3.957E+00	3.821E+00
		3	34.872	3.487E+00		
			1	0.406	4.057E-06	
b	1.00E-05	[1E-2, 1E2]	2	0.400	4.003E-06	4.925E-06
		3	0.672	6.716E-06		
			1	1.133	1.133E+03	
$k_1$	1.00E+03	[1E-2, 1E2]	2	1.407	1.407E+03	1.271E+03
		3	1.274	1.274E+03		
			1	13.939	1.394E+04	
$k_2$	1.00E+03	[1E-2, 1E2]	2	13.822	1.382E+04	1.363E+04
			3	13.136	1.314E+04	

Table 5.8 shows that the results of the structural mechanical parameter update in the three tests are stable and close. The average values of the updated mechanical parameters will be used as the initial values for structural damage identification in the next section.

# 5.5.2 Damage detection of damaged beams

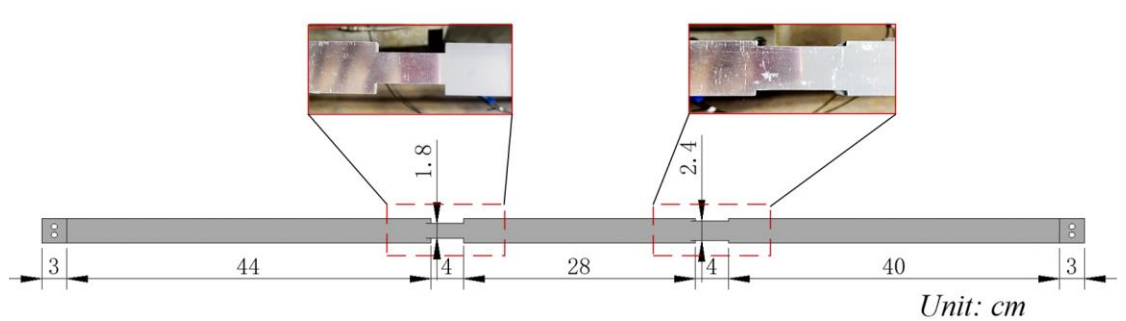


Figure 5.19 Location and depth of damage on the aluminum beam

In the second phase of laboratory testing, a damaged aluminum beam was installed and tested. The damage location and severity of the aluminum beam are shown in Fig. 5.19. The damage of the aluminum beam was simulated by reducing the width of the aluminum beam by 40% at  $x = 47 - 51 \, cm$  and 20% at  $x = 79 - 83 \, cm$ . This damage will cause the stiffness of elements 5 and 8 in the beam model to decrease by 40% and 20%, respectively. The same five accelerometers were installed on this damaged aluminum beam to record the vibration signals. The hammer applied a force at the mid-span to make the beam vibrate from rest.

A PI-FFNN model with the same parameters as in the undamaged beam case is built to detect beam damage. The elastic modulus E and damping coefficients a, b of the model are set as the updated values in Table 5.8. Since the damaged beam was newly installed on the supports, the tightening force of the bolts may have changed compared to the case of the intact beam. So, the support rotational stiffnesses are trained again and the initial values are set to the updated values in Table 5.8. A 10-element

damage index vector z is defined to quantify the stiffness reduction of the aluminum beam element, and its value range is 0.01-1.0. Another 2-element vector  $\gamma$  is defined to update the support rotational stiffnesses, and its value range is [0.01, 100]. The z vector and  $\gamma$  vector are trained together with the neural network model. The first 200 time steps of the five acceleration observations are utilized as the input data of the PI-FFNN model. To improve the sparsity and noise robustness of damage identification, according to the L-curve test, the weight of the regularization term  $\alpha$  is set to 10. After training 5000 iterations using the Adam optimizer with a learning rate of 0.001, the loss function of the PI-FFNN model has converged.

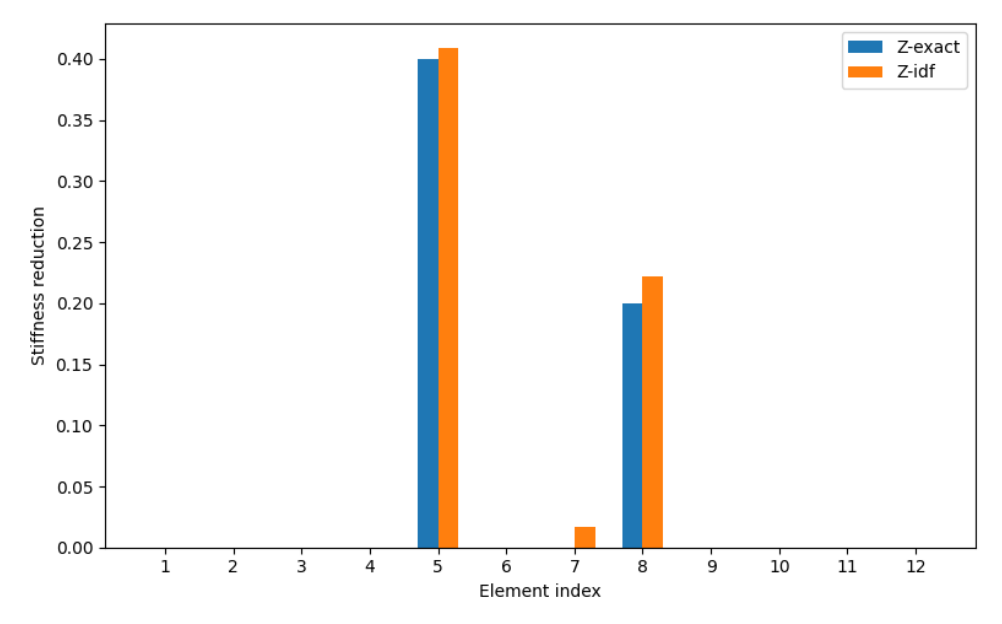


Figure 5.20 Results of stiffness reduction identified by the PI-FFNN model

Fig. 5.20. shows the result of structural damage detected by the PI-FFNN after model training. It shows that the PI-FFNN model successfully located and detected two damages on the aluminum beam. Due to the integration of regularization terms in the

loss function, the identified results maintain a very high sparsity. The detected stiffness reduction values are 40.869% (element 5) and 22.238% (element 8) respectively, with errors of 0.869% and 2.238% compared to the accurate values of 40% and 20%. According to Eq. (18), the overall error  $\varepsilon_z$  of the damage detection result is calculated to be 0.370%. In addition, PI-FFNN also reconstructed the external force from the hammer as shown in Fig. 5.21. It shows that the forces reconstructed from the PI-FFNN model show a high consistency with the measured values. Since external force is difficult to measure accurately, it is difficult to judge whether the measurement value from the force sensor or the reconstructed force is more accurate. For reference only, the relative L2 error between the reconstructed external force and the measured force is calculated to be 14.784%.

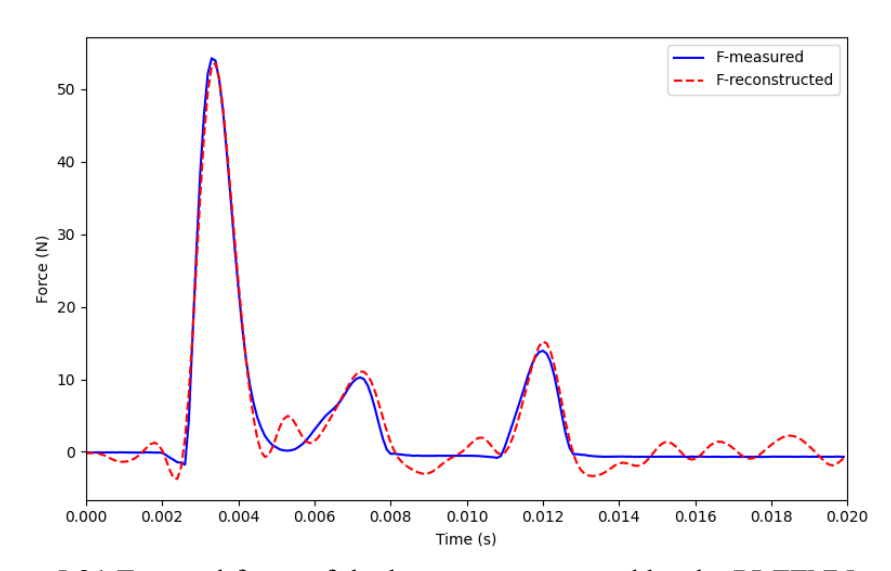


Figure 5.21 External force of the beam reconstructed by the PI-FFNN model

### 5.6 Summary

This study proposes a physics-informed Fourier feature neural networks (PI-

FFNN) framework for vibration-based structural damage identification with unknown external forces. In this framework, the external forces and damages of the structure are identified simultaneously without the input of external forces. A Fourier feature neural network is employed as the core of the framework to predict the external forces of the structure. The Fourier feature layer, which is proven to alleviate the spectral bias of the neural network model, is utilized to accurately express the multi-frequency characteristics of the external forces. PI-FFNN is a physical data coupled model that can utilize the Newmark-beta scheme of the motion equation as physical information to train the neural network model. A regularization term is also added to the loss function to improve the sparsity and noise robustness of the identification results. The integration of physical information enables PI-FFNN to train the model without any labeled data of structural damage, making it an unsupervised learning model.

Numerical examples of a cantilever beam and a plane truss are employed to verify the performance of the proposed method. The local damage and external forces on both structures are accurately identified even in the noisy data. In the cantilever beam case, the proposed method is also compared with the Markov parameters method with Tikhonov regularization and the original PINNs. The results show that PI-FFNN can obtain more accurate results in structural damage identification and force reconstruction. Afterward, a laboratory test is conducted on a beam structure. A PI-FFNN model is built to first identify the initial mechanical parameters of the intact beam and then accurately identify the damaged beam based on the identified initial mechanical parameters. The

external forces on the beam are also successfully identified showing a high agreement with the measured values.

# Chapter 6 Structural identification from unknown input excitations with physics-informed neural networks

#### 6.1 Introduction

Structural identification (Alvin et al., 2003; Noël & Kerschen, 2017) is the reverse modeling process of determining the characteristics and state of an unknown structure by analyzing the dynamic response and behavior of the structure. This process is crucial in the fields of engineering and infrastructure because it helps engineers assess the health of structures and detect potential damage and degradation in a timely manner. In recent years, with the rapid development of various advanced sensing methods and machine learning, a wide range of machine learning-based structural identification methods have been developed and applied in many engineering fields (D. Liu et al., 2023; Worden & Manson, 2007).

In theory, structural identification can be conceptualized as the inverse problem of discovering the intrinsic characteristics and behaviors of a structure from the observed data of the structure. Since the vibration acceleration response is easier to obtain than displacement and velocity, most methods of structural identification and structural damage detection are performed by analyzing the vibration response of the structure, which is the so-called vibration-based method (Avci et al., 2021; Fan & Qiao, 2011). After obtaining the vibration data, researchers will try to use various data analysis methods to process the measurement data. These analysis methods can be roughly

divided into two categories: physics-driven methods and data-driven methods. The former characterizes the physical characteristics of the structure by establishing physical models of the structure, such as the governing equations or finite element models (Girardi et al., 2020). Then the measured data is utilized to update the physical model so that the model can accurately represent the actual engineering structure. After decades of development, research work in the physical-driven direction has matured and has been successfully applied in many projects. For example, in (Arora et al., 2009), a damped finite element model updating procedure is proposed and tested with the objective that the proposed model is able to predict the measured FRFs accurately in a fixed beam structure and an F-shape structure.

The data-driven method has developed rapidly in recent years, with the explosive growth of machine learning and deep learning. In the data-driven method, structural identification is regarded as a pattern recognition problem, a problem that has been widely studied in the field of machine learning (Zhang et al., 2008). By establishing the characteristics of the structural vibration response related to the intrinsic properties of the structure, such as structural stiffness, the parameters of the structure are inversely identified by analyzing the characteristics of the vibration response. Among them, classic data-driven methods include Bayesian optimization (Z. Chen et al., 2020; Zuo & Guo, 2022), blind source separation (Sadhu et al., 2017; Zhou & Chelidze, 2007), and deep learning algorithms (Yu et al., 2019).

In the research that has been carried out, the external force input of the structure

is usually an important prior knowledge, which is used to input the physical model to predict the response in the physical-driven method and to extract the characteristics of the structural vibration in the data-driven method (Pan & Yu, 2019). However, in practical applications, the input excitations (such as earthquakes, wind loads, etc.) to the structure are often unknown, which poses a major challenge to existing structural identification. The dynamic characteristics and variability of these excitations make it difficult to accurately infer the true stress and deformation conditions of the structure based solely on the structural response data. Especially in the face of extreme weather or emergencies, failure to accurately identify the input excitation may lead to misjudgment of the health status of the structure, thereby affecting safety assessments and maintenance decisions. Therefore, solving the challenges brought by unknown input excitations is crucial to improving the accuracy and reliability of structural identification.

In order to deal with the limitations of unknown input excitation, we explored the feasibility of applying a new method called physics-informed neural networks (PINNs) in structural identification. PINNs framework is a new physics and data-coupled deep learning method proposed to solve the direct and inverse problems of nonlinear systems (Raissi et al., 2019). In PINNs, physical information described as various equations is seamlessly integrated into the training of machine learning models as prior information. Unlike purely data-driven methods, physics information is also considered as part of the model constraints to make the model's predictions endogenously consistent with

physical laws and improve the generalization and robustness of the model. The excellent performance of PINNs has been successfully obtained in many fields of physics and engineering, such as fluid mechanics (Mao et al., 2020), thermal analysis (He et al., 2021), and structural analysis (Abueidda et al., 2021). In this study, we develop a PINNs-based approach for structural identification from structural vibration measurements under unknown input excitations. In the proposed method, physical information is utilized to construct the mapping relationship between external loads and structural responses. A neural network model is employed to represent the unknown external excitations. The neural network model and the mechanical parameters of the structure are simultaneously updated to perform structural identification and external force reconstruction by minimizing the deviation between the predicted structural response and the vibration measurements. The nonlinearity in the structure can also be modeled by another neural network model to present the internal nonlinear restoring forces, which can also be identified together with the vibration response measurements.

The proposed framework contributes to the field of structural identification and health monitoring in terms of: (1) A PINNs framework is proposed to learn the governing dynamic characteristics of structural systems. The inherent physical laws of the model can be learned instead of just establishing an uninterpretable mapping relationship between input and output data. (2) The proposed method can perform structural identification under unknown external excitations using only the vibration response of the structure. This avoids the difficulty and cost of accurately measuring

external excitations. (3) The proposed method is applicable to both linear and nonlinear systems, forming a universal method in structural identification problems. The mechanical parameters of linear structural systems such as stiffness and damping can be directly inverted to discover the exact values. The nonlinear components can be modeled by establishing a surrogate model to characterize the nonlinear restoring forces.

The rest of the study is organized as follows: Section 2 introduces the background of the research. Section 3 presents the proposed method in detail. Section 4 and Section 5 verify the proposed method using numerical and experimental examples, respectively. Finally, the study is concluded in Section 6.

## 6.2 Background

#### **6.2.1** Motion equation of structural system

Consider a multi-degree-of-freedom structural system whose motion equation is

$$M\ddot{x} + C\dot{x} + Kx + f(x, \dot{x}) = F(t) \tag{6.1}$$

Here M is the mass matrix, C and K are the damping matrix and stiffness matrix of the structure.  $f(x, \dot{x})$  is the internal nonlinear restoring force, generated by the nonlinear stiffness or energy dissipation device. Eq. (6.1) is a second-order ordinary differential equation, which is usually solved by a numerical method to obtain the response of the structure  $(x, \dot{x}, \ddot{x})$  with the external force input F. Among these numerical methods, Newmark-beta is widely utilized because of its good numerical stability, flexibility, and accuracy. Specifically, the Newmark-beta method lists the following 4 equations at each time step and solves  $x_{n+1}$  and  $\dot{x}_{n+1}$  by inputting the

current state  $x_n$ ,  $\dot{x}_n$ , and the external forces  $F_n$  and  $F_{n+1}$ .

$$M\ddot{x}_n + C\dot{x}_n + Kx_n + f(x_n, \dot{x}_n) = F_n \tag{6.2}$$

$$M\ddot{x}_{n+1} + C\dot{x}_{n+1} + Kx_{n+1} + f(x_{n+1}, \dot{x}_{n+1}) = F_{n+1}$$
(6.3)

$$\dot{x}_{n+1} = \dot{x}_n + \Delta t \cdot ((1 - \gamma) \cdot \ddot{x}_n + \gamma \cdot \ddot{x}_{n+1}) \tag{6.4}$$

and

$$x_n = x_n + \Delta t \cdot \dot{x}_n + \frac{1}{2} \Delta t^2 \cdot ((1 - 2\beta) \cdot \ddot{x}_n + 2\beta \cdot \ddot{x}_{n+1})$$
 (6.5)

Here,  $0 \le \beta \le 0.5$  and  $0 \le \gamma \le 1$  are the parameters of the Newmark-beta method. By setting different combinations of values of  $\beta$  and  $\gamma$ , the Newmark method can be different schemes, such as the explicit central difference scheme ( $\beta$ =0,  $\gamma$ =0.5) and the average acceleration scheme ( $\beta$ =0.25,  $\gamma$ =0.5). In this study, the average acceleration scheme is used due to the advantages of its superior stability.

It is noted that the basis for using these numerical methods to solve Eq. (6.1) to obtain the structural response is that the structural parameters M, C, K, and the external force time series F(t) are all known. In general, the structural M matrix is easy to determine through weight measurement. However, the K and C matrices, as unobservable parameters of the structural system, usually need to be inversely determined through vibration testing. In addition, in actual engineering, the external forces of the structures are always difficult to measure accurately through sensors. The external forces also need to be inversely reconstructed through other measurement data. These studies on identifying structural parameters and reconstructing external forces from measurement data point to a research field called structural identification.

Theoretically, the purpose of structural identification is to estimate the physical parameters of the structure and identify unknown external excitations acting on the structure, such as earthquakes, wind loads, or other dynamic loads, by analyzing the dynamic response of the structure.

#### 6.2.2 Physics informed neural networks

Physics-informed neural networks (PINNs) (Raissi et al., 2019) are a type of neural network that integrates physical information as prior information to train the neural network, thereby reducing the demand for training data and increasing robustness to data sparsity and noise. For a physical system with the governing equation:

$$N(t, x, u(t, x); \theta) = f(t, x)$$
(6.6)

where  $N(\cdot)$  is a differential operator parameterized by  $\theta$ , and f(t,x) is the force term of the equation. PINNs can predict the exact value of u(t,x) given the parameter  $\theta$  and sufficient constraints, which is called the forward problem of the equation. PINNs can also use partial observations of u(t,x) to reversely discover the exact value of  $\theta$ , which is called the inverse problem. In solving the forward problem, unlike traditional deep neural networks, the loss function of PINNs is no longer defined as the residual between the predicted value and the training data, but is replaced by a physical loss function calculated as the residual of the governing equation as

$$Loss_{f} = \sum_{i=1}^{N_{f}} \left[ N(t_{i}^{f}, x_{i}^{f}, u(t_{i}^{f}, x_{i}^{f}); \theta) - f(t_{i}^{f}, x_{i}^{f}) \right]^{2}$$
 (6.7)

Here,  $N_f$  is the number of sampling points  $(t_i^f, x_i^f)$  in the equation domain, at which the residual of the governing equation is calculated. The constraints are also

embedded through a loss function calculated as

$$Loss_{u} = \sum_{i=1}^{N_{u}} [u(t_{i}^{u}, x_{i}^{u}) - u'(t_{i}^{u}, x_{i}^{u})]^{2}$$
(6.8)

Here,  $N_u$  is the number of sampling points  $(t_i^u, x_i^u)$  on the equation constraints, and u' is the exact value on the constraint conditions of the equation. By employing an optimizer to minimize  $Loss = Loss_f + Loss_u$ , the u(t,x) predicted by PINNs can gradually satisfy both the governing equation and the constraints, thus approaching the exact equation solution. With the support of physical information of the governing equation, PINNs can solve the forward problem of the physical system without any training data.

For the inverse problem, the residual of the governing equation referred to in Eq. (6.7) will also be utilized as part of the loss function. However, since the value of  $\theta$  is unknown, it is an ill-posed problem to discover the  $\theta$  value only with the governing equation. For this reason, some measurement points are recorded to form a loss function  $Loss_u$  as

$$Loss_{m} = \sum_{i=1}^{N_{m}} [u(t_{i}^{m}, x_{i}^{m}) - u^{m}(t_{i}^{m}, x_{i}^{m})]^{2}$$
(6.9)

Here  $N_m$  is the number of observations, and  $u^m$  is the observed value at the observation point  $(t_i^m, x_i^m)$ . Similarly, using an optimizer to minimize  $Loss = Loss_f + Loss_m$ , the u(t,x) predicted by PINNs can gradually approach the observed data and satisfy the physical information constraints described by the governing equations. In this way, PINNs can successfully discover the accurate value of  $\theta$  using only a small amount of observed data. Due to the constraints of physical information,

rather than relying solely on observed data, PINNs also show strong noise robustness (Arzani et al., 2021).

# 6.3 Methodology

In this section, we will develop a framework based on PINNs for structural identification. In reality, structures are often forced to vibrate due to external forces or displacement excitations rather than simply free vibrations. These external excitations, such as wind loads and water impacts, are difficult to measure accurately. Due to the inertia of the sensor, using the sensor directly in the path of the excitation will also affect the excitation on the structure. In addition, the internal restoring forces generated by the nonlinearity of the structure are also difficult to observe through sensors. These unobservable factors will restrict the application of traditional physical methods that rely on accurate force measurements, such as finite element model updating, on actual structures. Therefore, inspired by PINNs, in our proposed method, two neural network models are designed to represent the unknown external forces and internal restoring forces on the structure to fully utilize the powerful representation capabilities of the neural network model. Specifically, two neural network models with the input of time t output the external force and internal restoring force of the structure, respectively. Their physical relationships can be expressed as  $NN^{ex}(t) \rightarrow F_t^{ex}$  and  $NN^{in}(t) \rightarrow$  $F_t^{in}$  respectively.

Spectral bias (Wang et al., 2021) is a well-known shortcoming of neural networks, which manifests itself as neural networks preferentially learning low-frequency

components in the data and ignoring high-frequency components. Time series data of external forces and internal restoring forces of the structure are mostly composed of a mixture of multiple frequency components, which will easily fall into the trap of spectral bias when neural network models are utilized to represent these forces. Fourier feature layer (Wang et al., 2021) technology which has been proven to be an effective and simple way to mitigate the spectral bias of neural networks, has been applied and analyzed in (Sallam & Fürth, 2023; Song & Wang, 2023). In order to improve the ability of  $NN^{ex}$  and  $NN^{in}(t)$  models to represent multiple frequencies in the reconstructed force, a Fourier feature layer is established in both  $NN^{ex}$  and  $NN^{in}$  models. The mathematical relationship of the Fourier feature layer can be expressed as

$$L_{FF}(x,W) = \begin{bmatrix} \cos(2\pi W \cdot t) \\ \sin(2\pi W \cdot t) \end{bmatrix}$$
 (6.10)

Here  $L_{FF}$  is the output of the Fourier feature layer, and t is the input of the  $NN^{ex}$  model. W is the trainable parameter, the weight of the Fourier feature layer, which is initialized according to the distribution  $N(0, \sigma^2)$ .  $\sigma$  is a hyperparameter that controls the distribution range of W to determine the frequency distribution of the features established by the Fourier layer. The value of  $\sigma$  can be determined by observing the frequency spectrum of the vibration measurement data. Subsequently, the output from the Fourier feature layer is input into a fully connected neural network (FCNN) for nonlinear mapping. The FCNN model of  $NN^{ex}$  outputs unknown excitations on the structure, which are acceleration or external force of one or several degrees of freedom, or ground acceleration. The FCNN model of  $NN^{in}$  is used to

reconstruct the internal restoring force of one or several degrees of freedom. Both FCNN models consist of L hidden layers and one output layer. Each hidden layer includes H neurons. The hyperbolic tangent function is utilized as the activation function to provide nonlinear expression capabilities to FCNN models. It is worth noting that for time-invariant systems, the internal restoring force usually depends on the state of the structure  $(x, \dot{x})$  rather than on the time t, so this model will be replaced by another neural network model that takes the system state as input to discover the potential relationship between the structural state and the internal force after successfully reconstructing the internal restoring force.

In order to identify the accurate stiffness of the structural system, a stiffness update vector  $z^k$  is defined to update the stiffness of structural components. Assuming that the structure consists of  $N_i$  components and the initial stiffness of the i-th element is  $k_i^0$ . Then the component stiffness can be updated by

$$k_i^z = z_i^k \cdot k_i^0 \tag{6.11}$$

The  $z^k$  vector is initialized to an all-ones vector. The updated stiffness matrix  $K^z$  can be constructed using the updated stiffness of the components. The accurate mass matrix M is considered to be available, so it does not need to be updated. The damping matrix of the system is set to Rayleigh damping, which is calculated as

$$C^z = z_1^c \cdot a^0 \cdot M + z_2^c \cdot b^0 \cdot K^z \tag{6.12}$$

Here,  $z^c = [z_1^c, z_2^c]$  is a damping coefficient update vector with a size of 2 and initialized to an all-ones vector.  $a^0$  and  $b^0$  are the initial damping systems, and  $C^z$ 

is the updated damping matrix.  $z^k$  and  $z^c$  are two trainable vectors that will be updated together with the neural network model.

Now, the unknown external forces and internal restoring forces in Eq. (6.1) are represented by the neural network, and the K and C matrices are set as the updated  $K^z$ ,  $C^z$ . Then the predicted structural response can be calculated according to Eq. (6.1). Here, the mature numerical solver Newmark-beta method is utilized to estimate the predicted response of the structure to take full advantage of its efficiency and stability. Although PINNs have also been proven to be able to solve differential equations, the accuracy of the solution cannot be guaranteed due to the 'soft' embedding of constraints (X. Li et al., 2024) and the unbalanced convergence speed of multiple loss functions (Wang et al., 2022). Using the structural response calculated from the Newmark-beta method, a loss function is constructed by measuring the deviation between the calculated and measured values as

$$Loss_{pinn} = \sum_{i=1}^{N_m} [\ddot{x}^{pred}(t_i^m) - \ddot{x}^m(t_i^m)]^2$$
 (6.13)

Here,  $N_m$  is the number of observations.  $\ddot{x}^{pred}$  is the predicted value of the acceleration response obtained from the Newmark-beta method, and  $\ddot{x}^m$  is the measured value of the structural vibration response. By using a gradient descent-based optimizer, such as Adam (Kingma, 2014) to minimize the loss function, the output of the neural network  $NN^{ex}$  will approach the true external force and the output of  $NN^{in}$  will be close to the true internal restoring force.  $Z^k$  and  $Z^c$  will update  $K^z$  and  $K^c$  to discover the true parameters of the system, thereby completing system parameter

identification and internal and external forces estimation. The overall framework of the proposed method is shown in Fig. 6.1.

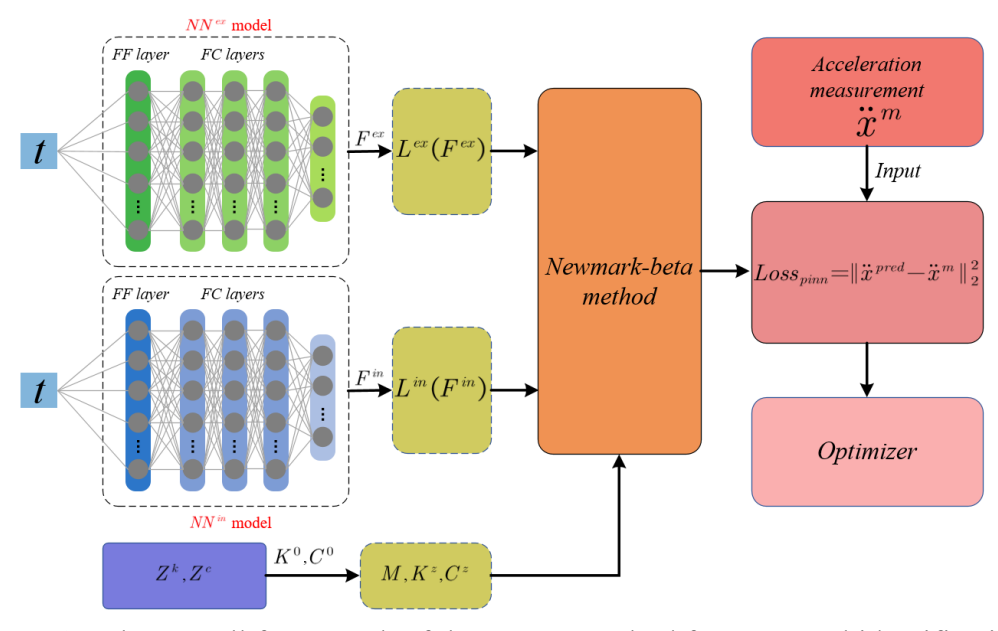


Figure 6.1 The overall framework of the PINNs method for structural identification.

In Fig. 6.1, model  $NN^{ex}$  and model  $NN^{in}$  are the neural network models for predicting external excitation and internal restoring force, respectively.  $L^{ex}$  and  $L^{in}$  are the mapping matrices of external excitation and internal restoring force, respectively.

It is noted that to ensure that the problem of structure identification is well-posed, the number of response observations needs to be greater than the number of unknown external and internal excitations. The unknown external forces and unknown internal restoring forces should not act on the same degree of freedom to avoid mutual interference. After successfully reconstructing the time series data of the system's internal restoring force, the identified structural model cannot be utilized to predict the structural response under new external loads. This is because the internal restoring force

usually depends on the structural system state  $(x, \dot{x})$ , rather than on t. Therefore, it is necessary to establish a mapping relationship between internal restoring force and structural system state  $(x, \dot{x})$  so that the identified model can predict the dynamic response of the structure under new loads. Generally, it is a feasible path to learn the mapping relationship between internal restoring force and structural state by establishing a new neural network model. However, the internal force we reconstruct usually has only a small number of time steps, typically a few hundred to a few thousand. The neural network model learned based on such a small number of samples will have a large deviation from the real physical relationship. Here, the advantage of PIML in learning physical mapping relationships from sparse data by using physical information enhancement is again utilized. An FCNN model as shown in Fig. 6.2 with the structural state  $(x, \dot{x})$  as input is established to approximate the internal restoring force of the structure, and its physical relationship can be expressed as  $FCNN^{in}(x_t, \dot{x}_t) \rightarrow f_t$ . Known physical information, such as the cubic relationship between internal force and displacement or the hysteresis governing equation, is utilized to provide prior physical information for the training of the FCNN<sup>in</sup> model. The reconstructed internal restoring force data from the NN<sup>in</sup> model is also used to determine the unknown parameter in the physical information. Specifically, the loss functions of FCNN<sup>in</sup> model are constructed as

$$Loss_{phy} = \sum_{i=1}^{N_m} [N(x_t, \dot{x}_t; \theta) - f^{rec}(t)]^2$$
 (6.14)

$$Loss_{data} = \sum_{i=1}^{N_m} [f^{pred}(x_t, \dot{x}_t) - f^{rec}(t)]^2$$
 (6.15)

and

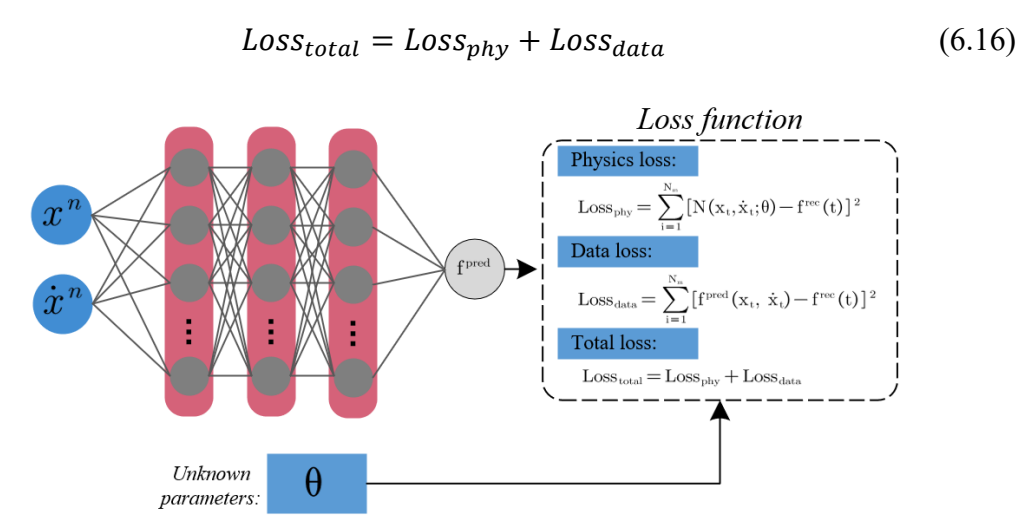


Figure 6.2 The architecture of the FCNN<sup>in</sup> model

Here  $N_m$  is the number of reconstructed internal restoring forces,  $f^{pred}$  is the restoring force predicted by the  $FCNN^{in}$  model, and  $f^{rec}$  is the restoring force reconstructed from the  $NN^{in}$  model shown in Fig. 6.1.  $N(\cdot)$  is a known physical relationship, with the unknown control parameter  $\theta$ . The unknown parameters  $\theta$  are also trained and updated together with the neural network model. A similar gradient descent-based optimizer is employed to minimize the loss function  $Loss_{total}$ , so that the  $FCNN^{in}$  model can successfully represent the internal restoring force and the value of the control parameter  $\theta$  in the physical relation  $N(\cdot)$  can be discovered. After training, the discovered control parameters  $\theta$  and physical information  $N(\cdot)$  can be used to estimate the internal restoring force depending on the state of the structure  $(x, \dot{x})$ . At this point, the PINNs framework proposed has the ability to predict the structural response under new external excitations. By inputting new external forces

to the PINNs framework and employing the discovered physical information  $N(x, \dot{x}, \theta)$  to predict the internal restoring force, the response of the structure can be predicted by the Newmark-beta method with the updated structural parameters  $K^z$  and  $C^z$ .

It is noted that our proposed PINNs method is not the first study on physics-informed machine learning (PIML) for structure identification. Several PIML frameworks for structural dynamic response prediction and structure damage detection have been published, among which the most well-known one for structure identification is the physics-informed neural ordinary differential equations (PI-NODE) framework (Lai et al., 2021). For comparison, the differences between our proposed framework and PI-NODE are summarized in Table 6.1.

Table 6.1 Summary of the differences between proposed framework and PI-NODE

	PI-NODE	Proposed framework
Model input	Structural state (displacement and velocity), external force	Vibration response
Mechanical parameters	Exact value	Initial guess
Neural network	NODE	FFNN, FCNN
Solver	ODE solver	Newmark-beta method

In structural identification, pure data-driven machine learning algorithms use the measured vibration responses of multiple degrees of freedom as training data to learn their potential mapping relationships and then use model extrapolation to predict the output. However, changes in the initial conditions of the structure and the external force

input will cause the mapping relationship to change, resulting in the failure of data-driven model prediction. The method we proposed is different from the simple input-output mapping relationship fitting of machine learning. The proposed method aims to explore the intrinsic physical information of the structural system, so as to more accurately reflect the fundamental dynamic characteristics of the system. In addition, due to the integration of the governing equation, the proposed method can adapt well to changes in structural input and initial conditions. In addition, physics-driven methods, such as finite element model updating and sensitivity-based methods, are input-output methods. This means that accurate measurement of the external excitation of the model is required, which is always difficult in actual engineering. Moreover, the difficulty in adapting to nonlinear restoring forces in the physics-driven methods also limits their scope of use.

#### **6.4 Numerical cases**

### 6.4.1 4-degree-of-freedom system

To demonstrate the proposed method, a 4-degree-of-freedom (4-DOF) dynamical system with cubic nonlinearity is studied as a numerical example. The system is shown in Fig. 6.3 as a spring-mass model commonly used in structural dynamic simulation. A nonlinear spring with cubic stiffness is added on  $m_1$ .

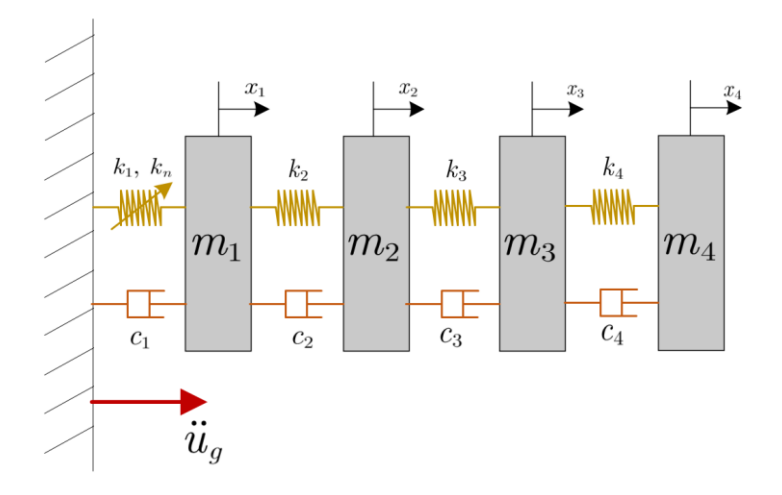


Figure 6.3 4-DOF structural dynamic system

The equation of motion for this 4-DOF structure can be expressed as

$$\begin{cases} m_1\ddot{x}_1(t) + (k_1 + k_2)x_1(t) - k_2x_2(t) + (c_1 + c_2)\dot{x}_1(t) - c_2\dot{x}_2(t) + k_nx_1^3(t) = m_1\ddot{x}_g(t) \\ m_2\ddot{x}_2(t) - k_2x_1(t) + (k_2 + k_3)x_2(t) - k_3x_3(t) - c_2\dot{x}_1(t) + (c_2 + c_3)\dot{x}_2(t) - c_3\dot{x}_3(t) = m_2\ddot{x}_g(t) \\ m_3\ddot{x}_3(t) - k_3x_2(t) + (k_3 + k_4)x_3(t) - k_4x_4(t) - c_3\dot{x}_2(t) + (c_3 + c_4)\dot{x}_3(t) - c_4\dot{x}_4(t) = m_3\ddot{x}_g(t) \\ m_4\ddot{x}_4(t) - k_4x_3(t) + k_4x_4(t) - c_4\dot{x}_3(t) + c_4\dot{x}_4(t) = m_4\ddot{x}_g(t) \end{cases}$$
(6.17)

Here, x,  $\dot{x}$ ,  $\ddot{x}$  are displacement, velocity, and acceleration, respectively. The linear stiffness system is  $k_1=k_2=k_3=k_4=100$ . The cubic stiffness of the nonlinear spring is  $k_n=1000$ . The masses of the four degrees of freedom are  $m_1=m_2=2.0$  and  $m_3=m_4=1.0$ . The damping matrix C is defined as C=0.45.  $M+0.018\cdot K$ . Assume that the structure vibrates from rest due to the ground acceleration. The ground acceleration is  $\ddot{x}_g=10sin(2\pi t)+3sin(4\pi t)+2sin(6\pi t)$ . An implicit second-order Runge-Kutta method (Iserles, 2008) is utilized as a numerical solver to calculate the vibration response of the structure as training data. The training time step is  $dt=0.01\,s$  and the calculation duration is  $5.0\,s$ . The time series data and frequency spectrum of the calculated vibration response are shown in Fig. 6.4.

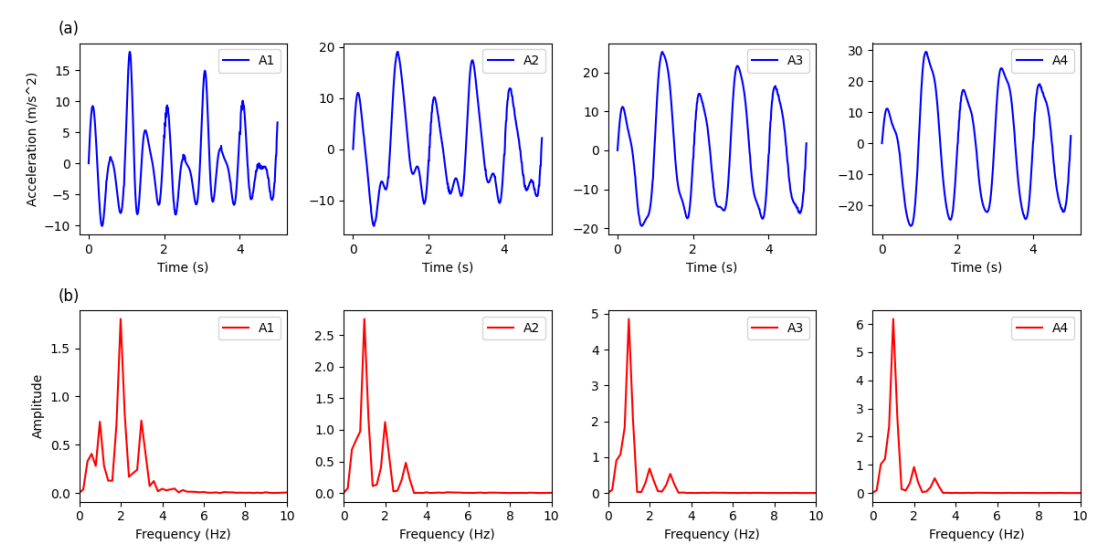


Figure 6.4 (a) Vibration response and (b) frequency spectrum of the structure calculated by the numerical solver

Assuming that the mass of the structure is known and the vibration responses of the four degrees of freedom as shown in Fig. 6.4 is recorded, a PINNs framework for structural identification as shown in Fig. 6.1 is built to reversely discover the accurate values of K and C and reconstruct the restoring force of the nonlinear stiffness spring. The initial guess of the stiffness of all linear springs is set to 50, and the initial value of the damping coefficients a and b is set to 0.1 and 0.001. Two update vectors  $z^k$  and  $z^c$  are initialized and trained to update the stiffness matrix K and damping matrix C of the structure. Two FFNN models are established to represent the unknown ground acceleration and the restoring force of the nonlinear spring, respectively. According to the frequency spectrum of the vibration response, the hyperparameter  $\sigma$  of the Fourier layer in the FFNN model is set to 10. The number of fully connected hidden layers in the FFNN is 2, and each layer contains 100 neurons. Using the ground acceleration and

internal restoring force predicted by the two FFNNs, as well as the updated  $K^z$  and  $C^z$  matrices, the response of the structure is predicted using the Newmark-beta method, and the loss function is constructed with the vibration response of the structure. Here, the noise-free vibration data of 0-2s is first considered as the training data. A gradient descent-based optimizer Adam is employed to minimize the loss function with a learning rate of 0.001. The entire framework is trained with 50,000 iterations, and the convergence process of the loss function is shown in Fig. 6.5. The entire training process of the model took 3563.16 seconds.

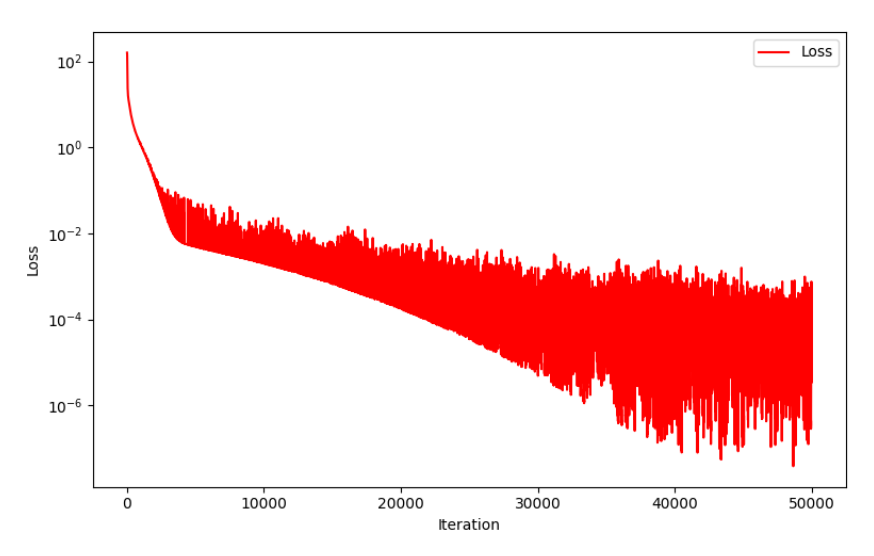


Figure 6.5 Convergence process of loss function

After training, Fig. 6.6 shows the predicted structural displacement, velocity, and acceleration responses of four degrees of freedom from 0 to 2 seconds. The results show that the prediction of the structural response of (0-2 s) is very close to the ground truth, which means that our framework successfully learns the input data of the model and reconstructs the velocity and displacement responses of the structural system.

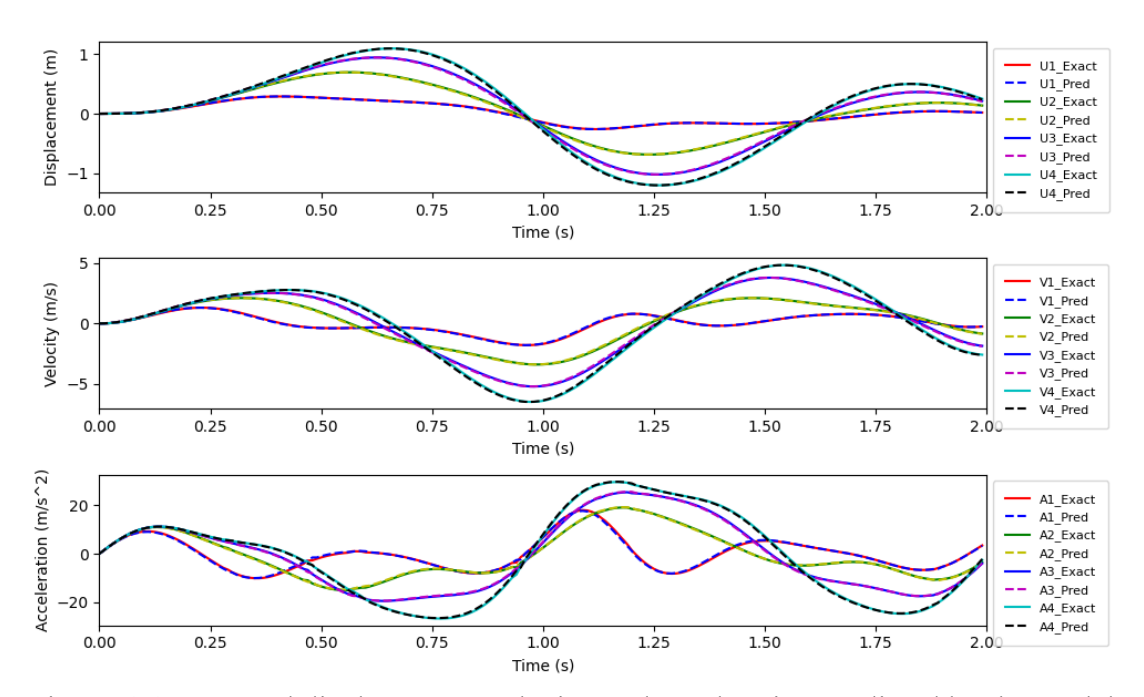


Figure 6.6 Structural displacement, velocity, and acceleration predicted by the model

From the output of the  $NN^{ex}$  model, the acceleration response of the ground is also reconstructed and is shown in Fig. 6.7. The results show that the  $NN^{ex}$  model successfully reconstructs the time series of ground acceleration based on the vibration measurements.

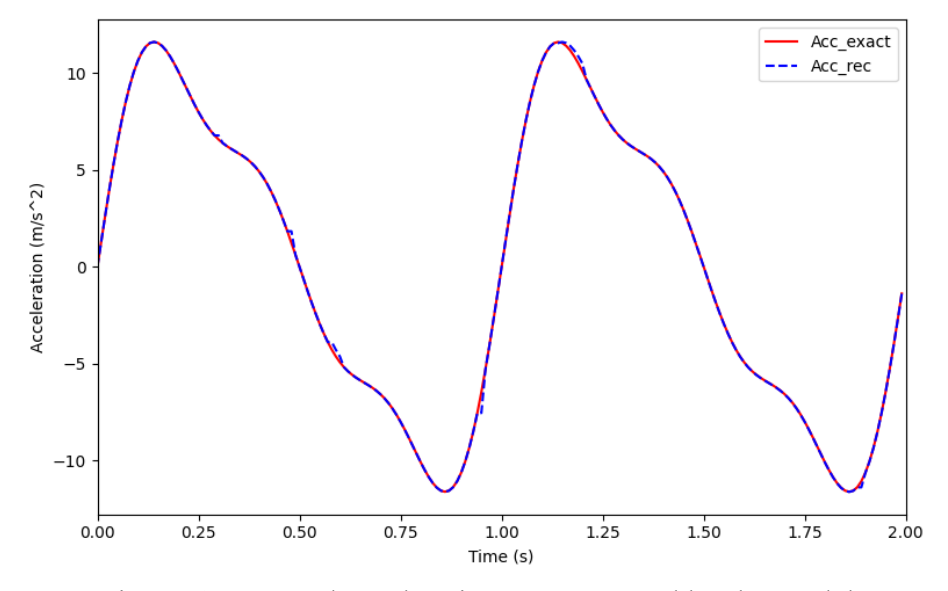


Figure 6.7 Ground acceleration reconstructed by the model

The structural stiffness discovered from the PINNs framework are  $k_1$ =72.67,  $k_2$  = 100.00,  $k_3$ =100.00,  $k_4$ =100.00. The discovered results show that the PINNs framework accurately discovered the accurate value of the structural stiffness of  $k_2$ ,  $k_3$ , and  $k_4$ . The discovered damping coefficients a = 0.450 and b = 0.018 are also consistent with the true value. The value of  $k_1$  is not accurately found because the partial restoring force of the linear spring  $k_1$  is also included in the force reconstructed by the  $NN^{in}$  model together with the restoring force of the cubic spring. To show the total restoring force of the nonlinear springs  $k_n$  and  $k_1$ , the predicted nonlinear restoring force output of the  $NN^{in}$  model and the predicted linear restoring force of  $k_1$  are summed as the total restoring force. The time series data of the internal restoring force reconstructed by  $NN^{in}$  model, the linear restoring force of  $k_1$ , and their sum values are shown in Fig. 6.8.

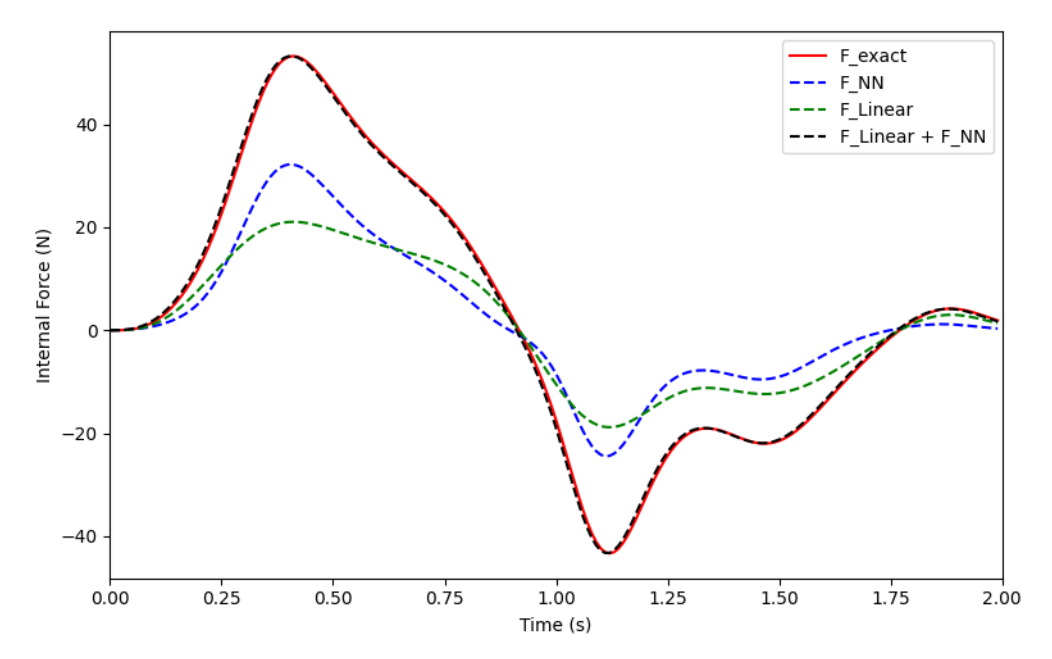


Figure 6.8 The time series data of the internal restoring force

Fig. 6.8 shows that the sum of the internal restoring force reconstructed by the  $NN^{in}$  model and the linear restoring force of  $k_1$  successfully reconstructs the total internal restoring force of the structure generated by linear springs and nonlinear springs. In order to make the PINNs model have the ability to extrapolate, i.e., to predict the structural response under a new external force, an FCNN model with input of the structural state is established to replace the  $NN^{in}$  model to predict the internal restoring force. This FCNN has 4 hidden layers, each consisting of 100 neurons. The prior physical knowledge of the linear and cubic relationship between the internal restoring force and the structural displacement response is utilized to train the FCNN model. The loss function of the FCNN model can be expressed as:

$$Loss_{phy} = \sum_{i=1}^{N_m} [\theta_1 \cdot x_i^3 + \theta_2 \cdot x_i - f^{rec}(t_i)]^2$$
 (6.18)

$$Loss_{data} = \sum_{i=1}^{N_m} [f^{pred}(x_i) - f^{rec}(t_i)]^2$$
 (6.19)

and

$$Loss_{total} = Loss_{phy} + Loss_{data} (6.20)$$

Here  $N_m = 200$  represents the reconstructed internal restoring force for 200 steps shown in Fig. 6.8.  $\theta = (\theta_1, \theta_2)$  are unknown parameters trained together with the FCNN model.  $f^{rec}$  is the reconstructed internal restoring force in Fig. 6.8 and  $f^{pred}$  is the restoring force predicted by the FCNN model. The Adam optimizer is employed to train this FCNN model 10,000 times with a learning rate of 0.001 until the loss function converges. After training,  $\theta_1$  and  $\theta_2$  converge to 995.56 and 27.14 respectively, and the restoring force of the nonlinear spring is identified as  $f_1^{in} =$ 

995.56 ·  $x_1^3$  + 99.81 ·  $x_1$ , which is close to the true value  $f_1^{in} = 1000 \cdot x_1^3 + 100 \cdot x_1$ .

Now, the identified expression for the nonlinear spring can be employed to predict the internal restoring forces according to the state of the structure, which enables PINNs to predict the structural response of this 4-DOF system under new forces. To verify the performance of PINNs, the ground acceleration of 2-5 s will be used as the external force and the calculation results of 2-5 s in Fig. 6.4 are used as ground truth. Here, the identified expression for the nonlinear spring is used to predict the internal restoring force  $F_t^{in}$  of the structure, and the external force  $F_t^{ex}$  is applied by ground acceleration. The parameters of the structure are set according to the discovered structural stiffness and damping coefficients. The Newmark-beta method in the PINNs framework is also utilized to predict the vibration response of the structure. The acceleration responses of this 4-DOF system predicted by PINNs are shown in Fig. 6.9. The results show that PINNs can accurately predict the seismic response of this 4-DOF structure under the ground acceleration.

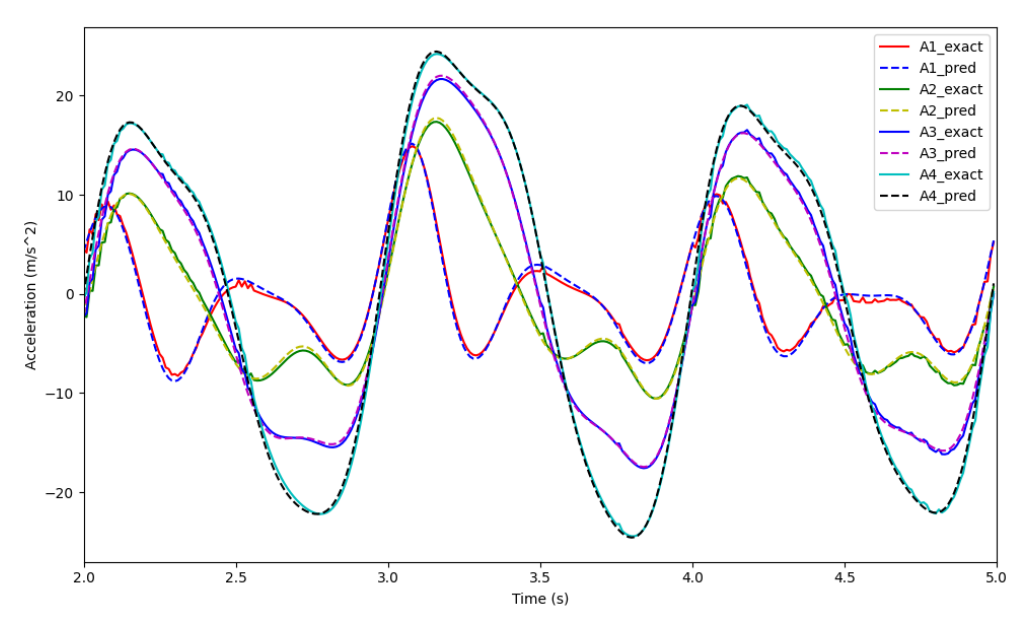


Figure 6.9 The acceleration responses predicted by PINNs model

We further discuss the performance of the proposed framework with noisy measured data. The above system identification process is performed on the training data containing 1% and 5% Gaussian noise. Table 6.2 shows the identified structural parameters from the noise measurement. The results show that the error of structural parameter identification increases with the increase of noise level. The damping coefficient a is more sensitive to noise than the stiffness k and the damping coefficient b. In the training data with 1% noise, the error of stiffness identification is less than 0.2%, and the damping coefficient b is accurately identified. In the training data with 5% noise, the error of stiffness identification is less than 3%, and the relative error of the damping coefficient b is 5.56%. The proposed method demonstrates excellent noise robustness in this case.

Table 6.2 Structural parameters identified from noisy training data

Noise level	$k_2$	$k_3$	$k_4$	а	b
1%	100.15	100.11	99.98	0.498	0.018
5%	98.68	97.12	100.44	0.260	0.019
Exact	100.00	100.00	100.00	0.450	0.018

In the cases of noisy training data, the internal restoring forces of the nonlinear springs are also reconstructed through the prediction of the  $NN^{in}$  model. Similarly, the total internal restoring forces are calculated as the sum of the internal restoring forces predicted by the  $NN^{in}$  model and the restoring force of the identified linear spring  $k_1$ . The results of total internal restoring force in the cases of noisy training data are shown in Fig. 6.10. The result shows that the nonlinear internal restoring forces of the structural system are successfully reconstructed in the cases of noisy training data. As the noise level in the training data increases, the error in the identified internal restoring forces increases.

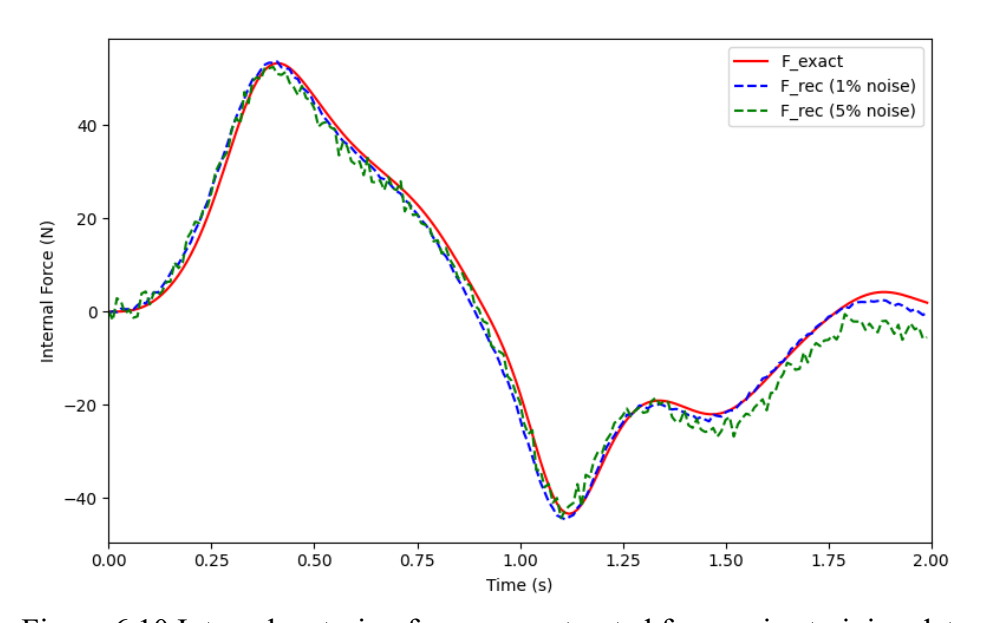


Figure 6.10 Internal restoring force reconstructed from noisy training data

Similar to the case of training data without noise, an FCNN model is also employed to learn the mapping between the internal restoring force and the displacement of  $m_1$  in the noisy training data. The linear and cubic relationship between the restoring force and displacement response of the nonlinear spring is used as prior physical information to train this FCNN model. The loss functions of the FCNN model are shown in (Eq. 6.17) – (Eq. 6.19). After 20,000 training iterations, the value of the unknown parameter theta has converged. The internal restoring forces of the identified nonlinear spring are  $f_1^{in} = 949.92 \cdot x_1^3 + 105.82 \cdot x_1$  (1% noise) and  $f_1^{in} = 762.07 \cdot x_1^3 + 110.63 \cdot x_1$  (5% noise). It is seen here that as the noise level increases, the error in the identified structure will also increase. After successful training, this identified expression of the restoring force is utilized to predict the internal restoring force of the structure so that the PINNs framework can predict the response of the structure under new external excitations. Similarly, the ground acceleration of 2-5 s is input as an external force and the calculated acceleration response results of the two noise cases are shown in Fig. 6.11. The results show that the identified structure can successfully and accurately predict the dynamic response of the structure under new external loads.

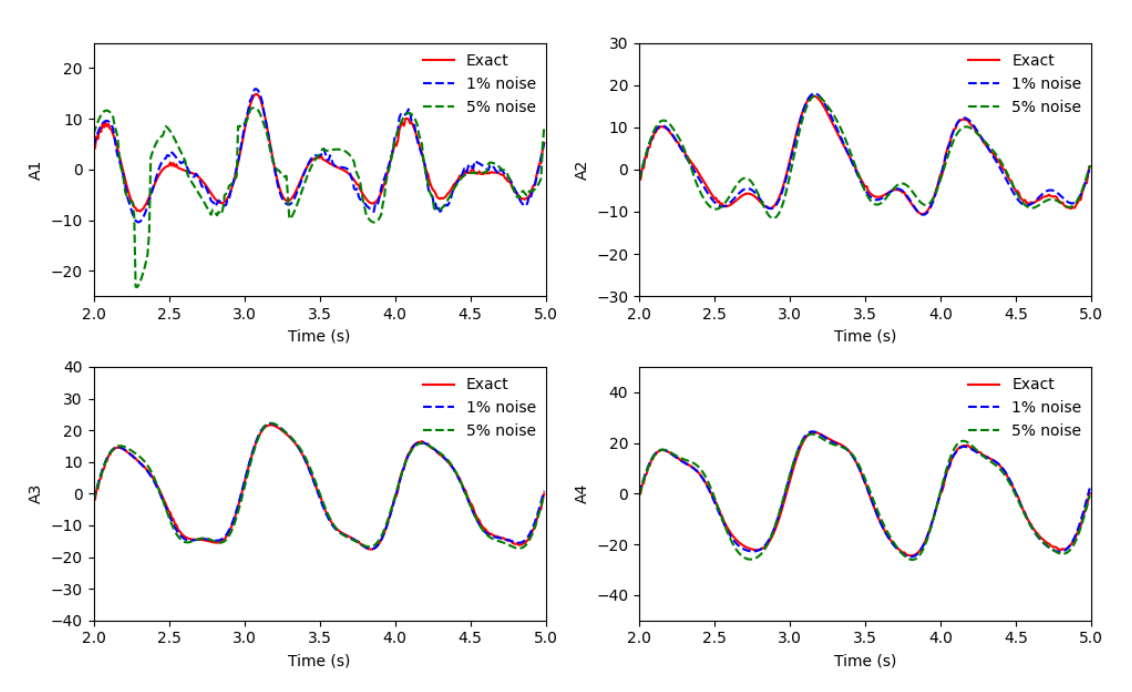


Figure 6.11 The calculated structural acceleration response of noisy cases

# 6.4.2 Bouc-Wen hysteresis system

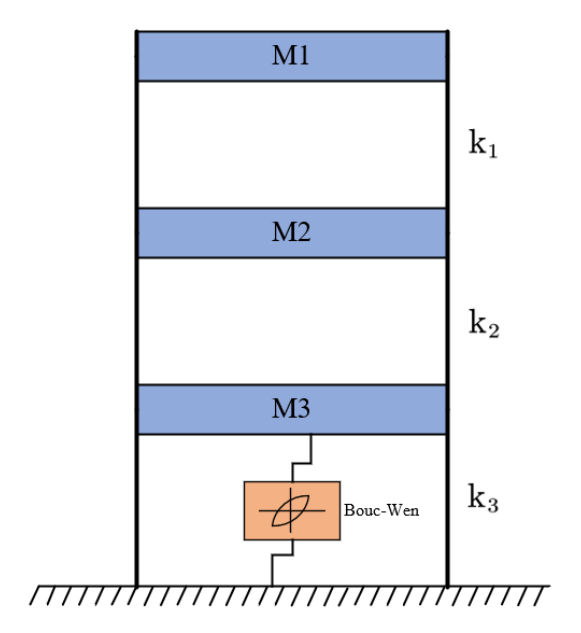


Figure 6.12 3-DOF system with Bouc-Wen hysteresis model

A 3-DOF system with Bouc-Wen hysteresis model as shown in Fig. 6.12 is analyzed as a numerical case for structural identification. The masses of the three

degrees of freedom are  $M_1 = 1kg$ ,  $M_2 = 2kg$ ,  $M_3 = 3kg$ . The stiffness of the linear springs is  $k_1 = 20N/m$ ,  $k_2 = 25N/m$ ,  $k_3 = 15N/m$ . The hysteresis force of the Bouc-Wen hysteresis model is calculated according to

$$F_{BW} = k_{BW} * z(t) \tag{6.21}$$

Here  $k_{BW}$  is the Bouc-Wen stiffness set to 15 N/m, z(t) is the unobservable hysteresis displacement, which obeys a nonlinear differential equation with initial condition z(0) = 0, as

$$\dot{z}(t) = \dot{u}(t) - \beta |\dot{u}(t)| |z(t)|^{n-1} z(t) - \gamma \dot{u}(t) |z(t)|^n$$
(6.22)

Here, the Bouc-wen parameters are set as  $\beta=0.75$ ,  $\gamma=0.5$ , n=2.0. This structural system vibrates under seismic acceleration of the amplified EI-Centro earthquake (Ha et al., 2004), as shown in Fig. 6.13. A second-order implicit Runge-Kutta method (Iserles, 2008) is used to calculate the vibration response of the structure, with a time step of 0.01s and a calculation time of 5s. The time domain curves and frequency distribution of the acceleration response of the three degrees of freedom are shown in Fig. 6.14.

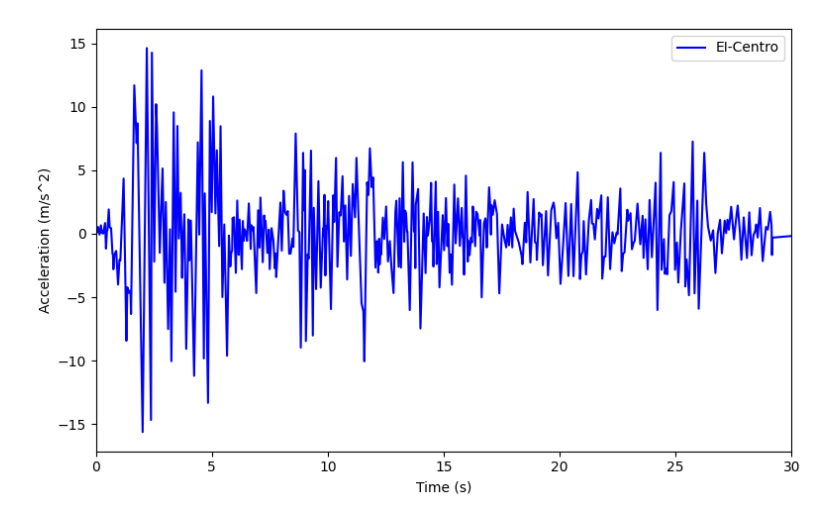


Figure 6.13 The amplified EI-Centro seismic acceleration

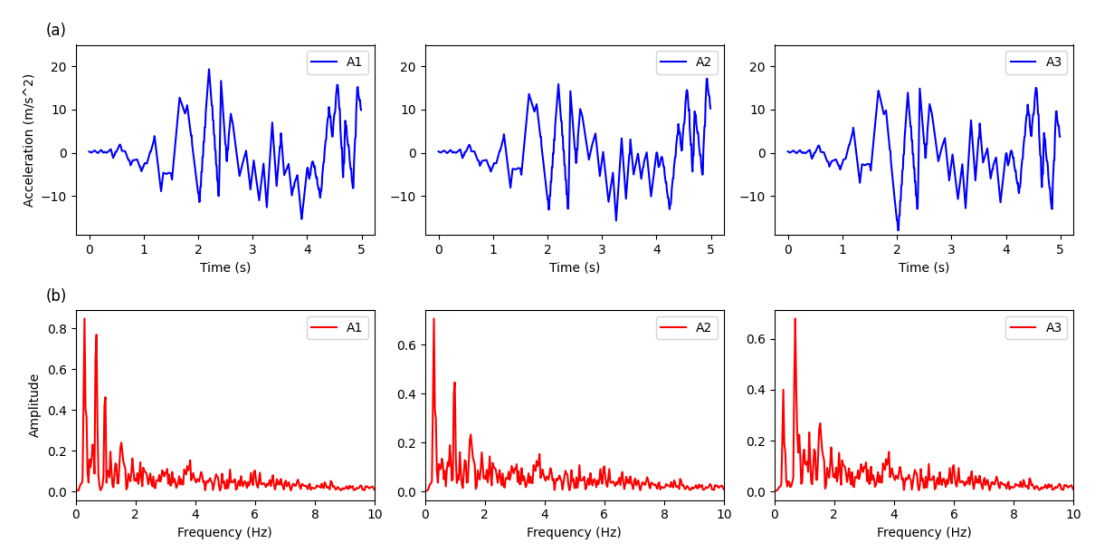


Figure 6.14 The time domain curves (a) and frequency distribution (b) of the acceleration response of the 3DOF system

Using the known mass matrix M and the calculated acceleration response as the measured vibration data, a PINNs model is established to identify the stiffness matrix K of the structure and reconstruct the external seismic acceleration and the internal restoring force generated by the Bouc-Wen model. The stiffness of linear springs is initialized to  $10 \, N/m$ , and a three-element update vector  $z^k$  is defined and initialized to an all-ones vector to update the stiffness of the linear springs by Eq. 6.11. Two FFNN models are established to represent the unknown ground acceleration and the restoring force of the Bouc-Wen system, respectively. According to the frequency spectrum of the vibration response shown in Fig. 6.14, the hyperparameter  $\sigma$  of the Fourier layer in the FFNN model is set to 10. The number of fully connected hidden layers in the

internal restoring force predicted by the two FFNN models, as well as the updated  $K^z$  matrix, the response of the 3-DOF system is predicted using the Newmark-beta method, and the loss function is constructed with the vibration response of the structure. Here, the noise-free vibration data of  $0-5\,s$  is considered as the training data. A gradient descent-based optimizer Adam is employed to minimize the loss function with a learning rate of 0.001. The entire framework is trained with 30,000 iterations, and the convergence process of the loss function is shown in Fig. 6.15.

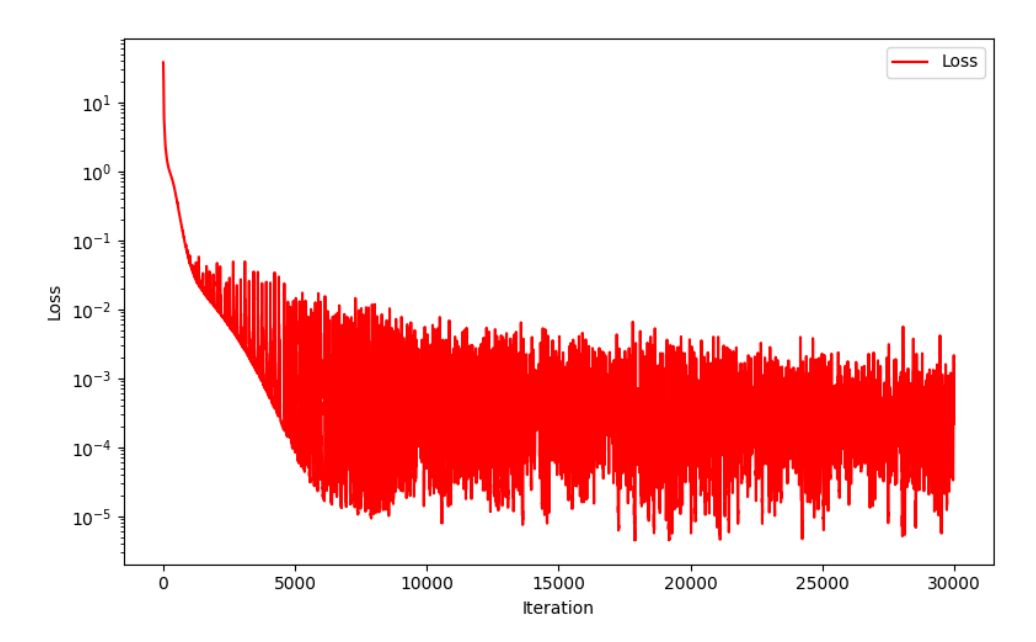


Figure 6.15 The convergence process of the loss function

After training, the displacement response of the 3-DOF system is also reconstructed as shown in Fig. 6.16 by the Newmark-beta method with the ground acceleration and internal restoring force predicted by the two FFNN models. This result shows that the reconstructed system responses are consistent with the benchmark solution. The ground acceleration is also reconstructed by *NN<sup>ex</sup>* as shown in Fig. 6.17.

The results show that our proposed PINNs also successfully reconstructed the unknown seismic acceleration on this 3-DOF system using the measurement of the structural vibration response.

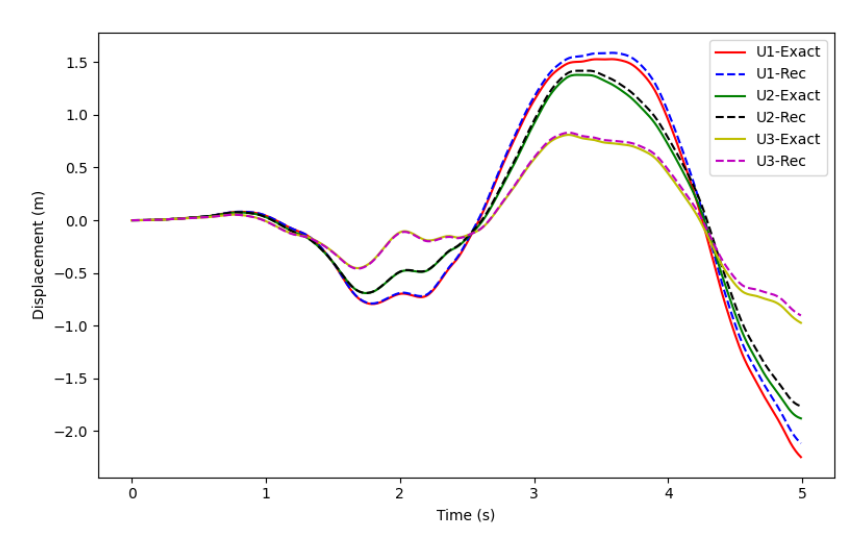


Figure 6.16 The reconstructed displacement response of the 3-DOF system

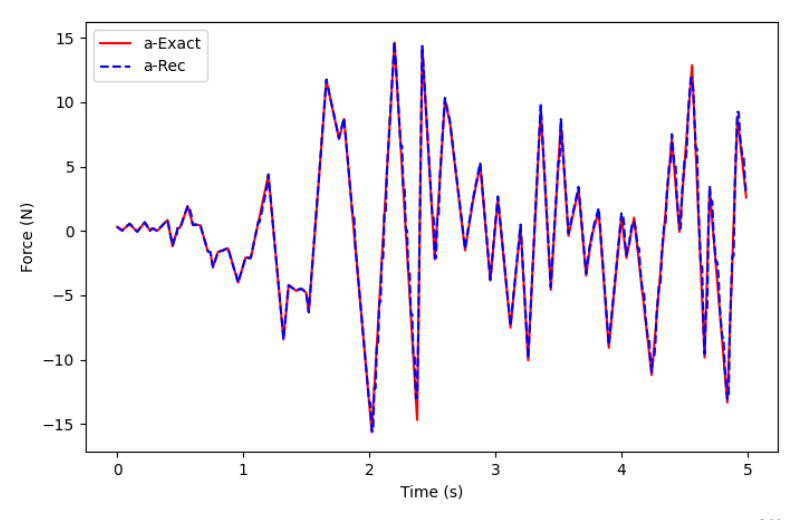


Figure 6.17 The reconstructed ground acceleration from NNex model

Using the updated vector  $z^k$ , the stiffness of the three linear springs is identified as  $k_1 = 20.00 N/m$ ,  $k_2 = 24.99 N/m$ ,  $k_3 = 13.57 N/m$ , which is close to the true value of the spring stiffness.  $NN^{in}$  also reconstructs the internal restoring force

generated by the Bouc-Wen model, as shown in Fig. 6.18.

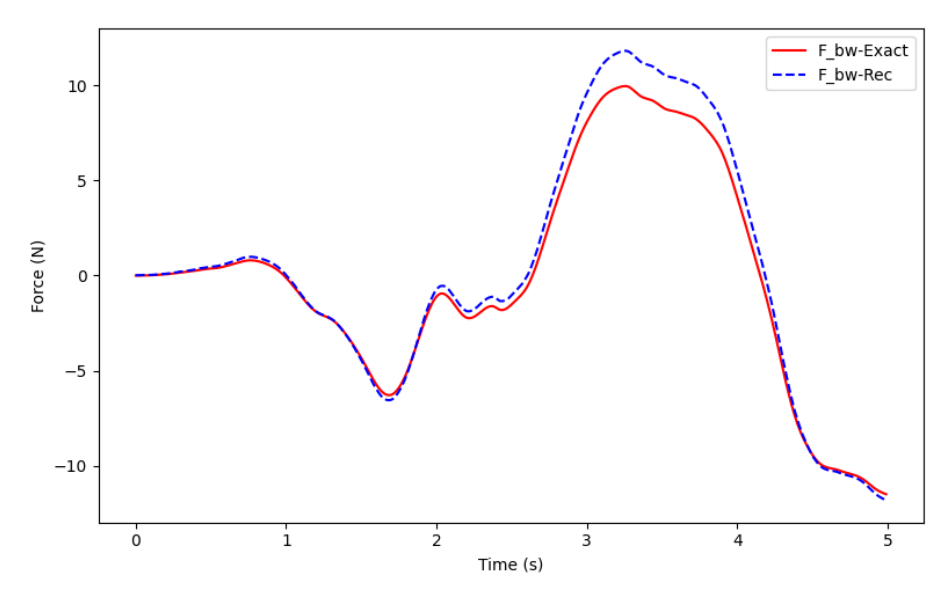


Figure 6.18 The reconstructed internal restoring force generated by the Bouc-Wen model

Fig. 6.18 shows that the identified hysteresis force of the Bouc-Wen is close to the calculated result as the ground truth, but there is still some error, which is considered to be caused by the inclusion of part of the linear restoring force in the identified hysteresis force. In order to make the PINNs model have the ability to predict the structural response under a new external force, an FCNN model with input of the structural state is established to replace the  $NN^{in}$  model to predict the internal restoring force generated by the Bouc-Wen model. This FCNN has 4 hidden layers, each consisting of 100 neurons. The input of the neural network model is t, and the output is the hysteresis displacement z(t) of the Bouc-Wen model. So, the loss function of the FCNN model is defined as

$$Loss_{phy} = \sum_{i=1}^{N_m} \left[ \dot{z}(t_i) - (\dot{u}(t_i) - \theta_1 |\dot{u}(t_i)| |z(t_i)|^{\theta_3 - 1} z(t_i) - \theta_2 \dot{u}(t_i) |z(t_i)|^{\theta_3} \right]^2$$
 (6.23)

$$Loss_{data} = \sum_{i=1}^{N_m} [\theta_4 z(t_i) - f^{rec}(t_i)]^2$$
 (6.24)

and

$$Loss_{total} = Loss_{phy} + Loss_{data} (6.25)$$

Here  $N_m = 500$  represents the reconstructed internal restoring force for 500 steps shown in Fig. 6.18.  $z(t_i)$  is the hysteresis displacement predicted by the FCNN model.  $\dot{z}(t_i)$  is calculated by the finite difference method as  $\dot{z}(t_i) = \frac{z(t_{i+1}) - z(t_i)}{\Delta t}$ .  $\dot{u}(t_i)$  is the reconstructed velocity response from the Newmark-beta method.  $\theta = (\theta_1, \theta_2, \theta_3, \theta_4)$  are unknown parameters representing the parameters  $\beta, \gamma, n, k_{BW}$  respectively, which are trained together with the FCNN model.  $f^{rec}$  is the reconstructed internal restoring force in Fig. 6.18. The Adam optimizer is employed to train this FCNN model 50,000 times with a learning rate of 0.001 until the loss function converges.

After training,  $\theta$  converges to (0.678, 0.389, 1.769, 16.466). The results show that the parameters of the Bouc-Wen model are successfully identified as  $k_{BW}=16.466 \,\mathrm{N/m}$ ,  $\beta=0.678$ ,  $\gamma=0.389$ , n=1.769. Now the structural system has been fully identified and has the ability to predict the response of the structure under new loads. A new seismic acceleration of the Chi-Chi earthquake as shown in Fig. 6.19 is applied to the 3-DOF system. The identified structural system is used to predict the response of the structure, and the structural vibration response calculated by the second-order implicit Runge-Kutta method is set as the benchmark solution. The structural vibration response predicted by the identified structural system is shown in Fig. 6.20.

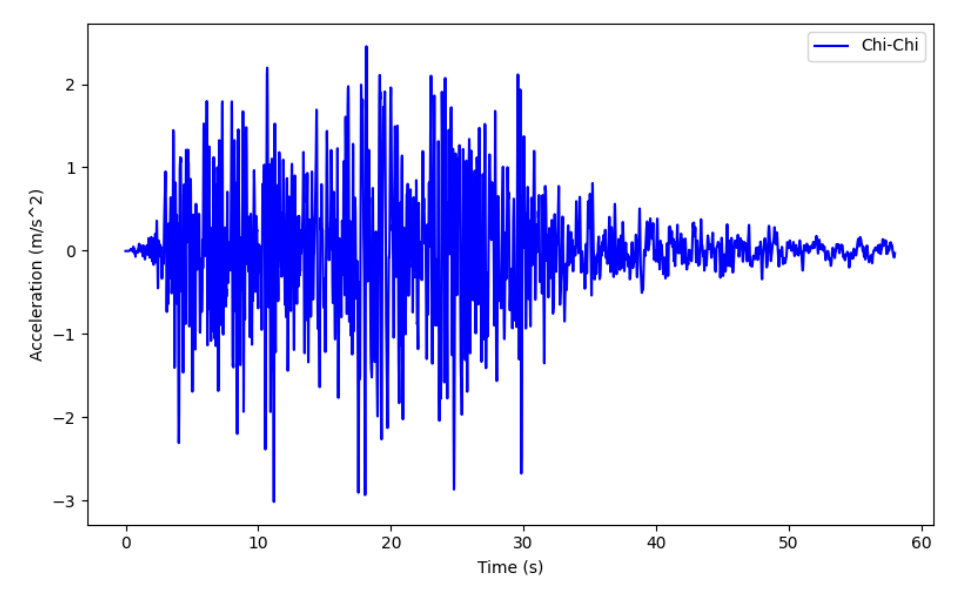


Figure 6.19 The seismic acceleration of Chi-Chi earthquake

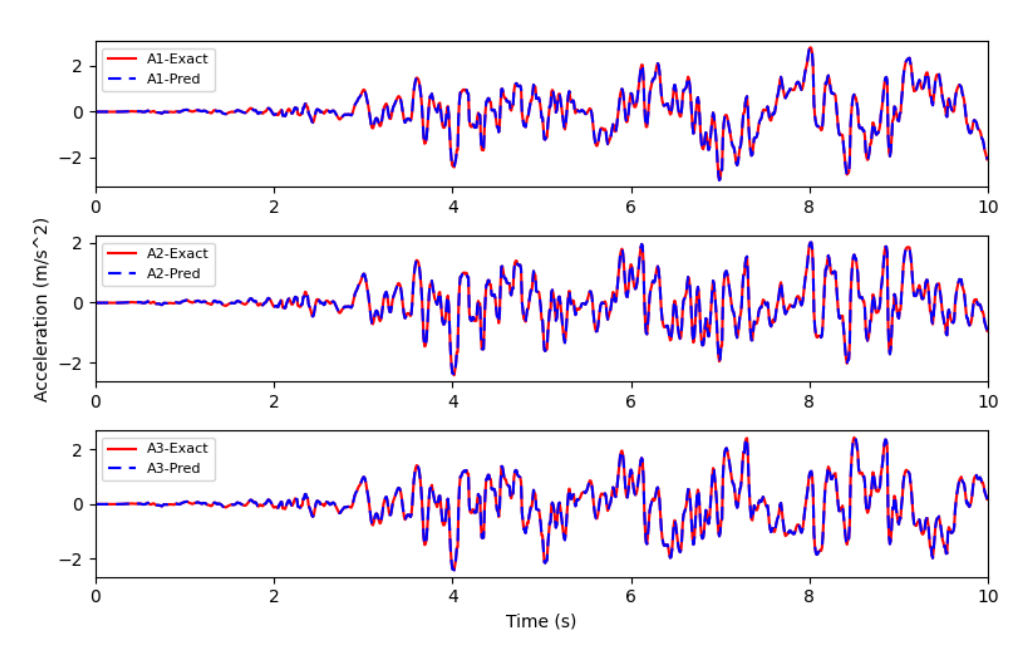


Figure 6.20 The structural vibration response predicted by the identified structural system

The results in Fig. 6.20 show that the identified structural system successfully and accurately predicts the vibration response of the structure under the new seismic acceleration. Fig. 6.21 shows the hysteresis force calculated by the identified Bouc-

Wen model. The results show that the hysteresis force generated by the Bouc-Wen model is also successfully characterized by the identified structural system.

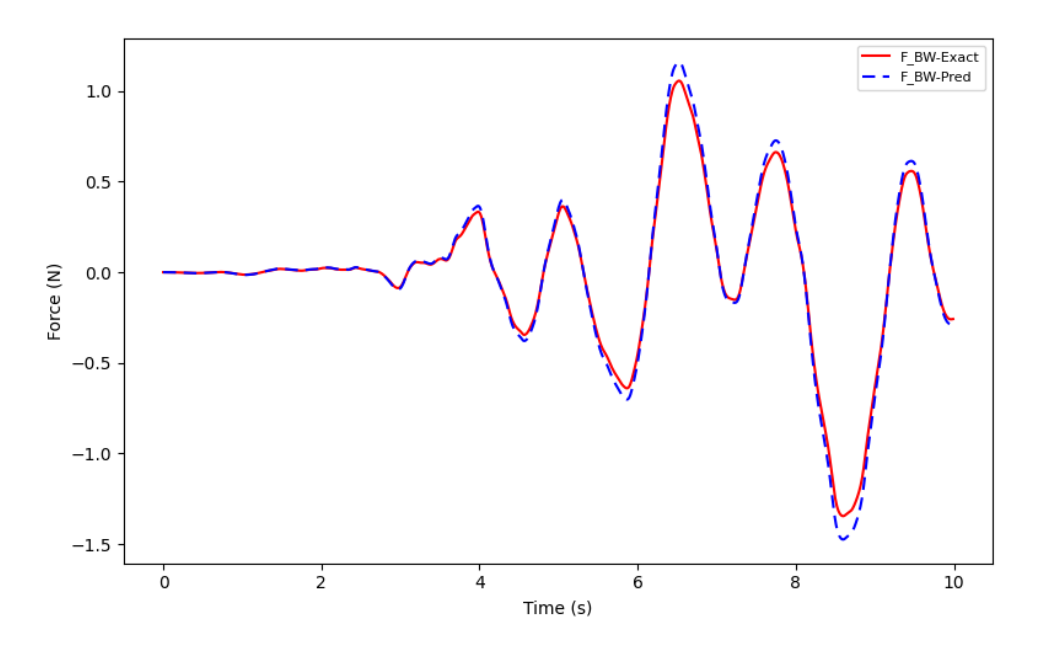


Figure 6.21 The hysteresis force calculated by the identified Bouc-Wen model

## **6.5** Experimental case

In order to further verify the proposed method through experimental data, a beam vibration test was carried out in the laboratory. As shown in Fig. 6.22, an aluminum beam mounted on two supports was tested. The size of the beam is 1260 \* 30 \* 5mm. The material is aluminum with a measured density of  $2683.08 \, kg/m^3$ . Both ends of the beam are bolted to the supports, and the length of the connecting section on each side is  $30 \, mm$ . These connections are considered rotational semi-rigid, where the beam displacement on the supports is constrained to 0, while the rotation is not 0. The angular moments of the supports on the beam are identified as the internal restoring forces. A hammer with a force sensor is used to apply a dynamic force at the mid-span

of the beam to make the beam vibrate. Five accelerometers are installed to measure the vibration response of the beam. The installation positions of the accelerometers and the additional weights added to the beam are listed in Table 6.3.



Figure 6.22 Vibration test of aluminum beam

Table 6.3 Installation position and weight of accelerometers

Sensor ID	Position (mm)	Weight (g)
A1	230	29.3
A2	430	31.8
A3	630	29.6
A4	830	35.8
A5	1030	29.5

A Dewesoft data logger and a laptop were used to collect and record the measurement data, with a sampling frequency of 10000 Hz. The beam vibrated from rest by applying a force with a hammer at the mid-span. The vibration responses of the five accelerometers were collected and Fourier transformed to analyze their frequency distribution. The results are shown in Fig. 6.23.

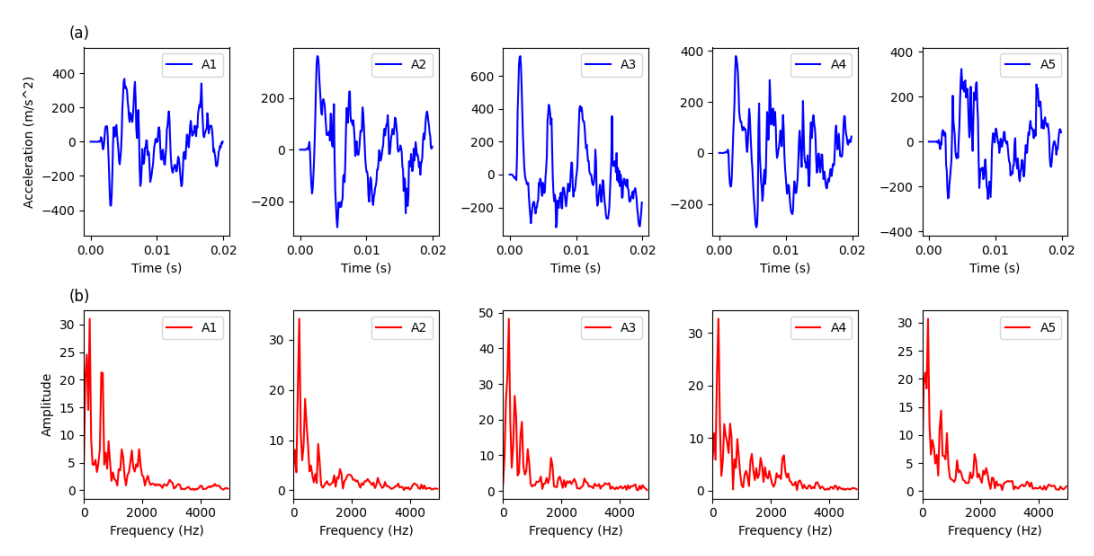


Figure 6.23 The collected vibration responses and frequency spectrum

The finite element model of the aluminum beam is constructed by discretizing it into 12 Euler-Bernoulli beam elements with consistent mass matrices. The length of the elements is 100 mm. The finite element model has a total of 13 nodes, 12 elements, and 24 degrees of freedom. A PINNs framework as shown in Fig. 6.1 is built to perform the structural identification of the beam. Since the aluminum beam is a homogeneous material and the cross-sectional size is consistent, a stiffness update coefficient  $z^k$  is used to update the elastic modulus of all beam elements to update the stiffness matrix. Here, the initial value of the elastic modulus is set as E = 65 GPa. Rayleigh damping is also employed to model the damping of the beam, with  $C = a \cdot M + b \cdot K$ . Here a and b are updated by a two-element damping update vector  $z^c$ . The initial values of a and b are set to 1e-1 and 1e-5, respectively.

Two FFNN neural network models are constructed to represent the external force at the mid-span and the internal restoring force from the two supports, respectively.

Both models have two fully connected hidden layers, each containing 100 neurons. According to the frequency distribution of the vibration response, the hyperparameter  $\sigma$  of the Fourier layer is set to 1000. In both FFNNs, the model  $NN^{ex}$  for predicting the external force at the mid-span takes as input t and outputs the external force  $F^{ex}$ of the structure. The model  $NN^{in}$  for predicting the angular moment from the supports takes t as input and outputs the angular moment of the two supports. The parameters of the two models, the stiffness update coefficient  $z^k$  and the damping update vector  $z^c$  are the trainable parameters of this PINNs framework. The first 200 time steps of the vibration measurement are input as the training data for the models. An Adam optimizer with a learning rate of 0.001 is employed to minimize the loss function of the model, which is calculated as the mean squared error between the predicted structural vibration and the measured data. The training is performed for 10,000 iterations, where the loss function is observed to converge. After the model is trained, the predicted structural vibration response at the accelerometer locations is shown in Fig. 6.24. The results show that the PINNs framework represents the structural vibration measurement data well.

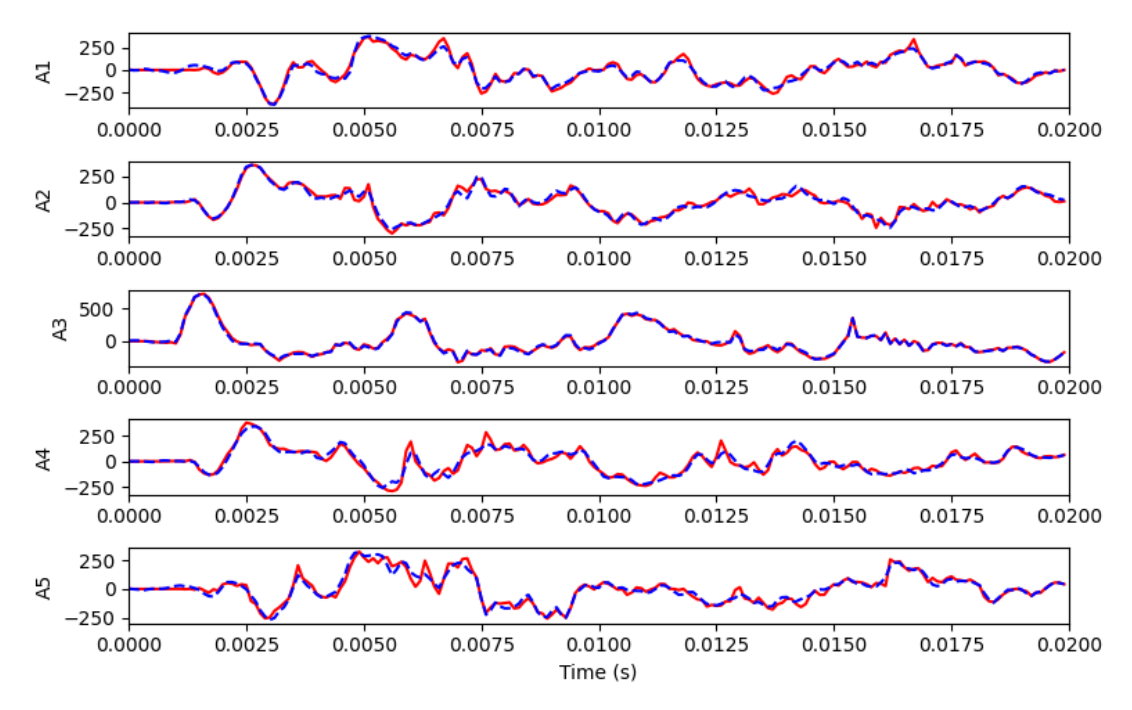


Figure 6.24 The comparison of the structural vibration response predicted by the model (blue) and measured data (red)

After training, the model parameters identified by PINNs are  $E^k = 70.213GPa$ , a = 2.483 and b = 4.814e - 6. PINNs also reconstructed the support angular moment and external force input as shown in Fig. 6.25. The measurement value from the force sensor of the hammer is also used as the reference for the external force input, although it is difficult to determine whether this measurement value is accurate. The results show that the external force reconstructed by PINNs is consistent with the measured data.

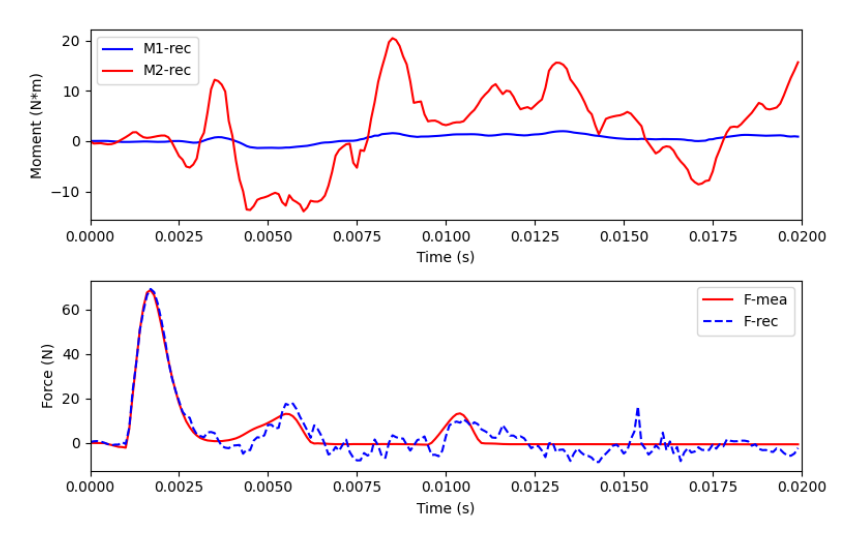


Figure 6.25 Reconstructed moments from supports (top) and reconstructed external force input (bottom)

In order to enable the PINNs framework to predict the structural response under new inputs, two FCNN models with input as the rotation angle of the support are built to replace the *NN*<sup>in</sup> model. FCNN models contain 4 hidden layers, each consisting of 100 neurons. The input of the model is the rotation angle at the support, and the output is the rotation moment of the support. The training data of the model is the reconstructed rotation moment shown in Fig. 18. The Adam optimizer is also used to minimize the difference between the moment predicted by the model and the reconstructed data. The model is trained 10,000 times with a learning rate of 0.001. Using the updated structural mechanics parameters and the trained FCNN model to predict the rotation moment, the PINNs model can now predict the structural response of this beam under the new external force. We conducted a new hammer test and input the external force recorded by the hammer into the PINNs. The comparison of the structural vibration response predicted by PINNs and the measured value is shown in Fig. 6.26.

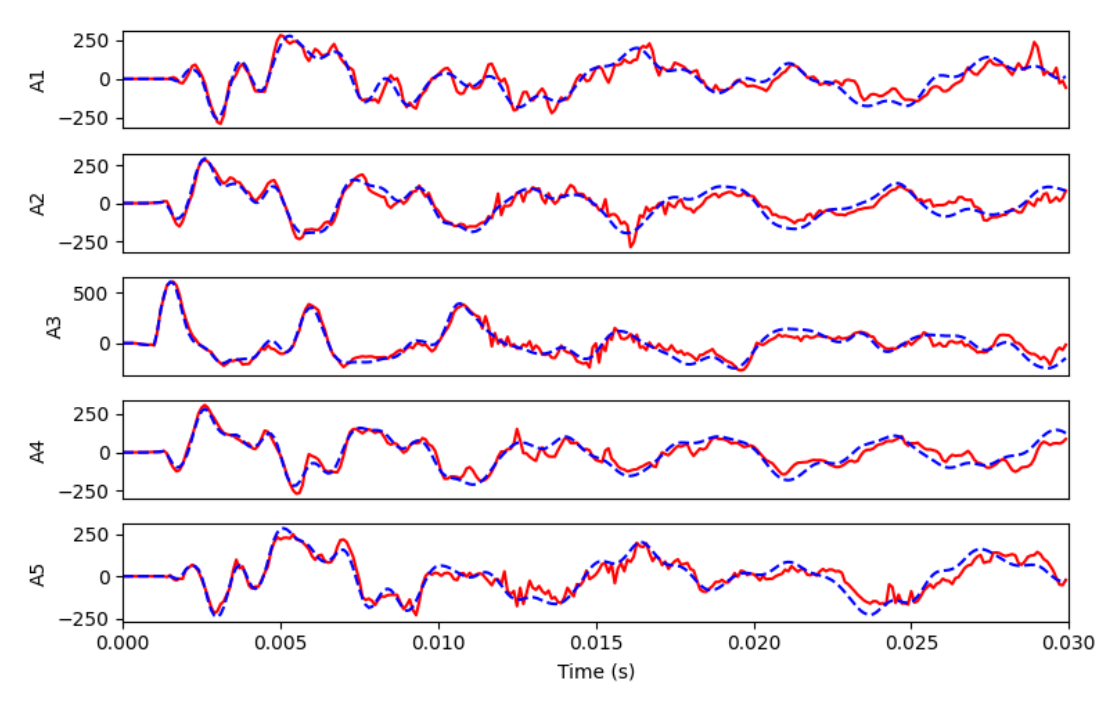


Figure 6.26 The comparison of the structural vibration response predicted by PINNs (blue) and the measured value (red)

Fig. 6.26 shows that under the new external excitation, the structural vibration response predicted by PINNs is highly consistent with the accelerometer measurements. which proves that PINNs successfully identify the dynamic characteristics of the structure.

## 6.6 Summary

This study investigates a promising approach for linear/nonlinear structure identification via physics-informed neural networks. The physical information of the structural vibration equations is seamlessly integrated into the proposed machine learning framework through a set of mathematical equations that describe the Newmark-beta derived relations of the dynamic system. By representing the external force input of the structure through a neural network, the proposed method can invert

the mechanical parameters of the structure based solely on the observed vibration response of the structure. For nonlinear structural systems involving nonlinear stiffness or damping, the internal restoring forces generated by the nonlinear components can also be accurately captured by another neural network model. To alleviate the spectral bias defect in neural networks, the Fourier feature layer is incorporated into the neural network model to form a Fourier feature neural network to improve the representation capability of multi-frequency features. A numerical example of a multi-degree-offreedom system involving cubic stiffness is tested to demonstrate the effectiveness of the proposed method. Based only on the vibration acceleration measurement data of the structure, the proposed method is shown to accurately reconstruct the unknown ground acceleration of the structural system and the restoring force generated by the nonlinear spring, and successfully identify the mechanical parameters of the structural system. Using these identified system parameters and the constructed surrogate model of the nonlinear spring, the response of the structure under new inputs is predicted and shown to be consistent with the ground truth. Another laboratory test of a beam with semirigid supports is carried out as a practical case to verify the proposed method. The results show that with a small number of vibration observations, the proposed method can accurately model the dynamic characteristics of the beam and predict the vibration response of the beam under new external excitations.

## **Chapter 7 Conclusions and recommendations**

### 7.1 Conclusions

After a decade of development, data-driven machine learning methods have become a preferred approach for researchers in many research fields due to their flexibility and powerful characterization capabilities. However, these purely datadriven methods still face some difficulties in solving forward and inverse problems in real physical systems. Since the machine learning model trained by various observational data can only fit the input-output mapping relationship at a shallow level, but cannot explore deeper physical characteristics, this shortcoming is reflected in the unsatisfactory generalization ability of the model, and the deviation between the predicted results and the real physical laws. Recently, a framework for seamlessly integrating physical information with machine learning models called physics-informed machine learning (PIML) has been developed to improve the ability of data-driven approaches to characterize physical constraints. Although PIML has been successful in many research and engineering fields, there are still some shortcomings to be solved in applying the existing PIML method directly to the forward and inverse problems of structural dynamics. First, the defects of spectral bias, 'soft' constraint embedding, and multi-loss convergence imbalance in PIML will be amplified in the structural dynamic response prediction, leading to prediction failure or obvious error. The inverse problem of structural damage identification from unknown forces makes the implementation of PIML difficult because of the unknown force terms in its governing equations. The uncertain nonlinearity of structures also poses some challenges to the accurate modeling of existing PIML methods.

In order to expand the research and application of PIML in structural dynamics, the research goal of this thesis is to develop advanced PIML methods for structural dynamic response prediction and structural damage identification. First, a PIML method of integrating physical information with a neural network model is proposed to solve the forward problem of structural dynamics. Here, how to accurately predict the vibration response of known linear/nonlinear physical systems under external excitation is first studied. To be specific, a novel recurrent convolutional neural network (RCNN) framework named structural dynamics learner (SDL) is proposed to predict the dynamic response of linear/nonlinear structural systems by employing an RCNN model to represent the physical state of the structure and incorporating the implicit Crank-Nicolson form of the system's motion equations into the SDL framework as physical information. The implicit Crank-Nicolson form of the motion equations gives SDL two significant advantages, including endogenous adaptability to linear and nonlinear systems and excellent numerical stability, especially in problems involving stiff equations. The RNN-based framework also makes SDL break through the defects of spectral bias, 'soft' constraint embedding and convergence imbalance of loss functions in the original PINNs, and improves the convergence speed of the model with the memory mechanism brought by its recurrent architecture. Several numerical cases involving nonlinear, stiff equations, hysteretic systems, and complex boundary conditions are carried out to validate the proposed framework, and the results are compared with traditional explicit numerical methods and original PINNs methods, respectively.

After that, the focus of this thesis turned to the research of inverse problems in structural mechanics. The reconstruction of structural external forces and dynamic responses is investigated first through a PIML framework that combines physical information with Markov parameters called physics-informed Markov parameters (PI-MP). The purpose of this research is to try to solve the problem often faced in practical structural engineering, i.e., how to accurately obtain the external excitation of the structure and how to reconstruct the unmeasured dynamic response through other measurement data when only part of the structure is observable. Here, the powerful representational power of neural networks is leveraged to represent the unknown external input of a structure. The motion equation of the structure, described as the Markov parameter in the state space, is integrated into the training of the neural network model as the prior physical information. By minimizing the deviation between the predicted structural acceleration response and the measured vibration response, PI-MP can reconstruct the external excitation input of the structure and predict the vibration response of all parts of the structure based on the reconstrated excitations. Even when the force points are unknown, PI-MP can also locate the exact force position by designing an optimization strategy that couples a greedy algorithm. Through two numerical cases and a laboratory test, the effectiveness and noise robustness of the proposed method are demonstrated.

The application of physical information machine learning for structural damage identification with unknown external forces from vibration measurements is further investigated. A physics-informed Fourier feature neural networks (PI-FFNN) framework is proposed to achieve this goal. In this framework, from vibration response measurements, the external forces and damages of the structure are identified simultaneously. A Fourier feature neural network, which is equipped with a Fourier feature layer to reduce the spectral bias of the model, is employed as the core of the framework to predict the external forces of the structure. Newmark-beta scheme of the motion equation as physical information to train the neural network model with a regularization term synergy to improve the sparsity and noise robustness of the identification results. The integration of physical information makes this approach an unsupervised learning method, the training of which does not rely on any damagerelated data labels. Two numerical experiments of beams and trusses and a laboratory test were carried out to verify the performance of the proposed method. The results show that the PI-FFNN method can locate and detect the structural damage and the external force of the reconstruction structure more accurately than the sensitivity-based method and the original PINNs method, even in the vibration measurement of noise.

Finally, our research focuses on the problem of structure identification of nonlinear vibration systems. Based on PINNs, we propose a framework for simultaneously

identifying structural mechanical parameters, reconstructing unknown external excitations on structures, and establishing alternative models for nonlinear systems. In this framework, two neural network models are employed to represent the structure's unknown external excitation and nonlinear internal restoring force, respectively. The mechanical parameters of the structure are updated along with the neural network model as trainable parameters. The physical information of the structural vibration equations is seamlessly integrated into the proposed machine learning framework through a set of mathematical equations that describe the Newmark-beta derived relations of the dynamic system. By minimizing the difference between the predicted structural response and the structural vibration observation, both the external excitation and the internal nonlinear restoring force of the structure can be reconstructed simultaneously and the exact values of the structural parameters can be discovered. In a numerical case and a laboratory test, the proposed framework successfully identifies the mechanical parameters of the structure and accurately predicts the vibration response of the structure under the new external excitation by learning from the observed data.

### 7.2 Recommendations for Further Research

This thesis presents several innovative PIML frameworks for solving forward and inverse problems in structural dynamics. Under the constraints of physical information, these frameworks demonstrate the independence of complex and large training data and

achieve excellent noise robustness and generalization. However, these methods are still based on theoretical assumptions of PIML. In PIML, researchers assume that the research object always obeys our established governing equations, such as the structural vibration equations. This assumption is obtained by simplifying the complex physical world into simple physical models. However, in the real physical world, material nonlinearity, inhomogeneity and the complexity of constraints are widespread. These complex characteristics are difficult to describe with a simple governing equation. And more complex physical relationships are difficult to exactly discover, so our proposed method is still based on this assumption and still faces limitations in the knowability and accuracy of exact physical laws. In addition to this assumption, our proposed method still faces the following limitations in practical applications.

The first limitation lies in the structural complexity of the PIML method. Unlike mature numerical analysis methods such as the finite element method, which can easily solve analysis problems involving millions of degrees of freedom, PIML, which relies on training machine learning models such as neural networks to solve the governing equations of the structure, has a model complexity far exceeding that of numerical analysis methods. Therefore, current research focuses only on problems with no more than a few hundred degrees of freedom. Limited by the available computing resources, it is still difficult to use these PIML methods to analyze large engineering structures. Fortunately, recent breakthroughs in large machine learning models, especially large language models, are expected to provide a new and promising path for the simulation

of large structures using machine learning and even PIML. This is a research direction worthy of further exploration in future studies.

The second limitation of the developed PIML for practical engineering applications is the computational efficiency of the model. In the proposed frameworks, neural network models such as convolutional neural networks, recurrent neural networks or Fourier eigen-neural networks need to be trained iteratively to reach convergence. Like the various deep neural network trainings applied in other research fields, the training process of these models takes a lot of time and computing resources, which is less efficient than traditional numerical analysis methods. This efficiency disadvantage will also limit its wider research and application. In future research, how to improve the training efficiency of the model is also a crucial bottleneck for the PIML method in structural dynamics. This problem may be alleviated by designing more efficient neural network frameworks and more advanced optimizers to train neural network models.

The third limitation is the applicability of PIML to big data. Current PIML methods, including our proposed frameworks, can still only process a small amount of training data, usually only several thousand time steps. However, in actual engineering, with the development of advanced sensors and data acquisition designs, the data acquisition frequency has reached several thousand hertz, which has accumulated a large amount of observation data in engineering. How to extract the long-term features of training data and couple the physical information to improve PIML's learning ability

of a large amount of training data over a long time is also a problem worth exploring in the future.

The last limitation is the convergence of the loss function of PIML methods. Since PIML methods rely entirely on the loss function to train the neural network model to approach the exact solution. The convergence of the loss function is a crucial criterion to ensure the accuracy of the results. However, in the existing framework, it is still difficult to ensure the convergence of the solution due to the imbalance of multiple loss functions or the non-convexity of the neural network model training problem. In recent years, some new techniques, such as energy-based loss functions, have been used to reduce the non-convexity of the model search space, thereby improving the convergence of the solution. These techniques have shown promising results to ensure the accuracy of the solution. Therefore, in future research, whether the several model frameworks proposed in this study can be improved from the perspective of energy-based loss functions is a direction worthy of further exploration.

### References

- Abueidda, D. W., Lu, Q., & Koric, S. (2021). Meshless physics-informed deep learning method for three-dimensional solid mechanics. *International Journal for Numerical Methods in Engineering*, 122(23), 7182-7201.
- Al-Adly, A. I., & Kripakaran, P. (2024). Physics-informed neural networks for structural health monitoring: a case study for Kirchhoff–Love plates. *Data-Centric Engineering*, 5, e6.
- Alkayem, N. F., Cao, M., Zhang, Y., Bayat, M., & Su, Z. (2018). Structural damage detection using finite element model updating with evolutionary algorithms: a survey. *Neural Computing and Applications*, *30*, 389-411.
- Alvin, K., Robertson, A., Reich, G., & Park, K. (2003). Structural system identification: from reality to models. *Computers & structures*, 81(12), 1149-1176.
- Arora, V. (2011). Comparative study of finite element model updating methods. *Journal* of Vibration and Control, 17(13), 2023-2039.
- Arora, V., Singh, S. P., & Kundra, T. K. (2009). Finite element model updating with damping identification. *Journal of Sound and Vibration*, 324(3), 1111-1123.
- Arzani, A., Wang, J.-X., & D'Souza, R. M. (2021). Uncovering near-wall blood flow from sparse data with physics-informed neural networks. *arXiv* preprint *arXiv*::08249, 33(7)
- Astroza, R., Nguyen, L. T., & Nestorović, T. (2016). Finite element model updating using simulated annealing hybridized with unscented Kalman filter. *Computers & structures*, 177, 176-191.
- Avci, O., Abdeljaber, O., Kiranyaz, S., Hussein, M., Gabbouj, M., & Inman, D. J. (2021).

  A review of vibration-based damage detection in civil structures: From traditional

- methods to Machine Learning and Deep Learning applications. *Mechanical Systems and Signal Processing*, 147, 107077.
- Bai, J., Rabczuk, T., Gupta, A., Alzubaidi, L., & Gu, Y. (2023). A physics-informed neural network technique based on a modified loss function for computational 2D and 3D solid mechanics. *Computational Mechanics*, 71(3), 543-562.
- Bao, Y., & Li, H. (2021). Machine learning paradigm for structural health monitoring. Structural Health Monitoring, 20(4), 1353-1372.
- Baydin, A. G., Pearlmutter, B. A., Radul, A. A., & Siskind, J. M. (2018). Automatic differentiation in machine learning: a survey. *Journal of machine learning research*, 18(153), 1-43.
- Bazmara, M., Silani, M., & Mianroodi, M. (2023). Physics-informed neural networks for nonlinear bending of 3D functionally graded beam. *Structures*, 49, 152-162.
- Beltran Carbajal, F. (2012). Advances in Vibration Engineering and Structural Dynamics. BoD–Books on Demand.
- Bowman, B., Oian, C., Kurz, J., Khan, T., Gil, E., & Gamez, N. (2023). Physics-informed neural networks for the heat equation with source term under various boundary conditions. *Algorithms*, *16*(9), 428.
- Brecht, R., & Bihlo, A. (2024). M-ENIAC: A physics-informed machine learning recreation of the first successful numerical weather forecasts. *Geophysical Research Letters*, 51(10), e2023GL107718.
- Burkart, N., & Huber, M. F. (2021). A survey on the explainability of supervised machine learning. *Journal of Artificial Intelligence Research*, 70, 245-317.
- Cai, S., Mao, Z., Wang, Z., Yin, M., & Karniadakis, G. E. (2021a). Physics-informed neural networks (PINNs) for fluid mechanics: A review. *arXiv* preprint *arXiv*:.09506,

- Cai, S., Mao, Z., Wang, Z., Yin, M., & Karniadakis, G. E. (2021b). Physics-informed neural networks (PINNs) for fluid mechanics: A review. *Acta Mechanica Sinica*, 37(12), 1727-1738.
- Cai, S., Wang, Z., Chryssostomidis, C., & Karniadakis, G. E. (2020). Heat transfer prediction with unknown thermal boundary conditions using physics-informed neural networks. Fluids Engineering Division Summer Meeting, 83730, V003T005A054.
- Cai, S., Wang, Z., Fuest, F., Jeon, Y. J., Gray, C., & Karniadakis, G. E. (2021). Flow over an espresso cup: inferring 3-D velocity and pressure fields from tomographic background oriented Schlieren via physics-informed neural networks. *Journal of Fluid Mechanics*, 915, A102.
- Cai, S., Wang, Z., Wang, S., Perdikaris, P., & Karniadakis, G. E. (2021a). Physics-informed neural networks for heat transfer problems. *Journal of Heat Transfer*, 143(6), 060801.
- Cai, S., Wang, Z., Wang, S., Perdikaris, P., & Karniadakis, G. E. (2021b). Physics-Informed Neural Networks for Heat Transfer Problems. *Journal of Heat Transfer*, 143(6)
- Cao, F., Guo, X., Gao, F., & Yuan, D. (2023). Deep Learning Nonhomogeneous Elliptic Interface Problems by Soft Constraint Physics-Informed Neural Networks.

  Mathematics, 11(8), 1843.
- Castro-Triguero, R., Murugan, S., Gallego, R., & Friswell, M. I. (2013). Robustness of optimal sensor placement under parametric uncertainty. *Mechanical Systems and Signal Processing*, 41(1-2), 268-287.
- Çevik, A., Kurtoğlu, A. E., Bilgehan, M., Gülşan, M. E., & Albegmprli, H. M. (2015). Support vector machines in structural engineering: a review. *Journal of Civil*

- Engineering and Management, 21(3), 261-281.
- Chai, X., Cao, W., Li, J., Long, H., & Sun, X. (2024). Overcoming the Spectral Bias Problem of Physics-Informed Neural Networks in Solving the Frequency-Domain Acoustic Wave Equation. *IEEE Transactions on Geoscience and Remote Sensing*, 62, 1-20.
- Chegeni, M. H., Sharbatdar, M. K., Mahjoub, R., & Raftari, M. (2022). New supervised learning classifiers for structural damage diagnosis using time series features from a new feature extraction technique. *Earthquake Engineering and Engineering Vibration*, 21(1), 169-191.
- Chen, C. (2024). PGNM: Using Physics-Informed Gated Recurrent Units Network Method to capture the dynamic data feature propagation process of PDEs. *Chaos, Solitons & Fractals*, 185, 115136.
- Chen, F., Sondak, D., Protopapas, P., Mattheakis, M., Liu, S., Agarwal, D., & Di Giovanni, M. (2020). Neurodiffeq: A python package for solving differential equations with neural networks. *Journal of Open Source Software*, 5(46), 1931.
- Chen, Z., & Chan, T. H. T. (2017). A truncated generalized singular value decomposition algorithm for moving force identification with ill-posed problems. *Journal of Sound and Vibration*, 401, 297-310.
- Chen, Z., Liu, Y., & Sun, H. (2021). Physics-informed learning of governing equations from scarce data. *Nature communications*, *12*(1), 1-13.
- Chen, Z., Weng, S., Yu, H., Li, J., Zhu, H., Yan, Y., & Wu, L. (2023). Bayesian-based method for the simultaneous identification of structural damage and moving force. *Mechanical Systems and Signal Processing*, 185, 109742.
- Chen, Z., Zhang, R., Zheng, J., & Sun, H. (2020). Sparse Bayesian learning for structural damage identification. *Mechanical Systems and Signal Processing*, 140,

106689.

- Cheng, C., & Zhang, G.-T. (2021). Deep learning method based on physics informed neural network with resnet block for solving fluid flow problems. *Water*, *13*(4), 423.
- Cheng, X., Dong, J., Han, X., & Fei, Q. (2018). Structural health monitoring-oriented finite-element model for a large transmission tower. *International Journal of Civil Engineering*, 16, 79-92.
- Cross, E. J., Gibson, S. J., Jones, M. R., Pitchforth, D. J., Zhang, S., & Rogers, T. J. (2022). Physics-informed machine learning for structural health monitoring. Structural Health Monitoring Based on Data Science Techniques, 347-367.
- Cunha, B. Z., Droz, C., Zine, A.-M., Foulard, S., & Ichchou, M. (2023). A review of machine learning methods applied to structural dynamics and vibroacoustic. *Mechanical Systems and Signal Processing*, 200, 110535.
- Dadras Eslamlou, A., & Huang, S. (2022). Artificial-neural-network-based surrogate models for structural health monitoring of civil structures: a literature review. *Buildings*, 12(12), 2067.
- Das, S., Saha, P., & Patro, S. K. (2016). Vibration-based damage detection techniques used for health monitoring of structures: a review. *Journal of Civil Structural Health Monitoring*, 6(3), 477-507.
- Dat, T. T., Matsumoto, Y., & Dang, J. (2023). A Preliminary Study on Physics-Informed Machine Learning-Based Structure Health Monitoring for Beam Structures. International Conference on Experimental Vibration Analysis for Civil Engineering Structures, 490-499.
- Delgadillo, R. M., & Casas, J. R. (2022). Bridge damage detection via improved completed ensemble empirical mode decomposition with adaptive noise and

- machine learning algorithms. Structural Control and Health Monitoring, 29(8), e2966.
- Denkena, B., Bergmann, B., & Stoppel, D. (2020). Reconstruction of process forces in a five-axis milling center with a LSTM neural network in comparison to a model-based approach. *Journal of manufacturing and materials processing*, 4(3), 62.
- Ding, Z., Li, J., Hao, H., & Lu, Z.-R. (2019). Structural damage identification with uncertain modelling error and measurement noise by clustering based tree seeds algorithm. *Engineering Structures*, 185, 301-314.
- Dong, Y., Li, Y., Lai, M., & Xiao, M. (2008). Nonlinear structural response prediction based on support vector machines. *Journal of Sound and Vibration*, 311(3), 886-897.
- Ereiz, S., Duvnjak, I., & Fernando Jiménez-Alonso, J. (2022). Review of finite element model updating methods for structural applications. *Structures*, 41, 684-723.
- Esfandiari, A., Bakhtiari-Nejad, F., Rahai, A., & Sanayei, M. (2009). Structural model updating using frequency response function and quasi-linear sensitivity equation. *Journal of Sound and Vibration*, 326(3-5), 557-573.
- Eshkevari, S. S., Takáč, M., Pakzad, S. N., & Jahani, M. (2021). DynNet: Physics-based neural architecture design for nonlinear structural response modeling and prediction. *Engineering Structures*, 229, 111582.
- Fallah, A., & Aghdam, M. M. (2024). Physics-informed neural network for bending and free vibration analysis of three-dimensional functionally graded porous beam resting on elastic foundation. *Engineering with Computers*, 40(1), 437-454.
- Fan, W., & Qiao, P. (2011). Vibration-based damage identification methods: a review and comparative study. *Structural Health Monitoring*, *10*(1), 83-111.
- Fang, Z. (2021). A High-Efficient Hybrid Physics-Informed Neural Networks Based on

- Convolutional Neural Network. *IEEE Trans Neural Netw Learn Syst*, *PP*(10), 1-13.
- Fang, Z., Wang, S., & Perdikaris, P. (2024). Learning only on boundaries: a physics-informed neural operator for solving parametric partial differential equations in complex geometries. *Neural Computation*, *36*(3), 475-498.
- Farhani, G., Kazachek, A., & Wang, B. (2022). Momentum diminishes the effect of spectral bias in physics-informed neural networks. *arXiv* preprint *arXiv*:2206.14862,
- Feng, W., Li, Q., Lu, Q., Wang, B., & Li, C. (2020). Time domain force localization and reconstruction based on hierarchical Bayesian method. *Journal of Sound and Vibration*, 472, 115222.
- Frei, S., & Singh, M. K. (2024). An Implicitly Extended Crank–Nicolson Scheme for the Heat Equation on a Time-Dependent Domain. *Journal of Scientific Computing*, 99(3), 64.
- Gang, X., Chai, S., Allemang, R. J., & Li, L. (2014). A new iterative model updating method using incomplete frequency response function data. *Journal of Sound and Vibration*, 333(9), 2443-2453.
- Gao, H., Sun, L., & Wang, J.-X. (2021). PhyGeoNet: Physics-informed geometry-adaptive convolutional neural networks for solving parameterized steady-state PDEs on irregular domain. *Journal of computational physics*, 428, 110079.
- Gao, H., Zahr, M. J., & Wang, J.-X. (2022). Physics-informed graph neural Galerkin networks: A unified framework for solving PDE-governed forward and inverse problems. *Computer Methods in Applied Mechanics and Engineering*, 390, 114502.
- Gardner, P., Lord, C., & Barthorpe, R. J. (2020). Bayesian history matching for structural dynamics applications. *Mechanical Systems and Signal Processing*, 143,

- Genikomsou, A. S., & Polak, M. A. (2015). Finite element analysis of punching shear of concrete slabs using damaged plasticity model in ABAQUS. *Engineering Structures*, 98, 38-48.
- Gharehbaghi, V. R., Noroozinejad Farsangi, E., Noori, M., Yang, T. Y., Li, S., Nguyen, A., Málaga-Chuquitaype, C., Gardoni, P., & Mirjalili, S. (2022). A Critical Review on Structural Health Monitoring: Definitions, Methods, and Perspectives. *Archives of Computational Methods in Engineering*, 29(4), 2209-2235.
- Ghiasi, R., Torkzadeh, P., & Noori, M. (2016). A machine-learning approach for structural damage detection using least square support vector machine based on a new combinational kernel function. *Structural Health Monitoring*, 15(3), 302-316.
- Giagopoulos, D., Arailopoulos, A., Dertimanis, V., Papadimitriou, C., Chatzi, E., & Grompanopoulos, K. (2019). Structural health monitoring and fatigue damage estimation using vibration measurements and finite element model updating. Structural Health Monitoring, 18(4), 1189-1206.
- Girardi, M., Padovani, C., Pellegrini, D., Porcelli, M., & Robol, L. (2020). Finite element model updating for structural applications. *Journal of Computational and Applied Mathematics*, 370, 112675.
- Gockenbach, M. S. (2016). *Linear inverse problems and Tikhonov regularization* (Vol. 32). American Mathematical Society.
- González--Pinto, S., Montijano, J. I., & Pérez--Rodríguez, S. (2004). Two-step error estimators for implicit Runge--Kutta methods applied to stiff systems. *ACM Transactions on Mathematical Software (TOMS)*, 30(1), 1-18.
- Grossmann, T. G., Komorowska, U. J., Latz, J., & Schönlieb, C.-B. (2024). Can physics-informed neural networks beat the finite element method? *IMA Journal of*

- Applied Mathematics, hxae011.
- Gui, G., Pan, H., Lin, Z., Li, Y., & Yuan, Z. (2017). Data-driven support vector machine with optimization techniques for structural health monitoring and damage detection. KSCE Journal of Civil Engineering, 21, 523-534.
- Guo, T., Wu, L., Wang, C., & Xu, Z. (2020). Damage detection in a novel deep-learning framework: a robust method for feature extraction. *Structural Health Monitoring*, 19(2), 424-442.
- Guo, X.-Y., & Fang, S.-E. (2024). A physics-informed auto-encoder based cable force identification framework for long-span bridges. *Structures*, *60*, 105906.
- Ha, Q., Wu, Y. M., Samali, B., & Li, J. (2004). Earthquake response of a building model with base-isolated active control. *IFAC Proceedings Volumes*, *37*(14), 641-646.
- Haghighat, E., Raissi, M., Moure, A., Gomez, H., & Juanes, R. (2021). A physics-informed deep learning framework for inversion and surrogate modeling in solid mechanics. *Computer Methods in Applied Mechanics and Engineering*, 379, 113741.
- Haidarpour, A., & Kong, F. T. (2020). Finite element model updating for structural health monitoring. *Structural Durability & Health Monitoring*, 14(1), 1.
- Hanrahan, S., Kozul, M., & Sandberg, R. (2023). Studying turbulent flows with physics-informed neural networks and sparse data. *International Journal of Heat and Fluid Flow*, 104, 109232.
- Hansen, P. C., & O'Leary, D. P. (1993). The use of the L-curve in the regularization of discrete ill-posed problems. SIAM Journal on Scientific Computing, 14(6), 1487-1503.
- Haywood-Alexander, M., & Chatzi, E. (2024). On the Application of Physics-Informed Neural-Networks for Identification and State Estimation of Vibrating Structures.

- International Operational Modal Analysis Conference, 642-651.
- He, Z., Ni, F., Wang, W., & Zhang, J. (2021). A physics-informed deep learning method for solving direct and inverse heat conduction problems of materials. *Materials Today Communications*, 28, 102719.
- Hennigh, O., Narasimhan, S., Nabian, M. A., Subramaniam, A., Tangsali, K., Fang, Z., Rietmann, M., Byeon, W., & Choudhry, S. (2021). NVIDIA SimNet<sup>TM</sup>: An AI-accelerated multi-physics simulation framework. International Conference on Computational Science, 447-461.
- Heo, G., & Jeon, J. (2016). An experimental study of structural identification of bridges using the kinetic energy optimization technique and the direct matrix updating method. *Shock and Vibration*, 2016(1), 3287976.
- Hosseini, M. Y., & Shiri, Y. (2024). Flow field reconstruction from sparse sensor measurements with physics-informed neural networks. *Physics of Fluids*, 36(7)
- Hou, X., Zhou, X., & Liu, Y. (2024). Reconstruction of ship propeller wake field based on self-adaptive loss balanced physics-informed neural networks. *Ocean Engineering*, 309, 118341.
- Hu, Y., Tsang, H.-H., Lam, N., & Lumantarna, E. (2023). Physics-informed neural networks for enhancing structural seismic response prediction with pseudo-labelling. *Archives of Civil and Mechanical Engineering*, 24(1), 7.
- Hua, X., Ni, Y., Chen, Z., & He, X. (2012). Monte Carlo study of the effect of measurement noise in model updating with regularization. *Journal of Engineering Mechanics*, 138(1), 71-81.
- Hua, X. G., Ni, Y. Q., Chen, Z. Q., & Ko, J. M. (2009). Structural Damage Detection of Cable-Stayed Bridges Using Changes in Cable Forces and Model Updating. *Journal of Structural Engineering*, 135(9), 1093-1106.

- Huang, B., & Wang, J. (2022). Applications of physics-informed neural networks in power systems-a review. *IEEE Transactions on Power Systems*, 38(1), 572-588.
- Huang, C., Tao, C., Ji, H., & Qiu, J. (2023). Impact force reconstruction and localization using Distance-assisted Graph Neural Network. *Mechanical Systems and Signal Processing*, 200, 110606.
- Huang, Y. H., Xu, Z., Qian, C., & Liu, L. (2023). Solving free-surface problems for non-shallow water using boundary and initial conditions-free physics-informed neural network (bif-PINN). *Journal of computational physics*, 479, 112003.
- Iserles, A. (2008). A First Course in the Numerical Analysis of Differential Equations (2 ed.). Cambridge University Press.
- Jacquelin, E., & Hamelin, P. (2003). Force recovered from three recorded strains. *International Journal of Solids and Structures*, 40(1), 73-88.
- Jafarkhani, R., & Masri, S. F. (2011). Finite Element Model Updating Using Evolutionary Strategy for Damage Detection. *Computer-Aided Civil and Infrastructure Engineering*, 26(3), 207-224.
- Jagtap, A., & Karniadakis, G. (2020). Extended physics-informed neural networks (XPINNs): a generalized space-time domain decomposition based deep learning framework for nonlinear partial differential equations. *Communications in Computational Physics*, 28(5), 2002-2041.
- Jeong, H., Bai, J., Batuwatta-Gamage, C. P., Rathnayaka, C., Zhou, Y., & Gu, Y. (2023).

  A Physics-Informed Neural Network-based Topology Optimization (PINNTO) framework for structural optimization. *Engineering Structures*, 278, 115484.
- Jiang, D., Zhang, M., Xu, Y., Qian, H., Yang, Y., Zhang, D., & Liu, Q. (2024). Rotor Dynamic Response Prediction Using Physics-informed Multi-LSTM Networks. Aerospace Science and Technology, 109648.

- Jiang, Q., Shu, C., Zhu, L., Yang, L., Liu, Y., & Zhang, Z. (2023). Applications of finite difference-based physics-informed neural networks to steady incompressible isothermal and thermal flows. *International Journal for Numerical Methods in Fluids*, 95(10), 1565-1597.
- Jin, G., Wong, J. C., Gupta, A., Li, S., & Ong, Y.-S. (2024). Fourier warm start for physics-informed neural networks. *Engineering Applications of Artificial Intelligence*, 132, 107887.
- Johnston, P. R., & Gulrajani, R. M. (2000). Selecting the corner in the L-curve approach to Tikhonov regularization. *IEEE Transactions on Biomedical Engineering*, 47(9), 1293-1296.
- Kapoor, T., Wang, H., Núñez, A., & Dollevoet, R. (2023). Physics-informed neural networks for solving forward and inverse problems in complex beam systems. *IEEE Transactions on Neural Networks and Learning Systems*,
- Karniadakis, G. E., Kevrekidis, I. G., Lu, L., Perdikaris, P., Wang, S., & Yang, L. (2021). Physics-informed machine learning. *Nature Reviews Physics*, *3*(6), 422-440.
- Kharazmi, E., Zhang, Z., & Karniadakis, G. E. (2021). hp-VPINNs: Variational physics-informed neural networks with domain decomposition. *Computer Methods in Applied Mechanics and Engineering*, 374, 113547.
- Kim, T., Kwon, O.-S., & Song, J. (2019). Response prediction of nonlinear hysteretic systems by deep neural networks. *Neural Networks*, *111*, 1-10.
- Kingma, D. P. (2014). Adam: A method for stochastic optimization. *arXiv preprint* arXiv:1412.6980,
- Kingma, D. P., & Ba, J. (2014). Adam: A method for stochastic optimization. *arXiv* preprint arXiv:1412.6980,
- Kissas, G., Yang, Y., Hwuang, E., Witschey, W. R., Detre, J. A., & Perdikaris, P. (2020).

- Machine learning in cardiovascular flows modeling: Predicting arterial blood pressure from non-invasive 4D flow MRI data using physics-informed neural networks. *Computer Methods in Applied Mechanics and Engineering*, 358, 112623.
- Koryagin, A., Khudorozkov, R., & Tsimfer, S. (2019). PyDEns: A python framework for solving differential equations with neural networks. *arXiv* preprint *arXiv*:1909.11544,
- Kudela, P., Moll, J., & Fiborek, P. (2020). Parallel spectral element method for guided wave based structural health monitoring. *Smart Materials and Structures*, 29(9), 095010.
- Kulkarni, N. N., & Sabato, A. (2024). Full-field expansion and damage detection from sparse measurements using physics-informed variational autoencoders. *Structural Health Monitoring*, 14759217241289575.
- Lai, Z., Alzugaray, I., Chli, M., & Chatzi, E. (2020). Full-field structural monitoring using event cameras and physics-informed sparse identification. *Mechanical Systems and Signal Processing*, 145, 106905.
- Lai, Z., Mylonas, C., Nagarajaiah, S., & Chatzi, E. (2021). Structural identification with physics-informed neural ordinary differential equations. *Journal of Sound and Vibration*, 508, 116196.
- Lakshminarayana, S., Sthapit, S., Jahangir, H., Maple, C., & Poor, H. V. (2022). Data-driven detection and identification of IoT-enabled load-altering attacks in power grids. *IET Smart Grid*, *5*(3), 203-218.
- Lakshminarayana, S., Sthapit, S., & Maple, C. (2022). Application of physics-informed machine learning techniques for power grid parameter estimation. *Sustainability*, 14(4), 2051.
- Laubscher, R. J. a. p. a. (2021). Simulation of multi-species flow and heat transfer using

- physics-informed neural networks. arXiv preprint arXiv:.14907,
- Law, S. S., Chan, T. H. T., & Zeng, Q. H. (1997). Moving force identification: a time domain method. *Journal of Sound and Vibration*, 201(1), 1-22.
- Lei, G., Lei, Z., Shi, L., Zeng, C., & Zhou, D.-X. (2025). Solving PDEs on spheres with physics-informed convolutional neural networks. *Applied and Computational Harmonic Analysis*, 74, 101714.
- Lei, X., Yang, Z., Yu, J., Zhao, J., Gao, Q., & Yu, H. (2020). Data-driven optimal power flow: A physics-informed machine learning approach. *IEEE Transactions on Power Systems*, 36(1), 346-354.
- Leung, W. T., Lin, G., & Zhang, Z. (2022). NH-PINN: Neural homogenization-based physics-informed neural network for multiscale problems. *Journal of computational physics*, 470, 111539.
- Li, Q., & Lu, Q. (2019). A revised time domain force identification method based on Bayesian formulation. *International Journal for Numerical Methods in Engineering*, 118(7), 411-431.
- Li, X., Deng, J., Wu, J., Zhang, S., Li, W., & Wang, Y. G. (2024). Physical informed neural networks with soft and hard boundary constraints for solving advection-diffusion equations using Fourier expansions. *Computers & Mathematics with Applications*, 159, 60-75.
- Li, X., & Zhang, W. (2022). Physics-informed deep learning model in wind turbine response prediction. *Renewable Energy*, 185, 932-944.
- Li, Y., Ni, P., Sun, L., & Xia, Y. (2024). Finite element model-informed deep learning for equivalent force estimation and full-field response calculation. *Mechanical Systems and Signal Processing*, 206, 110892.
- Liang, R., Liu, W., Fu, Y., & Ma, M. (2024). Physics-informed deep learning for

- structural dynamics under moving load. *International Journal of Mechanical Sciences*, 284, 109766.
- Lin, X., & Yuan, F. (2005). Experimental study applying a migration technique in structural health monitoring. *Structural Health Monitoring*, 4(4), 341-353.
- Linka, K., Schäfer, A., Meng, X., Zou, Z., Karniadakis, G. E., & Kuhl, E. (2022). Bayesian Physics Informed Neural Networks for real-world nonlinear dynamical systems. *Computer Methods in Applied Mechanics and Engineering*, 402, 115346.
- Liu, D., Bao, Y., & Li, H. (2023). Machine learning-based stochastic subspace identification method for structural modal parameters. *Engineering Structures*, 274, 115178.
- Liu, F., Li, J., & Wang, L. (2023). PI-LSTM: Physics-informed long short-term memory network for structural response modeling. *Engineering Structures*, 292, 116500.
- Liu, F., Yu, Q., Song, H., Li, X., Liu, L., & Liu, D. (2023). A novel physics-informed framework for real-time adaptive modal parameters estimation of offshore structures. *Ocean Engineering*, 280, 114517.
- Liu, J., & Hao, Y. (2022). Crank–Nicolson method for solving uncertain heat equation. Soft Computing, 26(3), 937-945.
- Liu, T., & Meidani, H. (2023). Physics-Informed Neural Networks for System Identification of Structural Systems with a Multiphysics Damping Model. *Journal of Engineering Mechanics*, *149*(10), 04023079.
- Liu, Y., Wang, L., Gu, K., & Li, M. (2022). Artificial Neural Network (ANN)-Bayesian Probability Framework (BPF) based method of dynamic force reconstruction under multi-source uncertainties. *Knowledge-Based Systems*, 237, 107796.
- Liu, Y., Wang, L., & Ng, B. F. (2024). A hybrid model-data-driven framework for inverse load identification of interval structures based on physics-informed neural

- network and improved Kalman filter algorithm. Applied Energy, 359, 122740.
- Lourens, E., Reynders, E., De Roeck, G., Degrande, G., & Lombaert, G. (2012). An augmented Kalman filter for force identification in structural dynamics.

  Mechanical Systems and Signal Processing, 27, 446-460.
- Lu, H., Wang, Q., Tang, W., & Liu, H. (2024). Physics-informed neural networks for fully non-linear free surface wave propagation. *Physics of Fluids*, *36*(6)
- Lu, L., Meng, X., Mao, Z., & Karniadakis, G. E. (2021). DeepXDE: A deep learning library for solving differential equations. *SIAM Review*, *63*(1), 208-228.
- Lu, L., Pestourie, R., Yao, W., Wang, Z., Verdugo, F., & Johnson, S. G. (2021a). Physics-informed neural networks with hard constraints for inverse design. *SIAM Journal on Scientific Computing*, 43(6), B1105-B1132.
- Lu, L., Pestourie, R., Yao, W., Wang, Z., Verdugo, F., & Johnson, S. G. (2021b). Physics-informed neural networks with hard constraints for inverse design. *arXiv* preprint arXiv:.04626,
- Ma, Z., Liao, H., Gao, J., Nie, S., & Geng, Y. (2023). Physics-informed machine learning for degradation modeling of an electro-hydrostatic actuator system. Reliability Engineering & System Safety, 229, 108898.
- Mahmoudabadbozchelou, M., Karniadakis, G. E., & Jamali, S. (2022). nn-PINNs: Non-Newtonian physics-informed neural networks for complex fluid modeling. *Soft Matter*, *18*(1), 172-185.
- Mai, H. T., Truong, T. T., Kang, J., Mai, D. D., & Lee, J. (2023). A robust physics-informed neural network approach for predicting structural instability. *Finite Elements in Analysis and Design*, 216, 103893.
- Malik, F. N., Ricles, J., Yari, M., & Nissar, M. A. (2023). Physics Informed Recurrent Neural Networks for Seismic Response Evaluation of Nonlinear Systems. *arXiv*

- preprint arXiv:2308.08655,
- Mao, Y. M., Guo, X. L., & Zhao, Y. (2010). A state space force identification method based on Markov parameters precise computation and regularization technique. *Journal of Sound and Vibration*, 329(15), 3008-3019.
- Mao, Z., Jagtap, A. D., & Karniadakis, G. E. (2020). Physics-informed neural networks for high-speed flows. *Computer Methods in Applied Mechanics and Engineering*, 360, 112789.
- Meng, S., Zhou, Y., Zheng, Q., Liao, B., Chang, M., Zhang, T., & Djerrad, A. (2024).
  SeisGPT: A Physics-Informed Data-Driven Large Model for Real-Time Seismic
  Response Prediction. arXiv preprint arXiv:2410.20186,
- Miele, S., Karve, P., & Mahadevan, S. (2023). Multi-fidelity physics-informed machine learning for probabilistic damage diagnosis. *Reliability Engineering & System Safety*, 235, 109243.
- Misyris, G. S., Venzke, A., & Chatzivasileiadis, S. (2020). Physics-informed neural networks for power systems. 2020 IEEE power & energy society general meeting (PESGM), 1-5.
- Mousavi, Z., Varahram, S., Ettefagh, M. M., Sadeghi, M. H., & Razavi, S. N. (2021). Deep neural networks—based damage detection using vibration signals of finite element model and real intact state: An evaluation via a lab-scale offshore jacket structure. *Structural Health Monitoring*, 20(1), 379-405.
- Najafabadi, M. M., Villanustre, F., Khoshgoftaar, T. M., Seliya, N., Wald, R., & Muharemagic, E. (2015). Deep learning applications and challenges in big data analytics. *Journal of big data*, 2, 1-21.
- Nellikkath, R., & Chatzivasileiadis, S. (2021). Physics-informed neural networks for minimising worst-case violations in dc optimal power flow. 2021 IEEE

- International Conference on Communications, Control, and Computing Technologies for Smart Grids (SmartGridComm), 419-424.
- Nellikkath, R., & Chatzivasileiadis, S. (2022). Physics-informed neural networks for ac optimal power flow. *Electric Power Systems Research*, *212*, 108412.
- Nevin, J. W., Vaquero-Caballero, F., Ives, D. J., & Savory, S. J. (2021). Physics-informed Gaussian process regression for optical fiber communication systems. *Journal of Lightwave Technology*, 39(21), 6833-6844.
- Ngo, Q.-H., Nguyen, B. L., Vu, T. V., Zhang, J., & Ngo, T. (2024). Physics-informed graphical neural network for power system state estimation. *Applied Energy*, *358*, 122602.
- Ni, P., Sun, L., Yang, J., & Li, Y. (2022). Multi-end physics-informed deep learning for seismic response estimation. *Sensors*, 22(10), 3697.
- Ni, Q., Ji, J., Halkon, B., Feng, K., & Nandi, A. K. (2023). Physics-Informed Residual Network (PIResNet) for rolling element bearing fault diagnostics. *Mechanical Systems and Signal Processing*, 200, 110544.
- Niu, Y., Fritzen, C. P., Jung, H., Buethe, I., Ni, Y. Q., & Wang, Y. W. (2015). Online Simultaneous Reconstruction of Wind Load and Structural Responses—Theory and Application to Canton Tower. *Computer-Aided Civil and Infrastructure Engineering*, 30(8), 666-681.
- Noël, J.-P., & Kerschen, G. (2017). Nonlinear system identification in structural dynamics: 10 more years of progress. *Mechanical Systems and Signal Processing*, 83, 2-35.
- O'Leary, J., Paulson, J. A., & Mesbah, A. (2022). Stochastic physics-informed neural ordinary differential equations. *Journal of computational physics*, 468, 111466.
- Oh, B. K., Park, Y., & Park, H. S. (2020). Seismic response prediction method for

- building structures using convolutional neural network. *Structural Control and Health Monitoring*, *27*(5), e2519.
- Pan, C., & Yu, L. (2019). Identification of external forces via truncated response sparse decomposition under unknown initial conditions. *Advances in Structural Engineering*, 22(15), 3161-3175.
- Pan, H., Lin, Z., & Gui, G. (2019). Enabling damage identification of structures using time series—based feature extraction algorithms. *Journal of Aerospace Engineering*, 32(3), 04019014.
- Pan, X., & Yang, T. (2020). Postdisaster image-based damage detection and repair cost estimation of reinforced concrete buildings using dual convolutional neural networks. *Computer-Aided Civil and Infrastructure Engineering*, 35(5), 495-510.
- Pang, G., & Karniadakis, G. E. (2020). Physics-informed learning machines for partial differential equations: Gaussian processes versus neural networks. In *Emerging frontiers in nonlinear science* (pp. 323-343). Springer.
- Pang, G., Lu, L., & Karniadakis, G. E. (2019). fPINNs: Fractional physics-informed neural networks. *SIAM Journal on Scientific Computing*, 41(4), A2603-A2626.
- Park, H.-W., & Hwang, J.-H. (2023). Predicting the Early-Age Time-Dependent Behaviors of a Prestressed Concrete Beam by Using Physics-Informed Neural Network. *Sensors*, 23(14), 6649.
- Paszke, A., Gross, S., Massa, F., Lerer, A., Bradbury, J., Chanan, G., Killeen, T., Lin, Z., Gimelshein, N., & Antiga, L. (2019). Pytorch: An imperative style, high-performance deep learning library. Advances in Neural Information Processing Systems, 32
- Patel, Y., Mons, V., Marquet, O., & Rigas, G. (2024). Turbulence model augmented physics-informed neural networks for mean-flow reconstruction. *Physical Review*

- Fluids, 9(3), 034605.
- Paz, M., & Kim, Y. H. (2018). Structural Dynamics (6 ed.). Springer Cham.
- Peeters, B., & Ventura, C. (2003). Comparative study of modal analysis techniques for bridge dynamic characteristics. *Mechanical Systems and Signal Processing*, 17(5), 965-988.
- Peng, Z., Li, J., & Hao, H. (2022). Structural damage detection via phase space based manifold learning under changing environmental and operational conditions. *Engineering Structures*, 263, 114420.
- Petersen, Ø. W., Øiseth, O., & Lourens, E. (2022). Wind load estimation and virtual sensing in long-span suspension bridges using physics-informed Gaussian process latent force models. *Mechanical Systems and Signal Processing*, 170, 108742.
- Prawin, J., & Rao, A. R. M. (2018). An online input force time history reconstruction algorithm using dynamic principal component analysis. *Mechanical Systems and Signal Processing*, 99, 516-533.
- Preetha Hareendran, S., & Alipour, A. (2022). Prediction of nonlinear structural response under wind loads using deep learning techniques. *Applied Soft Computing*, 129, 109424.
- Psaros, A. F., Meng, X., Zou, Z., Guo, L., & Karniadakis, G. E. (2023). Uncertainty quantification in scientific machine learning: Methods, metrics, and comparisons. *Journal of computational physics*, 477, 111902.
- Qiao, B., Ao, C., Mao, Z., & Chen, X. (2020). Non-convex sparse regularization for impact force identification. *Journal of Sound and Vibration*, 477, 115311.
- Qu, J., Cai, W., & Zhao, Y. (2022). Learning time-dependent PDEs with a linear and nonlinear separate convolutional neural network. *Journal of computational physics*, 453, 110928.

- Qu, W., & Liang, Y. (2017). Stability and convergence of the Crank-Nicolson scheme for a class of variable-coefficient tempered fractional diffusion equations.

  Advances in Difference Equations, 2017(1), 108.
- Raissi, M., Perdikaris, P., & Karniadakis, G. E. (2019). Physics-informed neural networks: A deep learning framework for solving forward and inverse problems involving nonlinear partial differential equations. *Journal of Computational physics*, 378, 686-707.
- Raissi, M., Yazdani, A., & Karniadakis, G. E. (2020). Hidden fluid mechanics: Learning velocity and pressure fields from flow visualizations. *Science*, *367*(6481), 1026-1030.
- Rao, C., Sun, H., & Liu, Y. (2020). Physics-informed deep learning for incompressible laminar flows. *Theoretical and Applied Mechanics Letters*, 10(3), 207-212.
- Ren, C., Wang, N., Liu, Q., & Liu, C. (2019). Dynamic force identification problem based on a novel improved Tikhonov regularization method. *Mathematical Problems in Engineering*, (1), 6095184.
- Rezaei, S., Harandi, A., Moeineddin, A., Xu, B.-X., & Reese, S. (2022). A mixed formulation for physics-informed neural networks as a potential solver for engineering problems in heterogeneous domains: Comparison with finite element method. *Computer Methods in Applied Mechanics and Engineering*, 401, 115616.
- Ribeiro, A. H., Tiels, K., Aguirre, L. A., & Schön, T. (2020). *Beyond exploding and vanishing gradients: analysing RNN training using attractors and smoothness*Proceedings of the Twenty Third International Conference on Artificial Intelligence and Statistics, Proceedings of Machine Learning Research.
- Rubio, P.-B., Louf, F., & Chamoin, L. (2018). Fast model updating coupling Bayesian inference and PGD model reduction. *Computational Mechanics*, 62, 1485-1509.

- Rudin, C. (2019). Stop explaining black box machine learning models for high stakes decisions and use interpretable models instead. *Nature machine intelligence*, *1*(5), 206-215.
- Rui, E.-Z., Chen, Z.-W., Ni, Y.-Q., Yuan, L., & Zeng, G.-Z. (2023). Reconstruction of 3D flow field around a building model in wind tunnel: a novel physics-informed neural network framework adopting dynamic prioritization self-adaptive loss balance strategy. *Engineering Applications of Computational Fluid Mechanics*, 17(1), 2238849.
- Rui, E.-Z., Zeng, G.-Z., Ni, Y.-Q., Chen, Z.-W., & Hao, S. (2024). Time-averaged flow field reconstruction based on a multifidelity model using physics-informed neural network (PINN) and nonlinear information fusion. *International Journal of Numerical Methods for Heat & Fluid Flow*, 34(1), 131-149.
- Rui, E. Z., Chen, Z. W., Ni, Y. Q., Yuan, L., & Zeng, G. Z. (2023). Reconstruction of 3D flow field around a building model in wind tunnel: a novel physics-informed neural network framework adopting dynamic prioritization self-adaptive loss balance strategy. *Engineering Applications of Computational Fluid Mechanics*, 17(1), 2238849.
- Rui, E. Z., Zeng, G. Z., Ni, Y. Q., Chen, Z. W., & Hao, S. (2024). Time-averaged flow field reconstruction based on a multifidelity model using physics-informed neural network (PINN) and nonlinear information fusion. *International Journal of Numerical Methods for Heat & Fluid Flow*, 34(1), 131-149.
- Russell, M., & Wang, P. (2022). Physics-informed deep learning for signal compression and reconstruction of big data in industrial condition monitoring. *Mechanical Systems and Signal Processing*, 168, 108709.
- Sadhu, A., Narasimhan, S., & Antoni, J. (2017). A review of output-only structural

- mode identification literature employing blind source separation methods.

  Mechanical Systems and Signal Processing, 94, 415-431.
- Sallam, O., & Fürth, M. (2023). On the use of Fourier Features-Physics Informed Neural Networks (FF-PINN) for forward and inverse fluid mechanics problems.

  Proceedings of the Institution of Mechanical Engineers, Part M: Journal of Engineering for the Maritime Environment, 237(4), 846-866.
- Sanchez, J., & Benaroya, H. (2014). Review of force reconstruction techniques. *Journal of Sound and Vibration*, 333(14), 2999-3018.
- Sarabian, M., Babaee, H., & Laksari, K. (2022). Physics-Informed Neural Networks for Brain Hemodynamic Predictions Using Medical Imaging. *IEEE Transactions on Medical Imaging*, 41(9), 2285-2303.
- Schommer, S., Nguyen, V. H., Maas, S., & Zürbes, A. (2017). Model updating for structural health monitoring using static and dynamic measurements. *Procedia engineering*, 199, 2146-2153.
- Sen, A., Ghajar-Rahimi, E., Aguirre, M., Navarro, L., Goergen, C. J., & Avril, S. (2024).

  Physics-Informed Graph Neural Networks to solve 1-D equations of blood flow.

  Computer Methods and Programs in Biomedicine, 257, 108427.
- Shang, Z., Sun, L., Xia, Y., & Zhang, W. (2021). Vibration-based damage detection for bridges by deep convolutional denoising autoencoder. *Structural Health Monitoring*, 20(4), 1880-1903.
- Sharma, P., Chung, W. T., Akoush, B., & Ihme, M. (2023). A Review of Physics-Informed Machine Learning in Fluid Mechanics. *Energies*, *16*(5), 2343.
- Shen, S., Lu, H., Sadoughi, M., Hu, C., Nemani, V., Thelen, A., Webster, K., Darr, M., Sidon, J., & Kenny, S. (2021). A physics-informed deep learning approach for bearing fault detection. *Engineering Applications of Artificial Intelligence*, 103,

104295.

- Shen, S., & Málaga-Chuquitaype, C. (2024). Physics-informed artificial intelligence models for the seismic response prediction of rocking structures. *Data-Centric Engineering*, 5, e1.
- Shi, Q., Lin, B., Yang, C., Hu, K., Han, W., & Luo, Z. (2024). Convex model-based regularization method for force reconstruction. *Computer Methods in Applied Mechanics and Engineering*, 426, 116986.
- Shin, H., & Choi, M. (2023). Physics-informed variational inference for uncertainty quantification of stochastic differential equations. *Journal of computational physics*, 487, 112183.
- Shu, D., Li, Z., & Farimani, A. B. (2023). A physics-informed diffusion model for high-fidelity flow field reconstruction. *Journal of computational physics*, 478, 111972.
- Shukla, K., Jagtap, A. D., & Karniadakis, G. E. (2021). Parallel physics-informed neural networks via domain decomposition. *Journal of Computational Physics*, 447, 110683.
- Song, C., & Wang, Y. (2023). Simulating seismic multifrequency wavefields with the Fourier feature physics-informed neural network. *Geophysical Journal International*, 232(3), 1503-1514.
- Song, M., Astroza, R., Ebrahimian, H., Moaveni, B., & Papadimitriou, C. (2020).

  Adaptive Kalman filters for nonlinear finite element model updating. *Mechanical Systems and Signal Processing*, 143, 106837.
- Spijker, M. N. (1996). Stiffness in numerical initial-value problems. *Journal of Computational and Applied Mathematics*, 72(2), 393-406.
- Stiasny, J., Zhang, B., & Chatzivasileiadis, S. (2024). PINNSim: A simulator for power system dynamics based on Physics-Informed Neural Networks. *Electric Power*

- *Systems Research*, 235, 110796.
- Stoffel, M., Bamer, F., & Markert, B. (2018). Artificial neural networks and intelligent finite elements in non-linear structural mechanics. *Thin-Walled Structures*, *131*, 102-106.
- Stoffel, M., Gulakala, R., Bamer, F., & Markert, B. (2020). Artificial neural networks in structural dynamics: A new modular radial basis function approach vs. convolutional and feedforward topologies. *Computer Methods in Applied Mechanics and Engineering*, 364, 112989.
- Su, C., Liang, J., & He, Z. (2024). E-PINN: A fast physics-informed neural network based on explicit time-domain method for dynamic response prediction of nonlinear structures. *Engineering Structures*, *321*, 118900.
- Sun, H., & Betti, R. (2015). A hybrid optimization algorithm with Bayesian inference for probabilistic model updating. *Computer-Aided Civil and Infrastructure Engineering*, 30(8), 602-619.
- Sun, X., Ilanko, S., Mochida, Y., & Tighe, R. C. (2023). A Review on Vibration-Based Damage Detection Methods for Civil Structures. *Vibration*, *6*(4), 843-875.
- Tang, Y., Fan, J., Li, X., Ma, J., Qi, M., Yu, C., & Gao, W. (2022). Physics-informed recurrent neural network for time dynamics in optical resonances. *Nature computational science*, 2(3), 169-178.
- Tartakovsky, A. M., Ma, T., Barajas-Solano, D. A., & Tipireddy, R. (2023). Physics-informed Gaussian process regression for states estimation and forecasting in power grids. *International Journal of Forecasting*, 39(2), 967-980.
- Teimouri, H., Milani, A. S., Loeppky, J., & Seethaler, R. (2017). A Gaussian process–based approach to cope with uncertainty in structural health monitoring. *Structural Health Monitoring*, 16(2), 174-184.

- Tondo, G. R., Rau, S., Kavrakov, I., & Morgenthal, G. (2023). Stochastic stiffness identification and response estimation of Timoshenko beams via physics-informed Gaussian processes. *Probabilistic Engineering Mechanics*, 74, 103534.
- Trinh, D. T., Luong, K. A., & Lee, J. (2024). An analysis of functionally graded thin-walled beams using physics-informed neural networks. *Engineering Structures*, 301, 117290.
- Tsai, L.-W., & Alipour, A. (2023). Physics-informed long short-term memory networks for response prediction of a wind-excited flexible structure. *Engineering Structures*, 275, 114968.
- Wang, L., Liu, J., & Lu, Z.-R. (2020). Bandlimited force identification based on sincdictionaries and Tikhonov regularization. *Journal of Sound and Vibration*, 464, 114988.
- Wang, L., Liu, Y., Gu, K., & Wu, T. (2020). A radial basis function artificial neural network (RBF ANN) based method for uncertain distributed force reconstruction considering signal noises and material dispersion. *Computer Methods in Applied Mechanics and Engineering*, 364, 112954.
- Wang, N., Liu, Q., Ren, C., & Liu, C. (2019). A novel method of dynamic force identification and its application. *Mathematical Problems in Engineering*, 2019
- Wang, S., & Perdikaris, P. (2021). Deep learning of free boundary and Stefan problems. *Journal of computational physics*, 428, 109914.
- Wang, S., Wang, H., & Perdikaris, P. (2021). On the eigenvector bias of Fourier feature networks: From regression to solving multi-scale PDEs with physics-informed neural networks. *Computer Methods in Applied Mechanics and Engineering*, 384, 113938.
- Wang, S., Yu, X., & Perdikaris, P. (2022). When and why PINNs fail to train: A neural

- tangent kernel perspective. Journal of Computational Physics, 449, 110768.
- Wang, X., Hill, T. L., Neild, S. A., Shaw, A. D., Haddad Khodaparast, H., & Friswell,
  M. I. (2018). Model updating strategy for structures with localised nonlinearities
  using frequency response measurements. *Mechanical Systems and Signal Processing*, 100, 940-961.
- Wei, D., Li, D., & Huang, J. (2022). Improved force identification with augmented Kalman filter based on the sparse constraint. *Mechanical Systems and Signal Processing*, 167, 108561.
- Weng, Y., & Zhou, D. (2022). Multiscale physics-informed neural networks for stiff chemical kinetics. *The Journal of Physical Chemistry A*, 126(45), 8534-8543.
- Wessels, H., Weißenfels, C., & Wriggers, P. (2020). The neural particle method—an updated Lagrangian physics informed neural network for computational fluid dynamics. *Computer Methods in Applied Mechanics and Engineering*, 368, 113127.
- Wight, C. L., & Zhao, J. (2021). Solving Allen-Cahn and Cahn-Hilliard equations using the adaptive physics informed neural networks. *Communications in Computational Physics*, 29(3), 930-954.
- Worden, K., & Manson, G. (2007). The application of machine learning to structural health monitoring. *Philosophical Transactions of the Royal Society A:*Mathematical, Physical and Engineering Sciences, 365(1851), 515-537.
- Wu, R.-T., & Jahanshahi, M. R. (2019). Deep convolutional neural network for structural dynamic response estimation and system identification. *Journal of Engineering Mechanics*, 145(1), 04018125.
- Wu, Y., Sicard, B., & Gadsden, S. A. (2024). Physics-informed machine learning: A comprehensive review on applications in anomaly detection and condition monitoring. *Expert Systems with Applications*, 124678.

- Würth, T., Freymuth, N., Zimmerling, C., Neumann, G., & Kärger, L. (2024). Physics-informed MeshGraphNets (PI-MGNs): Neural finite element solvers for non-stationary and nonlinear simulations on arbitrary meshes. *Computer Methods in Applied Mechanics and Engineering*, 429, 117102.
- Xiang, Z., Peng, W., Liu, X., & Yao, W. (2022). Self-adaptive loss balanced physics-informed neural networks. *Neurocomputing*, 496, 11-34.
- Xiao, Z., Ju, Y., Li, Z., Zhang, J., & Zhang, C. (2024). On the Hard Boundary Constraint Method for Fluid Flow Prediction based on the Physics-Informed Neural Network. Applied Sciences, 14(2), 859.
- Xiong, Q., Kong, Q., Xiong, H., Liao, L., & Yuan, C. (2024). Physics-informed deep 1D CNN compiled in extended state space fusion for seismic response modeling. *Computers & structures*, 291, 107215.
- Xu, J., Wei, H., & Bao, H. (2023). Physics-informed neural networks for studying heat transfer in porous media. *International Journal of Heat and Mass Transfer*, 217, 124671.
- Xu, S., & Noh, H. Y. (2021). PhyMDAN: Physics-informed knowledge transfer between buildings for seismic damage diagnosis through adversarial learning. *Mechanical Systems and Signal Processing*, 151, 107374.
- Xu, S., Sun, Z., Huang, R., Guo, D., Yang, G., & Ju, S. (2023). A practical approach to flow field reconstruction with sparse or incomplete data through physics informed neural network. *Acta Mechanica Sinica*, *39*(3), 322302.
- Xu, Z.-Q. J., Zhang, Y., & Luo, T. (2024). Overview Frequency Principle/Spectral Bias in Deep Learning. *Communications on Applied Mathematics and Computation*,
- Xue, J., & Ou, G. (2021). Predicting wind-induced structural response with LSTM in transmission tower-line system. *Smart structures and systems*, 28(3)

- Yamaguchi, T., & Mizutani, T. (2024). A Physics-Informed Neural Network for the Nonlinear Damage Identification in a Reinforced Concrete Bridge Pier Using Seismic Responses. *Structural Control and Health Monitoring*, 2024(1), 5532909.
- Yang, C. (2024). Interval strategy-based regularization approach for force reconstruction with multi-source uncertainties. *Computer Methods in Applied Mechanics and Engineering*, 419, 116679.
- Yang, L., Meng, X., & Karniadakis, G. E. (2021). B-PINNs: Bayesian physics-informed neural networks for forward and inverse PDE problems with noisy data. *Journal of computational physics*, 425, 109913.
- Yang, L., Zhang, D., & Karniadakis, G. E. (2018). Physics-informed generative adversarial networks for stochastic differential equations. *arXiv* preprint *arXiv*::02033,
- Yang, L., Zhang, D., & Karniadakis, G. E. (2020). Physics-informed generative adversarial networks for stochastic differential equations. *SIAM Journal on Scientific Computing*, 42(1), A292-A317.
- Yang, M., & Foster, J. T. (2022). Multi-output physics-informed neural networks for forward and inverse PDE problems with uncertainties. *Computer Methods in Applied Mechanics and Engineering*, 402, 115041.
- Yang, X., Barajas Solano, D., Tartakovsky, G., & Tartakovsky, A. M. (2019). Physics-informed CoKriging: A Gaussian-process-regression-based multifidelity method for data-model convergence. *Journal of computational physics*, 395, 410-431.
- Yang, Y., & Perdikaris, P. (2019). Adversarial uncertainty quantification in physics-informed neural networks. *Journal of computational physics*, 394, 136-152.
- Yang, Z., & Wang, L. (2010). Structural Damage Detection by Changes in Natural Frequencies. *Journal of intelligent material systems and structures*, 21(3), 309-319.

- Yao, Z., Zhang, T., Wu, L., Wang, X., & Huang, J. (2023). Physics-Informed Deep Learning for Reconstruction of Spatial Missing Climate Information in the Antarctic. *Atmosphere*, 14(4), 658.
- Yazdanpanah1a, O., & Seyedpoor, S. (2015). A new damage detection indicator for beams based on mode shape data. *Structural Engineering and Mechanics*, 53(4), 725-744.
- Yu, Y., Wang, C., Gu, X., & Li, J. (2019). A novel deep learning-based method for damage identification of smart building structures. *Structural Health Monitoring*, 18(1), 143-163.
- Yuan, B., Wang, H., Heitor, A., & Chen, X. (2024). f-PICNN: A physics-informed convolutional neural network for partial differential equations with space-time domain. *Journal of computational physics*, 515, 113284.
- Yuan, F.-G., Zargar, S. A., Chen, Q., & Wang, S. (2020). Machine learning for structural health monitoring: challenges and opportunities. *Sensors and smart structures technologies for civil, mechanical, and aerospace systems* 2020, 11379, 1137903.
- Yuan, L., Ni, Y.-Q., Deng, X.-Y., & Hao, S. (2022). A-PINN: Auxiliary physics informed neural networks for forward and inverse problems of nonlinear integrodifferential equations. *Journal of computational physics*, 462, 111260.
- Zargar, S. A., & Yuan, F.-G. (2024). Physics-informed deep learning for scattered full wavefield reconstruction from a sparse set of sensor data for impact diagnosis in structural health monitoring. *Structural Health Monitoring*, 14759217231202547.
- Zhai, W., Tao, D., & Bao, Y. (2023). Parameter estimation and modeling of nonlinear dynamical systems based on Runge–Kutta physics-informed neural network. Nonlinear Dynamics, 111(22), 21117-21130.
- Zhang, B., Wu, G., Gu, Y., Wang, X., & Wang, F. (2022). Multi-domain physics-

- informed neural network for solving forward and inverse problems of steady-state heat conduction in multilayer media. *Physics of Fluids*, *34*(11)
- Zhang, D., Guo, L., & Karniadakis, G. E. (2020). Learning in Modal Space: Solving Time-Dependent Stochastic PDEs Using Physics-Informed Neural Networks. SIAM Journal on Scientific Computing, 42(2), A639-A665.
- Zhang, D., Lu, L., Guo, L., & Karniadakis, G. E. (2019). Quantifying total uncertainty in physics-informed neural networks for solving forward and inverse stochastic problems. *Journal of computational physics*, 397, 108850.
- Zhang, E., Dao, M., Karniadakis, G. E., & Suresh, S. (2022). Analyses of internal structures and defects in materials using physics-informed neural networks. *Science Advances*, 8(7), eabk0644.
- Zhang, H.-F., Lu, X.-L., Ding, X., & Zhang, X.-M. (2024). Physics-informed line graph neural network for power flow calculation. *Chaos: An Interdisciplinary Journal of Nonlinear Science*, *34*(11)
- Zhang, J. (2020). A-stable two-step time integration methods with controllable numerical dissipation for structural dynamics. *International Journal for Numerical Methods in Engineering*, 121(1), 54-92.
- Zhang, J., Sato, T., Iai, S., & Hutchinson, T. (2008). A pattern recognition technique for structural identification using observed vibration signals: Linear case studies. *Engineering Structures*, 30(5), 1439-1446.
- Zhang, M., Guo, T., Zhang, G., Liu, Z., & Xu, W. (2024). Physics-informed deep learning for structural vibration identification and its application on a benchmark structure. *Philosophical Transactions of the Royal Society A*, 382(2264), 20220400.
- Zhang, R., Chen, Z., Chen, S., Zheng, J., Büyüköztürk, O., & Sun, H. (2019). Deep long short-term memory networks for nonlinear structural seismic response

- prediction. Computers & structures, 220, 55-68.
- Zhang, R., Liu, Y., & Sun, H. (2020a). Physics-guided convolutional neural network (PhyCNN) for data-driven seismic response modeling. *Engineering Structures*, 215, 110704.
- Zhang, R., Liu, Y., & Sun, H. (2020b). Physics-informed multi-LSTM networks for metamodeling of nonlinear structures. *Computer Methods in Applied Mechanics and Engineering*, 369, 113226.
- Zhang, R., Warn, G. P., & Radlińska, A. (2024). Dual state-parameter estimation of continuous structural systems with physics-informed parallel neural networks. *Journal of Sound and Vibration*, 571, 118138.
- Zhang, Y., Chen, N., Vialard, J., & Fang, X. (2024). A Physics-Informed Auto-Learning Framework for Developing Stochastic Conceptual Models for ENSO Diversity. *Journal of Climate*, 37(23), 6323-6347.
- Zhang, Z., & Sun, C. (2021). Structural damage identification via physics-guided machine learning: a methodology integrating pattern recognition with finite element model updating. *Structural Health Monitoring*, 20(4), 1675-1688.
- Zhang, Z., Yan, X., Liu, P., Zhang, K., Han, R., & Wang, S. (2023). A physics-informed convolutional neural network for the simulation and prediction of two-phase Darcy flows in heterogeneous porous media. *Journal of computational physics*, 477, 111919.
- Zhao, S., Peng, Y., Zhang, Y., & Wang, H. (2022). Parameter estimation of power electronic converters with physics-informed machine learning. *IEEE Transactions on Power Electronics*, 37(10), 11567-11578.
- Zhao, X., Gong, Z., Zhang, Y., Yao, W., & Chen, X. (2023). Physics-informed convolutional neural networks for temperature field prediction of heat source

- layout without labeled data. Engineering Applications of Artificial Intelligence, 117, 105516.
- Zheng, B., Li, T., Qi, H., Gao, L., Liu, X., & Yuan, L. (2022). Physics-informed machine learning model for computational fracture of quasi-brittle materials without labelled data. *International Journal of Mechanical Sciences*, 223, 107282.
- Zheng, Y., Hu, C., Wang, X., & Wu, Z. (2023). Physics-informed recurrent neural network modeling for predictive control of nonlinear processes. *Journal of Process Control*, 128, 103005.
- Zheng, Y., & Wu, Z. (2023). Physics-informed online machine learning and predictive control of nonlinear processes with parameter uncertainty. *Industrial & Engineering Chemistry Research*, 62(6), 2804-2818.
- Zhou, C., Chase, J. G., & Rodgers, G. W. (2021). Support vector machines for automated modelling of nonlinear structures using health monitoring results. *Mechanical Systems and Signal Processing*, 149, 107201.
- Zhou, W., & Chelidze, D. (2007). Blind source separation based vibration mode identification. *Mechanical Systems and Signal Processing*, 21(8), 3072-3087.
- Zhou, W., & Xu, Y. (2024). Damage identification for plate structures using physics-informed neural networks. *Mechanical Systems and Signal Processing*, 209, 111111.
- Zhu, H.-P., Mao, L., & Weng, S. (2014). A sensitivity-based structural damage identification method with unknown input excitation using transmissibility concept. *Journal of Sound and Vibration*, 333(26), 7135-7150.
- Zhu, H. P., Mao, L., & Weng, S. (2014). A sensitivity-based structural damage identification method with unknown input excitation using transmissibility concept. *Journal of Sound and Vibration*, 333(26), 7135-7150.

- Zhu, Q., Liu, Z., & Yan, J. (2021). Machine learning for metal additive manufacturing: predicting temperature and melt pool fluid dynamics using physics-informed neural networks. *Computational Mechanics*, 67(2), 619-635.
- Zobeiry, N., & Humfeld, K. D. (2021). A physics-informed machine learning approach for solving heat transfer equation in advanced manufacturing and engineering applications. *Engineering Applications of Artificial Intelligence*, 101, 104232.
- Zubov, K., McCarthy, Z., Ma, Y., Calisto, F., Pagliarino, V., Azeglio, S., Bottero, L., Luján, E., Sulzer, V., & Bharambe, A. (2021). NeuralPDE: Automating physics-informed neural networks (PINNs) with error approximations. arXiv preprint arXiv:2107.09443,
- Zuo, H., & Guo, H. (2022). Structural nonlinear damage identification based on Bayesian optimization GNAR/GARCH model and its experimental study. Structures, 45, 867-885.